
# Data-driven applications in ageing and inflammation of the retina

Thesis submitted in accordance with the requirements of

the University of Liverpool for the degree of Doctor in Philosophy

by

Dhanach Dhirachaikulpanich

October 2023

**Declaration**

This thesis is the result of work performed whilst registered as a candidate for the degree of Doctor of Philosophy at the University of Liverpool. I, Dhanach Dhirachaikulpanich, hereby declare that the work included in this thesis is my own. I incorporate published materials into the results chapters of this research degree thesis following the postgraduate research code of practice -Appendix 7- Annexe 2 (2022/2023) of the University of Liverpool. If the information has been derived from other sources, I have appropriately referenced them in this thesis. The following paragraphs outline the authors' contributions to each of studies that constitute the thesis results chapters.

Chapter 3: Dhanach Dhirachaikulpanich designed the study, performed the data analysis, wrote the first draft, and edited the manuscript. Xin Li checked the data analysis and edited the manuscript. Luminita Paraoan supervised and edited the manuscript. Louise Frances Porter edited the manuscript. All authors discussed the results, reviewed and approved the final manuscript.

Chapter 4: Dhanach Dhirachaikulpanich conceptualised the study, performed the analysis, wrote the first draft, and edited the manuscript. Kasit Chatsirisupachai helped conceptualised the study and edited the manuscript. Cyril Lagger checked, confirmed the data analysis, and edited the manuscript. Luminita Paraoan and Joao Pedro de Magalhaes conceived overall project, supervised the study, and provided critical insights for the interpretation of results. All authors contributed to the article and approved the final manuscript.

Chapter 5: Dhanach Dhirachaikulpanich conceptualised, designed, searched articles, and did data extraction and analysis. Nicholas Beare conceptualised and supervised data extraction/analysis. Kanat Chanthongdee participated in the search and selected articles. All authors read and reviewed the final manuscript. All authors read and approved the final manuscript.

Chapter 6: Dhanach Dhirachaikulpanich conceptualised, designed, contributed to data collection, did data analysis and wrote the first draft of the manuscript. Nicholas Beare conceptualised, designed, contributed to data collection, supervised data analysis and edited the manuscript. Savita Madhusudhan contributed to data collection and edited the manuscript. David Parry and Salma Babiker contributed to data collection. Yalin Zheng conceptualised and edited the manuscript. All authors read and reviewed the final manuscript. All authors read and approved the final manuscript.

Chapter 7: Dhanach Dhirachaikulpanich conceptualised, designed, contributed to data collection, did data analysis and wrote the first draft of the manuscript. Yalin Zheng conceptualised, designed, supervised data analysis and edited the manuscript. Nicholas Beare conceptualised, designed, contributed to data collection, supervised data analysis and edited the manuscript. Savita Madhusudhan contributed to data collection and edited the manuscript. Xiaoxin Li and Xiujen Chen contributed to data collection. Jianyang Xie confirmed data analysis and edited the manuscript. All authors read and reviewed the final manuscript. All authors read and approved the final manuscript.

Dhanach Dhirachaikulpanich, October 2023

**Acknowledgements**

First of all, I would like to sincerely express my deepest gratitude to my primary supervisor, Dr Nicholas Beare. I could not complete my PhD without his invaluable guidance and mentoring. Nick has guided me throughout the research and inspired me through his teaching and guidance with medical students, trainees and other consultants. He consistently mentors with kindness, constructive suggestion and encouragement. Nick inspires me to be a clinician-scientist and is my role model as a medical teacher. He is a beloved doctor among his patients, a good team player among other healthcare workers, and a lovely collaborator for his research team. Thus, it is my privileged, enjoyable moment and memorable opportunity to work with him.

I am grateful to my secondary supervisor, Professor Yalin Zheng, for his research knowledge and assistance. I have also gained much computer science knowledge while attending his lab meeting. He always guided with empowerment while always hitting the spot in every research question. I would like to acknowledge Dr Simon Tew for his help during the most challenging time of my PhD. He always supports me whenever I need it. I would like to thank Professor Luminita Paraoan for providing me with the opportunity to do my PhD, guiding me in molecular biology research and supporting my PhD works. I am also glad to be supervised by Professor Joao Pedro de Magalhaes. His imagination and passion for science always surprise me and make me enthusiastic about researching and being a scientist.

I thank my internal assessors, Professor George Bou-Gharios and Professor Stephen Kaye, for their guidance and support. I appreciate help from everyone at St. Paul's Eye Unit, especially Dr Savita Madhusudhan, David Parry, Dr Nima Ghadiri and Dr Salma Babiker. I have learned from every colleague and friend from the Institute of Life Course and Medical Sciences, especially Dr Dewi Romdhoniyyah, the Ocular Molecular Biology and Mechanisms of Disease group, especially Dr Wasu Supharattanasitthi, Kaiyue Teng and Xin Li, the Integrative Genomics of Ageing Group especially Dr Kasit Chatsirisupachai and Dr Cyril Lagger and Yalin's research group. I want to thank Dr Kanat Chanthongdee for helping with my systematic review work. All of them always support me and make my PhD life in Liverpool enjoyable.

I would like to acknowledge my sponsors Mahidol-Liverpool PhD scholarship, for supporting my PhD studies in Liverpool. I would like to recognise the support from every advisor from the Faculty of Medicine, Siriraj Hospital, Mahidol University, who has provided me with research opportunities since I was a medical student.

My life in Liverpool would not be happy without the support and friendship of all PhD-Thai friends, who always support me in every moment in Liverpool. I would also extend my gratitude to all my friends in Thailand and around the world. They are always present for me.

Finally, true love from my parents and two sisters always supported me unconditionally through every step of my life and participated in all my achievements.

**Table of contents**

**Declaration**.....2
**Acknowledgements**.....3
**List of figures**.....7
**List of tables**.....9
**List of publications/ presentations**.....10
**List of abbreviations**.....11
**Abstract**.....14
**Chapter 1 Introduction: Data-driven application of the retina**.....16
**1.1 The retina: structure and function**.....16
**1.1.1 Anatomy of the eye**.....16
**1.1.2 Neural retina**.....18
**1.1.3 The retinal pigment epithelium**.....19
**1.1.3.1 Structure of RPE**.....21
**1.1.3.2 Function of RPE**.....23
**1.1.4 Retinal vasculature and choroid**.....26
**1.1.5 Retinal diseases**.....28
**1.2 Omics data in the retina**.....30
**1.2.1 Omics**.....31
**1.2.2 Advancement in omics study of the retina**.....34
**1.3 Clinical images data**.....39
**1.3.1 Imaging in the retina**.....39
**1.3.2 From artificial intelligence to deep learning**.....43
**1.3.3 Deep learning and semantic segmentation**.....47
**1.3.4 Application of deep learning in retina**.....50
**Chapter 2 Literature review**.....53
**2.1 Introduction to the ageing retina and age-related macular degeneration**.....53
**2.1.1 Ageing of RPE**.....53
**2.1.2 Senescence, RPE and AMD**.....58
**2.1.3 Age-related macular degeneration**.....62
**2.1.4 Transcriptomic study of AMD RPE**.....71
**2.2 Introduction to retinal vasculitis**.....74
**2.2.1 Retinal vasculitis**.....74

**2.2.2 Clinical imaging of retinal vasculitis** ..... 79
**2.2.3 Retinal vasculitis classification** ..... 82
**2.3 Thesis aim and structure** ..... 84
**Chapter 3 Integrated microarray and RNAseq transcriptomic analysis of retinal pigment epithelium/choroid in age-related macular degeneration** ..... 88
**3.1 Introduction** ..... 90
**3.2 Methods** ..... 92
**3.3 Results** ..... 96
**3.4 Discussion** ..... 105
**Chapter 4 Intercellular communication analysis of the ageing RPE and choroid** ..... 111
**4.1 Introduction** ..... 113
**4.2 Methods** ..... 115
**4.3 Results** ..... 119
**4.4 Discussion** ..... 135
**Chapter 5. A systematic review of OCT and OCT angiography in retinal vasculitis** ..... 142
**5.1 Introduction** ..... 143
**5.2 Methods** ..... 145
**5.3 Results** ..... 147
**5.4 Discussion** ..... 162
**Chapter 6 Develop clinical grading of retinal vasculitis on a wide-field fluorescence angiography** ..... 168
**6.1 Introduction** ..... 169
**6.2 Methods** ..... 170
**6.3 Results** ..... 178
**6.4 Discussion** ..... 182
**Chapter 7 Develop computerised grading of retinal vasculitis on a wide-field fluorescence angiography** ..... 187
**7.1 Introduction** ..... 188
**7.2 Methods** ..... 189
**7.3 Results** ..... 194
**7.4 Discussion** ..... 199
**Chapter 8 Conclusion** ..... 203
**8.1 Summary** ..... 203
**8.2 Main findings and contributions** ..... 204
**8.2.1 Data-driven application in retinal research – novel findings** ..... 207
**8.2.2 Pathogenesis of AMD** ..... 207

**8.2.3 Clinical imaging of retinal vasculitis** ..... 208
**8.3 Future work** ..... 208
**8.3.1 Future work on ageing retinal disease** ..... 208
**8.3.2 Future work on inflammatory retinal disease** ..... 210
**References** ..... 213

## List of figures

Figure 1.1 Structure of the eye and retina. 18
Figure 1.2 RPE and its function. 20
Figure 1.3 Retinal vasculature and choroid. 27
Figure 1.4 Timeline of Ophthalmic Genomics. 36
Figure 1.5 Fluorescein angiography. 41
Figure 1.6 OCT and retina layers. 43
Figure 1.7 From artificial intelligence to deep learning. 44
Figure 1.8 Components of artificial neural networks. 45
Figure 1.9 Components of convolutional neural networks. 47
Figure 1.10 U-net architecture. 49
Figure 2.1 Colour fundus images of AMD. 66
Figure 2.2 Histopathologic examination of retinal vasculitis. 78
Figure 2.3 Clinical imaging of retinal vasculitis. 81
Figure 3.1 Data processing workflow and common genes between the datasets analyzed. 95
Figure 3.2 PCA plot of macular AMD RPE/choroid versus control RPE/choroid representing the datasets 97
Figure 3.3 PCA plot of non-macular AMD RPE/choroid versus control RPE/choroid representing the datasets 98
Figure 3.4 Venn diagram showing the overlap of differentially expressed genes identified by subgroup analysis in macular locations of RPE/choroid in AMD. 101
Figure 3.5 Zero order PPI network of meta-gene in macular AMD RPE/choroid. Downregulated nodes in red; upregulated nodes in green. 105
Figure 4.1 Summary of the RPE/choroid scRNA-seq dataset used for cell-cell communication analysis 120
Figure 4.2 Secreted proteins-mediated signalling involving RPE cells derived from CellChat results 121
Figure 4.3 ECM-related signalling in the RPE/choroid derived from CellChat results 123
Figure 4.4 Ligand and receptor genes differentially expressed with age in the RPE/choroid with their typical cell type-specific expression 127
Figure 4.5 Expression of senescence signature genes in RPE/choroid scRNA-seq and microarray data 129
Figure 4.6 Using senescence score to define senescent-like cells 131
Figure 4.7 scDiffCom intercellular communication results in the RPE/choroid with senescent-like subpopulations 132
Figure 4.8 Network representation of the impact of senescence on VEGF, BMP and TENASCIN intercellular communication in the RPE/choroid 133
Figure 5.1 OCT of a patient with active retinal 145
Figure 5.2 PRISMA flow diagram for study selection 148
Figure 5.3 Proposed mechanistic model of OCT/OCT-A findings related to pathogenic events of retinal vasculitis 165
Figure 6.1. Newly proposed retinal vasculitis grading scheme. 173
Figure 6.2 Example images for leakage score. 174
Figure 6.3 Example images for occlusion score. 175
Figure 6.4 Graph showing the relation between clinical grading and visual acuity 182
Figure 7.1 Training and Testing diagrams 193
Figure 7.2 Retinal vascular leakage image segmentation. 197
Figure 7.3 Retinal vascular occlusion image segmentation. 198

## List of tables

Table 2.1 Classifications of AMD ..... 64
Table 2.2 Transcriptome studies of postmortem human AMD RPE/choroid. ..... 71
Table 2.3 Retinal vasculitis's aetiology ..... 76
Table 2.4 Previous retinal vasculitis FA grading schemes ..... 82
Table 3.1 Meta-gene list showing top differentially expressed genes. ..... 98
Table 3.2 ORA analysis showing top KEGG pathways involving the meta-genes. ..... 102
Table 4.1 Ligands and receptors that are differentially expressed with age in RPE/choroid microarray samples and taking part in cell-cell interactions (detected by scDiffCom in scRNA-seq data) specifically from or to the RPE cell type. ..... 125
Table 5.1 Characteristics of included studies ..... 150
Table 6.1 Patients' characteristics of 50 recruited patients ..... 176
Table 6.2 Intra and interobserver reliability of retinal vasculitis grading from 4 independent graders. ..... 180
Table 6.3 Association between clinical variables includes retinal vasculitis grading with visual acuity using a Generalized Linear Model with a Generalized Estimating Equation. ..... 181
Table 7.1. Dataset characteristics ..... 191
Table 7.2 Dice score in different deep learning model to segment retinal vascular leakage and occlusion in retinal vasculitis ..... 195
Table 7.3 Studies reported segmentation of retinal vascular leakage and occlusion in FA ..... 200

## List of publications/ presentations

### Publications

Dhirachaikulpanich, D., Li, X., Porter, L.F., and Paraoan, L. (2020). Integrated Microarray and RNAseq Transcriptomic Analysis of Retinal Pigment Epithelium/Choroid in Age-Related Macular Degeneration. *Front Cell Dev Biol* 8**,** 808.

Dhirachaikulpanich, D., Lagger, C., Chatsirisupachai, K., De Magalhães, J.P., and Paraoan, L. (2022). Intercellular communication analysis of the human retinal pigment epithelial and choroidal cells predicts pathways associated with aging, cellular senescence and age-related macular degeneration. *Front Aging Neurosci* 14**,** 1016293.

Dhirachaikulpanich, D., Chanthongdee, K., Zheng, Y., and Beare, N.A.V. (2023). A systematic review of OCT and OCT angiography in retinal vasculitis. *J Ophthalmic Inflamm Infect* 13**,** 1.

Dhirachaikulpanich, D., Madhusudhan, S., Parry, D., Babiker, S., Zheng, Y., and Beare, N.A. V. (2023). Retinal vasculitis severity assessment: intra- and inter-observer reliability of a new scheme for grading wide-field fluorescein angiograms in retinal vasculitis. *Retina* 43**,** 1534-1543.

### Presentations

Dhirachaikulpanich, D., Madhusudhan, S., Parry, D., Babiker, S., Zheng, Y., and Beare, N.A. V. (2023, May). Validating a new grading scheme for retinal vasculitis. Poster presentation at the Royal College of Ophthalmologists Annual Congress 2023, Birmingham, UK.

Dhirachaikulpanich, D., Xie, J., Chen, X., Li, X., Madhusudhan, S., Zheng, Y., and Beare, N.A. V. (2023, September). Developing automated vascular leakage segmentation in retinal vasculitis patients using different deep learning architectures. Poster presentation at the International Ocular Inflammation Society Congress 2023, Berlin, Germany.

## List of abbreviations

| Abbreviation | Full name |
|---|---|
| A2E | N-retinldene-N-retinylethanolamine |
| ABCA | ATP-binding cassette protein |
| AGE | advanced glycation end products |
| AMD | age-related macular degeneration |
| AREDS | Age-Related Eye Diseases Study |
| ASUWOG | Angiography Scoring for Uveitis Working Group |
| BH | Benjamini-Hochberg |
| BMP | bone morphogenic proteins |
| CCIs | cell-cell interactions |
| CDK | cyclin-dependent kinase |
| cDNA | complementary DNA |
| CEP | acrolein and carboxyethylpyrrole |
| CFH | complement factor H |
| CI | confidence interval |
| CLAHE | contrast limited adaptive histogram equalisation |
| CMO | cystoid macular oedema |
| CONAN | Consensus on Neovascular AMD Nomenclature Study Group |
| CRALBP | cellular retinaldehyde binding protein |
| CRBP | cellular retinol-binding protein |
| CVA | corrected visual acuity |
| DE | differential expressed |
| ECM | extracellular matrix |
| FA | fluorescein angiography |
| FDR | false discovery rate |
| FN | false negative |
| FN1 | fibronectin 1 |
| FP | false positive |
| GA | geographic atrophy |
| GDF | growth differentiation factors |
| GEE | generalized estimating equations |
| GLM | generalized linear models |
| GLUT | glucose transporter |
| GPA | granulomatosis with polyangiitis |
| GRN | Granulin |
| GSE | Genomic Spatial Event database |
| GSEA | gene set enrichment analysis |
| GWAS | genome-wide association study |
| HDAC1 | histone deacetylase 1 |
| HGF | hepatocyte growth factor |
| HHE | 4-hydroxyhexenal |
| HNE | 4-hydroxynonenal |
| HTRA1 | high-temperature requirement serine peptidase 1 |
| IAMDGC | international age-related macular degeneration genomics consortium |

| | |
|---|---|
| ICC | intercellular communication |
| ICC | intra-class correlation coefficient |
| ICGA | indocyanine green angiography |
| IOU | intersect over union |
| IPM | interphotoreceptor matrix |
| IQR | interquatile range |
| IRBP | interphotoreceptor retinol-binding protein |
| IRVAN | idiopathic retinal vasculitis aneurysms and neuroretinitis |
| IU | intermediate uveitis |
| KEGG | Kyoto Encyclopedia of Genes and Genomes |
| LEPR | leptin receptor factor |
| LRAT | lecithin: retinol acyltransferase |
| LRI | ligand-receptor interactions |
| MCT | monocarboxylate transporter |
| MDA | malondialdehyde |
| MerTK | mer tyrosine kinase |
| MMP | matrix metalloproteinase |
| MNV | macular n-eovascularisation |
| Na+/K+-ATP | sodium/potassium adenosine triphosphatase |
| N-CAM | neural cell adhesion molecule |
| OCT | optical coherence tomography |
| OCT-A | optical coherence tomography angiography |
| OCT-EDI | enhanced-depth imaging OCT |
| OR | odd ratio |
| ORA | over-representation analysis |
| OS | outer segments |
| PCA | principal component analysis |
| PDGF | platelet-derived growth factor |
| PEDF | pigment epithelium-derived growth factor |
| PPI | protein-protein interactions |
| PTN | pleiotrophin |
| RDH | retinal dehydrogenase |
| RNAseq | RNA sequencing |
| RPE | retinal pigment epithelium |
| RPKM | reads per kilobase of gene model per million total reads |
| SA-beta-Gal | senescence-associated beta-galactosidase |
| SASP | senescence-associated secretory phenotype |
| scRNA-seq | single-cell RNA sequencing |
| SD-OCT | spectral-domain OCT |
| sl- | senescent-like |
| SLE | systemic lupus erythematosus |
| SM | segmentation models |
| SS-OCT | swept-source OCT |
| SUN | standardization of uveitis nomenclature |
| TGF | transforming growth factor |
| TGFβ | transforming growth factor β |

| | |
|---|---|
| TGN | trans-Golgi network |
| THBS | thrombospondin |
| TIMP | tissue inhibitors of metalloproteinases |
| TN | true negative |
| TNC | tenascin C |
| TP | true positive |
| TRH | thyrotropin releasing hormone |
| UWF | ultra-widefield |
| VEGF | vascular endothelial growth factors |
| VSN | variance stabilizing normalization |
| VTN | vitronectin |
| WF | widefield |
| WFFA | wide-field fluorescein angiography |

## Abstract

The retina comprises of neural retina which responds to light, and retinal pigment epithelium (RPE) which supports the neuroretina. Dysfunction of the retina threatens human sight and may result in visual impairment. With the increasing amount of data, data analysis and advancements in computer analysis, there is increasing information to aid the understanding of the retinal disease, both biologically and clinically. Omic's biological data is the product of massive sequencing technology, including genomic data and transcriptomic data. This omic data helps us to understand how biological molecules are involved with the development of disease and unravel pathways. On the other hand, clinical imaging data leads to more accurate clinical diagnosis and facilitates clinical work, but needs to be accurately and relevantly quantified. This can be facilitated by deep learning technology through the recognition and quantification of imaging data in clinical research and practice. This thesis presents the application of biomedical data analysis in the retina in both biological omics and clinical fields.

In the bioinformatics part of my PhD, I have explored biological data from RPE/choroid transcriptomics to investigate the pathogenesis of ageing and age-related macular degeneration (AMD). Transcriptomic data describes the complete gene expression change in tissues. Age and certain genetic alleles are the main risk factors for developing AMD, but the mechanism of gene expression leading to AMD remains unclear.

I extracted information from publicly available transcriptomic data (GSE29801, GSE135092, and GSE135922) to understand the differences in transcription between normal ageing and disease. I performed a meta-analysis of existing transcriptomic data of RPE/choroid from AMD patients. I integrated microarray data (GSE29801) with RNAseq data (GSE135092) to find important upregulated pathways in AMD-affected RPE/choroid. By using the combined p-values technique, the analysis suggested 764 meta-genes (366 downregulated and 398 upregulated) in macular AMD RPE/choroid (combined p-value $< 0.05$). Over-representation analysis of KEGG pathways showed two significant pathways among differential expressed (DE) genes in AMD, the neuroactive ligand-receptor interaction pathway (30 DE genes) and the extracellular matrix-receptor interaction signalling pathway (12 DE genes) (False Discovery Rate $< 0.05$).

After that, I explored the intercellular communication between RPE and the choroidal endothelium using a publicly available single-cell RNAseq dataset of RPE/choroid to identify pathways related to ageing, senescence and AMD. The CellChat/scDiffCom analysis of publicly available scRNA-seq data (one AMD and two normal eyes, GSE135922) suggested that VEGF-, BMP-, and tenascin-mediated pathways were among the most prominent cell-cell interactions between RPE cells, fibroblasts, and choroidal endothelial cells. Conducting a linear regression analysis across age on bulk microarray dataset (GSE29801) showed that the genes showing differential expression with age were part of VEGF-, BMP-, and tenascin-mediated pathways, including VEGFA, KDR, BMP7, BMPR2, SDC4, and TNXB (adjusted p-value $< 0.1$ and $|\log2(\text{fold change})| > \log2(1.5)/70$ years).

I also developed a senescence score using the ssGSEA approach. Notably, cells from an AMD patient exhibited a slightly higher average senescence score (mean = 0.21, SD = 0.21) compared to cells from healthy individuals (mean = 0.18, SD = 0.22) (Wilcoxon Rank Sum

Test, p-value = 1.37E-6) in scRNA-seq data. Additionally, I assigned a senescence score to each sample of the bulk microarray dataset, and the analysis suggested a significant correlation between the senescence score and age (Pearson's correlation R = 0.26, p-value = 0.0095). When examining the AMD subtypes, the geographic atrophy samples exhibited a notably lower senescence score compared to both non-AMD samples (p-value = 0.011) and neovascular AMD samples (p-value = 0.016). Overall, the intercellular communication analysis indicated VEGF-, BMP- and tenascin-mediated pathways among the strongest cell-cell interactions in RPE/choroid. Moreover, this analysis was the first to describe the distinction of senescence signature gene expressions between AMD subtypes. These results identify RPE signatures which contribute to a greater understanding of ageing RPE and AMD.

In the clinical aspect, I investigated clinical imaging data in retinal vasculitis. Retinal vasculitis is inflammation of retinal vessels, and progression to severe disease can lead to visual loss. The diagnosis of retinal vasculitis is confirmed using fluorescein angiography (FA), however, there is no accepted severity grading system for retinal vasculitis.

I developed a new severity grading system for retinal vasculitis based on wide-field fluorescein angiography (WFFA). This new grading scheme assesses both vascular leakage and occlusion, the main features of retinal vasculitis. I recruited 50 patients with retinal vasculitis, and their angiograms were graded by four observers: two specialist consultants, a specialist trainee, and an experienced ophthalmic grader. My analysis showed that the proposed grading scheme achieved good to excellent intra and interobserver reliability. The leakage score was significantly increased with worse concurrent visual acuity (generalised linear models, $\beta=0.090$, $p<0.01$) and at 1-year follow-up (generalised linear models, $\beta=0.063$, $p<0.01$).

Next, I developed a state-of-the-art deep learning technique for computerised grading for retinal vasculitis. I developed automated segmentation models for leakage and occlusion in retinal vasculitis patients based on several deep learning architectures; the model with the highest pixel-similarity dice score was selected as the best performing. The best segmentation model for leakage had a dice score of 0.6279 (95% confidence interval (CI) 0.5584-0.6974), while the best for occlusion had a dice score of 0.6992 (95% CI 0.6109-0.7874).

In order to consider non-invasive vascular imaging, I conducted a systematic review of optical coherence tomography (OCT) and OCT-angiography (OCT-A). My systematic review illustrated insufficient current evidence to support using OCT and OCT-A instead of fluorescein angiography to assess retinal vasculitis. However, some secondary complications of retinal vasculitis could be detected by OCT and may help indicate visual prognosis.

Overall, my PhD advances the application of data analysis in the retina, both in bioinformatics and clinical data. My transcriptomic data analysis in ageing RPE/choroid and AMD provides more understanding of gene expression difference between normal and disease, and links ageing, senescence and AMD. My clinical image analysis of retinal vasculitis develops a severity grading for clinicians and automated algorithm which may demonstrate utility for clinical and research applications.

# Chapter 1 Introduction: Data-driven application in the retina

In this chapter, I provide a brief introduction to data-driven applications in the retina. Firstly, I begin by discussing the basic structure and functions of the retina. Next, I introduce omics data in the context of the retina, emphasising its importance as a tool for understanding biological molecules to investigate retinal biology. Finally, I introduce clinical imaging, another aspect of data analysis in retinal studies. Moreover, I explain the potential role of artificial intelligence as a tool for analysing these imaging data.

The retina is the crucial part of the eye; it comprises of neural retina and retinal pigment epithelium (RPE). The neuroretina functions by sensing the light, while RPE in conjunction with the choroid supports the neuroretina. This introduction chapter briefly describes the anatomy and function of the retina, as well as the advancement in data-driven applications in retinal research.

## 1.1 The retina: structure and function

### 1.1.1 Anatomy of the eye

The human eye is a sensory organ in the visual system; it senses visible light stimuli and translates this signal to the brain. From the outside, the eye is a spherical shape that divides into an anterior and posterior chamber by a biconvex lens, which allows light to pass inside the eye (Costanzo, 2017). The eyewall composes of three layers: an outermost, a middle and an innermost (**Figure 1.1 Left**). The outermost layer has cornea and sclera; they protect the eye with their tough fibrous tissue. A transparent cornea, located in the front of the eyeball, lets light pass through, while the sclera is an opaque white coat covering most of the eyeball (Crossman and Neary, 2020).

The middle layer, or uvea, has an iris, ciliary body and choriocapillaris. The iris is a circular colourised muscle with a hole in the centre called the pupil; it controls the amount of light passing through an eye by dilating and contracting itself. The ciliary body produces aqueous humour, fluid inside the anterior chamber, while the posterior chamber contains a gel-like fluid called the vitreous humour. Choroid or choriocapillaris is a vascularised structure that supplies oxygen and nutrients to the innermost tissue (Forrester et al., 2016).

The outer corneoscleral and the middle uvea mainly protect and support the innermost layer, a neural tissue called the retina. This neuronal part detects the light, integrates and sends the signal to our brain through the optic nerve. In gross structure, the retina covers the posterior part of the eye except for an area of the optic nerve's head (optic disc) resulting in a blind spot (Provis et al., 2005). In contrast to the blind spot, the highest visual acuity locates in the macula, a yellowish centre part of the retina. Macula is about five to six millimetres in diameter; its central area, or fovea, is about two millimetres in diameter (Gregg et al., 2017). Under a microscope, the retina is a layered structure composed of many cell types and divides briefly into two parts: neuroretina and retinal pigment epithelium (RPE). The basement membrane of the RPE contacts with Bruch's membrane and choriocapillaris (Crossman and Neary, 2020).

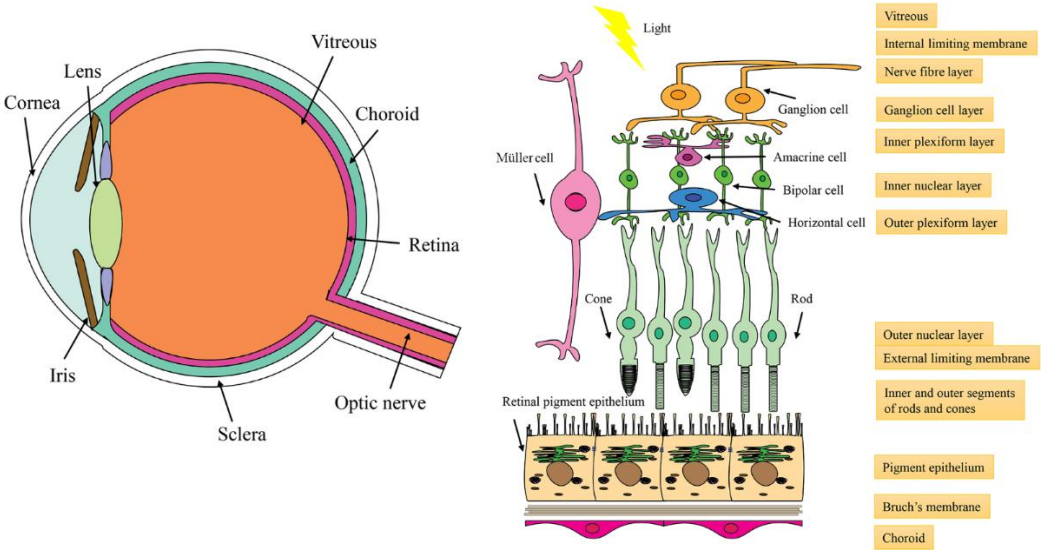


**Figure 1.1 Structure of the eye and retina.**

Schematic sagittal section of the eye with major components highlighted. The retina is located between the vitreous and choroid and comprises multiple layers and different cell types organised in a complex structure. Reprinted with permission under CC BY-NC-ND 4.0 license (Dhirachaikulpanich et al., 2020b)

### 1.1.2 Neural retina

The neural retina contains both neuronal cells that transfer neural response, such as photoreceptor, bipolar cell, horizontal cell, ganglion cell and amacrine cell; and non-neuronal cell that supports other functions, such as Muller cell, macroglia and microglia (Gregg et al., 2017;Schubert, 2019) (**Figure 1.1 Right**). The photoreceptor is the central neuronal component; it converts the light to a chemical signal through a process, called phototransduction. More than 100 million rods and 6 million cone photoreceptors are in the neural retina (Chen and Sampath, 2017). Rods distribute in the peripheral part of the retina and respond to the black and white vision. Cones distributes mainly in the macular, especially in the fovea, which contains only cones; these distributions make cones respond to high visual acuity and colour vision (Molday and Moritz, 2015). Phototransduction changes the membrane

potential of photoreceptors; this neuronal signal controls the communication between the synapse of the photoreceptor and interneuron (including bipolar cell, horizontal cell and amacrine cell). The sum-up of all interneuron responses then signals through the ganglion cells, whose axon forms the optic nerve and sends the neuronal response to the brain (Costanzo, 2017).

Phototransduction begins at the outer segments (OS) of photoreceptors. The OS contacts with RPE and composes of the thousand folded stacks of plasma membranes, called discs which contain rhodopsin, a pigmented molecule. Rhodopsin attaches with 11-cis-retinal (one form of vitamin A derivative), which is supplied by RPE (Strauss, 2005). When a photon hits rhodopsin, the activated rhodopsin initiates the chemical cascades, resulting in different levels of glutamate release at the synaptic vesicle of photoreceptors. After activation, 11-cis-retinal transforms to all-trans-retinal and returns to RPE (Sparrow et al., 2010). To increase photosensitivity, OS continuously renews itself; the rate of renewal depends on the species: around ten days in mice and around six weeks in frogs. The new OS discs begin at the base of the OS, and RPE eliminates the old OS by phagocytosis (Kevany and Palczewski, 2010).

Both OS of photoreceptors and RPE work collaboratively; they are crucial in the initiation part of phototransduction and the vitality of photoreceptors. Defects in this part of the retina can cause progressive photoreceptor degeneration, lead to retinal degenerative disease and finally result in permanent blindness (Molday and Moritz, 2015).

### 1.1.3 The retinal pigment epithelium

The human eye contains over 3 million mature RPE cells (Panda-Jonas et al., 1996). Lined between the photoreceptor and Bruch's membrane, RPE is a neuroectodermal-derived

epithelium. This pigmented cell has a hexagonal cobblestone appearance and is constructed as a simple cuboidal epithelium layer (Marmor, 2019). With its epithelium property, RPE forms a selective barrier by the tight junction and polarises itself into apical and basal sides. Apically, its microvilli are adjacent to the OS of the photoreceptor. Basally, it attaches to Bruch's membrane, an extracellular matrix (Caceres and Rodriguez-Boulan, 2020). With its unique architecture, The topography of the retina varies the shape of RPE: in the macula, RPE cells are tall and have a small diameter; elsewhere, RPE cells appear shorter and broader (Sparrow et al., 2010). RPE is crucial as a barrier between the retina and choroid and forms the outer blood-retina barrier; it supports the function of the photoreceptor (**Figure 1.2**). RPE is a dominant supplier of 11-cis-retinal that photoreceptors use for phototransduction; phagocytosis of OS; prevention of oxidative stress and phototoxicity; interaction with Bruch's membrane; secretory epithelium; and supporting nutrients to the photoreceptor (Strauss, 2005). RPE cells are postmitotic and one RPE cell supports around 40 photoreceptors, making it crucial to sight and also vulnerable to degenerative processes(Strauss, 2005;Sparrow et al., 2010).

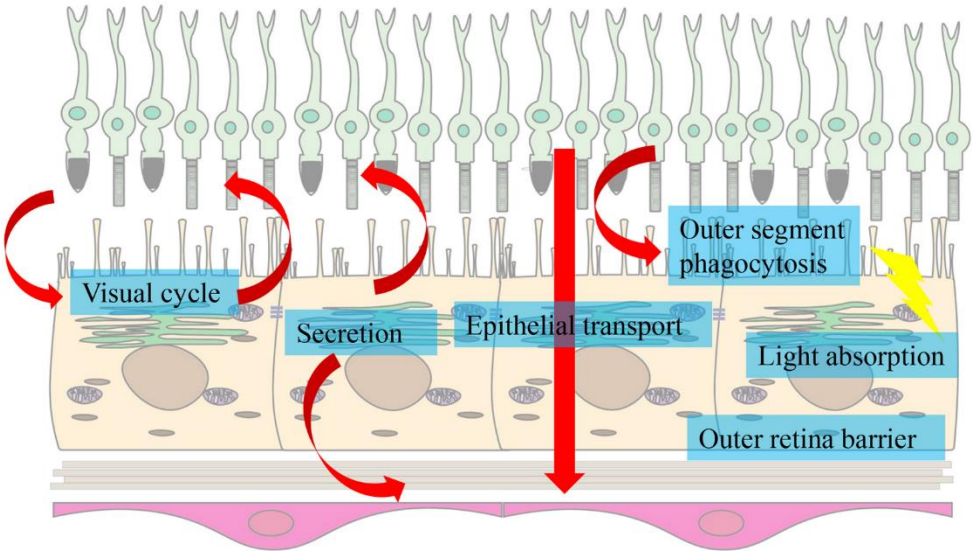


**Figure 1.2 RPE and its function.**

The RPE is a fascinating tissue, forming a tight monolayer of cells that separates the immune-privileged retina from the choroid blood supply. It is central to the maintenance of photoreceptors and the visual cycle. It regulates multiple processes in the adjacent environment by polarised secretion of various effector proteins, active transport of molecules across the blood-retinal barrier, phagocytosis of photoreceptor outer segments and absorption of light. Reprinted with permission under CC BY-NC-ND 4.0 license (Dhirachaikulpanich et al., 2020b).

#### 1.1.3.1 Structure of RPE

##### Pigmented epithelium

Under a microscope, RPE is recognised by its brown pigment; this pigment comes from the melanosome, a lysosomal organelle containing melanin pigment. Melanin granules reside in the apical part of RPE (Sparrow et al., 2010). RPE's density depends on the region of the retina, where high density belongs to the macula and lower in the peripheral. Melanosome generates this pigment and uses it to protect photoreceptors against phototoxicity by absorbing the light that passes through the retina. Apart from melanin, melanosome contains a lysosomal enzyme such as CathepsinD, which is a prominent protease in the degrading process of OS (Lakkaraju et al., 2020).

##### Polarisation

Although polarisation affects the distribution of cellular components and proteins in RPE similar to other epitheliums, RPE's apical surface is not adjacent to a lumen like other epithelia (Kay et al., 2013). Its apical surface faces the OS of the photoreceptor. RPE's microvilli pack with photoreceptors by interphotoreceptor matrix (IPM) and adhesive molecule on its apical surface, like neural cell adhesion molecule (N-CAM) (Handa, 2017). With this

unique feature of RPE, some surface proteins show reversed polarity. For example, sodium/potassium adenosine triphosphatase (Na+/K+-ATP) typically expresses at the basolateral surface of other epithelium but at the apical surface of RPE because this protein transports sodium to the photoreceptors(Sparrow et al., 2010). Apical surface protein supports other's RPE functions, such as Mer tyrosine kinase (MerTK), which supports OS phagocytosis(Kevany and Palczewski, 2010).

On the basal surface, the RPE cell has its basal membrane infolding (typically 1 micrometre in length) attached to Bruch's membrane. The Bruch's membrane is an acellular extracellular matrix membrane established between RPE and choriocapillaris. This membrane majorly contains elastin and collagen. With this structure, Bruch's membrane separates choroid vessels from the retina and regulates the transportation of fluid and nutrients between RPE and choriocapillaris(Curcio and Johnson, 2017). To attach to Bruch's membrane, RPE uses its basal protein such as α3β1, α6β1, and αvβ3 integrins. Other essential basal proteins, like bestrophin-1, a chloride anion channel, are associated with calcium influx (Handa, 2017). Despite attachment, RPE balances synthesis and degradation of Bruch's membrane; for instance, matrix metalloproteinase (MMP) and tissue inhibitors of metalloproteinases (TIMP)—both secreted from RPE—regulate the degradation of Bruch's membrane (Caceres and Rodriguez-Boulan, 2020).

This polarity reflects the collaborative functions of apical and basal transporters. Glucose transporter (GLUT1) expresses in both apical and basal domains. This transporter shifts glucose from the choriocapillaris, through RPE, to the photoreceptors. From glucose metabolism, the photoreceptor produces waste as lactate that later transports to

monocarboxylate transporters: MCT1 at the apical side and MCT3 at the basal side of RPE(Strauss, 2005;Handa, 2017).

Apart from proteins, RPE's organelles distribute by polarisation. Nucleus and Golgi stay on the basal side. Mitochondria tend to locate at the basal side due to high oxygen requirements from the choriocapillaris. Melanosomes and melanin granules reside in the apical side. Other organelles, like lysosomes and phagosomes, distribute equally throughout the cell (Handa, 2017).

**Blood-retina barrier formation**

At the apicolateral side of RPE, there are combinations of tight junctions, adherens junctions and gap junctions; these strong cell-cell adhesions of RPE create a blood-retina barrier that has high transepithelial resistance (Handa, 2017). They also prevent the paracellular transport of biomolecules and maintain RPE's apical and basal compartments. Abnormality in tight junctions decreases this barrier property and may result in the epithelial-mesenchymal transition of RPE(Caceres and Rodriguez-Boulan, 2020).

### 1.1.3.2 Function of RPE

**Visual cycle**

The goal of the visual cycle is to regenerate a visual pigment, 11-cis-retinal, for the phototransduction of the photoreceptors. During phototransduction, light isomerises 11-cis-retinal to all-trans-retinal within the OS of the photoreceptors, which is unable to regenerate 11-cis-retinal by itself. RPE is responsible for this metabolic pathway since it has many enzymes to convert all-trans-retinal back to 11-cis-retinal (Sparrow et al., 2010). After phototransduction, all-trans-retinal leaves the discs by ATP-binding cassette protein (ABCA4)

and retinal dehydrogenase (RDH8, RDH12) converses all-trans-retinal to all-trans-retinol by reduction process (Strauss, 2005). Interphotoreceptor retinol-binding protein (IRBP) binds to all-trans-retinol and sends it across the interphotoreceptor matrix, finally to RPE. Within RPE, all-trans-retinol attaches to cellular retinol-binding protein (CRBP), and this retinol undergoes a process of esterification by lecithin: retinol acyltransferase (LRAT) and an RPE protein, RPE65. LRAT and RPE65 converts all-trans-retinol into 11-cis-retinol, which is bound to cellular retinaldehyde binding protein (CRALBP). Afterwards, retinol dehydrogenase (RDH5) catalyses the oxidation of 11-cis-retinol into its aldehyde form,11-cis-retinal. Finally, RPE releases this vitamin A derivative,11-cis-retinal, back to OS of photoreceptors (Strauss, 2005;Kiser et al., 2012).

**Phagocytosis of OS**

OS of photoreceptors are exposed to intense light and phototransduction cascades that create oxidative stress and damage the OS of photoreceptors. To maintain their functions, the OS of photoreceptors need to shed and regenerate (Kevany and Palczewski, 2010). The shed OS is eliminated by RPE phagocytosis, which happens approximately 100 million times in each RPE's lifetime (Sparrow et al., 2010). The RPE begins this process by recognition of OS shedding through its apical surface proteins, such as αvβ3 and αvβ5 (Finnemann et al., 1997). After recognition, RPE binds and engulfs the shed OS as a phagosome. In RPE's cytoplasm, the microtubule transfers a phagosome by microtubule and myosin VIIa to the basal part of the cell, where phagosome degradation occurs. Subsequently, the OS phagosome fuses with the lysosome and interacts with Cathepsin D, a lysosomal protease. Apart from phagolysosome fusion, RPE uses autophagy to degrade the shed OS (Lakkaraju et al., 2020). After degradation, RPE recycles some OS products, such as vitamin A derivatives in the visual cycle and fatty

acids for its energy sources. The unwanted products finally liberate from RPE to the choriocapillaris(Strauss, 2005).

**Oxidative stress prevention**

Melanosomes and melanin pigments absorb the light, that is dangerous to RPE (Lakkaraju et al., 2020). Apart from light, RPE is exposed various oxidative stresses from the choriocapillaris and phagocytosis of the OS of the photoreceptors. Choriocapillaris contains high oxygen amounts that continuously perfuse the RPE's basal part (Strauss, 2005). Phagocytosis of the OS and following fatty acid metabolism via beta-oxidation creates hydrogen peroxide that is a devastating oxidative stress to RPE(Lakkaraju et al., 2020). To cope with this problem, RPE uses enzymatic antioxidants, including catalase and superoxide dismutase. It also activates the chronic oxidative stress response, such as glutathione and thioredoxin. Besides the enzymatic responses, accumulated carotenoids also act as antioxidants (Strauss, 2005;Handa, 2017).

**Transports of fluid and nutrients**

With the tight junction, RPE creates 10 times higher resistance for paracellular diffusion compared with transcellular transport. This barrier controls the fluids and nutrients transport through RPE, which delivers all ions, nutrients, fluids and wastes to their specific membrane transporters using active transport (Strauss, 2005). By transporting via GLUT1, RPE apically supplies glucose to the photoreceptors as their energy supplies. Similarly, photoreceptors' waste, such as lactic acid, exits the retina through RPE's MCT1 and MCT3 (Handa, 2017).

**Secretory function**

RPE secretes proteins in a polarised fashion using apical and basal sorting mechanisms that occur at the trans-Golgi network (TGN) and decide the fate of secreted proteins (Kay et al., 2013). After sorting, these proteins are crucial to their secreted locations, whether apical photoreceptors or basal Bruch's membrane (Caceres and Rodriguez-Boulan, 2020). The pigment epithelium-derived growth factor (PEDF) is among the most abundant apically secreted growth factor (Paraoan et al., 2020). With a neuroprotective effect, PEDF prevents and delays the photoreceptors' cell death. PEDF also has an antiangiogenic effect which inhibits the growth of the choriocapillaris. Oppositely, vascular endothelial growth factors (VEGF)—a basal-secreted growth factor— stabilise and promotes survival of the choriocapillaris (Strauss, 2005). In addition to growth factor secretion, RPE modifies components of Bruch's membrane by basal secreted proteins, for example, MMP and TIMP (Caceres and Rodriguez-Boulan, 2020).

### 1.1.4 Retinal vasculature and choroid

Whilst the nutrient needs of the outer retina are supplied through the RPE the inner retina is supplied by the retinal vasculature. The vasculature suppling the retina is complex. The primary source of the arterial supply is the ophthalmic artery, a branch of the internal carotid artery. The inner retina is supplied by the most crucial branch of the ophthalmic artery, the central retinal artery, which serves the inner two-thirds of the retina blood supply (Kiel, 2010). The choriocapillaris serves the outer retina, the vascular structure located below Bruch's membrane.

Retinal vessels are the branches of the central retinal artery. This central retinal artery has 4 major branches: superior nasal, superior temporal, inferior nasal and inferior temporal. Each branch supplies a separate quadrant of the retinal fundus. After that, the retinal vessels

enter and support the neural retina by forming three capillary layers: (1) the superficial retinal vasculatures, (2) the intermediate retinal vascular network and (3) the deep retinal vascular network (**Figure 1.3**) (Chen et al., 2016). These retinal vessels form an inner blood-retinal barrier and comprise a non-fenestrated endothelium.

The choroid is the thin vasculature layer supporting the outer retina, which is mainly comprised of the RPE and photoreceptors. The choroid originates from the short posterior ciliary arteries and the long posterior ciliary arteries; both are ophthalmic artery branches (Kiel, 2010). In contrast with the retinal vessels, choriocapillaris comprises a fenestrated endothelium that allows passive diffusion. The choroid has the highest blood flow among human tissues because it delivers oxygen and metabolites to high energy-demanded RPE and photoreceptors and the fact that the Bruch's membrane and RPE separate the choroid from photoreceptors making it not direct contact with the tissues it supplies oxygen (Spaide, 2020).

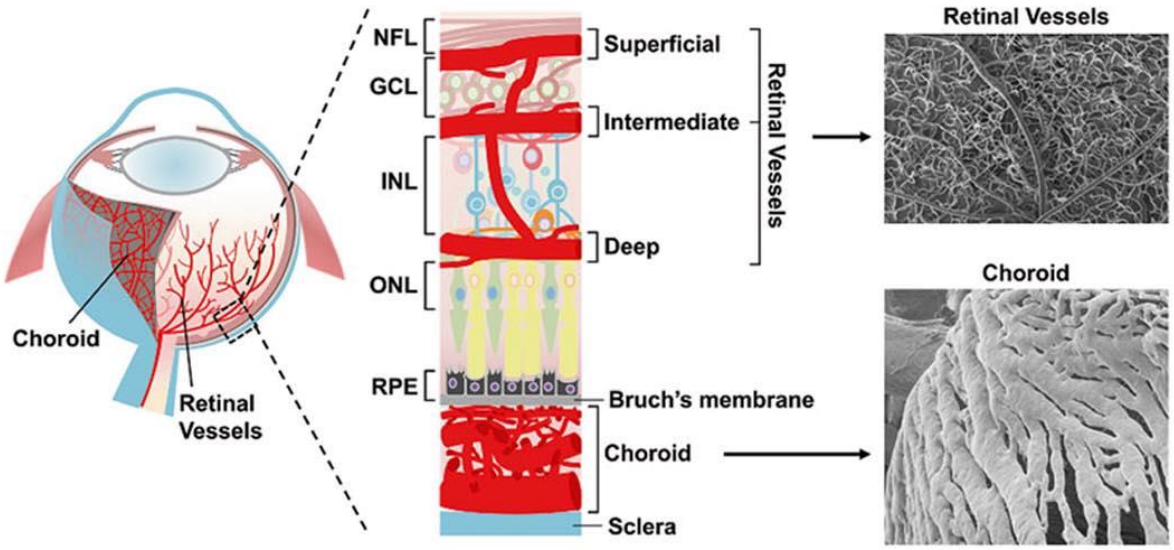


**Figure 1.3 Retinal vasculature and choroid.**

The illustration of the ocular vasculature shows three layers of retinal vessels: the superficial retinal vasculature, the intermediate and deep retinal vascular networks. Reprinted with permission License Number 5459411269155 (Chen et al., 2016).

### 1.1.5 Retinal diseases

The retina can be damaged by various causes, but is particularly susceptible to age-related degenerative changes, metabolic dysregulation such as diabetes, and inflammation because of its particular anatomy and physiology discussed above. The symptoms of retinal diseases are visual disturbance and vision loss (Landau and Kurz-Levin, 2011). This thesis focuses on age-related retinal or macular disease and inflammatory retinal disease. Below is a brief introduction to age-related and inflammatory retinal disease.

#### Age-related retinal disease

Age-related macular degeneration (AMD) is a leading cause of irreversible blindness in the world (Mitchell et al., 2018), and a systematic review predicted that it would affect about 300 million people by the end of 2040 (Wong et al., 2014). The symptoms of AMD can progress from asymptomatic to central vision blindness. In early AMD, there are abnormal pigmentation of RPE and the presence of drusen larger than 63 micrometres (drusen less or equal to 63 micrometres are considered normal ageing changes) (Ardeljan and Chan, 2013). AMD can be presented as neovascular AMD and atrophic AMD in the late stage. Neovascular AMD (exudative, wet) presents with macular neovascularisation (MNV), while atrophic AMD can progress to atrophy of the retina or geographic atrophy (GA) (Mitchell et al., 2018). Epidemiologic studies have shown that ageing, as well as genetic and environmental factors, are associated with AMD (Klein, 2007). Ageing is the strongest risk factor of AMD (Rudnicka et al., 2012); the prevalence of late AMD is less than 1% in people under 65 years old, while it

rises to about 13% in people over 85 years old (Colijn et al., 2017). Even though the clinical and epidemiologic data pinpoint ageing as the major risk factor, the disease mechanism still poorly understands how ageing RPE leads to AMD. These pathophysiologic events in AMD could involve a higher oxidative stress, inflammation, mitochondrial dysfunction, abnormal levels of proteolytic enzymes and cellular senescence (Ardeljan and Chan, 2013;Wang et al., 2019;Rozing et al., 2020). This unanswered question needs clarification through the research.

**Inflammatory retinal disease**

Inflammation and infection could affect different parts of the retina, including the neural retina, retinal vasculature and choroid. The Standardization of uveitis nomenclature (SUN) working group has classified the term posterior uveitis as the inflammation that has a primary site in the retina and choroid, including choroiditis, chorioretinitis, retinochoroiditis, retinitis and neuroretinitis (Jabs et al., 2005). The ocular inflammation that affects retinal vasculature is termed as retinal vasculitis. Inflammatory retinal disease is less commonly seen in the population than age-related retinal disease. Epidemiology studies have estimated that uveitis incidence is around 17-52/100,000 per year and 38-714/100,000 populations per year (Tsirouki et al., 2018). It should be noted that epidemiological studies conducted to estimate uveitis often use data from tertiary hospitals, while the denominators represent the total population in the geographical area. This estimation might be biased by factors such as referral systems and population distributions. More appropriate methods might involve using a national prospective birth cohort to estimate the incidence. Additionally, the heterogeneity of uveitis incidence may be influenced by endemic areas of specific uveitis entities. However, this estimation of incidence rates provides us with public health data on how rare uveitis is. Among uveitis, posterior uveitis is reported to be 15-30% of the cases. The mechanism of this inflammation in the retina is poorly understood. The eye is normally an immune privilege site,

but an insult, such as inflammation and infection, could break the blood-retinal barrier and cause disease (Forrester et al., 2018). The patients affected by posterior uveitis could be presented with abnormal vision or visual loss and may have another associated symptom of anterior uveitis, such as a painful eye (McClellan and Coster, 1987;Prete et al., 2014).

In contrast with AMD, which has a consensus of classification (Spaide et al., 2020), posterior uveitis, with its diverse aetiology and manifestations, still lacks agreement on classification, especially for retinal vasculitis (Jabs et al., 2005). Without accepted classification, it leads to poor and unquantified communication between researchers and clinicians. Both preclinical and clinical research is needed to understand disease mechanisms and implement meaningful clinical classification of the disease.

These retinal diseases are further discussed in subsequent Chapters. **Chapter 2.1** discusses ageing RPE and AMD as an age-related retinal disease, and **Chapter 2.2** discusses retinal vasculitis as an inflammatory retinal disease.

### 1.2 Omics data in the retina

The previous section explains the complex structure of the retina and its importance to human vision. Although there is no complete understanding of the retinal structure and the disease, one tool to elucidate this is through data analysis from multi-omic data of the retina. This section introduces the omic data analysis concept and suggests the previous omic research that investigates retinal biology.

### 1.2.1 Omics

In biology, the central dogma clarifies the molecular relationship between DNA, RNA and protein. RNA is the product of DNA transcription, and protein is the product of RNA translation (Franklin and Vondriska, 2011). With this concept, many diseases could be explained by altering these molecules. However, detecting DNA, RNA, or proteins required specific experiments and, in the past, was a very laborious task. After completing the human genome project in 2003 (International Human Genome Sequencing, 2004), the first and most complete human reference genome, the detecting of multiple molecules of DNA, RNA and proteins has accelerated (Gosálvez and Horcajadas, 2018). This human genome project could be marked as a significant milestone of the omic era, as it allows scientists to detect the new variations of the mutation using high-throughput sequencing technology and develop an understanding of how these molecules act differently in health and diseases.

The word 'Omics' is related to studying the collective of biological molecules within a cell. Different omics studies measure whole patterns of a specific molecule type, including DNA, RNA and proteins (Gosálvez and Horcajadas, 2018). Omics studies are trying to use these large-scale data as a whole to develop an understanding of the interaction of biological molecules (Yamada et al., 2021). The following terms are listed as examples of omics:

1. Genomics is the study of genomes, that is, the analysis of the whole genes in the cell by detecting the whole DNA using microarrays or next-generation sequencing (Sheffield and Stone, 2011).

2. Transcriptomics is the study of whole RNA in cells. Because the DNA is transcribed to RNA differently in each cell and tissue, the transcriptomic is also known as gene

expression studies or functional genomics (Tian et al., 2015). These patterns of RNA expressions reflect the molecular cascade in the cell since even if there is a gene mutation, that gene might not be transcribed in some tissues and is not the culprit of pathophysiology in some diseases. The technology for transcriptomics includes complementary DNA (cDNA) microarray, RNA sequencing (RNAseq) and single-cell RNA sequencing (scRNA-seq) (Voigt et al., 2021).

a. cDNA microarray: This is the multiple arrays of immobilised probes which could bind with specific cDNA. The machine with a laser scanner can then detect the quantity of cDNA throughout these arrays. The disadvantages of these arrays include a variety of microarray platforms from different companies (Gosálvez and Horcajadas, 2018), which may represent different regions of genes, and microarrays could not detect the absolute value of gene expression, making it hard to compare among samples using different platforms.

b. RNAseq: This is the technology to quantify absolute gene expression belonging to the whole RNA in the cells using sequencing technology (Tian et al., 2015). The advantage is that it could detect the less abundant of the transcript that may not be present in microarray probes and have more accurate quantification of gene expression than the microarrays. The disadvantage is that the methods require the pooling of cells to concentrate the amount of RNA in the samples, but the complex tissue, especially the retina, consists of different cell types. Therefore, quantifying gene expression of specific cell types in the retina could not be done precisely by either bulk RNAseq or microarrays.

c. scRNA-seq: The developed version of RNAseq technology by applying the cell sorting and microfluidic approaches that allow the detection of the whole transcriptome of an individual cell in the whole tissues. For instance, this technology can sequence the transcriptome and analyse the differential gene expression between RPE and choroid (Voigt et al., 2019;Voigt et al., 2021). The disadvantage is the higher cost, and the data analysis is complicated.

3. Proteomics analyses and quantifies protein profiles of cells, organisms or biological fluids. It is also able to detect the protein post-translational modification. The primary tool for proteomics is mass spectrometry (Jay and Gillies, 2012).

4. Metabolomics is the large-scale detection and quantification of metabolites in biological samples using tools such as mass spectrometry and nuclear magnetic resonance spectroscopy (Nazifova-Tasinova et al., 2020).

Not only is there technology required to detect omics in the biological samples, but there is also development in data analysis to understand the complexity of data generated from the omics technology. This data analysis is called bioinformatics (Gosálvez and Horcajadas, 2018). Bioinformatics methods require statistical knowledge and computational analysis to deal with the large amounts of data generated and facilitate the discovery of biological mechanisms. Examples are identifying disease biomarkers, finding differential gene expression and gene ontology (Yamada et al., 2021).

### 1.2.2 Advancement in omics study of the retina

Like in other tissues and organs, bioinformatics and omics are becoming crucial in understanding the retina's biology and pathogenesis of retinal disease and exploring new treatment possibilities for the retinal disease.

#### Genomic and retina

The study of genetics has had an impact on ophthalmology since the discovery of the retinoblastoma gene in 1985 (**Figure 1.4**). The new identification of causative genes allows clinicians to classify ophthalmic genetic conditions by genetic defect and better understand their mechanism and prognosis. Genetic diagnosis allows proper counselling to the patients, including the carrier risk to their descendants (Sheffield and Stone, 2011). Understanding causative genes also allows us to understand pathogenesis. For example, the mutation in *ABCA4* could cause autosomal recessive Stargardt disease (STGD1) by increasing the A2E toxic substances in the retina (Conley et al., 2012). The *ABCA4* gene has 50 exons, and the traditional Sanger sequencing of all 50 exons could discover around 66-80 per cent of diseases (Yatsenko et al., 2001;Tanna et al., 2017). The disadvantage of the traditional methods is that they are time-consuming and difficult to apply to a large cohort of patients (Al-Khuzaei et al., 2021). With next-generation sequencing, all exons are automated sequences at once, enabling the detection of known and novel variants of *ABCA4* (Fujinami et al., 2013;Khan et al., 2020).

Genomics is not only involved in detecting mutation from single-gene diseases but also contributes to complex inheritance disorders (Sheffield and Stone, 2011). Complex inheritance disorders such as AMD are affected by the interaction of multiple genes and environmental factors. The role of genetic testing in this complex disease is to observe a higher risk of disease but not claim that the mutation is causing the disease. Moreover, testing a single candidate gene

might be unable to find the culprit gene. The genome-wide association study (GWAS) is applied to identify genes involved in complex inheritance disorders. For instance, many GWAS identified genes associated with AMD, including the complement factor H (*CFH*) gene, which increases the risk of AMD (Raychaudhuri et al., 2011;Fritsche et al., 2013;Fritsche et al., 2016). One of the largest GWAS analysed 16,144 AMD patients and found 34 loci contributed to AMD (Fritsche et al., 2016).

The discovery of disease mechanisms at the molecular level also increases the possibility of new drug discovery. The discovery of vascular endothelial growth factor (VEGF) helped anti-VEGF development, which is an essential drug for neovascular AMD (Jager et al., 2008). The VEGF is the angiogenic factor meaning that it promotes forming new blood vessels in the tissues; thus, neutralizing this molecule leads to reduce neovascularisation, including in advanced AMD. Since 2004 when FDA approved the first anti-VEGF therapy for ocular neovascularisation, anti-VEGF has been the most prominent therapy for neovascular AMD (Kim and D'Amore, 2012;Fleckenstein et al., 2021).

Not only did identifying genes and molecules lead to the discovery of disease mechanisms and drug development, but more recently, the advance in genetics led to gene editing and gene therapy treatment. The idea of gene therapy is to correct the gene mutation by transferring a corrected gene to the patients. Mutations in *RPE65* cause Leber's congenital amaurosis type 2, which leads to early onset visual loss. Hopefully, gene therapy has recently become the therapeutic option for this disease. In 2017, the FDA approved the RPE65 gene therapy for Leber's congenital amaurosis type 2, which clinical trial showed improved vision (Miraldi Utz et al., 2018).

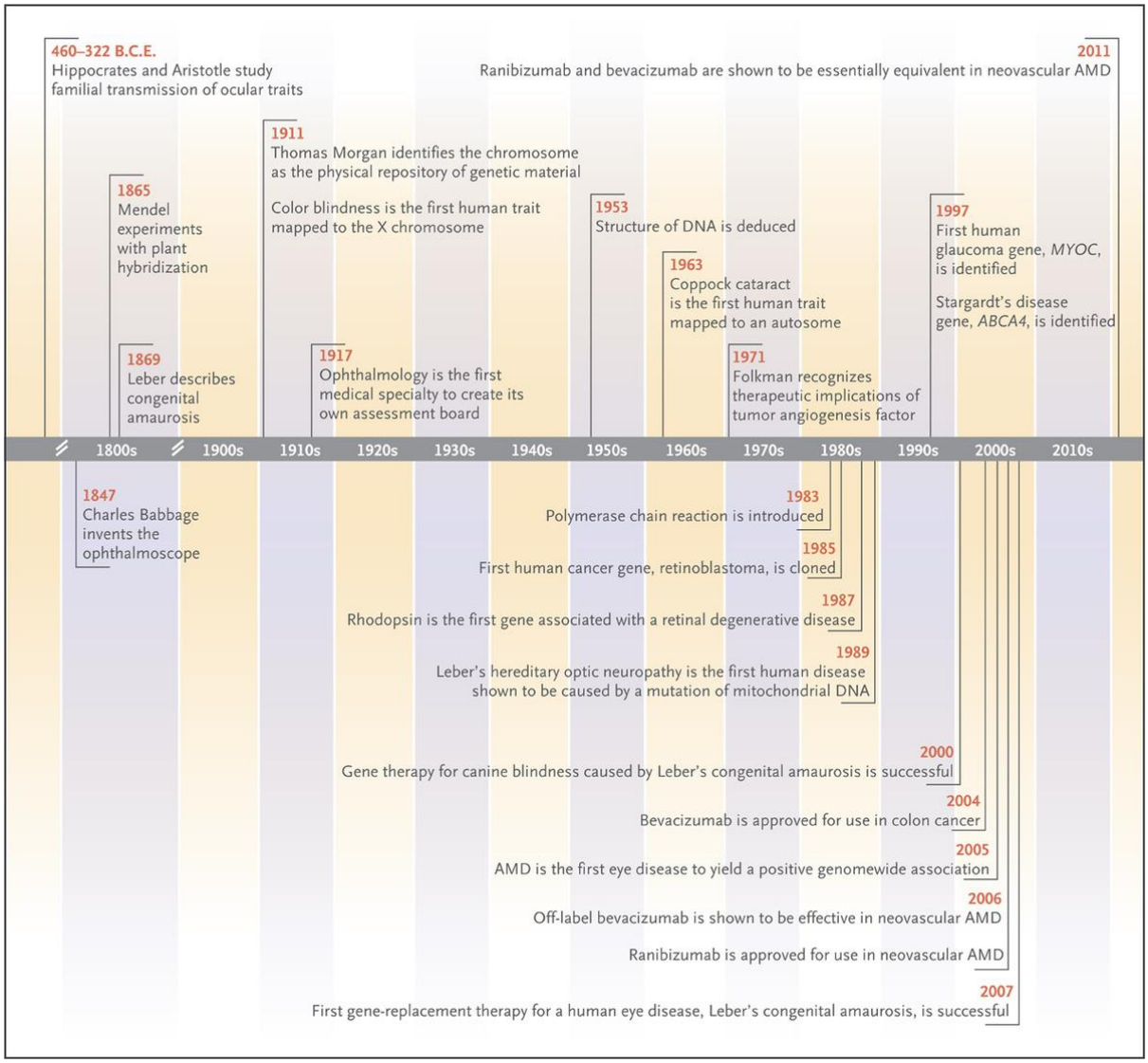


**Figure 1.4 Timeline of Ophthalmic Genomics.**

Schematic diagram describes the important events in molecular biology, genomics and vision research. Reproduced with permission from (scientific reference citation), Copyright Massachusetts Medical Society. (Sheffield and Stone, 2011)

### Transcriptomic and retina

As gene expression studies have allowed analysis of the difference between tissue expression, vision scientists have acquired the retinal tissue to study the gene expression among different anatomical structures and cellular types and compare between normal and disease. Different from the genomic, which would be the same genome throughout the body,

transcriptome depends on the tissue. To study this, vision scientists need the human eye tissue to enable RNA extraction and do transcriptomics and subsequent analysis (Tian et al., 2015). Despite difficulties in acquiring post-mortem human eye tissue, the early transcriptome study using microarray estimated 25,000 transcripts expressed in the neuronal retina (Swaroop and Zack, 2002). The pathway analysis using transcriptome data to evaluate the pathway involved in RPE/choroid tissue found retinol metabolism as a significant pathway expressed in RPE/choroid (Booij et al., 2010). (Whitmore et al., 2014) For AMD, Newman et al. compared the gene expression between normal and AMD human post-mortem retina tissue and found the differential gene expression in AMD related to other diseases such as Alzheimer's disease, cardiovascular disease and type 2 diabetes (Newman et al., 2012).

However, a problem with gene expression studies of the retina is that the difficulties in acquiring tissue lead to small sample sizes of human eye tissues, which could be less than 10 samples, in contrast with genomic studies, which could acquire more than 10 thousand human blood samples. The result between studies also tends to have minimal overlaps between gene expression analysis, leading to the question of analysis reliability (Tian et al., 2015). In **Chapter 3**, I discuss and analyse the integration among a different dataset of RPE/choroid transcriptome by using the analysis method that has been applied in other tissue leading to some hypotheses of the pathogenesis of AMD.

Using bulk transcriptome methods such as microarray and RNAseq also led to contamination between the neuronal retina and RPE/choroid and could not distinguish between different retinal cell types. The development of scRNA-seq tackles this problem (Voigt et al., 2021). With the more advanced techniques, the researchers could cluster the retina cell types using gene expression data, for instance, identifying RPE, endothelial cells, fibroblast and

immune cells among RPE/choroid tissue (Voigt et al., 2019). However, a similar problem with bulk RNAseq is that all transcriptome analyses need human tissues. In an attempt to gain more information from the few human eyes tissue acquired for scRNA-seq, I have compared the result with bulk transcriptome data leading to some aspect of AMD and ageing RPE/choroid in **Chapter 4**.

**Proteomic and retina**

Proteomic studies attempt to identify proteins in RPE leading to an understanding of RPE biology (Beranova-Giorgianni and Giorgianni, 2018). Alge et al. conducted a proteomic study that compared primary RPE obtained from a human with the cultured dedifferentiated human RPE and found that the cultured RPE was missing proteins related to the visual cycle, including RPE65 and CRALBP (Alge et al., 2003). Another study by Nordgaard et al. did a proteomic study of AMD RPE and identified some protein dysregulates associated with mitochondrial function (Nordgaard et al., 2006). Not only can a proteomic study be done with cells, but this technique can also be applied to secreted protein in the biological fluid. Kang et al. reported that aqueous humour proteins such as cathepsin D and cytokeratin 8 might be potential biomarkers in AMD patients (Kang et al., 2014).

**Metabolomic and retina**

The metabolomic study is another tool to understand the retina and suggest possible biomarkers for retinal disease (Kersten et al., 2018;Nazifova-Tasinova et al., 2020). The instability of the metabolome makes this technique more dynamic and time-sensitive compared with other omics (Koo et al., 2014). The metabolomic often performs in the biological fluid, especially blood, unlike transcriptomic and proteomics, where post-mortem tissue could be performed. Like other tissues, most metabolomic study in retinal disease also used patients'

blood samples (Hou et al., 2022). Laíns et al. conducted a metabolomics study comparing blood metabolites of 391 AMD patients and 100 controls (Lains et al., 2017). This study reported the difference in lipid profile and showed the difference in glycerophospholipid, purine, taurine and hypotaurine. Another recent metabolomic study compared the blood metabolite of 2267 AMD patients with 4266 control patients, and reported dysregulation of AMD patients' lipoprotein, amino acids and citrate levels (Acar et al., 2020). In short, these studies may give insights into the pathophysiology of AMD and lead to a potential blood biomarker for AMD.

### 1.3 Clinical images data

In the previous section, omics' preclinical data use has been discussed in relation to the retina. That information needs laboratory and biochemical techniques and may not appear routinely in clinical practice. The increasing of data-driven applications is also applied to clinical information, which, although unable to explain disease at the molecular pathogenesis level, also helps diagnose, predict prognosis and follow up on eye patient treatment. One of the most revolutionised methods in data analysis is deep learning applications, especially in clinical imaging. This section discusses the definition of these terms and how they influence the ophthalmology field.

#### 1.3.1 Imaging in the retina

Medical imaging is a crucial clinical tool to diagnose, treat and follow up with patients. Retinal imaging also provides anatomic and functional changes in retinal diseases. Retinal imaging techniques have been developed for about 170 years (Abràmoff and Kay, 2013). H. Helmholtz successfully invented the ophthalmoscope in 1851. Gullstrand developed the first fundus camera in 1910, and fundus photography is still widely used as an essential tool in retinal imaging. After that, the fluorescein dye-based technique was first described by Novotny

and Alvis in 1961; these fluorescein angiographic techniques allow visualization of retinal circulation. In 1987, optical coherence tomography (OCT) was described and extended to image retinal tissue structure (Huang et al., 1991). Nowadays, fundus imaging, fluorescein angiography (FA) and OCT are still used daily in the retinal clinic.

**Colour fundus photography**

The fundus camera utilises the projection of the 3D ocular fundus into a 2D image. The illumination sources are passed to contrast filters, including red, blue and green filters that enhance the visibility of ocular structures. The retinal structures, including the optic disc, retinal vasculature, and macula, could be seen through this technique (Badar et al., 2020).

**Fluorescein angiography**

The dye bases angiography techniques use the principle of the emitted photon from the excited dye (fluorescein or indocyanine green) to intensify the images (Badar et al., 2020). For FA, sodium fluorescein ($C_{20}H_{12}O_5Na$), a low molecular weight dye, is injected through the subject's circulation (Johnson et al., 2013). This dye could illuminate the retinal vascular circulation and assess the integrity of retinal vessels. With this property, FA is the standard method to display retinal vascular leakage and occlusion. The side effects of fluorescein injection include extravasation, local tissue necrosis and allergic reaction, which could be ranged from a mild allergic reaction to a severe adverse event such as anaphylaxis.

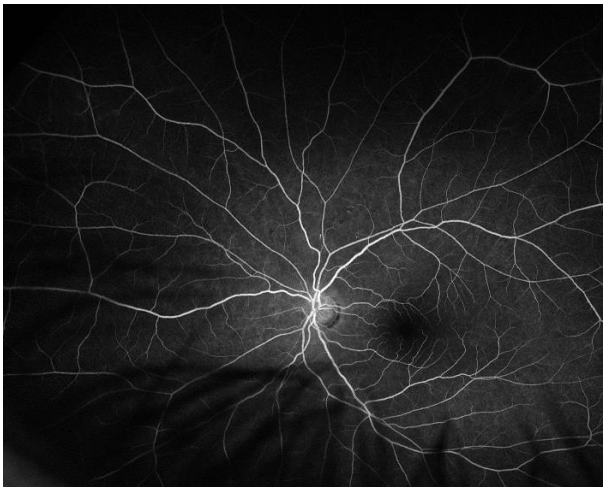

**Figure 1.5 Fluorescein angiography.**

An example of fluorescein angiography with an Optos P200DTx camera

**Indocyanine green angiography**

Indocyanine green angiography (ICGA) uses a high molecular weight, tricarbocyanine, anionic dye, which can bind to plasma proteins (Staurenghi et al., 2013). This dye could remain in the choroid vessels and make it the diagnostic imaging for choroidal abnormalities such as choroidal neovascularization and other abnormal vessels.

**Ultra-widefield fluorescein angiography**

The definition of widefield imaging has been agreed upon by a consensus of retinal experts based on retinal landmarks. In this consensus, the imaging needs to be a single capture centred on the fovea and can visualize four quadrants of the retina (Choudhry et al., 2019). Widefield (WF) images refer to the "retina extending from the vascular arcades to the posterior edge of vortex vein ampulla (field of view between 60-100 degrees)", and ultra-widefield (UWF) images refer to the "anterior edge of vortex vein ampulla and beyond to pars plana (field of view between 110-220 degrees)". This WFA or UWFA technique allows visualize the retina at a wider angle and reduces the difficulty for multiple captures of imaging and

montage images (Patel et al., 2020). These techniques could diagnose retinal disease in the peripheral part, such as retinal vasculitis. The example machine includes Heidelberg Spectralis (Heidelberg Engineering, Heidelberg, Germany) (field of view = 105 degrees), Optos 200Tx camera (Optos PLC, Dunfermline, United Kingdom) (field of view = 200 degrees) and Clarus 700 (Carl Zeiss Meditec, Jena, Germany) (field of view = 133 degrees) (Patel et al., 2020). The limitation of the current cameras is the inability to obtain the whole retina from ora to ora in one capture.

**Optical coherence tomography**

OCT techniques use near-infrared light with a wide spectrum range and can penetrate the scattering medium, allowing in vivo cross-sectional tomographic images of retinal microstructures (Abràmoff and Kay, 2013). The different type of OCT uses different light sources: spectral-domain OCT (SD-OCT) has a broadband light source, while a more recent swept-source OCT (SS-OCT) uses a swept laser light source and photodetector. This non-invasive, non-contact imaging modality is performed thirty million times a year (Tong et al., 2020). Currently, OCT is a standard for detecting macular diseases such as macular oedema.

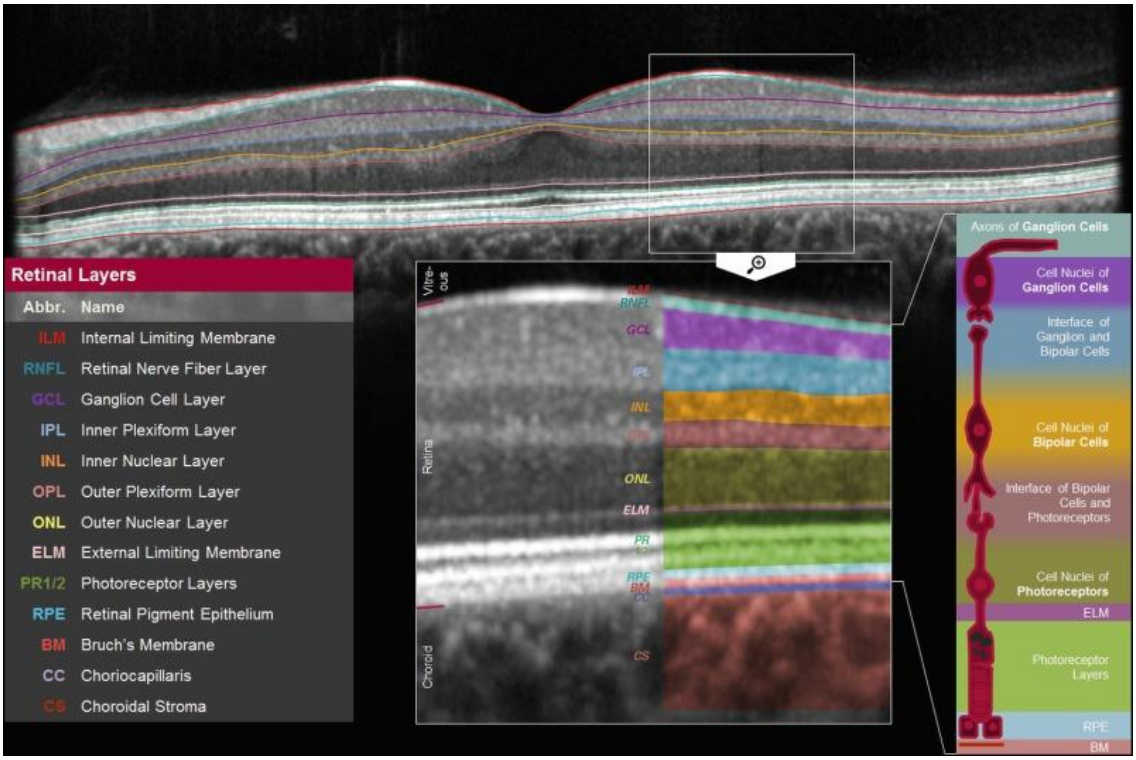


**Figure 1.6 OCT and retina layers.**

OCT image compared with different retina layers (Aumann et al., 2019).

**Optical coherence tomography angiography (OCT-A)**

The OCT-A uses multiple individual OCT repeatedly scans of the same location to acquire the image information that has changed over time (Haner et al., 2023). The result images could detect the particle movement, such as blood cells allowing this technique to reconstruct the retinal vasculature. It also allows differentiation between a superficial and deep capillary plexus. Examples of OCT-A vascular metrics are foveal avascular zone as capillary vessel density. In contrast with FA, OCT-A is non-invasive, and no dye injection is needed. However, OCTA cannot provide leakage information

### 1.3.2 From artificial intelligence to deep learning

The progress in retinal imaging technology allows the clinician to diagnose retinal disease. However, those defects in retinal diseases need clinical expertise to detect and give a

diagnosis. The manual evaluation by expertise is then prone to bias between clinicians, misdiagnosis, time-consuming and not applicable to large-scale analysis (Tong et al., 2020). Fortunately, artificial intelligence has been applied to medical diagnosis in different disciplines, including pathology, radiology and ophthalmology. Artificial intelligence is how computers try to do intellectual tasks similar to human thinking (Choi et al., 2020a). Machine learning refers to a branch of artificial intelligence that uses a computer to learn and predict from the provided datasets. In conventional machine learning, humans need to label and input the data to the computer or algorithm to predict desired outcomes (LeCun et al., 2015). Examples of conventional machine learning are logistic regressions, decision trees, random forests and support vector machines. This conventional method was time-consuming as it needed a large amount of manually labelled data.

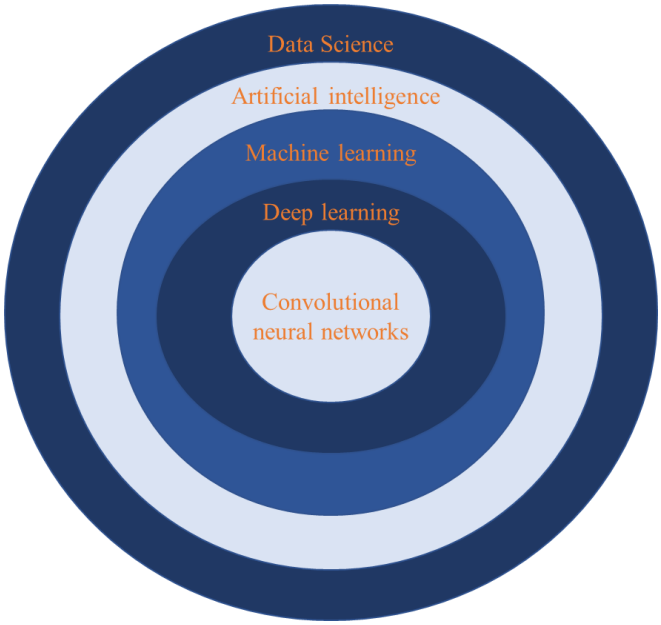


**Figure 1.7 From artificial intelligence to deep learning.**

Schematic diagram represents a relationship between data science, artificial intelligence, machine learning, deep learning and artificial neural networks (Choi et al., 2020a).

**Neural networks**

Deep learning is the most promising algorithm in machine learning. It is the resurrection of the machine learning method called artificial neural networks. Artificial neural network resembles biological neurons connecting in the animal brain, which contains multiple nodes or neurons communicating with other nodes (Schmidt-Erfurth et al., 2018b). These connections could travel from the input (first) layer, the process in the intermediate layers and provide the outcome in the output (last) layer. These connections are an analogy to how neurons synapse and analyse the signals in the brain. There are three parts of neural networks: the input layer, the hidden/ intermediate layers, and the output layer (Choi et al., 2020a). The input layer receive parameter provides for the network. The hidden layers transformed the information using activation functions such as the sigmoid function, hyperbolic tangent and rectified linear unit. For the output layer, the information from the hidden layer was sent and predicted using the activation function corresponding to the number of possible outcomes. For example, the binary classification, which predicts a yes or no outcome, contains the activation function that can predict two outcome classes (Choi et al., 2020a). During learning or training, another function called the loss function is set to estimate the discrepancy between the predicted outcome with the provided growth truth. The process called backward propagation is used to update the model (LeCun et al., 2015). The algorithm aims to minimize the loss function to create a more robust model.

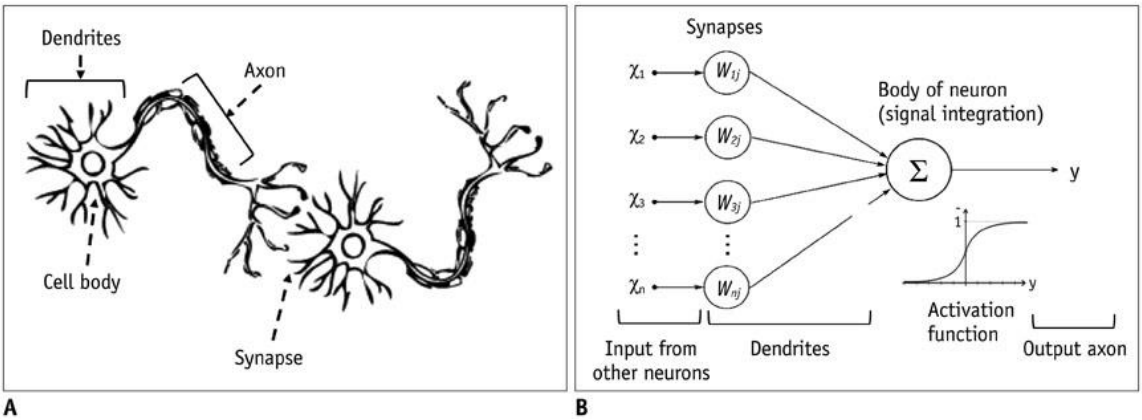


**Figure 1.8 Components of artificial neural networks.**

(A) Neurons and synapse (B) Artificial neural network (Lee et al., 2017b).

In fact, artificial neural networks have been proposed and successfully implemented in the screening of diabetic retinopathy since the 1990s (Gardner et al., 1996). However, at that time, the performance was still similar to the expert clinician. The development of graphic processing units with larger accessible datasets enables a new breed of deep neural networks that refurbish artificial neural networks with more hidden layers (LeCun et al., 2015). In 2012, the convolutional neural networks was applied to the Imagenet dataset, which contains 1.2 million images and can classify images into 1000 different classes with high performances (Krizhevsky et al., 2017). This development marks a new era in machine learning as deep learning could outperform classic machine learning and clinical expertise.

**Convolutional neural networks**

For image analysis, the input data are each pixel in the images. Each image is considered a matrix of pixel value if an image is grayscale and stacked of three matrices if the image is colour (LeCun et al., 2015). The deep neural network containing convolutional parameters that can extract information from the images is called a convolutional neural network. The convolutional neural network architecture comprises three special parts: convolutional, pooling and fully connected layers (Lee et al., 2017b). The convolutional layers are the filters that can extract features from images, such as lines, edges and shapes. Pooling layers aim to reduce the dimension of each feature to capture an increasingly larger field of the image. This pooling layer could be maximum, average or minimum. Lastly, the fully connected layers connect every part of the model and give the final outcome (Ting et al., 2019). This basic feature of convolutional neural networks has further developed by increasing the complexity of filters, layers and model sizes. Examples of well-known models are VGG, U-net, inception,

resnet, and efficientnet (Tan and Le, 2019). These models are applied to machine learning tasks for computer vision, including image classification and image segmentation.

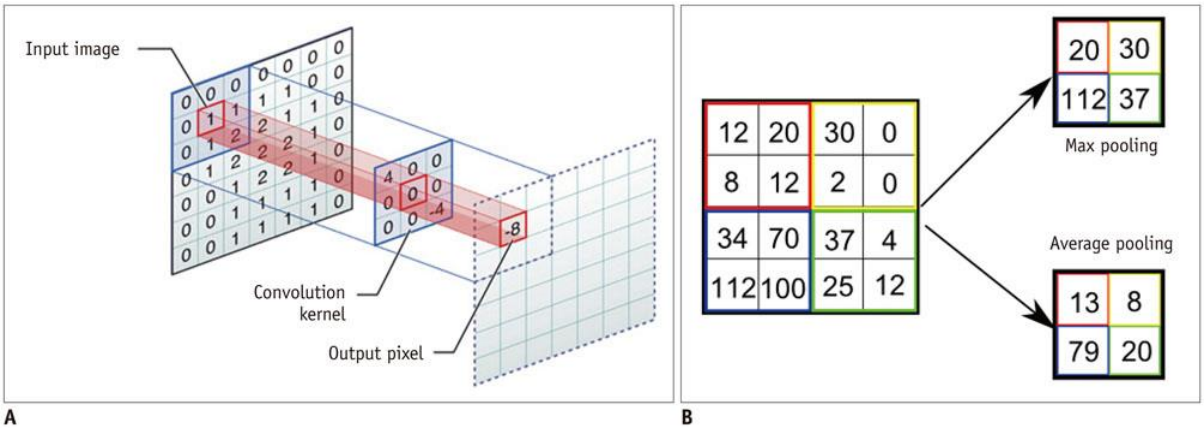


**Figure 1.9 Components of convolutional neural networks.**

(A) Convolutional layer (B) Pooling layers (Lee et al., 2017b).

### Training, validation and testing datasets

In machine learning, the dataset is split into training, validation and testing datasets (Ting et al., 2019). In this context, I am using the term 'validation' to refer to internal validation. These three datasets must not overlap to ensure the generalizability of the model. The training and validation are for the model building. The learning of the model is done by using this training dataset and then optimizing the parameter using the validation dataset. After completing the model, the model is evaluated by the testing dataset to report the machine learning model's performance (Ting et al., 2019).

## 1.3.3 Deep learning and semantic segmentation

The deep learning network could apply to many image tasks, including classification and segmentation. Classification is how computers characterize the image into different classes; for instance, classify the images into disease, normal or different stages (Ueda et al.,

2019). Segmentation is the method to identify objects' boundaries to represent the image's meaningful parts. This segmentation method could identify features such as optic disc or retinal vasculature from colour fundus photography (Schmidt-Erfurth et al., 2018b). Semantic segmentation is the type of segmentation where each pixel of images represents different labels (Ueda et al., 2019), such as a blood vessel. Below are two examples of the algorithms for semantic segmentation that have been applied to medical images.

**U-net**

U-net architecture contains two paths: contracting and expansive path. The contracting path is similar to the convolutional neural networks, which shrink the information and give the classification of each image pixel. The novelty is the expansive path that increases the resolution of the output. There is a skip connection connecting contracting and expansive path. The original U-net first experimented with segmenting neuronal structures in electron microscopes (Ronneberger et al., 2015). After that, it gains popularity in semantic segmentation for medical diagnosis. More than 300 publications during 2017-2020 adapted U-net for medical applications (Siddique et al., 2021). U-net architecture has been further developed to many variances, including 3D U-net, attention U-net and U-net++ (Yin et al., 2022).

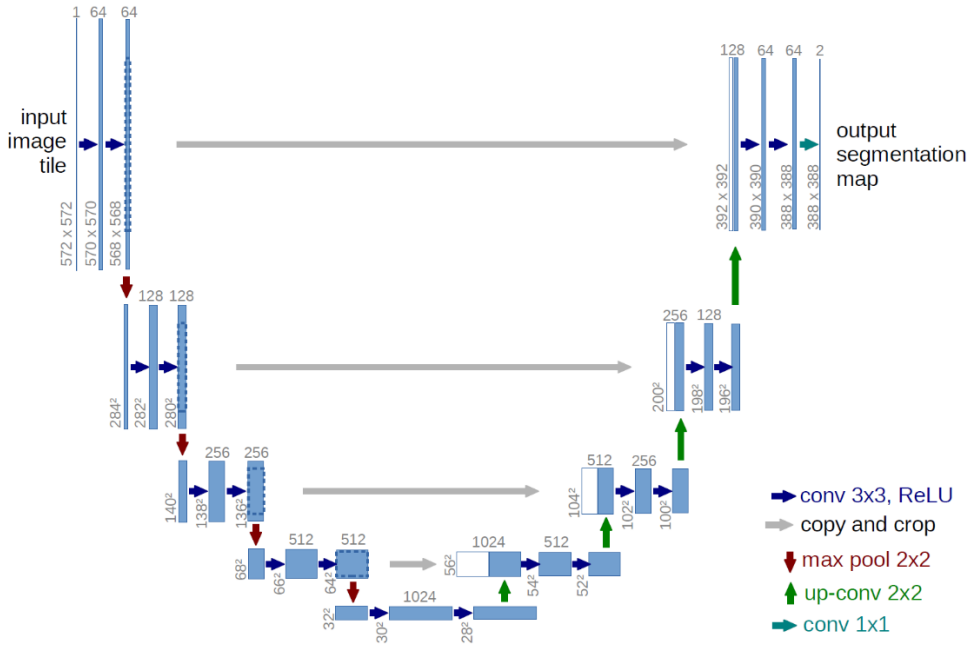


**Figure 1.10 U-net architecture.**

Schematic diagram describes U-net architecture. Reprinted with permission License Number 5491341213751(Ronneberger et al., 2015).

### Deeplab

Another popular semantic segmentation architecture is Deeplab. The uniqueness of this architecture is the particular convolution called atrous or dilated convolution (Chen et al., 2018b). This atrous convolution preserves the information's original size without increasing the filter size. The different versions of Deeplab are Deeplabv1, Deeplabv2, Deeplabv3 and Deeplabv3+(Chen et al., 2018a;Chen et al., 2018b).

### Evaluation metrics in image segmentation

To evaluate semantic segmentation models, the ground truth prediction needs to be compared with the predicted segmented image pixel by pixel. The values in the confusion matrix (true positive (TP), true negative (TN), false positive (FP) and false negative (FN)) are assigned to each pixel prediction. The accuracy could not represent a suitable matrix in

semantic segmentation because the accuracy may be high due to the true negative in the unbalanced dataset (Siddique et al., 2021). The dice score and intersect over union (also known as the Jaccard index) are two standard evaluation metrics that indicate the performance of the semantic segmentation model.

| | | |
|---|---|---|
| Accuracy | = | (TP + TN)/ (TP + TN+ FP + FN) |
| Dice score | = | 2 TP / (2 TP + FP + FN) |
| Intersect over union | = | TP / (TP + FP + FN) |

### 1.3.4 Application of deep learning in retina

The popularity of deep learning in the medical field has been applying to ophthalmology, especially retinal imaging (Choi et al., 2020a). One example is the identification of retinal landmarks such as the optic disc, fovea and retinal vasculature (Badar et al., 2020). In common retinal diseases, including AMD, and diabetic retinopathy, deep learning has been applied to disease screening, classification of diseases, segmentation of the pathological alteration and even visual prognosis prediction (Schmidt-Erfurth et al., 2018b).

The application in AMD is among the most successful story of artificial intelligence and deep learning. The recent systematic reviews explored the artificial intelligence application for detecting AMD using colour fundus imaging and found 13 articles (Dong et al., 2021). Among published studies, the largest dataset reported more than 300,000 colour fundus images to detect AMD (Zapata et al., 2020). The meta-analysis compared the algorithm with human grader references and reported a pooled sensitivity of 0.88 and specificity of 0.90 (Dong et al., 2021). For staging of AMD, one study reported the accuracy of deep learning between 0.88-0.92 using colour fundus imaging (Burlina et al., 2017). Schmidt-Erfurth et al. used deep learning to predict visual acuity in AMD after treatment with anti-VEGF (Schmidt-Erfurth et

al., 2018a). Not only colour fundus images but the OCT images of AMD are also extensively researched using deep learning. Kermany et al. used more than 100,000 OCT images for training classification of MNV, drusen, diabetic macular oedema and normal scans (Kermany et al., 2018). Deep learning has extended to the segmentation of AMD pathology in OCT, including intraretinal fluid (Lee et al., 2017a) and pigment epithelium detachment (Xu et al., 2017). Moreover, the algorithm is also applied to the clinical decision in AMD, such as deciding urgent referrals using OCT images (De Fauw et al., 2018).

Similar to AMD, deep learning applications have been applied to diabetic retinopathy. One of the most significant studies uses more than 400,000 colour fundus images to screen for diabetic retinopathy and achieve more than 0.9 sensitivity and specificity (Ting et al., 2017). More recently, deep learning was also applied to the FA images of diabetic retinopathy patients (Lee et al., 2022), although the number of patients and images in the study is relatively low compared to the study using colour fundus or OCT images.

Even though deep learning has been applied extensively in AMD and diabetic retinopathy, fewer studies were conducted on less common retinal diseases, such as inherited and inflammatory retinal diseases. Esengönül et al. conducted a systematic review and found 11 publications that used artificial intelligence to classify or segment inherited retinal diseases such as Stargardt Disease, Retinitis Pigmentosa and Best Disease (Esengonul et al., 2022). Unlike AMD, fewer patients are recruited in these studies ranging from 14-1670 total patients recruited. For inflammatory retinal diseases, only a few publications previously used deep learning (Zhao et al., 2017;Keino et al., 2022;Young et al., 2022). One study conducted the retinal vascular leakage segmentation using only 3 uveitis patients' FA images (Keino et al.,

2022). In summary, this scarcity indicates an opportunity to apply the deep learning method to less common retinal diseases, including inflammatory retinal diseases.

# Chapter 2 Literature review

In this chapter, I explore the literature that forms the foundation of our research on AMD and retinal vasculitis. I begin with a comprehensive understanding of the ageing process in the retina, focusing on the ageing of the retinal pigment epithelium (RPE) and its connection to AMD. This section also explores the concept of senescence and its relevance in the context of RPE and AMD. Subsequently, I delve into the importance of transcriptomic studies, particularly those related to AMD's RPE. Moving forward, I introduce retinal vasculitis, including clinical information, clinical imaging techniques employed for diagnosis, and the previous classification systems. Finally, I conclude with an overview of the aim and structure of this thesis.

## 2.1 Introduction to the ageing retina and age-related macular degeneration

### 2.1.1 Ageing of RPE

Ageing is an inevitable process that progresses the impairment of healthy tissue and typically happens in every organism. With the disposable soma theorem, the organisms allow a deficit in the repair mechanism in exchange for the increasing ability in development and reproduction; hence, it leads to the ageing process. The cellular event in ageing could vary from intra/extracellular debris accumulation to the cellular deficit, where debris accumulation/damages in subcellular components have not been repaired and might result in organ dysfunction (Kirkwood, 1977;Melzer et al., 2020).

Retina and RPE are complex tissue and also no exceptions for an ageing process. The unique ageing process and the dysfunctions of RPE could happen from the 50 years old human (Boulton et al., 2004). RPE is particularly prone to ageing due to its postmitotic highly differentiated nature, and its exposure to much oxidative stress from both choriocapillaris and

the photoreceptors. The defects in routine interaction of the photoreceptors and RPE result in waste production and accumulation: the visual cycle creates metabolic wastes, and phagocytosis of the OS creates lipofuscin and drusen. In addition, high metabolic activity from its mitochondria generates oxidative stress on the ageing RPE. Ageing processes change RPE structures and biochemical processes (Boulton et al., 2004). Structural changes in ageing RPE are loss of cell density, loss of melanin granules, stiffness of Bruch's membrane and abnormal deposits (Boulton and Dayhaw-Barker, 2001;Ardeljan and Chan, 2013). Abnormal deposition happens in both intracellular and extracellular compartments in ageing RPE (Boulton and Dayhaw-Barker, 2001). Lipofuscin is an intracellular deposit; it comprises lipoproteinaceous substances and toxic fluorophores such as N-retinldene-N-retinylethanolamine (A2E) (Lamb and Simon, 2007). Extracellularly, advanced glycation end products (AGE) deposit in Bruch's membrane (Pawlak et al., 2008;Glenn and Stitt, 2009). Another extracellular ageing deposit in RPE is drusen— a lipoproteinaceous substance between the basement membrane of RPE and Bruch's membrane. Drusen are a part of normal ageing but Each druse in normal ageing must be smaller than 63 micrometres (Ardeljan and Chan, 2013). Several biochemical changes happen in ageing RPE, including the increase in oxidative stress, DNA damage, mitochondrial defect, abnormal cellular signalling, and abnormal level of proteinase (Ardeljan and Chan, 2013;Hussain et al., 2020;Rozing et al., 2020). Crucially, all of these changes are associated with AMD.

**Structural change**

Ageing RPE exhibits cell density loss at 0.3% each year with prominent apoptotic cells in the macular region. Morphologically, ageing disorganises RPE's apical microvilli, reduces RPE's basal infolding and causes pigmentation abnormality such as hypo/hyperpigmentation.

Pigment abnormalities are a manifestation of RPE dyplasia. Eventually cell death leads to tissue loss and atrophy(Panda-Jonas et al., 1996;Boulton, 2013).

**Lipofuscin**

Lipofuscin is a small golden-yellow fluorescent granule (about 1 mm) in the cytoplasm of an ageing cell. In ageing RPE, lysosomes incompletely degrade the shedding OS. The abnormal autophagy and undigested OS then lead to the accumulation of lipofuscins in the RPE's basal part (Sparrow et al., 2012). These granules are composed of protein, lipid derivative and retinoid derivatives such as N-retinldene-N-retinylethanolamine (A2E) that can initiate RPE's apoptosis (Lamb and Simon, 2007). Lipofuscin with A2E accelerates the ageing process of the RPE by generating reactive oxygen species and inducing lipid peroxidation products. These lipid peroxidation main compounds include malondialdehyde (MDA), 4-hydroxynonenal (HNE),4-hydroxyhexenal (HHE), acrolein and carboxyethylpyrrole (CEP); and can be called together as advanced lipoxidation end products (ALEs). ALEs inhibit lysosomal enzymes such as CathepsinD; this process finally results in a vicious cycle by increasing lipofuscin production (Krohne et al., 2010).

**Melanosome**

Ageing changes the melanosome shape and reduces melanosome properties. Significant pigmentary changes include loss of melanin pigment, decrease in the number of melanosomes, and also increase in the amount of melanosome complexes such as melanolysosome and melanolipofuscin (Feeney-Burns et al., 1984). With this change, melanosomes may reduce photoabsorption and make RPE more vulnerable to oxidative stress (Boulton, 2013).

**Mitochondria**

Mitochondria dysfunction begins with mitochondria DNA damage, resulting from increased oxidative stress in ageing RPE. Mitochondria lose their cristae and reduce their matrix density. This mitochondria ageing is then associated with the defective metabolic activity of ageing RPE (Hyttinen et al., 2018)

**Lysosome**

Lysosomal enzymes try to increase their capacities in ageing RPE. Although this may break down more undigested shedding OS and keep the balance of waste product, the total waste lipofuscin and melanosome also increase. Therefore, the amount of lysosomal enzymes does not fit with the increased amount of waste and finally contributes to lipofusinogenesis (Boulton et al., 1994;Lakkaraju et al., 2020).

**Autophagy**

Autophagy is a cellular mechanism to cope with cell debris and unwanted organelles. RPE has this response to eliminate shedding OS and mitochondrial dysfunction. With ageing RPE autophagy becomes less effective and the ineffective autophagy then accumulates more intracellular cell debris and lipofuscin (Mitter et al., 2012).

**Antioxidant**

Because antioxidants can react with free radicals, they are essential in preventing oxidative stress and cellular damage. Unfortunatedly, the level of antioxidants is lower in ageing RPE. For example, vitamin E and superoxide dismutase levels are declining in the face of increased oxidative damage in the ageing RPE (Friedrichson et al., 1995;Gu et al., 2012).

**Bruch's membrane (extracellular matrix)**

The age-related change affects Bruch's membrane through structural change, waste deposition and reduction of its biochemical properties. By structural, Bruch's membrane thickness increases significantly with age, about two to three times in the macular area. The additional content is the collagen, which increases the membrane's strength but lowers its flexibility. Ageing Bruch's membrane loses its elastic layer and increases calcification, making it fragile and reducing its transport property. It also accumulates deposits of waste material, mainly lipid accumulation, drusen and advanced glycation end products (AGEs) (Curcio and Johnson, 2017).

The cause of these changes in Bruch's membrane may be the secondary to the ageing process of RPE. Because ageing RPE secretes a more inactive form of extracellular matrix proteinases such as MMP2 and MMP9 (Hussain et al., 2020), Bruch's membrane reduces its turnover rate, possibly leading to thickening. Moreover, the debris deposits, such as drusen, come from the ageing RPE.

The result of these ageing changes is a decline in the flow of fluid and nutrients and transport function of Bruch's membrane. These ageing changes reduce fluid flow and restrict the molecular transport between the choriocapillaris and the photoreceptors(Boulton, 2013). In addition to impeding fluid transport, ageing Bruch's with drusen and AGEs cause oxidative products associated with an inflammatory cascade to accumulate in the ageing RPE(Ardeljan and Chan, 2013).

**Drusen**

Drusen reside between the RPE's basement membrane and the Bruch's membrane. Its components consist of lipids, proteins, and cell debris. The deposition of drusen is associated with the ageing process of the RPE. (Wenick et al., 2017).

**Advanced glycation end products (AGEs)**

AGEs are the products of a non-enzymatic Maillard reaction that is the modification between the amino acid of proteins and the aldehyde group of sugars and dicarbonyls. AGEs accumulate in the extracellular matrix of the ageing tissue, and in the case of the retina, they accumulate in Bruch's membrane (Glenn and Stitt, 2009). These accumulations alter gene expression and proteome in RPE (Glenn et al., 2012), particularly the inflammatory response of the RPE, and may impair the lysosomal enzyme (Sharif et al., 2019), which is significant in autophagy and OS degradation. AGEs also elevate growth factors such as VEGF and platelet-derived growth factor (PDGF) (Ma et al., 2007).

### 2.1.2 Senescence, RPE and AMD

**Senescence**

Senescence is the process when cells permanently enter cell cycle arrest as the consequence of gradual deterioration with age (Blasiak, 2020). The process is originally identified as irreversible, resulting in the cessation of cell division. Cellular senescence was initially reported as a phenomenon in cell culture, but currently, it is known that various factors, including oxidative stress, DNA damage, viral infection, chemotherapy and ageing, can cause cellular senescence. The benefit of cellular senescence is essential for tumour suppression, wound repairing, and tissue remodelling (Sreekumar et al., 2020). However, the accumulation of senescent cells during ageing is associated with age-related abnormalities, including Alzheimer's disease, osteoarthritis and atherosclerosis. Morphologically, senescent cells are

flattened and enlarged in size; and have altered organelles morphology and function (Lee et al., 2021). For instance, impaired lysosomes in senescent cells cause protein aggregation, lipofuscin and mitochondrial turnover. With deficient mitochondria, the cells are susceptible to oxidative stress and increased reactive oxygen species production.

The molecular cascade of cellular senescence is triggered through the p16INk4a/Rb and p53/p21Cip1 pathways (Terao et al., 2022). The p53 and p16INk4a are tumour suppressors, and the loss of their functions resulting in malignant transformation. The p21Cip1 is a cyclin-dependent kinase (CDK) inhibitor encoded by the *CDKN1A* gene. The reactive oxygen species and DNA damage activate the p53/p21Cip1 pathway leading to cell cycle arrest.

Senescent cells also promote inflammation by secreting proinflammatory cytokines and growth factors as part of the complex senescence-associated secretory phenotype (SASP). These molecules include IL-6, IL-8, CXCL1, CXCL2, CSF-1, transforming growth factor (TGF), matrix metalloproteinases (MMPs), and VEGF (Blasiak, 2020). The inducers of SASP are NFkB, Notch, p38 mitogen-activated protein kinase, and mammalian target of rapamycin (mTOR) signalling. With SASP, senescent cells alter the expression and organisation of extracellular matrix components (Levi et al., 2020). This extracellular matrix change could influence their composition, topography and biomechanics. The increased stiffness and altered extracellular matrix component could be linked to age-related diseases such as osteoarthritis, COPD and cancer (Blokland et al., 2020).

Technically, there is no current single trait that could individually define cellular senescence. To identify senescence, multiple phenotypes must be confirmed, including several biomarkers (Itahana et al., 2007;Gonzalez-Gualda et al., 2021;Zhou et al., 2021). In brief, the

primary senescence marker detection includes cell cycle arrest, increased lysosomal content and senescence-associated beta-galactosidase (SA-beta-Gal) and detecting nuclear alterations. The detection of secondary senescence markers includes the SASP, mitochondria, reactive oxygen species and prosurvival pathways, and morphology and granularity of senescent cells.

Recently, to find cellular senescence signatures using transcriptomic data, a meta-analysis has combined microarray datasets to find senescence signature genes (Chatsirisupachai et al., 2019). With this approach, the study found that senescense signatures were expressed in ageing human tissues and cancer.

**Possible roles of senescence in RPE and AMD**

Even though RPE is a terminally differentiated, postmitotic tissue, which was previously thought as not able to undergo senescence (Malek et al., 2022), more evidence is identifying that cellular senescence can be found in post-mitotic neurons, brain tissue (von Zglinicki et al., 2021) as well as RPE.

Using RPE tissue culture, many research groups have shown the effects of cellular senescence on RPE cells. For example, A high passage (number of sub-cultures) of ARPE-19 (a human RPE cell line) showed the property of senescent cells, and they are more sensitive to VEGF (Kozlowski, 2015), which is known as the key marker associated with neovascular AMD. Comparing primary RPE cells cultured from ageing and young donors found increased expression of senescent markers, including p53, activated caspase-1, CDKN1A, CDKN2A (p16INK4a), TLR4, and IFNα in the primary RPE cultures from aged donors. (Chaum et al., 2015). A2E and cigarette smoke concentrate are examples of long-term and chronic oxidative stress associated with the pathogenesis of AMD; treating RPE culture with A2E and cigarette

smoke concentrate demonstrated cellular senescence by increasing reactive oxygen species level and senescence markers such as SA-beta-Gal (Marazita et al., 2016;Wang et al., 2018a). Apart from RPE, senescence also affects choroidal endothelial cells by increasing stiffness and susceptibility to the membrane attack complex deposition (Cabrera et al., 2016).

Although researchers can evidence RPE senescence through ARPE-19, ARPE-19 is not currently accepted as a good in vitro model of RPE (Malek et al., 2022). A poorly differentiated ARPE-19 lacks RPE differentiation markers such as RPE65 and lacks RPE properties such as polarization. Therefore, the current evidence on RPE senescence is still limited by the flawed ARPE-19 model and difficulty obtaining fresh tissue, hence might not reflect RPE senescence in humans.

Many hypotheses suggest that senescence occurs in ageing RPE and could potentially contribute to AMD, as senescence inducers such as chronic oxidative stress are relevant to AMD pathogenesis (Kozlowski, 2012;Blasiak, 2020;Lee et al., 2021). The SASP also could be a potential factor in increasing inflammation in AMD. With this concept, a potential alternative therapeutic option for AMD is using senolytic drugs to target senescent cells (Lee et al., 2021). Examples of senolytic drugs are quercetin and dasatinib. Quercetin was shown to reduce senescence markers in ARPE-19 treated with cigarette smoke extract (Zhu et al., 2019), while dasatinib might potentially suppress neovascular AMD (Seo and Suh, 2017) and retinal fibrosis (Ueda et al., 2021). Metformin is another drug that has properties related to senescence since it can inhibit SASP. A recent meta-analysis showed that metformin has a potential preventive effect for AMD (Romdhoniyyah et al., 2021). Moreover, the senolytic drug is currently ongoing in a clinical trial as a therapeutic option for neovascular AMD. The senolytics drug

UBX1325 is in phase 2 clinical trial for patients diagnosed with diabetic macular oedema and neovascular AMD (NCT04537884).

Overall, senescence of the RPE has been associated with AMD in vitro studies and in vivo observations. Given the lack of treatment for degenerative changes in AMD, there is a need for new drug discoveries, including senolytic drugs. Clinical trials are still required to determine whether senolytic drugs might be the potential treatment for AMD patients or not. However, the current knowledge on how possibly senescence might associate with RPE and AMD still needs to be investigated. In **Chapter 4**, I used a bioinformatic approach to investigate the senescence in RPE and AMD based on publicly available transcriptomic data.

### 2.1.3 Age-related macular degeneration

#### Presentation

In the early stage, patients usually have asymptomatic or mild symptoms such as a central vision defect, blurred vision and abnormal adaptation from bright to dim light. The symptoms then progress slowly over months to years into central visual loss. In neovascular AMD patients could experience sudden visual loss due to a haemorrhage, macular damage and fluid accumulation secondary to the primary lesion of AMD (Mitchell et al., 2018).

AMD symptoms affect mostly central vision; thus, this impairment declines the ability to read, drive, and facial recognition. Patients with AMD could also experience vision distortion or metamorphopsia. With advanced AMD, patients might not be totally blind, but the result of this central visual loss may lead to legal blindness in 12% of patients during the 5 years of advanced disease (Jager et al., 2008). The visual loss also declines the quality of life and increases the depressive symptom in one-third of the patients (Slakter and Stur, 2005).

**Type**

The presence of drusen and hypo/hyperpigmentation of RPE are the pathognomonic signs of AMD. These drusen are larger ( size more than 63 micrometres) than the small ones found in the normal ageing process (Ardeljan and Chan, 2013). Besides drusen, hypo/hyperpigmentation is the significant change of RPE in the early AMD (Rozing et al., 2020). In the intermediate stage, the drusen enlarge and fuse to be more confluent. In the late or advanced disease, patients may experience one of two forms: a non-neovascular AMD (dry AMD, geographic atrophy, non-exudative form) and a neovascular AMD (wet AMD, choroidal neovascularisation, macular neovascularisation, exudative form). The neovascular form has abnormal vascularisation arising in the choriocapillaris (or retina), while the late non-neovascular form is characterized by geographic atrophy, (Al-Zamil and Yassin, 2017).

Clinically AMD has several internationally accepted classification systems (**Table 2.1**). The epidemiological classification graded AMD into early and late stages (Klein et al., 2014). The Age-Related Eye Diseases Study (AREDS) categorized AMD into AREDS category 1 – 4, where AREDS category one indicates no AMD and four indicate advanced AMD (Age-Related Eye Disease Study Research, 2001a). Currently, the Beckman classification is the widely used classification based on colour fundus imaging in both research and clinical practice (Ferris et al., 2013). With this current classification, an early AMD is defined by a drusen size between 63-125 micrometres without any pigmentary abnormalities, while an intermediate AMD is defined as having drusen larger than 125 micrometres and/or the presence of any pigmentary abnormalities. Any neovascular AMD or GA are classified as late AMD. Previously, a neovascular AMD could be referred to as choroidal neovascularization, but recently in 2019, the Consensus on Neovascular AMD Nomenclature Study Group (CONAN) published a consensus classification of neovascular AMD based on OCT and OCT-A imaging

(Spaide et al., 2020). With this new framework, macular neovascularization (MNV) is a new term for choroidal neovascularization. The term macular neovascularization includes neovascularization originating from the choroid and retinal circulation, where neovascular from retinal circulation is classified as type 3 MNV. Apart from 3 types of MNV, polypoidal choroidal vasculopathy (PCV) is a variant of type 1 MNV characterized by the presence of a branching vascular network and distinct nodular vascular agglomerations, often called polyps. This variant is commonly seen in Asia. PCV typically demands a more rigorous regimen of anti-VEGF treatment compared to other types of neovascularization and may need additional treatment modalities like photodynamic therapy(Wong et al., 2016).

The classification system is important for treatment planning and prognosis since different stages have different outcomes. For instance, type 1 MNV may have better outcomes if left untreated, while type 3 MNV is associated with the worst outcomes if left untreated (Mathis et al., 2023). However, one disadvantage of the classification system is that it is based on clinical manifestations rather than molecular diagnoses, which may not accurately reflect the actual molecular events of the disease.

**Table 2.1 Classifications of AMD**

| Term | Definition |
|---|---|
| **The epidemiological classification (Klein et al., 2014)** | |
| Early AMD | Large (≥125 μm) drusen or retinal pseudodrusen, or pigmentary abnormalities |
| Late AMD | Neovascular AMD or geographic atrophy |
| **AREDS classification (Age-Related Eye Disease Study Research, 2001a)** | |
| category 1 (no AMD) | Drusen maximum size < 63 μm and total area < 125 $\mu m^2$ |
| category 2 | Presence of one or more of the following: |

| | |
|---|---|
| | (a) Drusen maximum size ≥ 63 μm but < 125 μm<br>(b) Drusen total area ≥ 125 $\mu m^2$<br>(c) Retinal pigment epithelial pigment abnormalities consistent with AMD, defined as one or more of the following in the central or inner subfields:<br>(1) Depigmentation present, (2) Increased pigment ≥ 125 μm, (3) Increased pigment present and depigmentation at least questionable |
| category 3 | Presence of one or more of the following:<br>(a) Drusen maximum size ≥ circle 125 μm<br>(b) Drusen maximum size ≥ 63 μm and total area > 360 $\mu m^2$ and type is soft indistinct<br>(c) Drusen maximum size ≥ 63 μm and total area > 656 $\mu m^2$ and type is soft distinct<br>(d) Geographic atrophy within grid but none at centre of macula |
| category 4 (advanced AMD) | Presence of one or more of the following:<br>(a) Geographic atrophy in central subfield with at least questionable involvement of centre of macula<br>(b) Evidence of neovascular AMD : (1) Fibrovascular/serous pigment epithelial detachment, (2) Serous (or hemorrhagic) sensory retinal detachment, (3) Subretinal/subretinal pigment epithelial haemorrhage, (4) Subretinal fibrous tissue (or fibrin), (5) Photocoagulation for AMD |
| **The Beckman classification (Ferris et al., 2013)** | |
| No apparent aging changes | No drusen and no AMD pigmentary abnormalities |
| Normal aging changes | Small drusen ≤63 μm and no AMD pigmentary abnormalities |
| Early AMD | Medium drusen >63 μm and ≤125 μm and no AMD pigmentary abnormalities |
| Intermediate AMD | Large drusen > 125 μm and/or any AMD pigmentary abnormalities |
| Late AMD | Neovascular AMD and/or any geographic atrophy |
| **The CONAN classification of neovascular AMD (Spaide et al., 2020)** | |

| | |
|---|---|
| Type 1 MNV | Ingrowth of vessels initially from the choriocapillaris into and within the sub-RPE space. Leads to varying types of pigment epithelium detachment. |
| Type 2 MNV | Neovascularization that originates from the choroid that traverses Bruch's membrane and the RPE monolayer and then proliferates in the subretinal space. |
| Type 3 MNV | Neovascularization that originates from the retinal circulation, typically the deep capillary plexus, and grows toward the outer retina. |

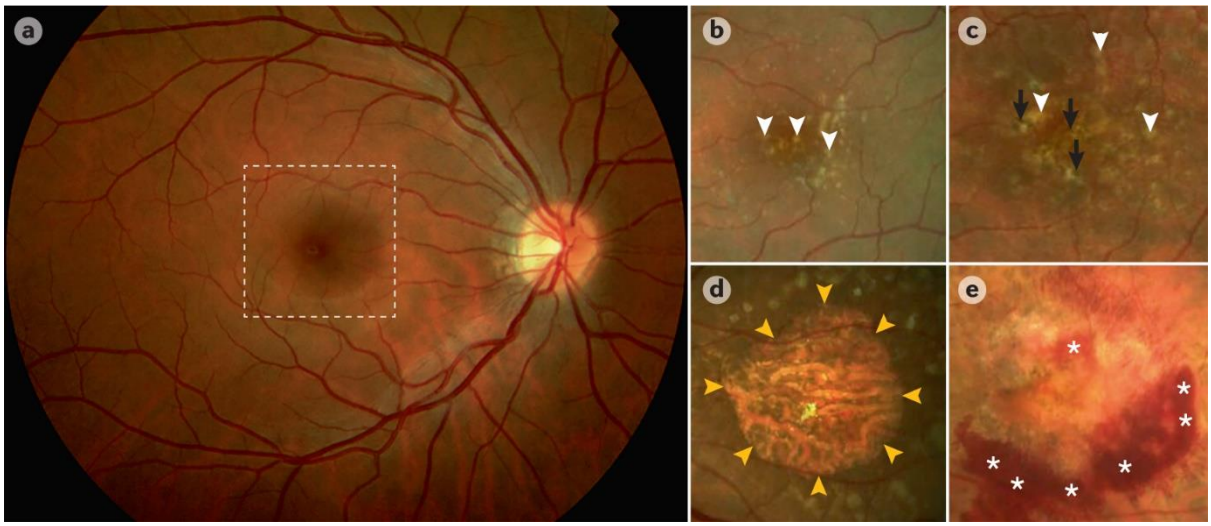


**Figure 2.1 Colour fundus images of AMD.**

The colour fundus images represent different stages of AMD. (A) Normal colour fundus image (the square represents the centre of the macula (a pigmented region in the centre of the retina, shaped like an oval and measuring approximately 5.5 mm in diameter)). (B) Early AMD (the arrows point to yellowish drusen). (C) Intermediate AMD (the white arrows point to large yellowish drusen, and the black arrows point to hyperpigmentation). (D) Geographic atrophy (the arrows point to the geographic atrophy area). (E) Neovascular AMD (the asterisks represent haemorrhage). Reprinted with permission License Number 5506660910686 (Fleckenstein et al., 2021).

**Risk factors**

The meta-analysis by Wong et al. showed that AMD prevalence is 8.7% of the world population (45-85 years) and could affect 288 million people by 2040 (Wong et al., 2014). The knowledge of the disease mechanism comes from the combination of epidemiological study, clinical imaging, histological study, genetic study and experimental study, but is incomplete and the exact mechanisms of AMD pathogenesis are unknown. Epidemiological studies has given us the essential background of risk associated with AMD (Handa et al., 2019;Rozing et al., 2020). Among the risks, ageing is the most prominent. The prevalence of late AMD is less than 1 per cent in people younger than 65, while it rises to about 13 per cent in people older than 85 (Colijn et al., 2017). Apart from ageing, risk factors include both environmental and genetic factors. Smoking increases the risk of AMD by two to four times and the risk of developing late AMD. Other less prominent risks are hyperlipidemia, obesity, hypertension, high fat intake, female sex and caucasian ethnicity (Al-Zamil and Yassin, 2017;Mitchell et al., 2018).

The genetic factor significantly influences the disease, as proven by the higher chance of people with positive family history developing AMD and a one-third chance of developing a disease in monozygotic twins (Hammond et al., 2002). To decode the culprit genetic factors, the international age-related macular degeneration genomics consortium (IAMDGC) used genome-wide association studies (Fritsche et al., 2016). The two most significant variants, complement factor H (*CFH*), and high-temperature requirement serine peptidase 1 (*HTRA1*) explain about half of the heritable AMD (DeAngelis et al., 2017). *CFH* gene is a complement inhibitor in the inflammatory process and is also a component found in drusen (Landowski et al., 2019). The *HTRA1* regulates extracellular matrix homeostasis (Lin et al., 2018). In addition to these two variants, others like *CST3*, *CFB*, *TIMP3*, *TLR3*, *LIPC*, and *C2* exhibit their role across a wide range of biological processes such as an inflammatory response, lipid metabolism

and extracellular matrix modification (Al-Zamil and Yassin, 2017). The large-scale GWAS have discovered 52 variants across 34 coding genes associated with AMD to date. However combining all 52 genetic variants could explain less than 30% of AMD cases, and the significant variants like *CFH* and *HTRA1* could not explain the non-caucasian population (DeAngelis et al., 2017). It is noteworthy that a GWAS is a type of study that examines the association between mutations and disease. Sometimes, a significant region identified through GWAS may not directly cause the disease but could be influenced by the linkage of certain genes(Tam et al., 2019). Moreover, the interaction between genetic mutations and environmental factors or epigenetics remains an area to be explored in relation to AMD. Therefore, these facts underscore the multifactorial nature of AMD and the necessity of studying ageing as the leading risk factor of AMD.

**Current treatment**

No current treatment can prevent or reverse AMD. The primary management is adjusting the modifiable risk to reduce disease progression, especially smoking cessation (Al-Zamil and Yassin, 2017) and support with vision loss. The antioxidant supplement is a therapeutic option used by some since it possibly prevents oxidative stress in the retina. The multicentre clinical trial study, the AREDS study suggested that the combination of vitamin C (500 mg), vitamin E (400 IU), beta-carotene (15 mg), copper (2 mg) and zinc (80 mg) —reduce the risk of developing advanced AMD (Age-Related Eye Disease Study Research, 2001b). However, the AREDS did not meet any of its primary endpoints and found no difference between the study arms. Only in a post-hoc sub-group analysis was a difference in progression to late AMD found, and there was no difference in vision between the arms. In the subsequent study, AREDS2 added lutein (10mg) and zeaxanthin (2mg), instead of beta-carotene to avoid the risk of lung cancer in smoking patients from the beta-carotene (Group et al., 2012). Because

there was no placebo group, AREDS2 did not add to our knowledge of efficacy of antioxidants in AMD. Due to the weakness in this evidence AREDS formulation antioxidants are not recommended by the National Institute for Health and Care Excellence

Repeated intravitreal anti-VEGF injection reduces neovascularization in neovascular AMD and improves vision on average, at least initially. Anti-VEGF bind to the VEGF, which promotes blood vessel growth from the choriocapillaris (Mitchell et al., 2018). However, non-neovascular AMD patients, do not have an available treatment option to improve their vision or even slow the decline. The absence of the available treatment again underlines the essence of studying the fundamental mechanism of the disease (Handa et al., 2019).

**The ageing process of RPE and its association with AMD**

Studying ageing RPE is crucial to understanding the exact molecular mechanism of AMD and the multiple interactions between the genetic, environmental and ageing factors (Rozing et al., 2020). Both intra and extracellular deposits occur in the ageing RPE. Lipofuscin, an intracellular ageing debris with lipid-rich content, together with A2E, induces the formation of ALEs. These accumulations disturb the proteostasis, leading to RPE degeneration and photoreceptor cell death in AMD (Krohne et al., 2010).

Reactive oxygen species increase from the ageing process and are the byproduct of OS phagocytosis. Oxidative stress is linked with senescence which could be relevant to the pathogenesis of AMD. This oxidative stress damages various molecules, including DNA and protein; it also disturbs the autophagy mechanism of RPE that digests the abnormal organelles and partially relates to the degradation of phagocytosed OS (Mitter et al., 2012). With abnormal digestion, the lipid and protein debris gather inside the ageing RPE cells, so impaired

autophagy could link to lipofuscinogenesis (Lakkaraju et al., 2020). Apart from autophagy, oxidative stress also harms the mitochondria and their DNA. The compromised mitochondria cannot adequately supply energy to the cell; finally, the inability to manage oxidative stress creates more reactive oxygen species and leads to apoptosis of RPE cells (Handa et al., 2019).

The extracellular waste AGEs deposit in the ageing Bruch's membrane. When AGEs interact with their AGE receptor (RAGE), they activate the inflammatory response and induce the oxidation of lipoprotein substances (Glenn and Stitt, 2009). Moreover, the stiffness and thickening of senescent Bruch's membrane reduce the permeability to transport waste that could lead to drusen formation (Curcio and Johnson, 2017). Altogether the compromised ageing RPE with both intra and extracellular debris is vulnerable to environmental factors accelerating the progression to AMD (Rozing et al., 2020).

Although various studies have associated risks that link RPE to AMD, including ageing, environmental and genetic factors, the exact cellular event of AMD is still unclear. The challenge is how to identify all of the different aspects of AMD simultaneously; and how to combine multiple risk factors and understand their consequence molecular event in the RPE (Handa et al., 2019). With the advance in bioinformatics technology, omic approaches such as genomic, proteomic and transcriptomic allow us to uncover molecular events simultaneously. This omics approach is a systematic one and, when used with fresh postmortem human donor specimen, gives us possible information contribute to our understanding of AMD pathobiology (DeAngelis et al., 2017).

### 2.1.4 Transcriptomic study of AMD RPE

A transcriptomic analysis is a potential tool to explore disease pathogenicity at the molecular level. By using differential gene expression analysis, the abnormal gene expression between healthy and diseased can be observed in tissues (Tian et al., 2015). The subsequent analysis can group genes differentially expressed to understand disease-related pathways or analyse the interaction between those genes. The transcriptomic analysis has been applied to various disease conditions, including AMD. Because the techniques are specific to tissue and require RNA in the cellular component, studying RPE transcriptomic currently inevitable needs postmortem samples (Voigt et al., 2021). Due to the difficulties in obtaining the donor's postmortem sample with specific pathology, the information gained from one donor is priceless. **Table 2.2** summarize the previous research on AMD RPE transcriptome. The previous transcriptomic studies included two microarray studies, one RNAseq and one scRNA-seq study.

**Table 2.2 Transcriptome studies of postmortem human AMD RPE/choroid.**

| Year | Title | Method |
|---|---|---|
| 2012 | Systems-level analysis of age-related macular degeneration reveals global biomarkers and phenotype-specific functional networks (Newman et al., 2012) | Microarray |
| 2013 | Altered gene expression in dry age-related macular degeneration suggests early loss of choroidal endothelial cells (Whitmore et al., 2013) | Microarray |
| 2018 | Complete Transcriptome Profiling of Normal and Age-Related Macular Degeneration Eye Tissues Reveals Dysregulation of Anti-Sense Transcription (Kim et al., 2018) | RNAseq |
| 2019 | Single-cell transcriptomics of the human retinal pigment epithelium and choroid in health and macular degeneration (Voigt et al., 2019) | scRNA-seq |

| | | |
|---|---|---|
| 2020 | Integration of eQTL and a Single-Cell Atlas in the Human Eye Identifies Causal Genes for Age-Related Macular Degeneration (Orozco et al., 2020) | RNAseq, scRNA-seq |

In 2012, Newman et al. conducted a transcriptomic analysis using microarrays to understand the molecular mechanisms of AMD by using 79 AMD RPE/choroid and 96 control RPE/choroid. Their analysis highlighted the cell-mediated immune responses were globally over-expressed in AMD samples (Newman et al., 2012). Whitmore et al. conducted microarray analysis using 9 early AMD RPE/choroid compared with 9 control RPE/choroid. Their pathway analysis suggested that genes upregulated in early AMD were possibly related to the biosynthesis of unsaturated fatty acids (*FADS1, FADS2, PTPLA*), while the genes in pathways associated with vision sensory perception and the plasma membrane were downregulated (Whitmore et al., 2013). They also indicated the early AMD samples lost choroidal endothelial-specific gene expressions. However, both studies conducted a transcriptomic analysis using microarrays, which would be limited by microarray technology that could not detect the absolute value of gene expression and only provided gene expression data for predefined genes on the arrays.

For RNAseq, Kim et al. sequenced 8 AMD RPE/choroid/sclera and 8 control RPE/choroid/sclera, in which they reported 310 differential expressed genes in AMD (Kim et al., 2018). In 2019, Voigt et al. applied the latest technology of scRNA-seq to RPE/choroid tissues using 1 neovascular AMD patient and 2 control RPE/choroid. In this scRNA-seq analysis, using cluster analysis of gene expression data, they reported cells clusters in RPE/choroid tissue include fibroblasts, melanocytes, pericyte, B-cell, T/NK-cell, Schwann cells, RPE, macrophages, endothelial cells, and mast cells (Voigt et al., 2019). Recently, Orozco et al. did RNAseq of 49 AMD RPE/choroid and 217 control RPE/choroid specimens.

Apart from that, they also did scRNA-seq of 5 postmortems control whole retina samples (Orozco et al., 2020).

Despite the low sample size, the AMD RPE transcriptomic studies are diverse in techniques and pathology. Due to the difficulties in gaining tissue samples, the attempts to utilise all the transcriptomic data using a data-driven approach are essential to gain more understanding of AMD pathogenesis. More specifically, the existing literature on transcriptomic analysis in the context of AMD presents two distinct gaps that have motivated the studies presented in this thesis. First, there is a limited overlap in differentially expressed genes when comparing transcriptomic data of AMD and normal RPE/choroid. This discrepancy may result from individual underpowered studies. Therefore, employing an integrative quantitative method to analyse combined datasets has the potential to mitigate bias between transcriptomic analyses and could enhance the power to detect differentially expressed genes. Another gap relates to the pathogenesis of AMD and its association with senescence. The current understanding of how senescence might be linked to RPE and AMD remains unexplored through transcriptomic analysis. Overall, the motivation behind this thesis is to address these disparities by analysing publicly available transcriptomic data, aiming to explore molecular determinants in RPE/choroid dysfunction in AMD. In **Chapter 3**, I conducted the meta-analysis using two distinct transcriptome platforms to find differentially expressed genes in AMD RPE/choroid compared with normal RPE/choroid, as well as pathways associated with those genes. In **Chapter 4**, the scRNA-seq of RPE/choroid has been re-evaluated to find the intercellular communication interaction between different genes expressed in RPE/choroid. My analysis also attempted to investigate how senescence might influence RPE/choroid and AMD using transcriptomic data from both previously published scRNA-seq and microarray datasets.

## 2.2 Introduction to retinal vasculitis

### 2.2.1 Retinal vasculitis

Retinal vasculitis is a subset of a broader disease category known as posterior uveitis, the inflammation at the back part of the eye the inflammation and has a primary site in the retina and choroid, including choroiditis, chorioretinitis, retinochoroiditis, retinitis and neuroretinitis. Retinal vasculitis is a conglomerate descriptive term for posterior uveitis that presents with inflammation occurring with the retinal vasculatures. It can often coexist with other manifestations of posterior uveitis. The term is used for the clinical diagnosis distinctively from vasculitis at the other part of the body or systemic vasculitis (Rosenbaum et al., 2016). While systemic vasculitis is evidenced by the pathologic process of vascular inflammation and necrosis, retinal vasculitis is evidenced through ophthalmic examinations (Datoo O'Keefe and Rao, 2021). The retrospective analysis spanning 25 years of data from the uveitis clinic at Oregon Health and Sciences University estimated that retinal vasculitis comprised 15% of all uveitis cases (Rosenbaum et al., 2012).(Do and Giovinazzo, 2016). There is no gender difference, and it is more common in patients aged less than 40 (Do and Giovinazzo, 2016). The overall incidence of retinal vasculitis is approximately 1-2 in 10,000 US and Western Europe populations (Hughes and Dick, 2003).

This rare disease could be presented as retinal vascular sheathing or classical tram line appearance on fundoscopic examination or colour fundus photography (Agarwal et al., 2017). The disease could be severe and sight-threatening as it could develop macular oedema, ischemia, epiretinal membrane and neovascularisation in the later stage (Mir et al., 2017). The symptoms of patients affected by retinal vasculitis are painless visual loss, blurred vision, scotoma, floaters and less common symptoms, including metamorphopsia and alteration of

colour vision (Levy-Clarke and Nussenblatt, 2005;Do and Giovinazzo, 2016). The patient could also experience pain if retinal vasculitis is associated with anterior uveitis or panuveitis. (Levy-Clarke and Nussenblatt, 2005;Do and Giovinazzo, 2016)

**Aetiology**

The causes of retinal vasculitis are broadly associated with inflammation, autoimmune, infection, drug-induced, malignancy and idiopathic (**Table 2.3**) (Agarwal et al., 2022). Retinal vasculitis could present as an isolated ocular disease or be associated with other systemic or ocular diseases. More than 25% of retinal vasculitis patients have an associated systemic or ocular disease, but only 1.4% of systemic vasculitis patients presented with retinal vasculitis (Rosenbaum et al., 2016). However, some systemic vasculitis diseases have a higher incidence of retinal vasculitis; for example, Behcet's disease has about 19.3% of patients with retinal vasculitis (Turk et al., 2021). Demographic background and ethnicity also affect the distribution of retinal vasculitis aetiology; including endemic tuberculosis areas would have a higher incidence of retinal vasculitis associated with tuberculosis (Apinyawasisuk et al., 2013;Agrawal et al., 2017); Behcet's disease has been found more common along the ancient Silk Road (Turk et al., 2021).

In addition to the known aetiology of retinal vasculitis, conditions have recently been associated with retinal vasculitis as aetiologies, including post-vaccination and drug-induced. Intracameral vancomycin injections have already been known to cause haemorrhagic occlusive retinal vasculitis through type 3 hypersensitivity reaction for drug-induced retinal vasculitis (Witkin et al., 2017).

In 2019, the US FDA approved brolucizumab, a humanised monoclonal single-chain Fv antibody fragment, for the treatment of neovascular AMD. Brolucizumab is an anti-VEGF which could bind with both VEGF receptor-1 and VEGF receptor-2 (Baumal et al., 2021). However, after it was approved, there were significant reports of intraocular inflammation following injection, including retinal vasculitis (Baumal et al., 2020). The post hoc analysis reported a 3.3 % incidence of retinal vasculitis (36 retinal vasculitis cases from 1,088 patients treated with brolucizumab in HAWK and HARRIER studies) (Mones et al., 2021). The possible explanation is unclear, but it is hypothesised that locally-generated antibodies to the drug might cause intraocular inflammation (Baumal et al., 2021). Recently, some case reports published COVID19-vaccines related ocular inflammation, including retinal vasculitis (Li et al., 2022;Mohamed et al., 2023;Yi et al., 2023). However, the number of reports is relatively small compared to the worldwide use of COVID19-vaccines. More studies and causal effects may need to be determined in COVID19-vaccines relates cases. Even though retinal vasculitis is rare, the fact that new aetiologies, such as broculizumab could cause it, highlights the importance of research in retinal vasculitis.

**Table 2.3 Retinal vasculitis's aetiology** (Walton and Ashmore, 2003;Agarwal et al., 2022)

| Ocular disorders | Infectious disorders | Systemic disorders |
|---|---|---|
| Idiopathic | Tuberculosis | Behcet's disease |
| Eales disease | Toxoplasmosis | Sarcoidosis |
| Birdshot Chorioretinopathy | Syphilis | Multiple sclerosis |
| Intermediate uveitis | Lyme disease | Crohn disease |
| Idiopathic retinal vasculitis aneurysms and neuroretinitis (IRVAN) | Cytomegalovirus | Systemic lupus erythematosus |
| Vogt-Koyanagi-Harada syndrome | Herpes simplex | Granulomatosis with polyangiitis |
| Sympathetic ophthalmia | Varicella zoster | Ankylosis spondylitis |
| Acute multifocal haemorrhagic retinal vasculitis | Whipple disease | Polyarteritis nodosa |
| | Endophthalmitis | Bueger disease |
| | Human T-cell lymphoma virus type 1 | Relapsing polychondritis |
| | Brucellosis | Antiphospholipid syndrome |

| | | |
|---|---|---|
| | Hepatitis | Chur-Strauss syndrome |
| | Cat scratch disease | Sjögren syndrome |
| | AIDS | Polymyositis |
| | Candidiasis | Rheumatoid arthritis |
| | Leptospirosis | Dermatomyositis |
| | Coccidioidomycosis | Takayasu disease |
| | Mononucleosis | Primary central nervous system lymphoma |
| | Rickettsia | Acute leukaemia |
| | Amebiasis | Cancer-associated retinopathy |
| | West Nile virus | Susac's syndrome |
| | Dengue virus | Drug-induced/ Post-vaccination |

**Pathogenesis**

The pathogenesis process in retinal vasculitis is believed to be an autoimmune or inflammatory process that affects small vessels. Previous research hypothesised that retinal vasculitis's pathogenesis is related to type III hypersensitivity (Levy-Clarke and Nussenblatt, 2005). The histologic study found CD4+ T-cell accumulation around the retinal vessels, which is more likely to be perivasculitis (**Figure 2.2**) (Do and Giovinazzo, 2016). The hypothesis postulates that ocular or systemic inflammation leads to a blood-retinal barrier breakdown and retinal vascular leakage evident in the ophthalmic examination. However, the scarcity of direct evidence due to hard-to-obtain histologic tissue specimens hinders the understanding of this disease's exact pathogenesis.

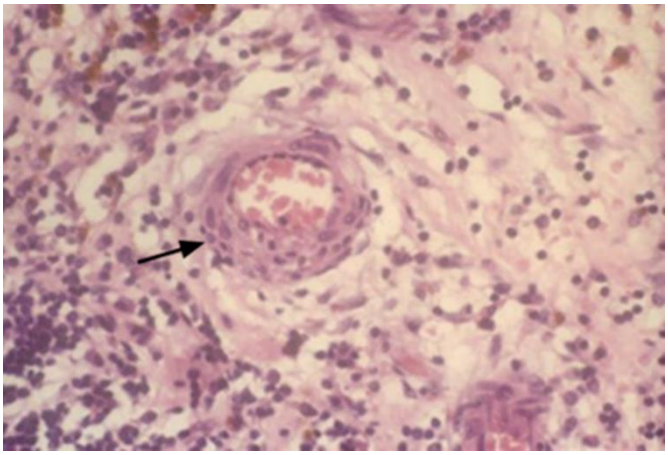

**Figure 2.2 Histopathologic examination of retinal vasculitis.**

Histopathologic examination shows Behçet's retinal vasculitis; the arrow represents perivascular inflammation. Reprinted with permission License Number 5523800985322 (Do and Giovinazzo, 2016).

**Management**

Due to the heterogeneity of the disease, the investigation of an underlying cause is essential. History taking, ocular and systemic examination, and laboratory tests should be done to differentiate infectious from noninfectious causes (Agarwal et al., 2022). This search for underlying systemic disease is crucial because retinal vasculitis could sometimes present as their first manifestation. (Datoo O'Keefe and Rao, 2021)Other specific laboratory tests could be done to investigate specific autoimmune or infectious diseases as suspected. After identifying the cause, the treatment is tailored to reflect the underlying pathology. The aim of treatment is to subside the intraocular inflammation and prevent long-term complications and visual loss (Levy-Clarke and Nussenblatt, 2005). Antimicrobial treatment is given to the infectious form of retinal vasculitis.

The follow-up and observation alone without intervention may be used in a retinal vasculitis case with minimal changes. Although there is currently no FDA-approved drug specifically for retinal vasculitis (Rosenbaum et al., 2016), immune suppression agents, including corticosteroids, steroid-sparing immunosuppressive drugs, and biologic agents, are the mainstay in non-infectious retinal vasculitis. Before starting immune suppression, the baseline laboratory includes a complete metabolic panel, chest X-ray, and hepatitis should be performed (Datoo O'Keefe and Rao, 2021). In the late stage of neovascularisation, panretinal photocoagulation and anti-VEGF may be beneficial to prevent further complications (Do and

Giovinazzo, 2016). Pars plana vitrectomy could be done in the case where vitreous haemorrhage is present (Datoo O'Keefe and Rao, 2021).

### 2.2.2 Clinical imaging of retinal vasculitis

#### Colour fundus imaging

Colour fundus imaging could demonstrate vascular sheathing or classical tram line appearance (Shulman et al., 2015), perivascular retinal infiltrates, perivascular haemorrhages, non-perfused retina or retinal vascular occlusion, vessel beading, cotton-wool spots, irregular vessel calibre, ghost vessels and neovascularisation secondary to ischaemia (Do and Giovinazzo, 2016;Agarwal et al., 2017). However, the findings in colour fundus photography can be minimal and not specific to retinal vasculitis.

#### Fluorescein Angiography

FA is the current gold standard for diagnosing retinal vasculitis (Jabs et al., 2005). The fluorescein dye bases angiography techniques use the principle of the emitted photon from the excited dye – fluorescein which was injected through the subject's circulation (Johnson et al., 2013). Hence, this technique could be invasive, and even the side effects of fluorescein injection are rare; they could range from extravasation to a severe adverse event such as anaphylaxis.

WFFA or UWFA is a more acceptable tool because retinal vasculitis could be presented in the peripheral retinal (Leder et al., 2013). The limited field of view in traditional FA can lead to misdiagnosis. The major characteristic feature is retinal vascular leakage which is the leakage of dye through the breakdown of the inner blood-retina barrier. The leakage is present as a progression of hyperfluorescence coming from retinal vessels, which could involve

retinal arteries, veins, capillaries or mixed (Agarwal et al., 2017). Hyperfluorescence can also occur a vessel wall staining, defined as vessel wall hyperfluorescence evident from mid-run onwards without expansion (Johnson et al., 2013) and not considered related to disease activity. The hyperfluorescent area could be either segmental, focal or diffuse/widespread. Many studies found that retinal vascular leakage indicates the inflammatory status of the disease (Kim et al., 2015;Onal et al., 2018).

The inflamed vessels could lead to occluded retinal vessels, which present as retinal non-perfusion or capillary dropout in FA images. If extensive, retinal non-perfusion can initiate retinal neovascularisation and haemorrhage (Ali et al., 2014).

**OCT**

OCT is a non-invasive technique that visualises the retinal microstructures in cross-section. No specific signs in OCT that indicate retinal vasculitis have been established. However, OCT is performed regularly in uveitis practice and could be used to follow up on the consequences of retinal vasculitis, such as macular oedema (Agarwal et al., 2017). Enhanced-depth imaging OCT (OCT-EDI) is the improved version of OCT that enhance choroidal structures visualisation (Laviers and Zambarakji, 2014). Choroidal thickness measuring through OCT-EDI could refer to the inflammatory activity of posterior uveitis (Balbaba et al., 2020;AlBloushi et al., 2021). OCT angiography (OCT-A) is the most recent technology that can visualise retinochoroidal vasculature without dye injection (Spaide et al., 2018;Invernizzi et al., 2019). The OCT-A is a potential tool to identify the non-perfusion area in retinal vasculitis (Emre et al., 2019), but one limitation is the current very limited field of view. Hence, OCT imaging modalities are the potential tools to visualise and use for follow-up patients with retinal vasculitis. To understand the role of OCT, **Chapter 5** systematically explores the literature on using OCT imaging modalities in retinal vasculitis.


**Figure 2.3 Clinical imaging of retinal vasculitis.**

Clinical imagings show Behçet's retinal vasculitis in right (A,C,E) and left (B,D,F) eyes. (A,B) Fundus imaging shows multifocal retinal infiltrates (white arrow), intraretinal haemorrhages (dotted arrow) and cotton wool spots (red arrow). (C) OCT shows cystoid macular oedema and serous retinal detachment. (D) normal OCT. (E,F) UWFA shows retinal vascular leakage. Reprinted with permission License Number 5523810587924 (Rosenbaum et al., 2016).

### 2.2.3 Retinal vasculitis classification

Retinal vasculitis has a vague definition and no accepted classification systems. In 2005, the SUN working group agreed upon the term retinal vasculitis, which describes the ocular inflammation associated with retinal vascular changes (Jabs et al., 2005). This international group considered the sign of retinal vascular disease on FA image, including retinal vascular leakage and occlusion associated with retinal vasculitis. However, they concluded that the definition of retinal vasculitis required more work and did not provide any classifications for retinal vasculitis severity. An accepted classification system is essential to understand the condition's aetiology, prognosis, and potential treatment options. It would allow clinicians to accurately diagnose and classify the severity of retinal vasculitis, develop treatment options, and be necessary for communication among clinicians, patients and researchers.

Similar to the SUN working group statement, uveitis specialists and researchers have used FA as the gold standard diagnosis for retinal vasculitis. However, no consistent classification or severity grading of the disease has emerged. Classification systems are sparse in the literature but appear to specifically be used to define or classify retinal vasculitis for individual research (**Table 2.4**). Some researchers grade retinal vascular leakage in FA into mild, moderate and severe (Keino et al., 2011;2014;Shirahama et al., 2019). However, these appear to have a vague distinction between each scoring system or have no clear anatomical landmark between different graders. Moreover, these classification systems have not been validated or applied to clinical practice.

**Table 2.4 Previous retinal vasculitis FA grading schemes**

| Study | A brief explanation of each retinal vasculitis FA grading scheme |
|---|---|

| | |
|---|---|
| (Suhler et al., 2005) | FA grading for uveitis includes assessment of media opacity, cystoid macular oedema, disc leakage, retinal vascular leakage, diffuse leakage and choroidal filling defect. |
| (Tugal-Tutkun et al., 2010a;Tugal-Tutkun et al., 2010b;Kang and Lee, 2014;Moon et al., 2017;Kim et al., 2022) | The Angiography Scoring for Uveitis Working Group (ASUWOG) has developed a 40-point scoring scheme to evaluate FA imaging for posterior uveitis. The items are optic disc hyperfluorescence, macular oedema, retinal vascular staining/leakage, capillary leakage, retinal capillary nonperfusion, neovascularization of the optic disc, neovascularization elsewhere, pinpoint leaks, and retinal staining/pooling. |
| (Keino et al., 2011;2014;Shirahama et al., 2019) | This scheme grades retinal vascular leakage on a scale of 0 to 3 (0 =none, 1=mild,2=moderate, 3=severe) for the peripheral retina, the macula and the optic disc. |
| (Leder et al., 2013) | Only ask the grader's opinion that the images are active or not active retinal vasculitis. |
| (Umazume et al., 2018) | Assess the optic nerve, posterior pole, peripheral retina findings and neovascularisation (total score = 12). |
| (Laovirojjanakul et al., 2019) | This scheme divides retinal vascular leakage into no leakage, peripheral leakage and diffuse leakage. |
| (Zarei et al., 2021) | This is a 43-point scoring scheme for evaluating Behcet's retinal vasculitis. The items are optic disc hyperfluorescence, macular hyperfluorescence, large retinal vessel wall hyperfluorescence, posterior capillary fluorescein leakage, peripheral capillary fluorescein leakage and hazy media. |

Although Angiography Scoring for Uveitis Working Group (ASUWOG) scoring of FA is not specific to retinal vasculitis, it has been repeated by other studies (Tugal-Tutkun et al., 2010a;Tugal-Tutkun et al., 2010b;Kang and Lee, 2014;Moon et al., 2017;Kim et al., 2022). This grading system has a total score of 40. It was validated in FA and UWFA (Tugal-Tutkun et al., 2010b); and used to follow up on Behcet's disease(Kim et al., 2022). Even if

implemented more than ten years ago, this complicated scoring system is not applied in clinical practice, trials, or follow-ups with other retinal vasculitis patients. This thesis is motivated by the fact that FA is the current technique to diagnose retinal vasculitis, and currently, there is no accepted FA grading system for this disease. The absence of an accepted grading system would make communication between clinicians and researchers inconsistent and hinder the development of new treatment options for this condition. Therefore, there is a current need to implement a new classification system for retinal vasculitis.

To address the classification issue of retinal vasculitis, I proposed and validated the new retinal vasculitis grading scheme in **Chapter 6**. Apart from the clinical grading, I also utilised a data-driven application approach using artificial intelligence to identify retinal vascular leakage and occlusion in retinal vasculitis, which is presented in **Chapter 7**.

## 2.3 Thesis aim and structure

### Aim and objectives

The increasing availability of data and advancements in data analysis and computing offer an opportunity to develop our understanding of retinal diseases. Omic's biological data, derived from advanced sequencing techniques, have the potential to provide more information on disease mechanisms, while clinical imaging data could improve diagnosis and workflows. In the case of AMD, disparities in gene expression data motivate a quantitative approach using a meta-analysis technique trying to mitigate biases. Additionally, exploring the link between senescence and AMD remains an unexplored area by bioinformatics. On the other hand, inflammatory retinal diseases, specifically retinal vasculitis, lack a precise classification system for FA imaging. Developing such a system has the potential to enhance prognosis, treatment, and communication. This thesis aims to develop a new grading scheme, explore the role of

artificial intelligence in retinal vasculitis, and explore OCT and OCT-A features for the retinal vasculitis.

In ageing retinal diseases, a common retinal disease where clinical and epidemiologic studies could provide ageing as the important risk factor for AMD, the pathogenesis of AMD is still unknown. This thesis aims to use the data-driven application to explore how RPE's transcriptomic data might contribute to AMD's pathogenesis. The specific objectives for these present studies are as follows:

1. To utilise RPE transcriptomic data analysis to develop an understanding on pathogenesis of ageing and AMD

1.1. To explore genes and functional pathways underpinning pathological processes occurring in ageing RPE/AMD by exploring existent AMD/controls RPE transcriptomic data.

1.2. To investigate intercellular communication of the RPE/choroid in the context of ageing, senescence and AMD by using an integrated analysis of RPE transcriptomic datasets obtained through different approaches (microarrays and scRNA-seq)

In contrast to common retinal diseases, inflammatory retinal diseases, especially retinal vasculitis, still have problems with consensus on their clinical imaging. This thesis aims to use the data-driven application to explore the clinical imaging of retinal vasculitis. The specific objectives for this present study are as follows:

2. To utilise clinical imaging data to better classify and segmentation of retinal vasculitis.

2.1. To conduct a systematic review to understand the features of retinal vasculitis in OCT imaging.

2.2. To develop and test the reliability of a novel grading scheme for retinal vasculitis.

2.3. To develop a computerised analysis of retinal vasculitis grading using artificial intelligence.

**Thesis structure**

Previously, in this chapter (**Chapter 2**), I described the literature that forms the foundation of my research, explained the literature gaps and identified my thesis objectives. To achieve the objectives of utilising advancement in data analysis the retinal disease, **Chapter 3-4** shows the utilising of transcriptomic data analysis in the ageing retina and age-related macular degeneration. **Chapter 3** used meta-analysis techniques to combine publicly available gene expression AMD data. **Chapter 4** bioinformatically explored senescence gene expression in RPE/choroid using transcriptomic data. **Chapter 5-7** shows the utilising of clinical data analysis for retinal vasculitis. **Chapter 5** explored the role of OCT and OCT-A on retinal vasculitis through a systematic review. **Chapter 6** added the new retinal vasculitis grading scheme for WFFA images. **Chapter 7** applied and developed a computerised segmentation method for retinal vasculitis. The five results chapters are adapted from studies written for publication, including a detailed introduction, methods, results and discussion. Lastly, **Chapter 8** summarised the findings in this thesis.

The work in **Chapter 3** was published in Frontiers in Cell and Developmental Biology.

The work in **Chapter 4** was published in Frontiers in Aging Neuroscience.

The work in **Chapter 5** was published in Journal of Ophthalmic Inflammation and Infection.

The work in **Chapter 6** was published in Retina.

The work in **Chapter 7** has been submitted to Ocular Immunology and Inflammation.

It is noteworthy that the shift between the topic from the ageing retinal disease in Chapter 3-4 and inflammatory retinal disease in Chapter 5-7 is the result of the supervisor's departure at the end of the second year of my PhD. The Postgraduate Research Team of the University of Liverpool acknowledges the shift of the topic. However, I believe this thesis has elaborated on utilising state-of-the-art data analysis in both preclinical and clinical data for retinal diseases.

# Chapter 3 Integrated microarray and RNAseq transcriptomic analysis of retinal pigment epithelium/choroid in age-related macular degeneration

In this chapter, I present my study that was published in Frontiers in Cell and Developmental Biology.

Dhirachaikulpanich, D., Li, X., Porter, L.F., and Paraoan, L. (2020). Integrated Microarray and RNAseq Transcriptomic Analysis of Retinal Pigment Epithelium/Choroid in Age-Related Macular Degeneration. *Front Cell Dev Biol* 8, 808.

This chapter reports for the first time an integrated transcriptomic analysis of RPE/choroid dysfunction in AMD (mixed stages) based on combining data from publicly available microarray (GSE29801) and RNAseq (GSE135092) datasets aimed at increasing the ability and power of detection of differentially expressed genes and AMD-associated pathways. The analysis approach employed an integrating quantitative method designed to eliminate bias among different transcriptomic studies. The analysis highlighted 764 meta-genes (366 downregulated and 398 upregulated) in macular AMD RPE/choroid and 445 meta-genes (224 downregulated and 201 upregulated) in non-macular AMD RPE/choroid. Of these, 731 genes were newly detected as differentially expressed (DE) genes in macular AMD RPE/choroid and 434 genes in non-macular AMD RPE/choroid compared with controls. Over-representation analysis of KEGG pathways associated with these DE genes mapped revealed two most significantly associated biological processes in macular RPE/choroid in AMD, namely the neuroactive ligand-receptor interaction pathway (represented by 30 DE genes) and the extracellular matrix-receptor interaction signaling pathway (represented by 12 DE genes). Furthermore, protein-protein interaction (PPI) network identified two central hub genes involved in the control of cell proliferation/differentiation processes, *HDAC1* and *CDK1*.

Overall, the analysis provided novel insights for broadening the exploration of AMD pathogenesis by extending the number of molecular determinants and functional pathways that underpin AMD-associated RPE/choroid dysfunction.

## 3.1 Introduction

The pathogenesis of AMD, a leading cause of irreversible blindness in the world, is linked to degenerative changes in the retina, RPE and choroid. Major risk factors for AMD are advanced age, family history and smoking (Klein et al., 2007;Wang et al., 2007). At the cellular level, DNA damage, oxidative stress, inflammation, mitochondrial dysfunction, cellular senescence, abnormal metabolism and aberrant proteolysis contribute to AMD development (Kay et al., 2014;Wang et al., 2019;Blasiak, 2020). Located between the neuroretina and choriocapillaris, the RPE is a major tissue involved in pathogenesis sustaining retinal function through metabolite exchanges, protein secretion, phagocytosis of spent photoreceptor outer segments, and immune barrier function through interaction with Bruch's membrane, the basement membrane of the RPE (Strauss, 2005) (Sparrow et al., 2010). Impaired RPE function has been shown to precede photoreceptors' death in AMD, leading to progressive degeneration of the neuroretina. Accumulation of medium and large-size drusen, lipo-proteinaceous deposits found below the RPE's basement membrane (Mitchell et al., 2018) (Wang et al., 2019) (Blasiak, 2020) is a significant factor in AMD progression from early to the advance disease, evidenced by population-based cohorts (Klein et al., 2007) (Wang et al., 2007). The choriocapillaris, a vascular endothelium situated just beneath the RPE and Bruch's membrane provides nutrients and oxygenation to the RPE (Whitmore et al., 2015) and also represents a major site of age-related degenerative changes with reduced vascular endothelial density (Ramrattan et al., 1994), vulnerability to inflammation through the membrane attack complex with increasing age, together contributing to AMD (Mullins et al., 2014). However, to date the precise molecular mechanisms of AMD pathogenesis and progression from early to advanced stages are incompletely understood (Ardeljan and Chan, 2013). Significant amount of research in recent years has concentrated on the complement pathway and inflammatory processes, but new emerging treatments targeting only the complement pathway failed to improve clinical

outcomes in phase 3 trials (Mitchell et al., 2018). Clearly, an integrated research approach considering other contributing pathogenic mechanisms is needed to identify novel and viable therapeutic targets.

Transcriptomic data, gathered by microarray (Booij et al., 2009;Newman et al., 2012) (Whitmore et al., 2013), RNAseq (Whitmore et al., 2014;Kim et al., 2018) or very recently advanced scRNA-seq (Voigt et al., 2019;Orozco et al., 2020) studies provide a solid starting point for the study of the molecular determinants of RPE/choroid dysfunction in AMD (Morgan and DeAngelis, 2014;Tian et al., 2015). Publicly available transcriptomic datasets allow targeted analyses of specific cellular processes, pathways, and their interactions. To date, transcriptomic RPE/choroid analyses focused on topographic regions, specifically macular versus non-macular retinal regions, have revealed different transcription profiles in these regions associated with various macular dystrophies and degenerative retinal diseases, including Best disease, Stargardt's disease and retinitis pigmentosa (Whitmore et al., 2014;Ashikawa et al., 2017). However, identification of the causative differentially expressed genes between AMD and age-matched controls from individual experiments is far from conclusive to date, conceivably due to the relatively small sample sizes of many datasets often compounded by AMD phenotype heterogeneity within the datasets (early and advanced AMD, geographic atrophy (GA) and neovascular AMD samples) and further confounded by the transcriptomic characteristics of ageing biology (de Magalhaes et al., 2009;Whitmore et al., 2013;Orozco et al., 2020). This is reflected in the generally small overlap between differentially expressed genes from specific AMD datasets. Other confounding factors may also include different sample preparation methods, transcriptomic platforms and data analysis methods employed across different studies (Tian et al., 2015).

An integrating quantitative method of analysis of combined datasets can eliminate bias between transcriptomic studies and increase the power of detection of differentially expressed genes (Zhou et al., 2016;Brown et al., 2017;Ma et al., 2017;Alimadadi et al., 2020). Here, this chapter describes such an analysis approach applied to investigate different platforms of publicly available transcriptomic datasets of post-mortem human AMD RPE/choroid. The differential gene expression patterns, pathway analysis and networks of protein-protein interactions (PPI) were explored in the combined datasets.

## 3.2 Methods

### Data collection

Publicly available post-mortem human AMD RPE/choroid transcriptome datasets were accessed through the NCBI GEO and ArrayExpress databases combined with a literature review for individual datasets. The post-mortem human AMD RPE/choroid transcriptome data generated by microarrays and RNAseq were selected and filtered using the following criteria: (1) data published between January 2010 and February 2020; (2) complete gene expression data available (raw or normalized); (3) sample size equal or higher than 10 in each group (AMD and control); (4) original specimens divided into macular and non-macular samples. Only two datasets passed these criteria and were included in this analysis, the Genomic Spatial Event database (GSE) 135092 and GSE29801. GSE135092 originated from an RNAseq study performed by Illumina HiSeq2500. The respective gene expression data provided by this dataset was quantified by HTSeqGenie as reads per kilobase of gene model per million total reads (RPKM), then normalized by DESeq2 (Orozco et al., 2020). GSE29801 dataset originated from a study using the Agilent G4112F array, obtained after quality control, background subtraction and normalization as described by Newman et al., 2012.

**Data analysis**

To integrate the different study platforms, this analysis used the two-step conventional metanalysis approach described by Ma et al. (Ma et al., 2017) For each platform, individual analyses were performed separately using the appropriate and specific bioinformatics pipeline for the respective application (e.g. edgeR or DESeq2 or limma for RNAseq and limma for microarray). I then combined the p-values obtained, setting the statistical significance threshold for each gene based on the result of this combined p-value (Tseng et al., 2012). The combined p-value is widely used in meta-analysis statistics of differential expressed genes since it is simple and versatile – it was shown to be applicable to analysis of both multiple microarray datasets and combined microarray and RNAseq datasets (Tseng et al., 2012;Ma et al., 2017). This meta-analysis technique was very convincing as it was applied to detect more DE genes in other diseases, including dilated cardiomyopathy (Alimadadi et al., 2020), Alzheimer's disease (Su et al., 2019), tuberculosis (Wang et al., 2018b), rheumatoid arthritis (Badr and Hacker, 2019) and helminth infection (Zhou et al., 2016). The diagram of data processing is shown in **Figure 3.1**. The gene expression table from each individual dataset was annotated and analyzed by the web-based analysis tool Networkanalyst (https://www.networkanalyst.ca/) (Xia et al., 2014;Xia et al., 2015;Zhou et al., 2019). The identifiers (IDs) from different platforms (ENSEMBL gene IDs for RNAseq and probe IDs for microarrays) were converted to Entrez gene IDs. The log transformation by variance stabilizing normalization (VSN) in combination with quantile normalization was performed for microarray data. Similarly, RNAseq data were transformed to log2 counts per million by the log2 count procedure. Differential expression (DE) analysis of each study was performed by limma using adjusted p-value <0.05 from Benjamini-Hochberg's False Discovery Rate (FDR) (Ritchie et al., 2015). The reason to use Benjamini-Hochberg's FDR correction controls was that it was less stringent than the more conservative methods like Bonferroni correction, so the results would increase

statistical power and expect to discover more potential genes. The disadvantage was that this method also increased Type I errors. To make data comparable, the batch effect between studies was minimized using the ComBat algorithm and then examined by principal component analysis (PCA) (Figure 3.2-3.3) (Johnson et al., 2007). This approach standardises the gene expression data by minimising both additive and multiplicative batch effects. The batch effect removal algorithm (ComBat) was also beneficial in background noise reduction, through the removal of genes with totally absent expression in more than 80 per cent of samples whilst equally reducing the variability of gene expression levels between batches (Johnson et al., 2007;Zhou et al., 2016). Using Fischer's approach for meta-analysis, each study p-value was combined together using the formula below.

$$F_g = -2\sum_{s=1}^{s}\left(\ln(P_{gs})\right)$$

A calculated combined p-value for each gene was considered significant if lower than 0.05 (Fisher, 1992;Xia et al., 2015;Alimadadi et al., 2020). Here, the differential significant gene list obtained was called the meta-gene.

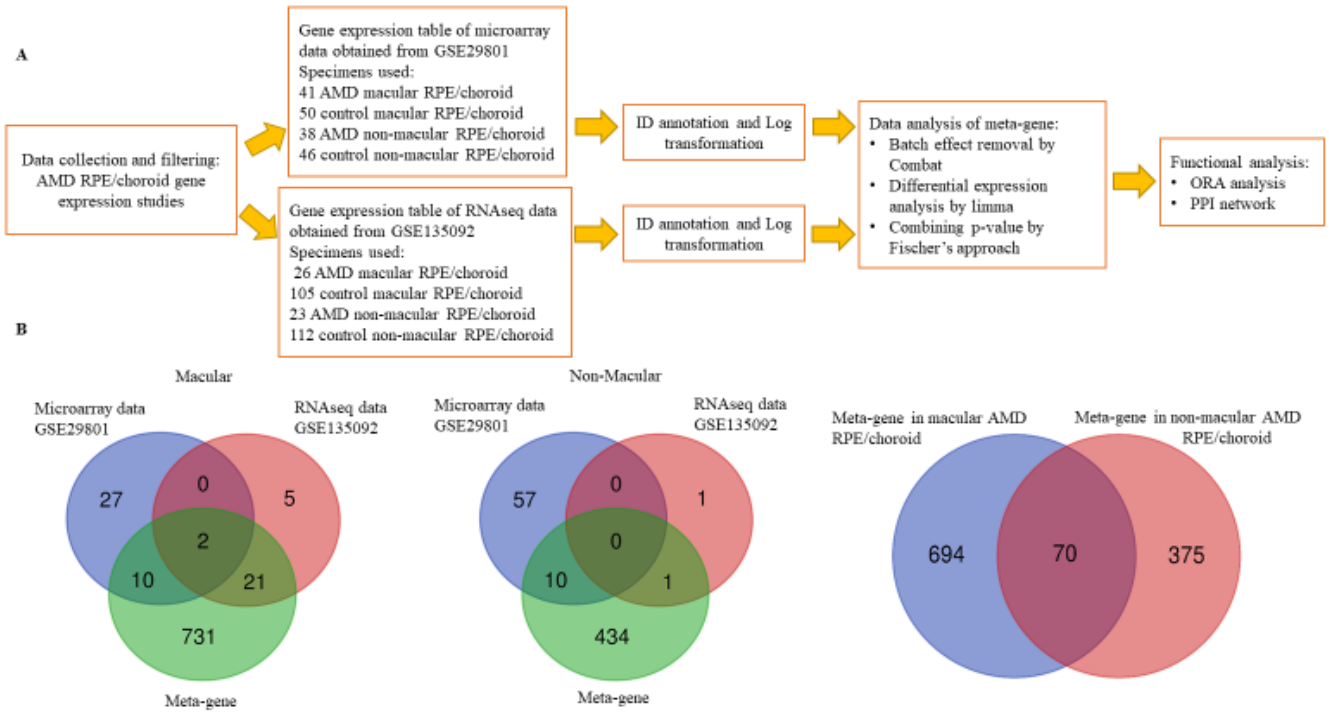


**Figure 3.1 Data processing workflow and common genes between the datasets analyzed.** (A) Data processing workflow; (B) Venn diagram showing the overlap of differentially expressed genes identified by microarrays, RNAseq and meta-gene in macular and non-macular locations of RPE/choroid in AMD.

### Data interpretation and functional analysis

The resulting meta-gene list was compared with the original DE gene list in each of the original studies. To identify significant pathways from the meta-gene list, over-representation analysis (ORA) was performed using Kyoto Encyclopedia of Genes and Genomes (KEGG) and p-values were adjusted by Benjamini-Hochberg's False Discovery Rate (FDR). A protein-protein interaction (PPI) network was constructed based on STRING database (Szklarczyk et al., 2019) and then visualized by a web-based tool (https://www.networkanalyst.ca/) (Xia et al., 2014;Xia et al., 2015;Zhou et al., 2019). Hub nodes were identified by high degrees and

high centrality from the PPI network. The results were then compared with the network constructed by WEB-based GEne SeT AnaLysis Toolkit (Zhang et al., 2005;Wang et al., 2013) (Wang et al., 2017;Liao et al., 2019).

### 3.3 Results

#### RPE/choroid AMD transcriptomic datasets

Five post-mortem human RPE/choroid AMD transcriptome studies were identified through the literature review: two microarrays studies, one RNAseq, one scRNAseq and a recent study using both RNAseq and scRNAseq (**Table 2.2**). All of these datasets were accessible through the NCBI GEO database but only two fulfilled the study's inclusion criteria, as follows. The dataset GSE29801 was generated by a study using Agilent Whole Human Genome 4 × 44K *in situ* oligonucleotide array platform (G4112F array) (Newman et al., 2012). This bulk microarray dataset was derived from RPE/choroid samples isolated from human donor eyes, which were obtained from the University of Iowa and the Lions Eye Bank of Oregon. However, it is worth noting that this dataset lacks comprehensive clinical information and the only quality control mentioned in the publication was RNA integrity analysis. In this study eyes with either a clinical or pathological diagnosis of AMD and with age ranging from 43 to 101 years were analyzed making use of 41 AMD macular RPE/choroid specimens (9 advanced AMD, 16 intermediate, 10 early and 6 undefined stage using the AREDS classification), 50 control macular RPE/choroid specimens, 38 AMD non-macular RPE/choroid specimens (9 advanced, 14 intermediate, 9 early and 6 undefined stage) and 46 control non-macular RPE/choroid specimens. The GSE135092 dataset was provided by an RNAseq study of eyes with a clinical diagnosis of AMD using the AREDS classification and ages ranging from 59 to 98 years, performed using the Illumina HiSeq2500 platform (Orozco et al., 2020). Post-mortem human eyes were processed by the Florida Lions Eye Institute for Transplant and Research. The study

analyzed 26 AMD macular RPE/choroid specimens (mixed advanced stages), 105 control macular RPE/choroid specimens, 23 AMD non-macular RPE/choroid specimens and 112 control non-macular RPE/choroid specimens (**Figure 3.1**). The limitation of using this RNA-seq dataset was the mixture of advanced stages of AMD samples, including GA and neovascular AMD.

**Meta-gene dataset**

The DE genes identified as a result of the combined analysis are referred to as meta-genes. DE genes were analyzed by integration of the two selected datasets through Networkanalyst web-based software. Initial analysis of individual datasets by limma with an FDR<0.05 found only 10 DE genes in macular and 57 DE genes in non-macular AMD RPE/choroid. To further interrogate the differences between AMD and control RPE/choroid, a more sensitive method involving Fischer's approach was then applied to the integrated data. After data normalization and batch effect adjustment, the PCA plot did not show major differences between studies, which indicated that the batch effect was reduced between the two studies (**Figures 3.3 and 3.3**).

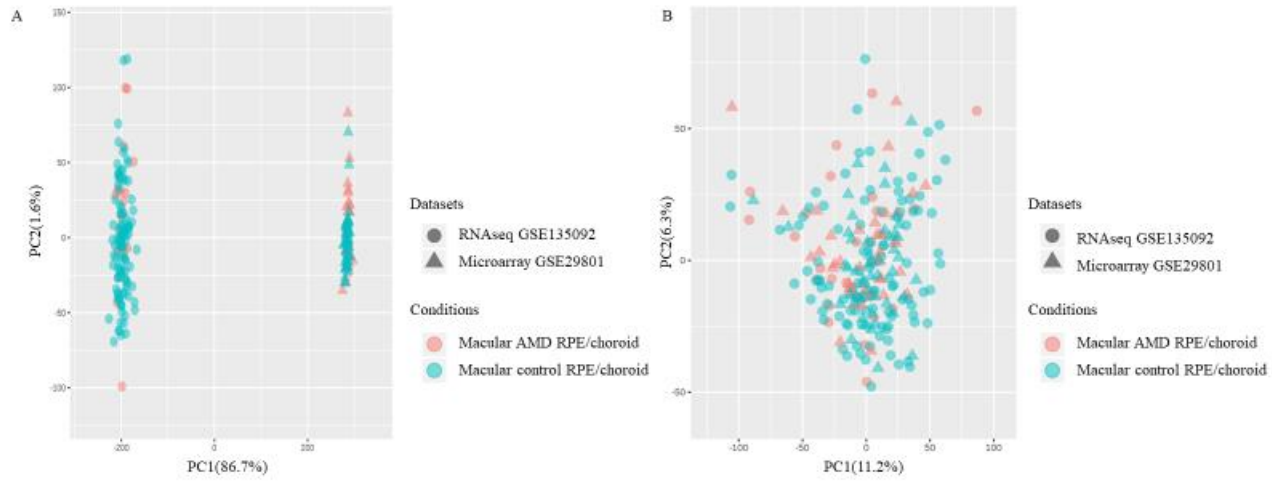


**Figure 3.2 PCA plot of macular AMD RPE/choroid versus control RPE/choroid representing the datasets** (A) before and (B) after applying ComBat algorithm

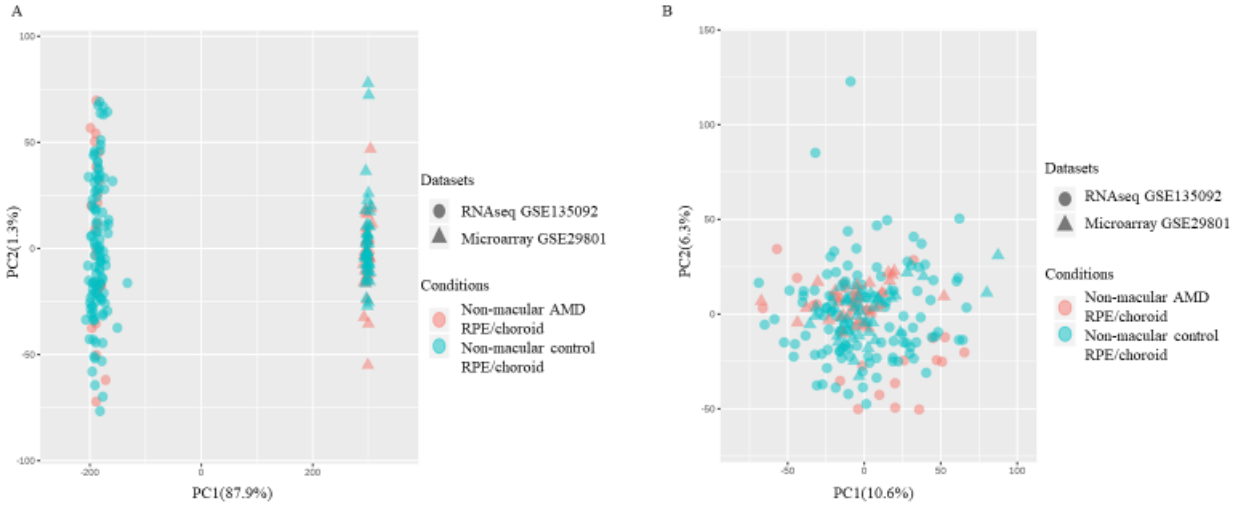


**Figure 3.3 PCA plot of non-macular AMD RPE/choroid versus control RPE/choroid representing the datasets** (A) before and (B) after applying ComBat algorithm

By using Fisher's approach for combining p-value, 764 significant meta-genes (366 down-regulated and 398 up-regulated) were detected in macular AMD RPE/choroid and 445 meta-genes (244 down-regulated and 201 up-regulated) in non-macular AMD RPE/choroid By ranking the combined p-values, the top 20 significant genes in macular and non-macular AMD RPE/choroid, respectively, were obtained and shown in **Table 3.1**.

**Table 3.1 Meta-gene list showing top differentially expressed genes.**

**Differential expressed genes identified in macular AMD RPE/choroid vs macular control RPE/choroid**

| EntrezID | Gene symbol | $F_g$ | Combined p-value | Effect |
|---|---|---|---|---|
| 84624 | FNDC1 | -47.991 | 1.72E-05 | Up-regulated |
| 4060 | LUM | -46.502 | 1.75E-05 | Up-regulated |
| 131578 | LRRC15 | -40.042 | 0.00019 | Up-regulated |
| 5803 | PTPRZ1 | -38.086 | 0.00032 | Up-regulated |
| 9547 | CXCL14 | -38.22 | 0.00032 | Up-regulated |
| 8148 | TAF15 | -35.072 | 0.00102 | Up-regulated |
| 4804 | NGFR | -34.669 | 0.00109 | Up-regulated |
| 3381 | IBSP | -31.756 | 0.00272 | Up-regulated |
| 3371 | TNC | -31.912 | 0.00272 | Up-regulated |
| 1118 | CHIT1 | -31.852 | 0.00272 | Up-regulated |
| 1515 | CTSV | -31.612 | 0.00272 | Up-regulated |
| 84466 | MEGF10 | -31.106 | 0.00278 | Up-regulated |
| 2224 | FDPS | -31.247 | 0.00278 | Up-regulated |
| 6695 | SPOCK1 | -30.827 | 0.00287 | Up-regulated |
| 55827 | DCAF6 | 40.05 | 0.00019 | Down-regulated |
| 64093 | SMOC1 | 37.387 | 0.00039 | Down-regulated |
| 7066 | THPO | 31.517 | 0.00272 | Down-regulated |
| 1E+08 | OST4 | 31.747 | 0.00272 | Down-regulated |
| 2619 | GAS1 | 32.158 | 0.00272 | Down-regulated |
| 83473 | KATNAL2 | 31.124 | 0.00278 | Down-regulated |

**Differential expressed genes identified in non-macular AMD RPE/choroid vs non-macular control RPE/choroid**

| EntrezID | Gene symbol | $F_g$ | Combined p-value | Effect |
|---|---|---|---|---|
| 54108 | CHRAC1 | -40.355 | 0.00066 | Up-regulated |
| 10648 | SCGB1D1 | -36.412 | 0.00216 | Up-regulated |
| 64116 | SLC39A8 | -31.469 | 0.00826 | Up-regulated |
| 84656 | GLYR1 | -30.629 | 0.00826 | Up-regulated |
| 79095 | C9orf16 | -30.731 | 0.00826 | Up-regulated |
| 6422 | SFRP1 | -28.224 | 0.01414 | Up-regulated |
| 1974 | EIF4A2 | 32.756 | 0.0081 | Down-regulated |
| 58155 | PTBP2 | 30.667 | 0.00826 | Down-regulated |
| 400073 | C12orf76 | 31.225 | 0.00826 | Down-regulated |
| 146225 | CMTM2 | 29.187 | 0.0118 | Down-regulated |
| 65982 | ZSCAN18 | 29.314 | 0.0118 | Down-regulated |
| 23564 | DDAH2 | 29.244 | 0.0118 | Down-regulated |
| 115761 | ARL11 | 28.924 | 0.01223 | Down-regulated |
| 6404 | SELPLG | 27.816 | 0.01414 | Down-regulated |
| 84695 | LOXL3 | 27.903 | 0.01414 | Down-regulated |
| 8936 | WASF1 | 27.635 | 0.01414 | Down-regulated |
| 8675 | STX16 | 27.52 | 0.01414 | Down-regulated |
| 8803 | SUCLA2 | 27.535 | 0.01414 | Down-regulated |
| 54816 | ZNF280D | 28.257 | 0.01414 | Down-regulated |
| 3187 | HNRNPH1 | 27.798 | 0.01414 | Down-regulated |

The extent of overlap between meta-genes and original DE genes detected in each study is shown in the Venn diagrams in **Figure 3.1**. A higher degree of overlap was identified in macular AMD RPE/choroid, with *PRSS33* and *SMOC1* detected as common DE genes in all datasets. No overlap of DE genes was detected between all three groups of genes in non-macular AMD RPE/choroid. Thirty-one genes were common between the microarray or RNAseq datasets, and the meta-genes of macular AMD RPE/choroid, while 11 common genes were detected in non-macular AMD RPE/choroid. In this analysis, 731 genes were newly detected as DE genes in macular and 434 genes in non-macular AMD RPE/choroid. Among the meta-genes, 70 genes were similarly differentially expressed in both macular and non-macular AMD RPE/choroid.

Furthermore, because AMD samples in GSE135092 consisted of mixed advanced stages of AMD (GA and neovascular AMD), and samples in GSE29801 consisted of advanced stages (GA and neovascular AMD), intermediate, and early stage of AMD, I performed subgroup analysis combining each AMD stage subgroup (early, intermediate, "mixed" advanced AMD) from GSE29801 with all GSE135092 samples. Interestingly, the presence of advanced AMD predominantly influenced the expression of genes included in the 764 meta-genes identified as DE in macular RPE/choroid, a stepwise reducing trend identified in intermediate then early stage of AMD, respectively (**Figure 3.4**). However, to maximize the number of samples and therefore power in this analysis, we used the meta-genes from all RPE/choroid samples in further downstream analyses.

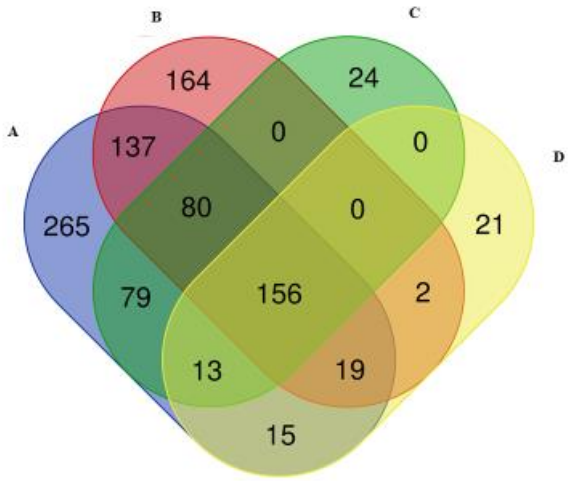


**Figure 3.4 Venn diagram showing the overlap of differentially expressed genes identified by subgroup analysis in macular locations of RPE/choroid in AMD.**

(A) Meta-gene of Microarray data (mixed stages of AMD) + RNAseq data

(B) Meta-gene of Microarray data (only advanced AMD) + RNAseq data

(C) Meta-gene of Microarray data (only intermediate AMD) + RNAseq data

(D) Meta-gene of Microarray data (only early AMD) + RNAseq data

**KEGG pathway analysis**

To interrogate the functional significance of meta-genes, over-representation analyses (ORA) of KEGG pathways were applied to both macular and non-macular meta-genes identified. Applying FDR<0.05, the interactions with the neuroactive ligand-receptor and the extracellular matrix (ECM)-receptor interaction pathways were statistically significant in macular AMD RPE/choroid, while there was no statistically significant pathway identified in non-macular AMD RPE/choroid. **Table 3.2** shows the top 5 KEGG pathways and meta-genes in each pathway found in macular and non-macular AMD RPE/choroid.

**Table 3.2 ORA analysis showing top KEGG pathways involving the meta-genes.**

| Macular AMD RPE/choroid vs macular control RPE/choroid | | | |
|---|---|---|---|
| **Pathway** | **p-value** | **FDR** | **Differential expressed gene (Gene symbol)** |
| Neuroactive ligand-receptor interaction | 0.000126 | 0.0297 | CHRNA1;GRIA1;OXTR;GABRB1;NPFFR1;SCT; GRIK3;ADRA1D;TRH;HTR2A;GRPR;ADRA1A; C5;P2RY2;PENK;LEPR;BDKRB2;BDKRB1;GABRE; PTGDR;CHRNB4;EDN3;GCGR;NPY1R;GRIN2C; GABRG3;MTNR1A;ADRB3;MC5R;RLN3 |
| ECM-receptor interaction | 0.000187 | 0.0297 | COMP;RELN;IBSP;ITGB4;ITGA3;TNC;SPP1; COL6A3;COL9A3;COL9A2;THBS2;THBS4 |
| AMPK signaling pathway | 0.000626 | 0.0664 | SREBF1;CAB39L;IRS2;PPP2R3A;FOXO3;EEF2; ADRA1A;G6PC2;PFKL;SCD;FASN;LEPR;PPARG;PCK2 |
| Wnt signaling pathway | 0.00126 | 0.0999 | APC2;CAMK2B;MMP7;FZD9;WNT9B;CACYBP; DKK1;DKK2;SFRP1;SFRP2;APC;TBL1XR1;BAMBI; RSPO3;GPC4;LGR5 |
| Fatty acid metabolism | 0.0018 | 0.102 | ELOVL3;FASN;ACAT2;FADS2;HADHB;HSD17B4; SCD;FADS1 |
| **Non-macular AMD RPE/choroid vs non-macular control RPE/choroid** | | | |
| **Pathway** | **p-value** | **FDR** | **Differential expressed gene (Gene symbol)** |
| Choline metabolism in cancer | 0.00445 | 0.363 | WASF1;WAS;PLA2G4C;AKT2;PIK3R3;DGKH;MAPK10 |
| Regulation of actin cytoskeleton | 0.00495 | 0.363 | WASF1;DIAPH2;WAS;TMSB4X;ITGA3;SPATA13; PIK3R3;ITGA6;ITGAE;ARHGEF7;FGD3 |
| Osteoclast differentiation | 0.00511 | 0.363 | OSCAR;IFNAR1;TYROBP;AKT2;PIK3R3;TGFB2; MAPK10;LCK |
| Influenza A | 0.00796 | 0.363 | HLA-DRB5;DNAJB1;IFNAR1;XPO1;AKT2;IL18; PIK3R3;PYCARD;IFNA10 |
| Hypertrophic cardiomyopathy (HCM) | 0.00836 | 0.363 | PRKAB2;ITGA3;ITGA6;TGFB2;CACNA1C;DAG1 |

Among the identified significant genes associated with the neuroactive ligand-receptor interaction, 13 genes were found down-regulated in macular AMD RPE/choroid including *ADRA1A, LEPR, PENK, SCT, BDKRB1, ADRB3, PTGDR, BDKRB2, RLN3, C5, EDN3, GABRE* and *NPY1R*. *LEPR* or Leptin Receptor Factor was the second highest significant down-regulated gene. LEPR was initially identified as a satiety factor, but was subsequently shown to play a role in normal ageing and neuroprotective processes (Gorska et al., 2010;Seshasai et al., 2015;Wauman et al., 2017). Other genes upregulated in the neuroactive ligand-receptor interaction pathway included *GRIK3, GRPR, CHRNA1, ADRA1D, OXTR, NPFFR1, P2RY2, MC5R, GABRB1, GRIA1, TRH, GCGR, MTNR1A, HTR2A, GRIN2C, CHRNB4* and *GABRG3*. All 12 significant genes associated with the ECM-receptor interaction pathway were upregulated in macular AMD RPE/choroid, with a distinct sub-pathway represented by a group of collagen genes including *COL6A3, COL9A3* and *COL9A2*. The most statistically significant gene in the ECM group was *TNC* or Tenascin C, which encodes a key ECM component in the nervous system altered in various eye diseases (Kobayashi et al., 2016b). Tenascin C also plays a role in inflammation process by regulating transforming growth factor β (TGFβ) (Reinhard et al., 2017). Noteworthy, *TGFB2* gene, an isoform of TGFβ, was also identified as up-regulated in both macular and non-macular meta-gene lists. Although not reaching statistical significance in this analysis, the fatty acid metabolism pathway was also among the enriched pathways in macular AMD RPE/choroid. Remarkably, all meta-genes associated with this pathway, consisting of *ELOVL3*, *FASN*, *ACAT2, FADS2*, *HADHB, HSD17B4, SCD* and *FADS1*, were not differentially expressed in non-macular AMD RPE/choroid.

**PPI network analysis**

Since the macula is the primary anatomical area affected in AMD, I sought to get more insight into the genes differentially expressed in macular AMD RPE/choroid by further exploring them by through a PPI network. For this purpose, a PPI network was constructed using STRING database and Networkanalyst web-based tools, with the input of 764 significant genes from macular AMD RPE/choroid meta-gene list. Initially, a first order network created an extensive network comprising 1718 nodes and 2578 edges. To improve the clarity of the network and obtain more important nodes, I created a zero order PPI network (**Figure 3.5**). This network contains 14 nodes with the highest degree of 7. Two downregulated genes with the highest degrees and high centrality were Histone Deacetylase 1 (*HDAC1*) and Cyclin-dependent kinase 1 (*CDK1*). HDAC1 and CDK1 are both cell cycle regulators (Goder et al., 2018) suggesting altered cell proliferation responses in macular AMD RPE/choroid. I also input these 764 DE genes in AMD macular RPE/choroid into the WEB-based pathway analysis tool "GEne SeT AnaLysis Toolkit". GEne SeT AnaLysis Toolkit constructs networks by using Network Topology-based Analysis method and used PPI BIOGRID as its reference list (Liao et al., 2019). The result revealed HDAC1 and CDK1 among the top five per cent of these genes when ranked by random walk probability.

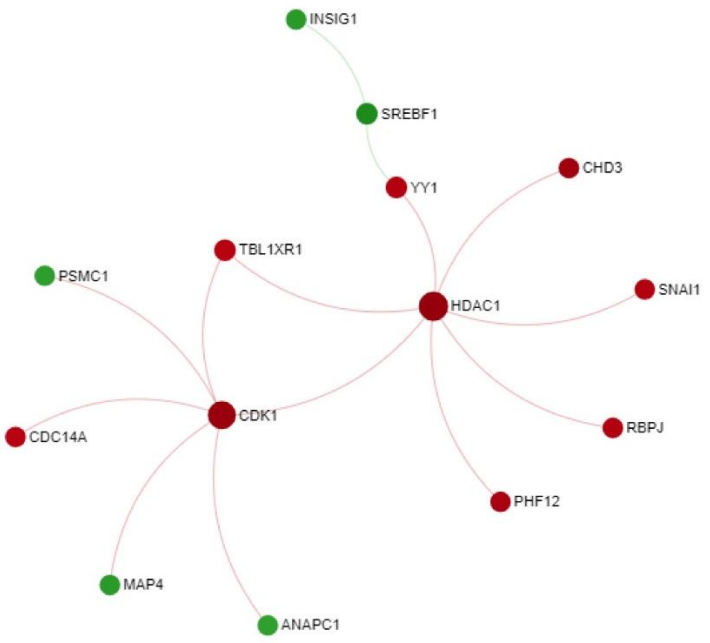


**Figure 3.5 Zero order PPI network of meta-gene in macular AMD RPE/choroid.**

Downregulated nodes in red; upregulated nodes in green.

### 3.4 Discussion

The increasing microarray and RNAseq transcriptomic datasets available provide an important resource for exploring, at a molecular level, the pathogenic machinery of AMD through bioinformatics approaches (Morgan and DeAngelis, 2014;Tian et al., 2015). However, analysis of individual AMD transcriptomic datasets with conventional statistical approaches may not enable comprehensive identification of DE genes and pathways in functionally impaired RPE/choroid. For example, the microarray analysis undertaken by Whitmore et al. (2013) concluded that there were no significantly DE genes when FDR was applied to the respective AMD RPE/choroid dataset. Similarly, the RNAseq analysis described by Orozco et al. (2020) also highlighted less than 30 putative causal genes for AMD RPE/choroid. Analysis approaches combining different transcriptomic datasets obtained from different platforms were recently used to detect more DE genes in various diseases, such as dilated cardiomyopathy

(Alimadadi et al., 2020), Alzheimer's disease (Su et al., 2019), tuberculosis (Wang et al., 2018b), rheumatoid arthritis (Badr and Hacker, 2019) and helminth infection (Zhou et al., 2016). My integrated analyses expand the number of specimens analyzed and are also well suited for AMD, given the multifactorial nature of the disease.

Here, I report an analysis of normal and AMD RPE/choroid transcriptome data performed by integrating microarray and RNAseq datasets employing the web-based tool Networkanalyst (Xia et al., 2015) with Fischer's method (Fisher, 1992;Alimadadi et al., 2020). This analysis extended the number of statistically significant differentially expressed RPE/choroid genes in AMD from 2 to 764 in macular RPE/choroid, and from 0 to 445 in non-macular AMD RPE/choroid. The resulting meta-genes identified as significantly differentially expressed in macular AMD RPE/choroid in comparison with normal RPE/choroid highlighted two significantly enriched pathways of potential functional importance in AMD pathogenesis, the neuroactive ligand-receptor interactions and extracellular matrix (ECM)-receptor interactions.

The most significant pathway in macular AMD RPE/choroid, the neuroactive ligand-receptor interactions had a FDR equal to 0.0297 by ORA analysis. This pathway regulates multiple neuroreceptors and their associated distant signaling molecules such as leptin, thyrotropin releasing hormone (TRH) and epinephrine (Biernacka et al., 2013;Kanehisa et al., 2016). It was previously shown to be functionally significant in neurotransmitter-mediated disorders such as alcohol dependence disorder (Biernacka et al., 2013), autism spectrum disorders (Wen et al., 2016), Parkinson's disease (Hardy, 2010;Hamza et al., 2011;Kong et al., 2015), as well as some types of lung cancer (Ji et al., 2018). My analysis suggested that 30 genes associated with this pathway may be linked to AMD, including *LEPR*, a receptor of leptin, which was initially identified in adipocytes (Gorska et al., 2010). Noteworthy, decreased serum leptin was

observed in AMD patients in a case-control study and leptin was hypothesized to have a neuroprotective function and to lower the risk of AMD by removing extracellular β-amyloid in drusen deposits, decreasing triglyceride fatty acid synthesis and downregulating genes such as lipogenic enzyme, oxidative stress and inflammation related genes (Seshasai et al., 2015;Wauman et al., 2017). My integrated data analysis identified the downregulation of leptin receptor in macular RPE/choroid in AMD for the first time. Cholinergic Receptor Nicotinic Alpha 1 Subunit (*CHRNA1*) and Cholinergic Receptor Nicotinic Beta 4 Subunit (*CHRNB4*), encoding two of the twelve gene subunits of the nicotinic acetylcholine receptor (Conti-Fine et al., 2000;Barrie et al., 2017), were found upregulated among the AMD meta-genes. The increased expression of these genes is associated with higher risk of lung cancer in smokers as the binding of the receptor by nicotine can stimulate angiogenesis especially within a context of inflammation and tumorigenesis (Yoo et al., 2014). The upregulation of *CHRNA1* and *CHRNB4* in AMD RPE/choroid may underlie one mechanism that contributes to the increased risk of AMD in smokers. Thyroid releasing hormone (TRH) has a central role in the thyroid hormone pathway that is found abnormal in some AMD patients. (Gopinath et al., 2016;Yang et al., 2018;Ma et al., 2020a). My analysis also suggested that TRH, another gene linked to the neuroactive ligand receptor pathway, is upregulated in the AMD RPE/choroid.

Genes associated with the ECM-receptor interaction pathway in AMD, highlighted by my analysis, have previously been shown to have high variability of expression between individuals (Booij et al., 2009). The finding of multiple significantly upregulated genes associated with this pathway in AMD RPE/choroid underpins wound healing responses as putative pathophysiological mechanisms implicated in AMD (Newman et al., 2012). It was not surprising that the results of my analysis could predict the similar pathway as Newman because the Newman dataset was one of the two inputs in the current meta-analysis. However, it is

important to note that the Newman data may be limited by a lack of detailed pathology of post-mortem tissues and the fact that this microarray study was published 10 years ago. Nevertheless, since it represented the largest accessible dataset for transcriptomics that included various disease stages, its inclusion in the analysis was crucial.

Tenascin C, the most statistically significant differentially expressed gene in this ECM-receptor interaction pathway, can upregulate TGFβ and promote inflammatory processes (Reinhard et al., 2017), in line with the increased level of Tenascin C identified in surgically excised choroidal neovascular membranes (Nicolo et al., 2000) and observation of its secretion in neovascular AMD (Kobayashi et al., 2016b;Reinhard et al., 2017). Furthermore, although the fatty acid metabolism pathway was not found to be statistically significantly associated with AMD in my analysis, the finding that all differentially expressed genes in this pathway were found exclusively in macular RPE/choroid underlines the geographical differences in gene expression patterns between macular and non-macular RPE/choroid regions, previously suggested by Whitmore et al., 2014 and Ashikawa et al., 2017. Specific examples of genes with a macular pattern of differential expression were Fatty Acid Desaturase 1 (*FADS1*) and Fatty Acid Desaturase 2 (*FADS2*), genes encoding delta-5 and delta-6 desaturases, implicated in drusen formation in a recent study (Ashikawa et al., 2017). Hence, fatty acid metabolism abnormalities may contribute to drusen formation, an area of interest following the suggestion of secretion by the RPE of the lipid component of soft drusen, a hallmark of AMD progression (Curcio, 2018a).

The PPI network analysis highlighted two central hub genes involved in the control of cell proliferation/differentiation processes, *HDAC1* and *CDK1*. *HDAC1* encodes an isoform of histone deacetylase that is ubiquitously expressed and has a role in transcriptional repression

(Hassig et al., 1998). Modification of chromatin structure through histone deacetylation has been identified as a mechanism of epigenetic regulation associated with various neurodegenerative diseases (Anderson et al., 2015). HDAC family members are involved in multiple biological processes including angiogenesis, inflammation and cell cycle progression, all of which play an important role in the pathophysiology of AMD (Tang et al., 2013). Noteworthy in this respect are the findings from a comparative study of Alzheimer's disease and AMD donors that showed that *HDAC1, 2, 5,* and *6* expression decreased in the retina and frontal cortex of affected individuals (Noh et al., 2008). The other hub node identified, *CDK1* or cyclin-dependent kinase 1 plays an important role in the regulation of mitotic transition and phosphorylation of Bcl-2, Bcl-XL, and Mcl–1 proteins (Harley et al., 2010;Terrano et al., 2010). In the context of AMD, a retinal transcriptome analysis of senescence-accelerated OXYS rats revealed a possible role of CDK1 in the retinal extrinsic apoptotic processes associated with AMD. Specifically, the study associated the increased apoptotic activity with *CDK1*, which was identified as a hub gene for functional clusters associated with the MAPK and p53 signaling pathways in the interaction network constructed from the respective transcriptomic data (Telegina et al., 2015).

A limitation of this analysis is due to the paucity of samples representing the individual disease stage phenotypes and respective subgroup analyses of AMD (early, intermediate, advanced) in the original studies (**Figure 3.4**) resulting in reduced power and the ensuing application of pathway analyses on combined datasets of mixed disease stages. Thus the advanced AMD refers here to mixed advanced stages of AMD (both GA and neovascular AMD). Clearly, an increase in the clinical data available with postmortem RPE/choroid samples used in omic technologies could enable more detailed studies into the

pathophysiological processes particular to each stages of AMD highlighting key progression factors to target for further therapeutic intervention research (Handa et al., 2019).

In conclusion, integration of microarray data and RNAseq data allows transcriptomic analyses of increased power and identification of DE meta-genes in AMD RPE/choroid. Taking such an approach, this study suggested two novel pathways characterized by significant enrichment of DE genes in AMD RPE/choroid, namely the neuroactive-ligand receptor interaction pathway and the ECM-receptor interaction pathway. In addition, the PPI network analysis highlighted two hub nodes that may link apoptotic and angiogenesis pathological processes in AMD. The integrated functional analysis of DE genes in AMD also revealed genes previously linked to other neurodegenerative disease such as Alzheimer's disease and Parkinson's disease. The approach used to integrate publicly available transcriptomic datasets obtained through different experimental platforms provided a novel insight and broadened the exploration of a larger number of potential genes and functional pathways with roles in AMD pathogenesis.

## Chapter 4 Intercellular communication analysis of the ageing RPE and choroid

In this chapter, I present my study that was published in Frontiers in Aging Neuroscience.

Dhirachaikulpanich, D., Lagger, C., Chatsirisupachai, K., De Magalhães, J.P., and Paraoan, L. (2022). Intercellular communication analysis of the human retinal pigment epithelial and choroidal cells predicts pathways associated with aging, cellular senescence and age-related macular degeneration. *Front Aging Neurosci* 14, 1016293.

The RPE and the choroid are ocular tissues with fundamental roles in supporting neuroretinal function. The pathogenesis of AMD, a leading cause of irreversible blindness for which ageing is the highest risk factor is closely linked with progressive impairment of various functions of these tissues. Cellular senescence, marked by cell cycle arrest and secretion of proinflammatory factors, is known to be associated with ageing and has been proposed as a potential driver of AMD. Here, this chapter investigated the role played by intercellular communication in the RPE/choroid within the context of ageing, senescence and AMD. The analysis inferred cell-cell interactions in the RPE/choroid by applying CellChat and scDiffCom on a publicly available scRNA-seq dataset from three human donors with and without AMD. I identified age-regulated ligand and receptor genes by using limma on a separate publicly available bulk microarray dataset providing RPE/choroid samples at multiple time points. Cellular senescence was investigated by assigning a score to each cell and each sample of these scRNA-seq and microarray datasets, respectively, based on the expression of key signature genes determined by a previous senescence meta-analysis. I identified VEGF-, BMP- and tenascin-mediated pathways supporting some of the strongest cell-cell interactions between RPE cells, fibroblasts and choroidal endothelial cells and as strong intercellular communication

pathways related to both ageing and senescence. Their signalling strength was enhanced between subpopulations of cells having high senescence scores. Predominant ligands of these pathways were upregulated with age whereas predominant receptors were downregulated. Globally, I also observed that cells from AMD samples presented slightly bigger senescence scores than normal cells and that the senescence score positively correlated with age in bulk samples ($R = 0.26$, p-value$<0.01$). Hence, my analysis provides novel information on RPE/choroid intercellular communication that gives insights into the connection between ageing, senescence and AMD.

## 4.1 Introduction

AMD is the leading cause of irreversible blindness in adults in developed countries (Wong et al., 2014), which has been linked to numerous genetical and environmental risk factors and most importantly age (Group et al., 2012;Wong et al., 2014). However, the molecular mechanisms by which ageing contributes to AMD pathogenesis are far from being fully characterized. One hypothesis suggests cellular senescence of the RPE, the cell monolayer with essential role in supporting the function of the neuroretina, as a key process promoting the development of AMD (Kozlowski, 2012). Cellular senescence impairs the ability of self-renewal – a biological process that is particularly important for the mitotically inactive RPE – and contributes to an increased inflammatory phenotype, mostly through the secretion of inflammatory cytokines and proteases, collectively defined as the senescence-associated secretory phenotype (SASP) (Kozlowski, 2012;Wang et al., 2019;Basisty et al., 2020). Age-related factors like increased oxidative stress, altered proteostasis and DNA damage are thought to promote senescence in several age-related neurodegenerative diseases such as Alzheimer's disease and Parkinson's disease (Kritsilis et al., 2018;Martinez-Cue and Rueda, 2020). An increase in senescent cells in aged RPE and choroid tissues has also been reported (Chaum et al., 2015;Cabrera et al., 2016) consistent with altered cell signalling known to promote chronic inflammation and RPE cellular dysfunction (Cao et al., 2013). Senescent RPE cells likely influence neighbouring cells, potentially contributing to the development of AMD characteristics such as increased choroidal endothelial stiffness and membrane attack complex deposition (Cabrera et al., 2016;Lee et al., 2021). Although an ongoing effort is trying to connect ageing, cellular senescence and the pathogenesis of AMD, the molecular mechanisms underlying their relationship are still not well established (Blasiak et al., 2017;Sreekumar et al., 2020).

The RPE and the choroid form a system that plays crucial roles in the normal function of the neuroretina as well as in the pathology of AMD (Strauss, 2005). It supports the neuroretinal metabolism by supplying nutrients and facilitating the removal of waste. The junctional complex of the RPE is critical for the blood-brain barrier while the tissue itself acts as a secretory machinery to support the communication between the choroid and the retina (Paraoan et al., 2020). During AMD, lipoproteinaceous and other extracellular debris accumulate between the RPE and the choroid, leading to the formation of drusen (Ardeljan and Chan, 2013). Previous research investigating how this system ages focused on the RPE or the choroid alone (Paraoan et al., 2000;Kay et al., 2013;Kay et al., 2014;Porter et al., 2019;Sharif et al., 2019;Voigt et al., 2019;Dhirachaikulpanich et al., 2020a;Voigt et al., 2020;Butler et al., 2021;Saptarshi et al., 2021). However, given that the RPE/choroid system is a complex microenvironment composed of many cell types functioning together, including RPE cells, endothelial cells, fibroblasts and immune cells (Voigt et al., 2021;Voigt et al., 2022), the communication between the cellular components of the RPE/choroid needs also to be characterised.

The advent of scRNA-seq and the development of cell-cell communication software now enables the investigation of the interactions between different cell types in a tissue (Armingol et al., 2021). In this context, intercellular communication (ICC) is defined as a set of signalling interactions involving secreted proteins (ligands) from one cell type and membrane-bound proteins (receptors) from another (or the same) cell type (Jin et al., 2021). Inferring such intercellular communication patterns, including secreted protein crosstalk and extracellular matrix receptor interactions, could prove useful to identify key signalling pathways in normal and disease conditions (Armingol et al., 2021;Jin et al., 2021). This type of analysis has been applied to a variety of diseases, including COVID-19 (He et al., 2021;Yang

et al., 2021), wound healing (Hu et al., 2021), inflammatory bowel disease (Corridoni et al., 2020). However, no study has yet investigated intercellular communication of the RPE/choroid in the context of ageing, senescence and AMD. For this purpose here I leveraged publicly available microarray and scRNA-seq datasets of the RPE/choroid to investigate cell-cell signalling altered by ageing and senescence in normal and AMD tissues. My analysis predicts three specific age-related pathways (VEGF, BMP and tenascin) that are enriched in interactions taking place between a set of fibroblasts, RPE cells and endothelial cells characterized by high expression of senescence signature genes.

## 4.2 Methods

### Single-Cell RNA-seq Data Acquisition and Processing

I retrieved publicly available scRNA-seq RPE/choroid data (GSE135922) containing samples from three human donors, including two normal eyes and one uncharacterised neovascular AMD eye (Voigt et al., 2019). This dataset was downloaded as a Seurat object through the human cell atlas galaxy portal (Moreno et al., 2020;Papatheodorou et al., 2020). The subsequent analysis was done in R (version 4.0.2). Cells were filtered out if they had unique gene counts lower than 300 or more than 7000. Log normalisation was performed with a scale factor of 10,000 using Seurat (version 4.0.1). The Seurat functions FindNeighbors and FindClusters were used to cluster the cells based on the first 10 principal components returned by the function RunPCA. For visualization purposes, UMAP dimensional reduction was performed with the function RunUMAP using the same 10 principal components (Hao et al., 2021). The gene markers' identifier of each cell cluster was done with the function FindAllMarkers. These markers were used to annotate each cluster by cell types similarly to Voigt et al. (Voigt et al., 2019).

**Intercellular Communication Analysis**

Intercellular communication (ICC) analysis was performed on the pre-processed Seurat object described above with two R packages relying on different detection methods: CellChat (Jin et al., 2021) and scDiffCom (Lagger et al., 2021). Both algorithms combine the cell type-specific expression of known ligand and receptor genes with permutation tests to assess the biological relevance of potential cell-cell interactions (CCIs). They differ in the way they quantify the strength of these interactions (respectively referred to as "communication probability" and "CCI score") and in their internal statistical implementations. scDiffCom was also specifically designed to perform differential ICC analysis between biological conditions, but this functionality was not used in the current study because of the low sample size of the aforementioned scRNA-seq dataset. Default settings of CellChat (version 1.0.0) were used as recommended (Jin et al., 2021). scDiffCom (version 0.2.3) was used in "detection-mode-only" with default parameters, except for the number of permutations that was set to 10,000 (instead of 1000) and the "quantile expression threshold" that was set to 0 (instead of 0.2). The latter parameter is used by scDiffCom to filter out statistically significant but lowly expressed CCIs. As such filtering is not performed by CellChat by default, it was disabled in this analysis to obtain more similar results. Detection of CCIs by both packages crucially depends on the prior database of curated ligand-receptor interactions (LRI) they rely on. Such LRIs can be pairs of genes (e.g. AMD:CALCR) or include additional factors to describe heteromeric complexes (e.g. ANGPT2:ITGA1-ITGB1). CellChat manually created a curated list of 1939 human LRIs principally based on knowledge extracted from the KEGG database (Kanehisa et al., 2016). However, scDiffCom relies on a larger collection of 4785 LRIs obtained by combining seven LRI databases that had been manually curated by previous studies, including CellChat itself. Therefore, scDiffCom has the potential to detect more CCIs than CellChat.

Network analysis to compute centrality scores of outgoing, incoming or mediator communication pathways was performed with CellChat built-in function netAnalysis_computeCentrality. The determination of the dominant and most relevant pathways was performed by exploring and comparing network results manually and by using either visualization tools provided by CellChat (e.g. netAnalysis_signalingRole_network) or custom scripts for scDiffCom results.

**Differential Analysis of Ligand/Receptor Genes in Ageing RPE/Choroid Microarray**

Transcriptomic microarray data were retrieved from GSE29801 (Newman et al., 2012). This dataset contained 96 post-mortem RPE/choroid samples with no previous ocular disease. The donors' age ranged from 9 to 93 years old. I identified genes differentially expressed with age using the R package limma (Ritchie et al., 2015) with the linear model indicated below,

$$Y_{ij} = \alpha Age_i + \beta Sex_i + \gamma Macular/non\text{-}Macular_i + \varepsilon_{ij}$$

In this regression model, $Y_{ij}$ is the expression level of gene j in sample i; $Age_i$ denotes the age of sample i; $Sex_i$ denotes the sex of sample i and $Macular/non\text{-}Macular_i$ denotes the anatomical location of RPE/choroid of sample i.

The genes were filtered to include only factors relevant to intercellular communication. As a reference, the list of the genes was used from the LRI database of scDiffCom (that also includes those from CellChat, as explained above). Age-associated differential expression was considered significant for adjusted p-values (Benjamini-Hochberg) less than 0.1 and absolute $\log_2$ fold change bigger than $\log_2(1.5)/70$years.

**Senescence Gene Expression and Intercellular Communication Analysis**

I scored each cell from the scRNA-seq dataset and each sample from the microarray dataset in relation to the level of expressed senescence signature genes. Such signatures were obtained from a recent meta-analysis that identified genes up- and down-regulated with senescence across 20 microarray datasets (Chatsirisupachai et al., 2019). This dataset provided 1232 senescence signature genes. As recommended in the GSEA user guide to limit gene set within 500 genes (Hanzelmann et al., 2013), I selected only genes with a q-value from the meta-analysis less than 0.001, and obtained 135 upregulated and 271 downregulated genes. The senescence score was defined as follows:

Senescence score = upregulated GSEA score – downregulated GSEA score,

where each term corresponds to a gene set enrichment analysis (GSEA) score computed either on each cell or sample (ssGSEA) using the upregulated, respectively downregulated, senescence signatures as gene sets. The assumption underlying this score was that if a sample exhibits senescence, it might share similar gene expression patterns with previously identified senescence-related gene expressions from meta-analysis. However, a limitation of scoring using the ssGSEA method was that it may not prioritise genes that had a greater influence on this pathway because each gene was scored equally. ssGSEA scores were computed from the scRNA-seq Seurat object described above by using the function enrichIt from the R package escape (version 1.1.1) (Borcherding et al., 2021). ssGSEA scores for microarray samples were computed using the R package gsva (version 1.38.2) (Hanzelmann et al., 2013).

## 4.3 Results

### Inferring Intercellular Communication in the RPE/Choroid

To initiate the analysis of the intercellular communication occurring at the level of the RPE and choroid, I used RPE/choroid scRNA-seq data from the publicly available dataset GSE135922 (Voigt et al., 2019) that had been obtained from post-mortem tissues of 3 donors, including one patient with neovascular (wet) AMD and two non-AMD patients (**Figure 4.1 A**). Following standard pre-processing (see Methods), I annotated 4,766 cells based on previously reported cell-type-specific marker genes as follows: fibroblasts (APOD), melanocytes (PMEL), lymphocytes (CXCR4), Schwann cells (PLP1), RPE (RPE65), macrophages (IGKC), endothelial cells (VWF) and mast cells (TPSB2) (**Figure 4.1 B-E**). My annotation is similar to the original work from Voigt et al. (Voigt et al., 2019), although they have described more specific clusters such as subpopulations of Schwann cells and lymphocytes that are not relevant to my current study. I next applied the CellChat algorithm to the healthy and AMD samples separately and detected 3600 and 3430 cell-type to cell-type interactions (CCIs), respectively. As it has been recently pointed out that different intercellular communication algorithms might be prone to returning different results (Dimitrov et al., 2021;Dimitrov et al., 2022), I with the help of Dr Cyril Lagger also used a second package, scDiffCom, to further confirm CellChat findings. When using the same prior LRI database as CellChat, scDiffCom returned 2597 and 2081 CCIs in normal and AMD samples, respectively. Out of those, 2274 and 1827 CCIs, respectively, were commonly detected by both packages, indicating that the scDiffCom algorithm is generally more conservative. As expected, when using its extended curated database including more LRIs than those present in CellChat, scDiffCom returned significantly more CCIs, namely 8629 and 7176 respectively. The detected interactions provide a global atlas of intercellular communication in the human RPE/choroid. Although I considered normal

and AMD tissues separately, I note that a sample size of only three patients was not large enough to perform a complete differential ICC analysis.

A

| Sample | Age [years] | Sex | Disease |
|---|---|---|---|
| 1 | 54 | M | Normal |
| 2 | 82 | F | Normal |
| 3 | 79 | M | wet AMD |

B

| Cell type | Count | Percentage |
|---|---|---|
| fibroblast | 1766 | 37.1 |
| melanocyte | 902 | 18.9 |
| lymphocyte | 615 | 12.9 |
| Schwann cell | 526 | 11.0 |
| RPE | 415 | 8.71 |
| macrophage | 267 | 5.60 |
| endothelial | 217 | 4.55 |
| mast cell | 58 | 1.22 |

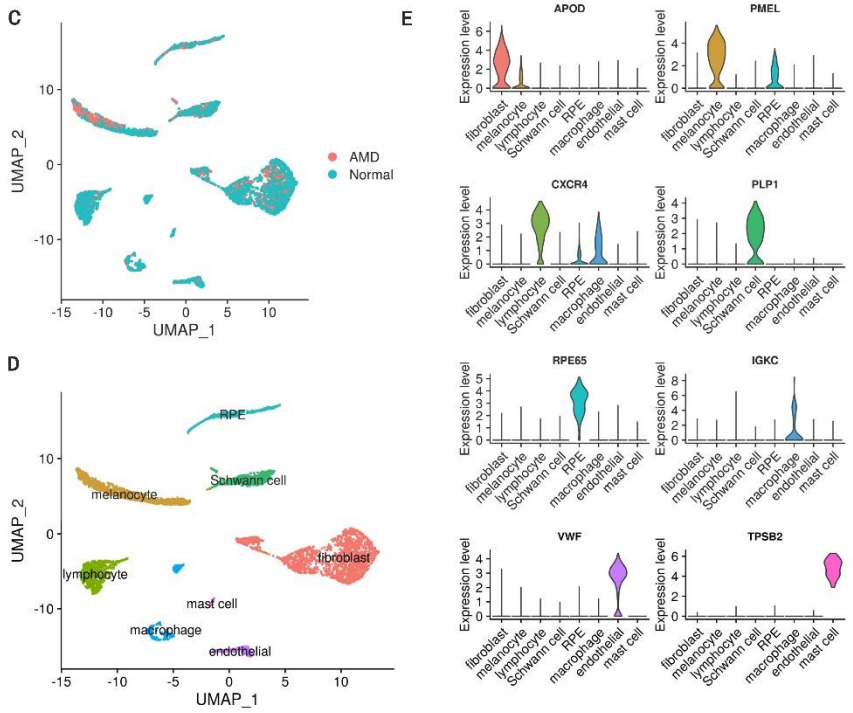


**Figure 4.1 Summary of the RPE/choroid scRNA-seq dataset used for cell-cell communication analysis**

(A) Demographic data including disease status of 3 RPE/choroid donors from GSE135922. (B) Count and percentage of each specific cell type detected from the 4,766 cells of the scRNA-seq data. (C-D) Dimensionality reduction (UMAP) of the scRNA-seq data showing eight cell types in the RPE/choroid. (C) Cells are colored by disease status (normal or AMD). (D) Cells are colored by cell-type annotations. (E) Violin plots showing the expression of marker genes used to annotate cell clusters.

### Secreted Proteins-Mediated Signalling and Extracellular Matrix Interactions

As the RPE plays an important role in the homeostasis of surrounding tissues, I was particularly interested in secreted proteins-mediated signalling pathways engaging RPE and/or other cells. Network centrality analysis on CellChat data revealed that vascular endothelial

growth factor (VEGF), bone morphogenic proteins (BMP), pleiotrophin (PTN), growth differentiation factors (GDF), granulin (GRN) and hepatocyte growth factor (HGF) were among the top such pathways between RPE cells and cells from the choroid (**Figure 4.2 A**).

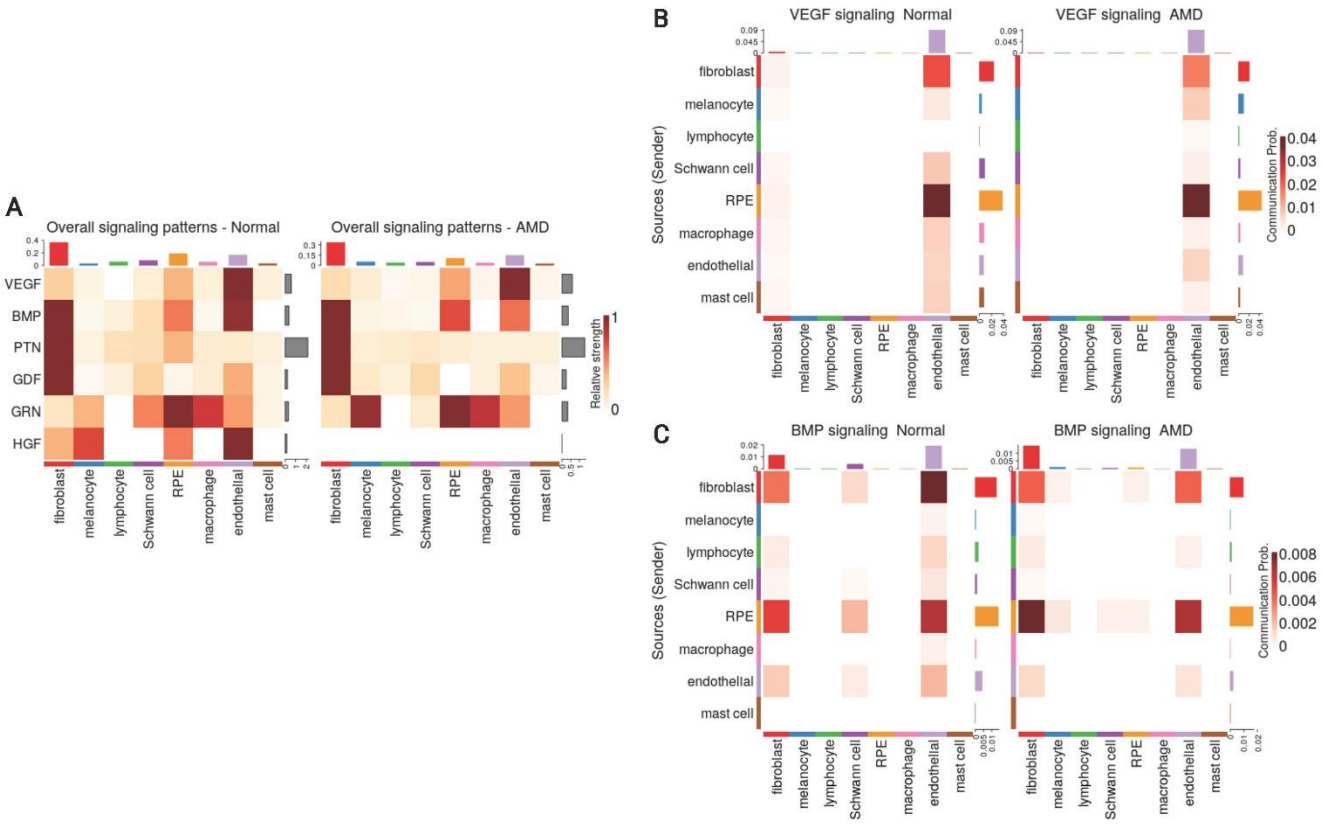


**Figure 4.2 Secreted proteins-mediated signalling involving RPE cells derived from CellChat results**

(A) Heatmap showing the relative strength of selected signalling pathways across cell types in both normal and AMD tissues in the scRNA-seq dataset from Voigt et al (2019). Pathways were selected as those being the most relevant to communication patterns involving RPE cells. (B) Cell-type to cell-type heatmap of CellChat communication probabilities aggregated from each VEGF LRI. VEGF signalling was predominantly targeting endothelial cells and was especially elevated when originating from RPE cells. (C) Cell-type to cell-type heatmap of CellChat communication probabilities aggregated from each BMP LRI. BMP signalling was predominantly targeting fibroblasts and endothelial cells and was especially elevated when originating from RPE cells and fibroblasts.

The CellChat cell-type-specific networks of VEGF and BMP (**Figure 4.2 B-C**) showed that RPE cells are the prominent source of secretion of effectors for these two pathways whereas endothelial cells and respectively fibroblast/endothelial cells are the major targets. Results derived from scDiffCom also confirmed these findings.

VEGF denotes a group of signal proteins that promote blood vessel formation or angiogenesis (Senger et al., 1983;Ferrara et al., 2003;Gogat et al., 2004) that have been studied in various diseases (Ellis and Hicklin, 2008) as their main inhibitor (anti-VEGF) could reduce the severity of many pathological conditions, including wet AMD (Schmidt-Erfurth et al., 2014). BMP are cytokines related to tissue regeneration and development (Sieber et al., 2009). BMP has been associated with the development of the neural retina and RPE (Hocking and McFarlane, 2007), RPE migration and maintenance of RPE barrier integrity (Ibrahim et al., 2020). Here, my cell-cell communication analysis highlighted VEGF and BMP as dominant signalling pathways from the RPE to the choroid.

As alterations of the extracellular matrix have been associated with dysfunction of the RPE/choroid and with AMD, especially in relation to migration/wound healing and angiogenesis (Pouw et al., 2021), I then extracted all CCIs detected by CellChat and scDiffCom involving ECM-receptor interactions. Prominent ECM-related pathways included collagen, laminin, fibronectin 1 (FN1), thrombospondin (THBS), tenascin and vitronectin (VTN) (**Figure 4.3 A**). CellChat cell-type-specific networks showed that fibroblasts, Schwann cells and endothelial cells were the major sources of effectors for these pathways (**Figures 4.3 B-D**). Again, the same patterns were revealed by scDiffCom.

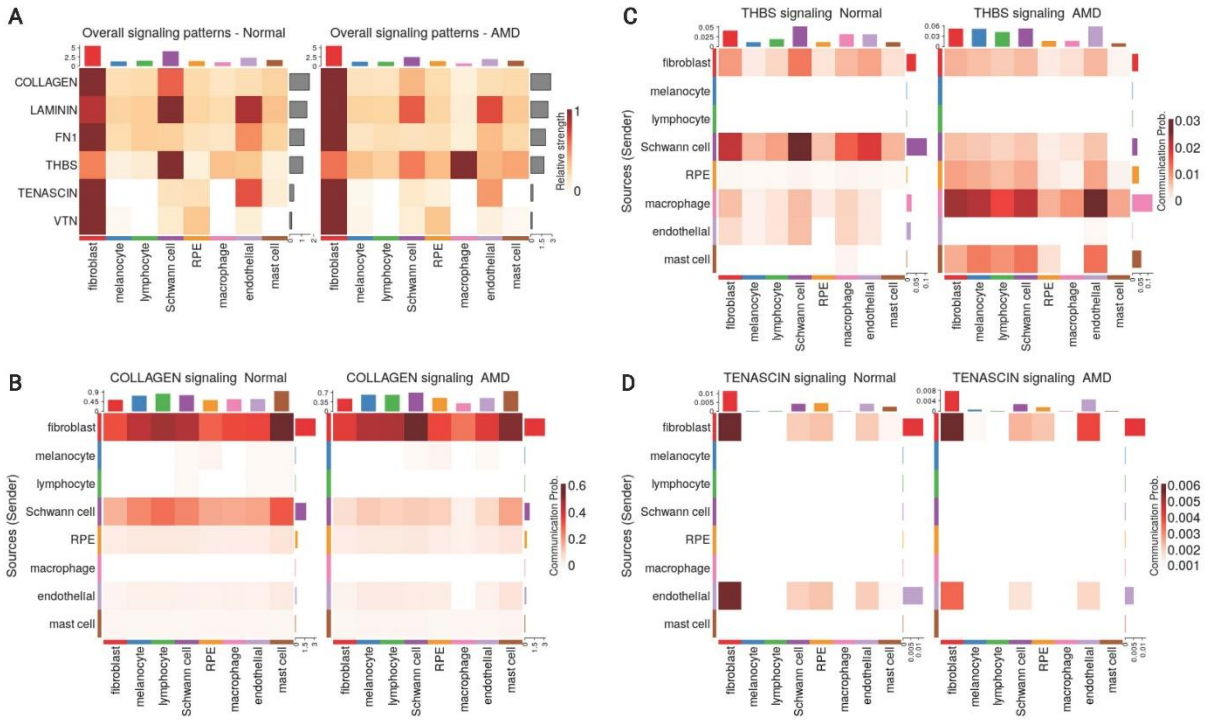


**Figure 4.3 ECM-related signalling in the RPE/choroid derived from CellChat results**

**(A)** Heatmap showing the relative strength of highly expressed ECM-related pathways across cell types in both normal and AMD tissues in the scRNA-seq dataset from Voigt et al (2019). **(B)** Cell-type to cell-type heatmap of CellChat communication probabilities aggregated from each COLLAGEN LRI. COLLAGEN signalling was mostly originating from fibroblast and Schwann cells targeting all cell types similarly. **(C)** Cell-type to cell-type heatmap of CellChat communication probabilities aggregated from each thrombospondin LRI. Thrombospondin signalling was mostly originating from fibroblast and Schwann cells and targeting various cell types. **(D)** Cell-type to cell-type heatmap of CellChat communication probabilities aggregated from each tenascin LRI. Tenascin signalling was mostly originating from fibroblast and endothelial cells targeting predominantly themselves as well as RPE and Schwann cells to a lesser extent.

**Age-Associated Ligands and Receptors in the RPE/Choroid**

As there is currently no scRNA-seq dataset of the RPE/choroid across the human lifespan, I relied on the bulk microarray data from (Newman et al., 2012) to investigate potential age-related expression changes in ligand and receptor genes. I performed a linear regression across age and accounted for potential confounding factors such as retinal location (macular versus non-macular). Out of the 1854 unique ligand/receptor genes present in the scDiffCom LRI database, I found that 60 and respectively 103 of them were upregulated, respectively downregulated with age in the bulk data (BH adjusted p-value < 0.1 and |log2(fold change)| > log2(1.5)/70years). To focus on the communication between the RPE and the cell types of the choroid, I then selected the genes that were explicitly taking part in a least one cell-cell interaction detected by scDiffCom either originating from or targeting the RPE. I obtained 46 and 43 ligand/receptor genes upregulated and respectively downregulated with age (**Table 4.1**).

**Table 4.1 Ligands and receptors that are differentially expressed with age in RPE/choroid microarray samples and taking part in cell-cell interactions** (detected by scDiffCom in scRNA-seq data) specifically from or to the RPE cell type.

| Ligands | | | |
|---|---|---|---|
| Regulation | Gene | log2FC | Adj. p-value |
| UP | AREG | 0.020 | 0.061 |
| | BMP7 | 0.019 | 0.032 |
| | BSG | 0.011 | 0.012 |
| | C1QTNF5 | 0.012 | 0.032 |
| | CDH3 | 0.011 | 0.067 |
| | CIRBP | 0.013 | 0.010 |
| | CNTN3 | 0.015 | 0.044 |
| | COL20A1 | 0.017 | 0.007 |
| | COL8A1 | 0.013 | 0.024 |
| | EFNA2 | 0.009 | 0.005 |
| | FNDC5 | 0.012 | 0.032 |
| | GDF11 | 0.012 | 0.069 |
| | MYOC | 0.020 | 0.025 |
| | OMG | 0.016 | 0.095 |
| | PTN | 0.009 | 0.096 |
| | SAA1 | 0.021 | 0.048 |
| | SERPINF1 | 0.013 | 0.055 |
| | SFRP1 | 0.024 | 0.008 |
| | SPON1 | 0.013 | 0.051 |
| | SPTBN2 | 0.015 | 0.002 |
| | THBS2 | 0.012 | 0.090 |
| | THBS4 | 0.017 | 0.011 |
| | TTR | 0.025 | 0.016 |
| | VEGFA | 0.012 | 0.002 |
| | ZP3 | 0.009 | 0.078 |
| DOWN | ADM | -0.011 | 0.048 |
| | ANGPT1 | -0.027 | 0.000 |
| | COL3A1 | -0.013 | 0.010 |
| | CXCL12 | -0.012 | 0.013 |
| | EFNB2 | -0.011 | 0.002 |
| | FBN1 | -0.011 | 0.021 |
| | FGF12 | -0.014 | 0.010 |
| | FSTL1 | -0.008 | 0.051 |
| | HBEGF | -0.010 | 0.051 |
| | JAG1 | -0.009 | 0.005 |
| | LTB | -0.011 | 0.064 |
| | NRG1 | -0.012 | 0.022 |
| | RSPO3 | -0.020 | 0.001 |
| | S100A4 | -0.011 | 0.010 |
| | SEMA3E | -0.008 | 0.057 |
| | SEMA5A | -0.011 | 0.006 |
| | SLIT2 | -0.011 | 0.007 |
| | SLIT3 | -0.011 | 0.002 |
| | TF | -0.013 | 0.032 |
| | TNFSF10 | -0.009 | 0.049 |
| | TNFSF13B | -0.013 | 0.012 |
| | TNXB | -0.014 | 0.004 |

| Receptors | | | |
|---|---|---|---|
| Regulation | Gene | log2FC | Adj. p-value |
| UP | APLP1 | 0.011 | 0.005 |
| | ATP1A3 | 0.008 | 0.010 |
| | EZR | 0.015 | 0.022 |
| | F2RL2 | 0.024 | 0.015 |
| | FAS | 0.010 | 0.025 |
| | FGFRL1 | 0.010 | 0.017 |
| | GPC1 | 0.010 | 0.001 |
| | INSR | 0.009 | 0.021 |
| | ITGA6 | 0.008 | 0.084 |
| | ITGB8 | 0.027 | 0.008 |
| | LRP8 | 0.016 | 0.024 |
| | LSR | 0.012 | 0.017 |
| | MERTK | 0.009 | 0.025 |
| | NETO2 | 0.023 | 0.007 |
| | PTPRZ1 | 0.011 | 0.063 |
| | SCARB1 | 0.009 | 0.007 |
| | SDC4 | 0.010 | 0.056 |
| | SLC16A1 | 0.016 | 0.010 |
| | STRA6 | 0.014 | 0.051 |
| | TRPM3 | 0.021 | 0.010 |
| | VASN | 0.017 | 0.002 |
| DOWN | ADRB2 | -0.009 | 0.019 |
| | AR | -0.010 | 0.010 |
| | BAMBI | -0.011 | 0.002 |
| | BMPR2 | -0.010 | 0.006 |
| | EPHA4 | -0.009 | 0.069 |
| | FZD2 | -0.008 | 0.021 |
| | FZD8 | -0.009 | 0.063 |
| | HHIP | -0.012 | 0.032 |
| | IGF2R | -0.011 | 0.030 |
| | IL6ST | -0.009 | 0.032 |
| | ITGA9 | -0.009 | 0.044 |
| | JAML | -0.012 | 0.055 |
| | KDR | -0.011 | 0.025 |
| | KIT | -0.009 | 0.095 |
| | KLRG1 | -0.011 | 0.003 |
| | NRP1 | -0.012 | 0.002 |
| | NRP2 | -0.011 | 0.017 |
| | PLXNA4 | -0.012 | 0.053 |
| | PRTG | -0.009 | 0.010 |
| | PTPRB | -0.010 | 0.069 |
| | TLR4 | -0.009 | 0.069 |

Several of the genes differentially expressed with age were part of the top secreted pathways detected by CellChat/scDiffCom from or to RPE cells, including *VEGFA*, *KDR*, *BMP7*, *BMPR2*, *PTN*, *SDC4* and *GDF11* (**Table 4.1**). Regarding VEGF pathway, the ligand gene VEGFA was upregulated with age in RPE/choroid bulk data (**Figure 4.4 A**) and mainly expressed by RPE cells (**Figure 4.4 A**) in scRNA-seq data. *KDR*, a receptor of the VEGF pathway, was downregulated with age in RPE/choroid bulk data (**Figure 4.4 A**) and predominantly expressed by endothelial cells in scRNA-seq data (**Figure 4.4 B**). Regarding the BMP pathway, the ligand gene *BMP7* was upregulated in ageing RPE/choroid bulk data (**Figure 4.4 C**) and mainly expressed by RPE cells (**Figure 4.4 D**) in scRNA-seq data. *BMPR2*, a receptor of the BMP pathway, was downregulated with age in RPE/choroid bulk data (**Figure 4.4 C**) and mainly expressed by endothelial cells (**Figure 4.4 D**). Collectively, these results support the idea that ageing RPE cells tend to increase the secretion of VEGF and BMP factors towards the choroid, whereas endothelial cells tend to decrease the expression of the corresponding receptors, suggesting a potential compensatory mechanism, which may offer some protection against initial pathological changes.

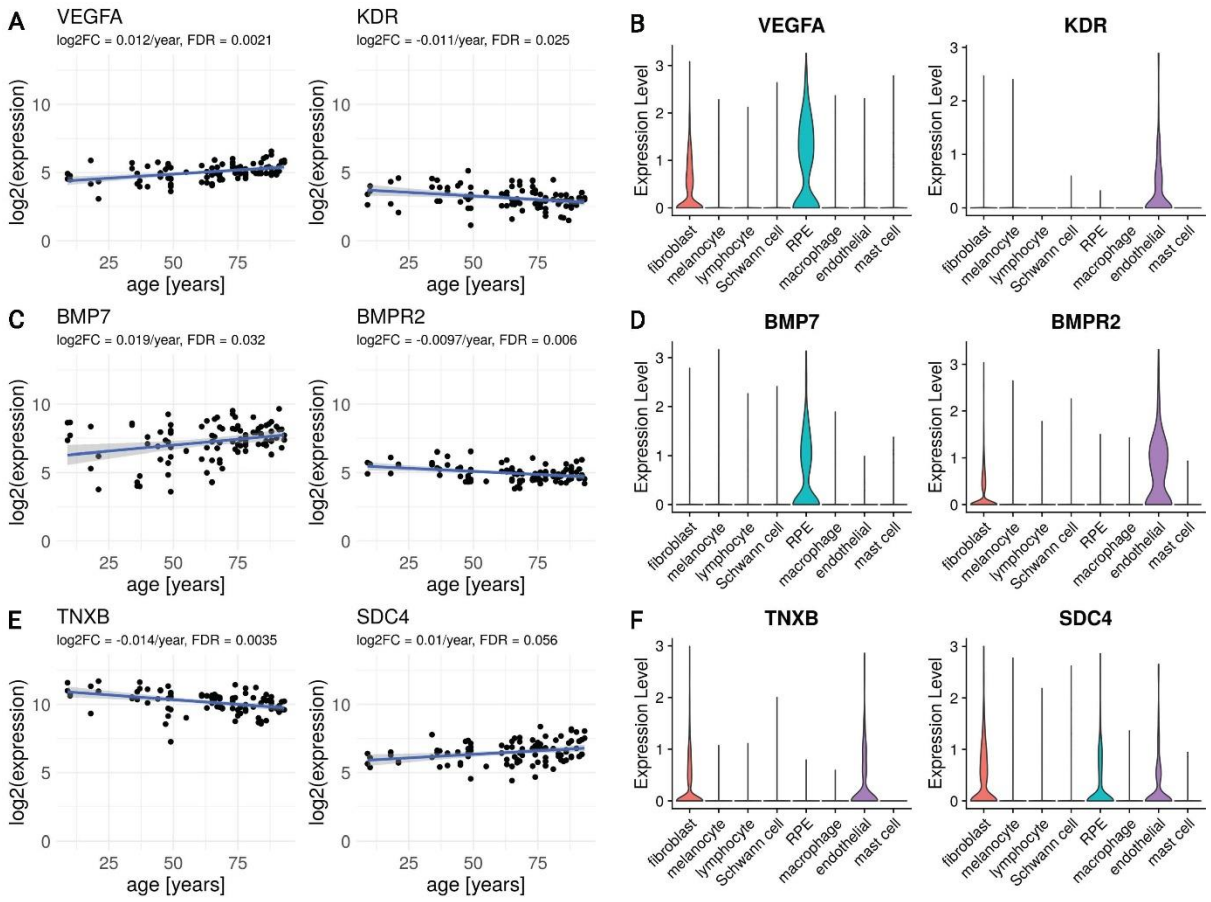


**Figure 4.4 Ligand and receptor genes differentially expressed with age in the RPE/choroid with their typical cell type-specific expression**

**(A, C, E)** Scatter plots of selected ligands and receptors showing expression changes with age in human RPE/choroid microarray samples from Newman et al. (2012). Displayed Log2FC and FDR are those computed with Limma according to the linear model described in Methods. **(B, D, F)** Violin plots showing expression levels of corresponding genes in RPE/choroid cell types from scRNA-seq samples of Voigt et al. (2019).

Several genes belonging to the top ECM-related pathways detected by CellChat from the scRNA-seq data were also differentially expressed with age in the bulk dataset, including collagen and integrin genes, *THBS2*, *THBS4*, *SDC4* and *TNXB* (**Table 4.1**). Among these, the ligand-receptor pair TNXB/SDC4 was particularly noteworthy. *TNXB* was expressed mostly by fibroblasts and endothelial cells in the scRNA-seq data (**Figure 4.4 F**) and downregulated

with age in the bulk data (**Figure 4.4 E**). *SDC4* was expressed by RPE cells, fibroblasts and endothelial cells in the scRNA-seq data (**Figure 4.4 F**) and upregulated with age in the bulk data (**Figure 4.4 E**). Changes in tenascin expression have been previously related to development and ageing (Choi et al., 2020b;Matsumoto and Aoki, 2020) as well as to pathologic conditions such as cancer, inflammation and fibrosis (Albacete-Albacete et al., 2021;Tajiri et al., 2021). Disruption of the tenascin pathway also results in promoting inflammatory processes and angiogenesis (Kobayashi et al., 2016a). Tenascin pathway genes were also reported as being enriched among differentially expressed genes in the RPE/choroid in AMD, including Tenascin-C (Dhirachaikulpanich et al., 2020a) and *TNXB* (Porter et al., 2019).

**Effects of Cellular Senescence on the RPE/Choroid Intercellular Communication**

I next sought to characterize potential cellular senescence signatures in the RPE/choroid as well as their effects on intercellular communication. I first assigned a senescence score to each cell of the RPE/choroid scRNA-seq dataset from Voigt et al. (2019), using the ssGSEA approach (Barbie et al., 2009;Borcherding et al., 2021). As reference signatures, I used the results from a previous meta-analysis that inferred genes up- and down-regulated with senescence by comparing 20 bulk transcriptomics datasets (Chatsirisupachai et al., 2019). The senescence score was defined as the difference between the ssGSEA score of upregulated signature genes and the ssGSEA score of downregulated signature genes (**Figure 4.5 A**). I noticed that cells from the patient with AMD had a slightly larger average senescence score (mean = 0.21, SD = 0.21) compared to cells from healthy samples (mean = 0.18, SD = 0.22) (Wilcoxon Rank Sum Test, p-value = 1.37E-6) (**Figure 4.5 B**). However, more data with a larger sample size in terms of patients will be required in the future to better establish if AMD is consistently associated with an increased expression of senescence-related genes.

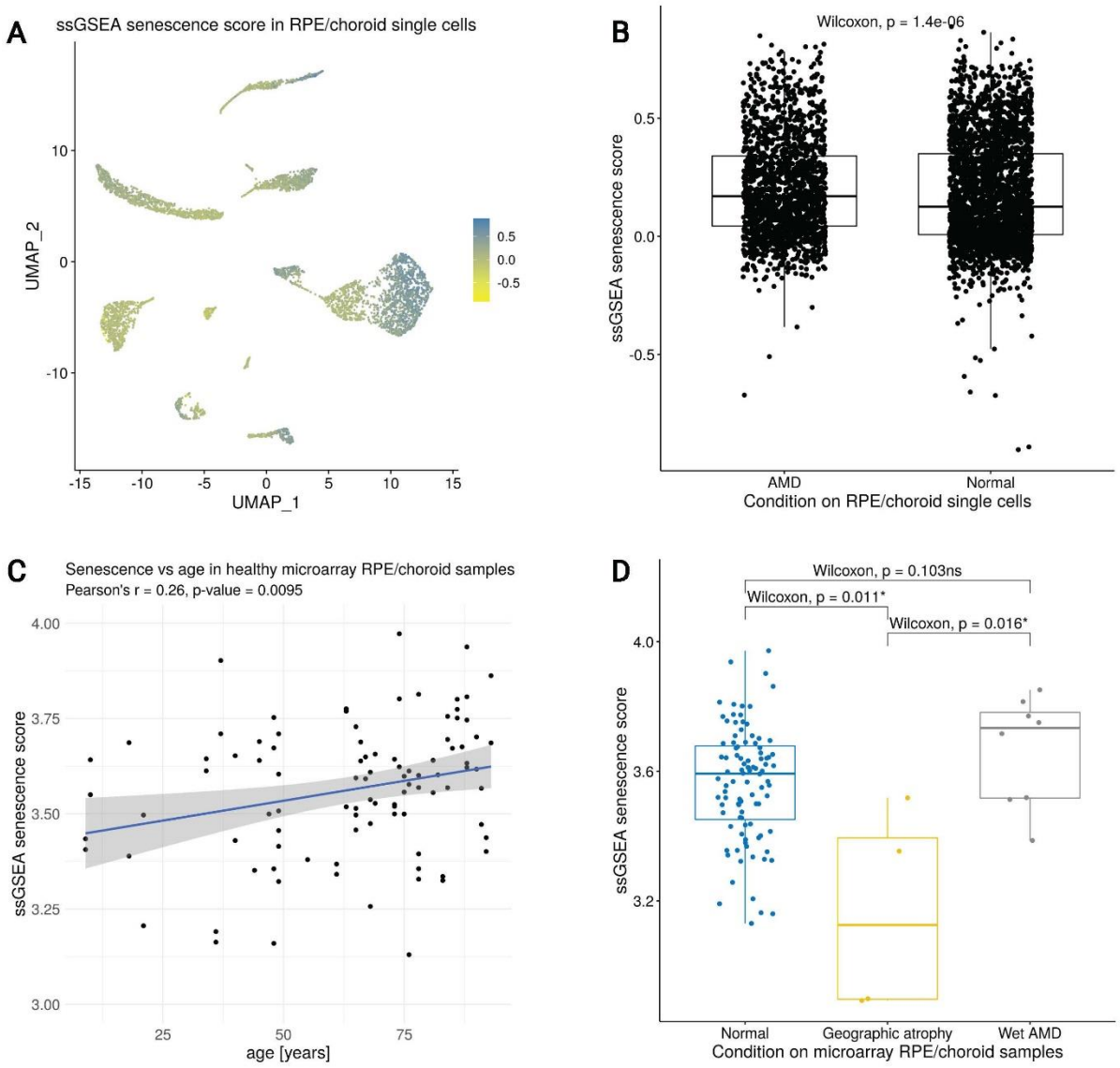


**Figure 4.5 Expression of senescence signature genes in RPE/choroid scRNA-seq and microarray data**

**(A)** Dimensionality reduction (UMAP) showing the ssGSEA senescence score of each cell in the scRNA-seq dataset from Voigt et al. (2019). **(B)** Boxplot showing a slight increase in the senescence score of AMD cells compared to normal cells from Voigt et al. (2019). **(C)** Positive correlation between senescence scores and age in the non-AMD microarray samples of Newman et al. (2012) (Pearson's correlation R = 0.26, p-value = 0.0095). **(D)** Boxplot showing significant and non-significant differences in senescence scores between normal, wet AMD and geographic atrophy RPE/choroid samples from Newman et al. (2012).

I then used the senescence score to label cells as either "normal" or "senescent-like". It is important to note that this method did not allow us to claim with certainty that cells with high scores were actually in a senescent state before being captured for sequencing. Nevertheless, it allowed us to extract cells that at least showed a senescence-like gene expression profile. In practice, I with the help of Dr Cyril Lagger defined such cells as those having a score in the top 20% of all senescence scores across all cell types (**Figure 4.6 A-C**). We did not find any relevant differences in the distribution of the number of such senescent-like cells across cell types between the three donors. However, I confirmed that the expression of genes involved in typical senescence pathways, including *TP53*, *CDKN1A*, *RB1*, *NFKB1* and *NOTCH1*, was generally higher in senescent-like cells compared to normal cells (**Figure 4.6 D**).

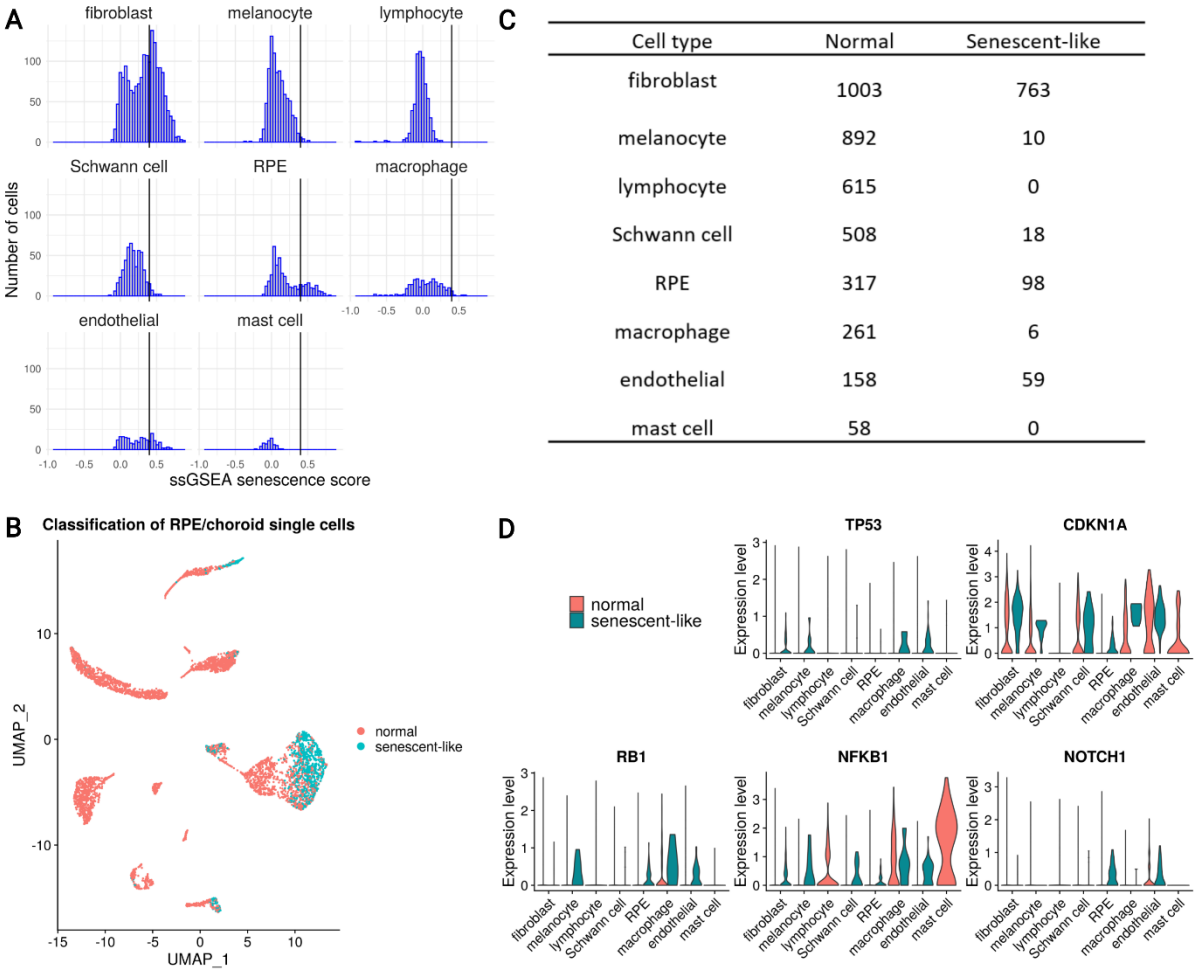


| Cell type | Normal | Senescent-like |
|---|---|---|
| fibroblast | 1003 | 763 |
| melanocyte | 892 | 10 |
| lymphocyte | 615 | 0 |
| Schwann cell | 508 | 18 |
| RPE | 317 | 98 |
| macrophage | 261 | 6 |
| endothelial | 158 | 59 |
| mast cell | 58 | 0 |

**Figure 4.6 Using senescence score to define senescent-like cells**

**(A)** Distribution of ssGSEA senescence scores across cells from Voigt et al. (2019) by cell types. The vertical line indicates the threshold used to separate normal cells from senescent-like cells. **(B)** Dimensionality reduction (UMAP) showing cells from Voigt et al. (2019) colored by their senescence status. **(C)** Number of normal and senescent-like cells per cell type. **(D)** Violin plot of the expression of typical senescence markers in Voigt et al. data (2019) for each cell type and the two senescence statuses.

I performed a new intercellular communication analysis on the same scRNA-seq data as above by splitting each cell type into the two subpopulations of normal and senescent-like cells (and by merging the samples of all three donors together). As I did not consider groups with less than 11 cells, the analysis was performed on 12 subpopulations (**Figure 4.6 C**). When using the LRI database from Cellchat, CellChat and scDiffCom returned respectively 11162 and 5637 CCIs, out of which 5044 were detected by both methods (**Figure 4.7 A**). When using its extended LRI database, scDiffCom returned 18908 CCIs.

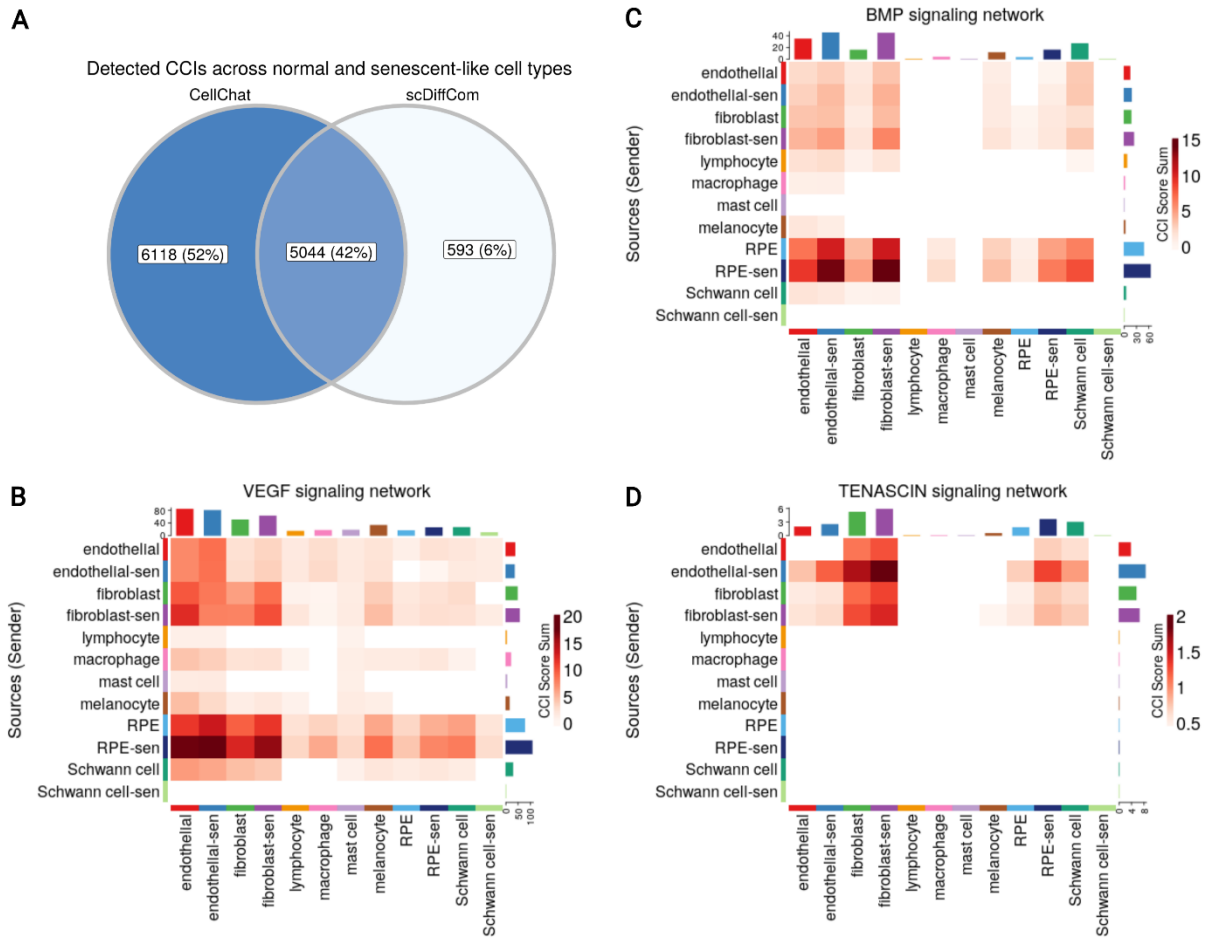


**Figure 4.7 scDiffCom intercellular communication results in the RPE/choroid with senescent-like subpopulations**

**(A)** 11162 and 5637 CCIs were considered biologically relevant by CellChat, respectively scDiffCom, in normal samples when using the CellChat database of LRI. scDiffCom was more conservative (6% of unique CCIs compared to 52% for CellChat). **(B)** Cell-type to cell-type heatmap showing the sum of scDiffCom CCI scores over VEGF LRIs. **(C)** Cell-type to cell-type heatmap showing the sum of scDiffCom CCI scores over BMPLRIs**. (D)** Cell-type to cell-type heatmap showing the sum of scDiffCom CCI scores over tenascin LRIs.

Ranking pathways according to centrality measures with CellChat revealed that the pathways previously found to be associated with ageing were among the top signalling patterns associated with senescent cell subpopulations. VEGF was predominantly expressed from

senescent-like (sl-) RPE cells toward sl-endothelial cells (**Figure 4.8 A**). Similarly, BMP showed stronger signalling from sl-RPE cells towards sl-endothelial cells, sl-Schwann cells and sl-fibroblasts compared to all other cell types (**Figure 4.8 B**). Finally, tenascin-mediated signalling was also stronger between sl-fibroblasts and sl-endothelial cells and from these two cell populations towards sl-RPE cells (**Figure 4.8 C**).

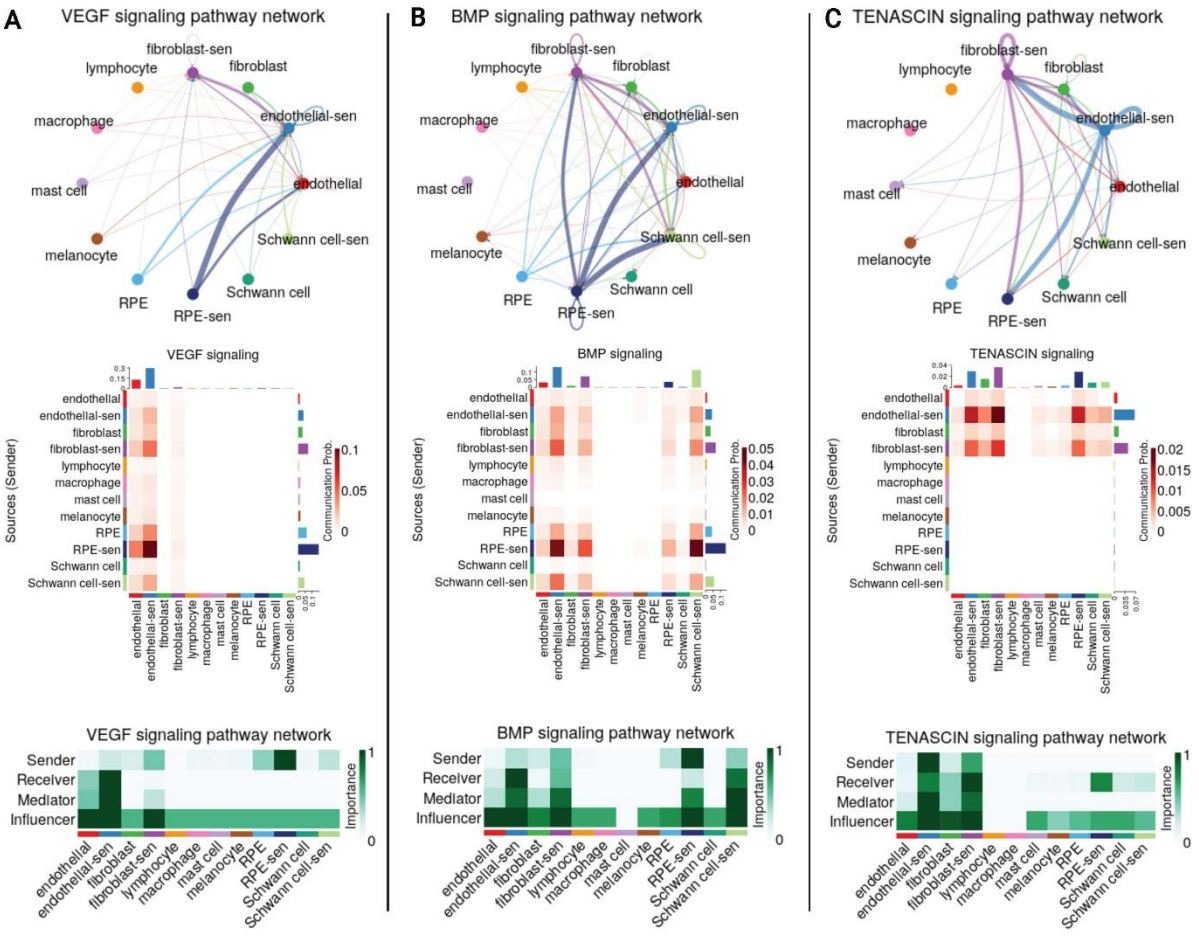


**Figure 4.8 Network representation of the impact of senescence on VEGF, BMP and TENASCIN intercellular communication in the RPE/choroid**

Signaling network summary between senescent-like and non-senescent cell types for **(A)** VEGF, **(B)** BMP and **(C)** TENASCIN pathways. Cell type to cell type networks (top panels) and heatmaps (middle panels) show the CellChat communication probability (aggregated over all LRIs from the given pathway) between each cell type pair. Centrality heatmaps (bottom

panels) show the various CellChat centrality scores across each cell type for the selected pathways.

Results from scDiffCom generally recapitulated most of these findings from CellChat, with some differences to mention. First, scDiffCom did not predict as CellChat that sl-endothelial cells were more targeted by VEGF than endothelial cells. Instead, these two cell populations shared similar overall "receiver scores" (**Figure 4.7 B**). It still noted, in agreement with CellChat, that VEGF was secreted more by sl-RPE cells than by RPE or other cells. Second, scDiffCom did not predict a strong BMP signalling from sl-RPE cells towards sl-Schwann cells, but instead towards Schwann cells (**Figure 4.7 C**). Finally, although scDiffCom predicted as CellChat a strong tenascin signalling from sl-endothelial cells towards sl-fibroblasts, the opposite signalling from sl-fibroblasts towards sl-endothelial cells was much weaker than as predicted by CellChat (**Figure 4.7 D**). Also more generally, the overall decrease of tenascin signalling involving fibroblasts compared with sl-fibroblasts appeared less prominent when looking at scDiffCom compared to CellChat analysis.

Despite these differences, the results from both CellChat and scDiffCom analyses highlighted how senescence state might influence RPE/choroid tissue in both normal and AMD, specifically by enhancing ICC via VEGF, BMP and tenascin pathways.

**Effects of Age on Cellular Senescence Scores in Microarray RPE/Choroid Data**

As I showed that senescence might influence ICC in the RPE/choroid, I further explored other potential factors that might be related to senescence in this tissue. To test the hypothesis that senescence might increase with age in the RPE/choroid, I assigned a senescence score to each sample of the bulk microarray dataset from Newman et al. (2012) and explored its

evolution with time. I found that the senescence score was significantly correlated with age (Pearson's correlation R =0.26, p-value = 0.0095) (**Figure 4.5 C**). This is consistent with earlier observations reporting a similar accumulation of senescent cells in different other tissues (Chatsirisupachai et al., 2019). I also compared the senescence score between control (non-AMD) samples and different types of AMD, including neovascular AMD and geographic atrophy (an end-stage non-neovascular type AMD). The results showed that neovascular AMD samples (n=8) had a slightly, but non-significantly, higher senescence score than non-AMD ones (n=96) (Wilcoxon Rank Sum Test, p-value = 0.103), while geographic atrophy samples (n=4) had a significantly lower senescence score than non-AMD samples (n=96) (p-value = 0.011) and neovascular AMD samples (n=8) (p-value = 0.016) (**Figure 4.5 D**). Overall, these two analyses suggested that the senescence score in the RPE/choroid may be affected by both age and AMD types. However, the fact that when comparing non-AMD to wet AMD there is no significant difference in the bulk microarray dataset (**Figure 4.5 D**) but a significant difference in the single-cell dataset (**Figure 4.5 B**) shows that further studies leading to more data and further analyses are necessary. Nevertheless, the fact that the RPE/choroid cells with high senescence scores presented increased signalling via VEGF, BMP and tenascin pathways suggests a possible connection between senescence and AMD RPE/choroid.

## 4.4 Discussion

An increasing number of patients suffer from the main age-related degenerative eye disease involving retinal tissues, AMD, which may lead to irreversible blindness. Current standard treatments can only address a small subset of the disease by slowing down the disease progression (Wong et al., 2014;Mitchell et al., 2018), highlighting the importance and need for better understanding the biology of the RPE/choroid tissue in the context of ageing and cellular senescence (Sreekumar et al., 2020;Lee et al., 2021). At the histological level, it is known that

ageing leads to abnormality of pigmentation with increase of soft drusen (a lipoproteinaceous deposit) between the RPE and the underlying choroid (Boulton et al., 2004;Curcio et al., 2009;Ardeljan and Chan, 2013;Curcio, 2018b). At molecular level, a recent first RNA-seq global gene expression study of the ageing human RPE reported upregulation of the visual cycle genes in the RPE with increasing age (Butler et al., 2021) and bulk and single-cell gene expression analyses of the ageing human choriocapillaris reported an increase of the pro-inflammatory environment in the choroid (Voigt et al., 2020). Nevertheless, there hasn't been any research conducted to explore the intercellular communication between the RPE/choroid in the context of aging, senescence, and AMD.

The study presented herein focused on the communication occurring at the level and between these two tissues, and on the effect that the ageing process has on this communication. By applying algorithms that have proved useful to study intercellular communication in various tissues from scRNA-seq data (Armingol et al., 2021;He et al., 2021;Hu et al., 2021;Jin et al., 2021;Lagger et al., 2021), I was able to extract important signalling patterns between the RPE and the choroid. Together with my ageing and cellular senescence analyses, my analysis predicted three pathways (VEGF, BMP and tenascin) that support some of the strongest RPE/choroid cell-cell interactions, while being significantly affected by age and enhanced between subpopulations of cells showing a senescent-like gene expression profile.

The analysis of secreted molecules with roles in cell signalling revealed age-related changes in communication involving VEGF and BMP. VEGF signalling has been studied extensively in many retinal diseases, especially AMD and diabetic retinopathy (Marneros, 2016). Treatments targeting VEGF can slow down the progression of neovascular AMD, despite not reversing it (Schmidt-Erfurth et al., 2014). VEGFA is secreted basolaterally from

the RPE and interacts with VEGF receptors such as KDR and VEGFR-2 (Blaauwgeers et al., 1999;Gogat et al., 2004;Hocking and McFarlane, 2007). By combining my ageing analysis on bulk microarray samples with cell-type-specific gene expression knowledge extracted from scRNA-seq data, this analysis suggested that ageing correlated with increased *VEGFA* expression in RPE cells and with decreased expression of the *KDR* in choroidal endothelial cells. Similarly, I identified BMP as another signalling pathway of the RPE/choroid affected by ageing. BMP signalling is involved in cell regulation processes, including cell proliferation, differentiation and eye morphogenesis (Solursh et al., 1996;Ibrahim et al., 2020). BMP7 plays a role in epithelial-mesenchymal transition, angiogenesis, and antifibrotic activity (Yang et al., 2020). A previous study showed that BMP7 could reduce proliferative vitreoretinopathy, a major complication of end-stage retinal detachment, by inhibiting RPE cells' fibrosis in a rabbit model (Yao et al., 2019). My findings indicated an increase in *BMP7* expression in RPE cells and a decreased expression of the *BMPR2* receptor in choroidal endothelial cells during human ageing. This result underscores the importance of the BMP signalling pathway for the homeostasis of the RPE/choroid. Although it is unclear why the expression of the receptor and ligand genes change in opposite directions, I hypothesised that it could be a protective adaptation to maintain the overall activity level of these two signalling pathways during ageing. Although available data do not provide information about the precise dynamics of molecular interactions between ligands and receptors, I suggest that a decrease in receptor expression might be a compensatory response to maintain a relatively stable level of signalling when facing an increase in ligand concentration. It has also been reported that choriocapillaris coverage of Bruch's membrane decreases with age (Ramrattan et al., 1994;Lutty et al., 2020) , while some reports point towards changes in the number of RPE cells during ageing (Gao and Hollyfield, 1992;Harman et al., 1997;Del Priore et al., 2002;Ach et al., 2014). Whether

compensatory gene expression occurs in ageing in order to maintain an appropriate level of cellular signalling needs to be investigated further experimentally.

Age-associated changes in the extracellular matrix of the RPE/choroid have been observed in both fundus and post-mortem tissues (Ardeljan and Chan, 2013;Boulton, 2013;Sura et al., 2020). Typically, AMD is associated with a thickening of the RPE basal lamina-Bruch's membrane complex driven by the accumulation of basal laminar deposit (Sura et al., 2020). Genes associated with ECM were also reported to be altered in AMD, including factors regulating wound healing and angiogenesis (Pouw et al., 2021). Here, my analysis suggested that the tenascin-mediated pathway might have an age-related significance to the RPE/choroid intercellular communication. The tenascin pathway contributes to ECM maintenance (Reinhard et al., 2017;Matsumoto and Aoki, 2020;Miller, 2020) and the absence of *TNXB* was reported to cause a reduction of collagen and of tissue strength (Mao et al., 2002). Tenascin has also a proangiogenic effect when interacting with the VEGF pathway (Ikuta et al., 2000). Our group previously identified *TNXB* as a methylation target that shows a decrease in methylation in its exon3 in RPE/choroid affected by AMD (Porter et al., 2019). Genome-wide association studies (GWAS) previously identified *TNXB* as a genetic variant associated with AMD (Cipriani et al., 2012;Fritsche et al., 2016). My current analysis suggested that *TNXB* is expressed by choroidal fibroblasts and endothelial cells and is globally downregulated with age while its receptor *SDC4* is expressed by fibroblasts, RPE cells and endothelial cells and is globally upregulated with age. This again suggested a potential compensatory mechanism. Together, my transcriptomic analysis and previous studies on DNA methylation and genetic variants emphasised the importance of *TNXB* and the tenascin pathway on the pathological mechanisms associated with ageing and AMD, especially in relation to ECM interactions between the RPE and the choroid affected by AMD.

I acknowledge that this current analysis has several limitations. Firstly, the single-cell data I retrieved contains only provided 3 RPE/choroid samples: two from normal eyes and one from an eye with neovascular AMD (Voigt et al., 2019). It needs to be emphasised that having only three samples might not represent the biology of RPE/choroid and AMD comprehensively, especially when there was only one sample from AMD, which is known to have several stages of the disease. To the best of my knowledge, there are currently no other public datasets that contain more samples suitable for my analysis. For example, although a recent scRNA-seq dataset from Voigt et al. 2022 contains more eye samples, it is not suitable for this intercellular communication study. Specifically, as cells have been sorted based on CD31 expression to enable the capture of endothelial cells, only a low number of RPE cells are present in the dataset and they are moreover confounded with photoreceptors (Voigt et al., 2019;Voigt et al., 2022). Secondly, the bulk microarray dataset that I used for this ageing-related analysis is missing clinical details regarding the post-mortem normal eyes (Newman et al., 2012). The only quality control that is provided is RNA integrity but not the detailed pathology of these eyes. Along the same line, both the scRNA-seq data (Voigt et al., 2019) and the bulk microarray data (Newman et al., 2012) are missing a clear nomenclature of neovascular AMD. The diagnosis of neovascular AMD was acquired from ophthalmic notes for the scRNA-seq dataset, while the diagnosis for the bulk microarray dataset was obtained from retina specialists and fundus photographs. However, the current clinical nomenclature (Jung et al., 2014;Spaide et al., 2020) indicates more specific subtypes of neovascularisation, such as intraretinal neovascularisation, and may influence different gene expression profiles. This emphasises the importance of improving the clinical documentation of recovered samples in future experiments and data collections. Thirdly, a common limitation of both the single-cell and bulk datasets I analysed is the absence of detailed spatial information. As samples originate

from 8-mm tissue punches, details regarding regional differences such as between the fovea, parafovea and perifovea are lost. Indeed, several studies such as some based on imaging techniques have illustrated the importance of the topographic nature of AMD. For example, a higher concentration of melanolipofuscin is found in foveal RPE (Bermond et al., 2020). Other studies using optical coherence tomography suggest that hyperreflective foci (potentially associated with AMD progression) may be due to migrating RPE cells undergoing transdifferentiation (Ouyang et al., 2013;Cao et al., 2021), highlighting the three-dimensional nature of the disease.

Some recent studies indicate that senescent RPE cells accumulate during AMD in human donors, primates and RPE cell cultures (Wang et al., 2019;Blasiak, 2020;Lee et al., 2021), thus raising the interest in the role of cellular senescence in AMD. In addition to RPE, cellular senescence also may affect choroidal tissues and the neuronal retina (Ma et al., 2013;Cabrera et al., 2016). However, it is still unclear what are the causal role and function of the potential senescent cells in human pathology as most studies are limited to animal models and cell cultures (Cao et al., 2013;Chaum et al., 2015;Cabrera et al., 2016). My results further highlight the importance of cellular senescence in the RPE/choroid tissues in relation to prominent cell-cell communication pathways mediated by VEGF, BMP and tenascin. These findings support potential alternative treatment approaches for AMD based on targeting senescent cells using senotherapies and senolytic drugs. The strategy to target senescent cells to prevent or slow down the progress of AMD has also been independently suggested by a recent review (Lee et al., 2021). A proposed approach is to inhibit pro-inflammatory signalling molecules and to regulate oxidative stress-induced senescence (Sreekumar et al., 2020). Notably, as my results suggested that different subtypes of AMD (geographic atrophy and neovascular AMD) may present differences in senescence status, such subtypes should be taken into consideration

before applying senotherapies. To achieve this promising goal, further studies on the biological mechanisms of senescence in AMD and further clinical studies using senotherapies to treat AMD are needed (El-Nimri et al., 2020)

## Chapter 5. A systematic review of OCT and OCT angiography in retinal vasculitis

In this chapter, I present my study that was published in Journal of Ophthalmic Inflammation and Infection.

Dhirachaikulpanich, D., Chanthongdee, K., Zheng, Y., and Beare, N.A.V. (2023). A systematic review of OCT and OCT angiography in retinal vasculitis. *J Ophthalmic Inflamm Infect* 13, 1.

Retinal vasculitis is a component of uveitis for which the SUN working group has no standard diagnostic criteria or severity grading. Fluorescein angiography is the gold standard test to assess retinal vasculitis, but is invasive and time-consuming. OCT provides non-invasive detailed imaging of retinal structures and abnormalities, including blood vessel architecture and flow with OCT-A. However, use of OCT in retinal vasculitis beyond assessing macular oedema, is not well established. A systematic review was conducted to understand the features of retinal vasculitis in OCT, OCT-EDI and OCT-A imaging. The systematic search was done in March 2022 and updated in January 2023, through PubMed, EMBASE and the Web of Science database for studies related to OCT, OCT-EDI and OCT-A findings and retinal vasculitis. Bias assessment was assessed using JBI Critical Appraisal Checklist, and any findings associated with retinal vasculitis were extracted by qualitative analysis. This current study identified 20 studies, including 8 articles on OCT, 6 on OCT-EDI and 6 on OCT-A. The studies included analytical retrospective studies, case-series, and a case-control study. Five OCT studies reported secondary complications could be detected, and four reported retinal thickness alteration in retinal vasculitis. Five studies explored choroidal thickness alteration in OCT-EDI, and four explored capillary density alterations in retinal vasculitis using OCT-A. The heterogeneity in the studies' analysis and design precluded a meta-analysis. There were no

clear OCT, OCT-EDI or OCT-A findings that demonstrated potential to supersede fluorescein angiography for assessing retinal vasculitis. Some signs of macular structural effects secondary to retinal vasculitis may help prognostication for vision. The OCT signs of inflamed retinal vessels and perivascular tissue is an unexplored area.

## 5.1 Introduction

Retinal vasculitis is one of the presentations of posterior uveitis (Walton and Ashmore, 2003). The causes of retinal vasculitis are heterogenous ranging from infections such as tuberculosis (Agrawal et al., 2017) to systemic inflammatory diseases such as Behcet's disease, systemic lupus erythematosus (SLE) and sarcoidosis (Rosenbaum et al., 2016;Agarwal et al., 2022). Retinal vasculitis can also be drug-induced or idiopathic (Mir et al., 2017). Assessing retinal vasculitis can be challenging. Fundoscopic findings may be minimal, non-specific or not differentiate active disease. Fluorescein angiography, preferably wide-field, is needed to determine the presence of active vasculitis and its severity. However, there is no consensus accepted classification or grading system for retinal vasculitis(Jabs et al., 2005;Agarwal et al., 2017;Datoo O'Keefe and Rao, 2021). Fundoscopic findings include, vascular sheathing or classical tram line appearance (Shulman et al., 2015), perivascular retinal infiltrates, perivascular haemorrhages, retinal vessel occlusion, vessel beading and neovascularisation secondary to ischaemia. On fluorescein angiography (Tugal-Tutkun et al., 2010a;Leder et al., 2013;Sheemar et al., 2019), retinal vasculitis shows breakdown of the inner blood-retina barrier (vascular leakage) or occlusion of vessels. Leakage can be segmental or widespread, affect any vessel and is widely seen as a marker of inflammatory activity(Rosenbaum et al., 2016). Occlusion can be in the form of capillary non-perfusion or of larger vessels and may be due to previous vasculitis which is currently inactive. Staining of vessel walls can also be seen in

active and inactive disease. Fluorescein angiography is time-consuming and invasive as it requires intravenous dye injection (Agarwal et al., 2017;Diala et al., 2021).

OCT is a non-invasive imaging modality that shows details of retinal structures and abnormalities (Gallagher et al., 2007;Pichi et al., 2020). Retinal pathology associated with posterior uveitis can easily be observed using OCT, such as changes in retinal thickness, disruption of retinal layers and macular oedema (Onal et al., 2014;Kang et al., 2018). OCT of inflamed retinal vessels can identify enlarged vessels, hyperreflective vessel walls, hyperreflective lumen, inflammatory material in the adjacent vitreous and thickened perivascular retina (**Figure 5.1**). OCT-EDI better visualises choroidal structures,(Laviers and Zambarakji, 2014) and changes in choroidal thickness can relate to posterior uveitis (Balbaba et al., 2020;AlBloushi et al., 2021). OCT-A non-invasively images perfused retinal and choroidal vessels of the central macula (Spaide et al., 2018;Invernizzi et al., 2019). OCT-A can identify vessel closure and non-perfusion but not blood-retina barrier breakdown.

Previous non-systematic reviews have examined multimodal imaging in uveitis and retinal vasculitis but OCT modalities in retinal vasculitis has not been reviewed (Agarwal et al., 2017;Accorinti et al., 2020;Diala et al., 2021;Ebrahimiadib et al., 2021). Because the previous reviews are narrative, the findings reported might cause a selection bias and not cover all evidence related to retinal vasculitis. Therefore, this systematic review was initiated to understand the findings in OCT, OCT-EDI and OCT-A associated with retinal vasculitis.

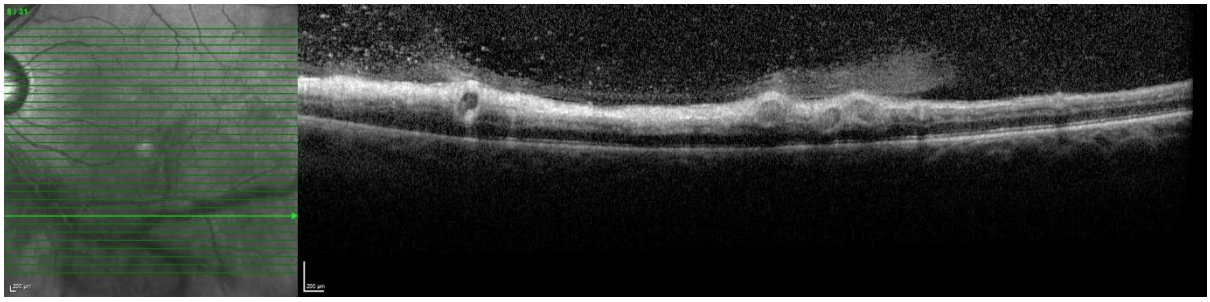

**Figure 5.1 OCT of a patient with active retinal vasculitis** in Behcet's Disease showing enlarged retinal vessels with hyperreflective walls, hyperreflective lumens and adjacent vitritis.

## 5.2 Methods

### Search Strategies and Data Sources

This systematic review was done following the guidelines of PRISMA 2020 (Page et al., 2021). This study was a systematic review of previous studies without new intervention; hence, ethical approval was not required.

A systematic electronic search of Pubmed/Medline, Web of Science and Embase was done in March 2022 and updated in January 2023. The following search terms were used "oct" OR "optical coherence tomography" AND "retinal vasculitis". Duplication in the included papers was removed using Endnote's deduplicate and manual removal by the authors, Dhanach Dhirachaikulpanich and Kanat Chanthongdee.

### Study Selection

Eligible studies met following criteria: (1) the study was on patients diagnosed with retinal vasculitis (2) the diagnosis of retinal vasculitis was based on medical records and/or fluorescein angiography imaging (3) the study reported features of retinal vasculitis on OCT or OCT-EDI or OCT-A (4) case-control, cross-sectional, prevalence or case-series studies were

included (5) the study was a peer-reviewed article. Studies were excluded if (1) it was a review, (2) the article was not in English (3) a case report/case series which reported less than 5 patients. Notably, many uveitis studies are case reports, and excluding all case reports might result in excluding a significant number of pieces of evidence. Moreover, including only articles published in English might exclude patients from different geographic areas and ethnicities. Two authors, Dhanach Dhirachaikulpanich and Kanat Chanthongdee, independently conducted a study selection and exclusion. Discordance was resolved by the senior author, Nicholas Beare.

**Data Extraction and Bias assessment**

Two authors, Dhanach Dhirachaikulpanich and Nicholas Beare, collaboratively performed bias evaluation and did data extraction. The following data were tabulated and extracted: Study site and year of publication, imaging modalities, age of participants (mean and range), number of participants with retinal vasculitis, sex, the causative disease of retinal vasculitis, retinal vasculitis diagnostic criteria of the study and the study type.

Bias assessment was conducted using JBI Critical Appraisal Checklist(Porritt et al., 2014) for analytical cross-sectional studies, prevalence studies, case-control studies or case series, depending on the type of each study. This JBI Critical Appraisal Checklist provides a tool to assess the quality of a study, including its design, conduct and analysis. We selected this bias assessment tool because it is the only tool covering studies with different study designs, including case series. The included studies were used in the data synthesis (Munn et al., 2015;Ma et al., 2020b). Studies were only included if they scored more than half of each JBI Critical Appraisal Checklist.

### Data synthesis

It was not possible to perform quantitative analysis or meta-analysis due to each associated publication's different nature and parameters. For qualitative analysis, the main OCT, OCT-EDI or OCT-A findings associated with retinal vasculitis were descriptively reported.

## 5.3 Results

### Searching results and the included studies' characteristics

**Figure 5.2.** summarises the search methodology following PRISMA2020 guidance. We retrieved a total of 1,176 articles from Pubmed/MEDLINE (n=424), EMBASE (n=580) and the Web of Science databases (n=172). We removed duplicate articles using an automatic function in Endnote X9 programs and also by manual detection. Of the 893 remaining articles, 774were excluded by initial screening of the title and abstract. One hundred and nineteen articles remained for the full-length article review and 99 were excluded. Finally, 20 articles were included in this systematic review.

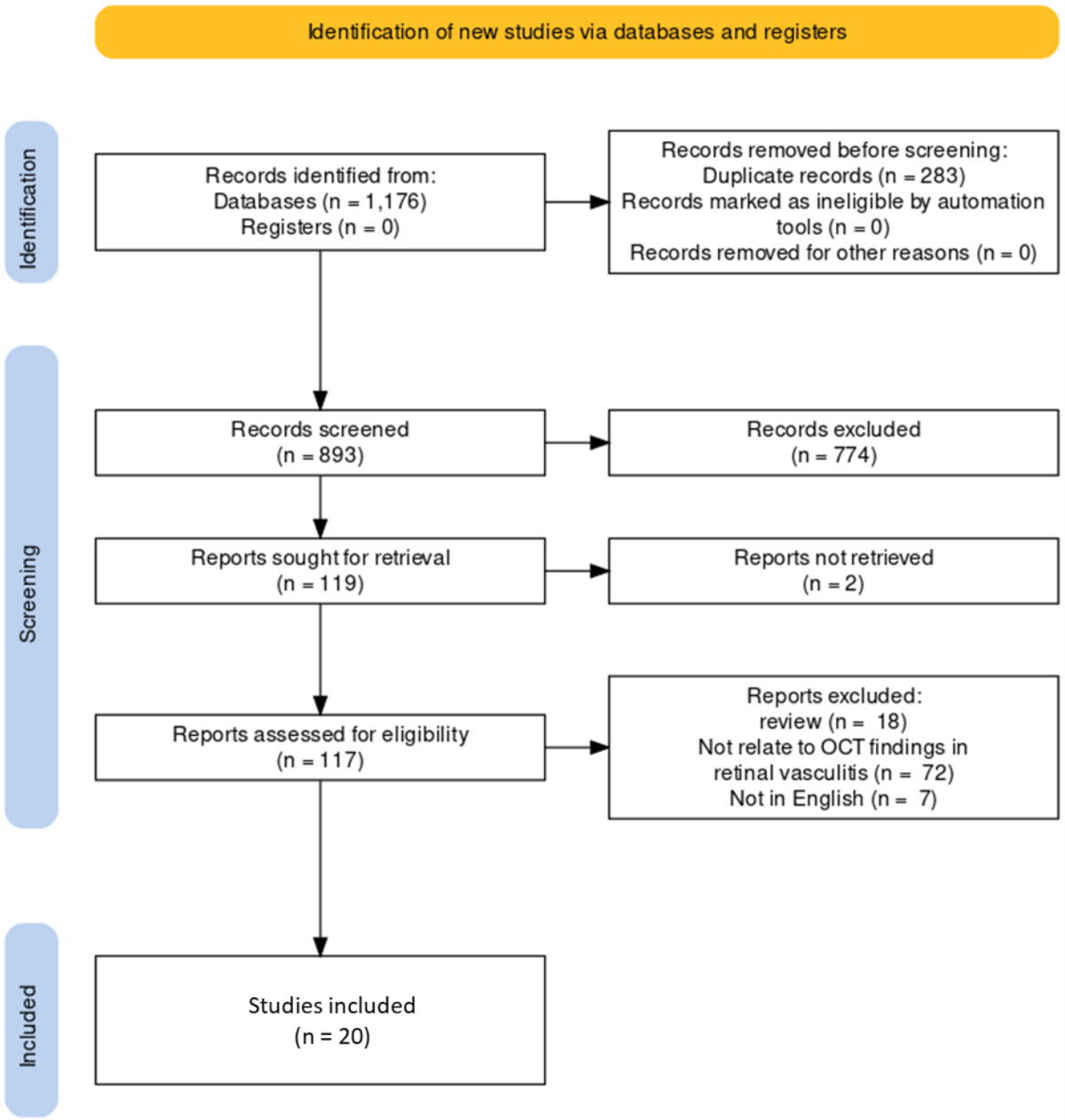


**Figure 5.2 PRISMA flow diagram for study selection**

The study types included 13 analytical cross-sectional studies(Monnet et al., 2007;Karampelas et al., 2015;Boni et al., 2016;Maleki et al., 2016;Onal et al., 2018;Emre et al., 2019;Shirahama et al., 2019;Tian et al., 2019a;Tian et al., 2019b;Abroug et al., 2021;Bousquet et al., 2021;Zarei et al., 2021;Silpa-Archa et al., 2022), 6 case series(Birnbaum et al., 2014;Teussink et al., 2016;Abucham-Neto et al., 2018;Goel et al., 2018;Knickelbein et al., 2018;Noori et al., 2021) and 1 case-control study (Kumar et al., 2021). The characteristics

of all included studies are shown in **Table 5.1**. 8 articles (Monnet et al., 2007;Karampelas et al., 2015;Maleki et al., 2016;Teussink et al., 2016;Goel et al., 2018;Knickelbein et al., 2018;Zarei et al., 2021;Silpa-Archa et al., 2022) reported features of retinal vasculitis on OCT , 6 on OCT-EDI (Birnbaum et al., 2014;Boni et al., 2016;Onal et al., 2018;Shirahama et al., 2019;Bousquet et al., 2021;Kumar et al., 2021) and 6 on OCT-A (Abucham-Neto et al., 2018;Emre et al., 2019;Tian et al., 2019a;Tian et al., 2019b;Abroug et al., 2021;Noori et al., 2021). The underlying diagnosis of uveitis reported in the included studies included idiopathic retinal vasculitis, Birdshot Chorioretinopathy, Eales disease, sarcoidosis, tuberculosis, rheumatoid arthritis, multiple sclerosis, SLE, acute retinal necrosis, Behcet's Disease, c-ANCA related systemic vasculitis, HIV, Toxoplasmosis, Takayasu arteritis, Rickettsial infection, idiopathic retinal vasculitis aneurysms and neuroretinitis syndrome, west Nile virus infection, cytomegalovirus retinitis, endogenous endophthalmitis, Susac syndrome, measles, poststreptococcal uveitis, Toxocariasis, pars planitis, intraocular lymphoma, syphilis and Crohn's disease.

**Table 5.1 Characteristics of included studies**

| Study | Country | Age of participants in diseases group (range(mean), years) | Image modality | Number of participants in diseases group | Sex (female: male) | Disease | Criteria for the diagnosis of retinal vasculitis | Study type | JBI Critical Appraisal Checklist score |
|---|---|---|---|---|---|---|---|---|---|
| *(Monnet et al., 2007) | France | 21-79 (median=55.9) | OCT | 80 | 51:29 | Birdshot Chorioretinopathy | previous medical record, clinical examination at baseline, and FA imaging(scoring) | analytical cross-sectional study | 8/8 |
| (Karampelas et al., 2015) | UK | 19-85 (median = 45) | OCT | 82 | 37:45 | idiopathic, sarcoidosis, tuberculosis, rheumatoid arthritis, multiple sclerosis, SLE, acute retinal necrosis, Bechet, cANCA, HIV | previous medical record and FA imaging(scoring) | analytical cross-sectional study | 6/8 |
| (Maleki et al., 2016) | USA | 7-83(42.7) | OCT | 80 | 55:25 | idiopathic | previous medical record, clinical examination at baseline, and FA imaging | analytical cross-sectional study | 8/8 |
| (Teussink et al., 2016) | Netherlands | 25-76 (51) | OCT | 21 | 9:12 | Birdshot Chorioretinopathy | previous medical record and FA imaging | case series | 10/10 |
| (Goel et al., 2018) | India | 16-54(27.97) | OCT | 66 | 4:62 | Eales disease | previous medical record, clinical examination at baseline, and FA imaging | case series | 8/10 |
| (Knickelbein et al., 2018) | USA | 38-64(55.5) | OCT | 11 | 9:2 | Birdshot Chorioretinopathy | previous medical record and FA imaging | case series | 10/10 |
| (Zarei et al., 2021) | Iran | 18-48 (31.6) | OCT | 15 | 4:11 | Behcet's Disease | previous medical record, clinical examination at baseline, FA imaging (scoring) | analytical cross-sectional study | 6/8 |
| (Silpa-Archa et al., 2022) | Thailand | 15-73 (40) | OCT | 48 | 28:20 | retinal vasculitis with positive QuantiFERONTB Gold Test | previous medical record, clinical examination at baseline, FA imaging | analytical cross-sectional study | 8/8 |
| (Birnbaum et al., 2014) | USA | 44-68 (58) | OCT-EDI | 14 | 12:2 | Birdshot Chorioretinopathy | previous medical record, clinical examination at baseline, and FA imaging (scoring) | case series | 9/10 |
| (Boni et al., 2016) | USA | (57.3) | OCT-EDI | 76 | 54:32 | Birdshot Chorioretinopathy | previous medical record | analytical cross-sectional study | 8/8 |
| (Onal et al., 2018) | Turkey | 18-46 (29.75) | OCT-EDI | 28 | 9:19 | Behcet's Disease | previous medical record, clinical examination at baseline, FA imaging (scoring) | analytical cross-sectional study | 6/8 |
| (Shirahama et al., 2019) | Japan | (45) | OCT-EDI | 30 | 10:20 | Behcet's Disease | previous medical record and FA imaging | analytical cross-sectional study | 6/8 |
| *(Bousquet et al., 2021) | France | (60) | OCT-EDI | 80 | 48:32 | Birdshot Chorioretinopathy | previous medical record and clinical examination at baseline | analytical cross-sectional study | 8/8 |
| (Kumar et al., 2021) | India | (34.61) | OCT-EDI | 23 | 3:20 | idiopathic | previous medical record, clinical examination at baseline, and FA imaging | case-control study | 8/10 |

*, ** = same group of researchers, FA= fluorescein angiography

**Table 5.1 (continued) Characteristics of included studies**

| Study | Country | Age of participants in diseases group (range(mean), years) | Image modality | Number of participants in diseases group | Sex (female: male) | Disease | Criteria for the diagnosis of retinal vasculitis | Study type | JBI Critical Appraisal Checklist score |
|---|---|---|---|---|---|---|---|---|---|
| (Abucham-Neto et al., 2018) | Brazil | 24-67 (36) | OCTA | 10 | 7:3 | Behcet's Disease, Toxoplasmosis, Sarcoidosis, Takayasu arteritis, idiopathic | previous medical record and FA imaging | case series | 6/10 |
| **(Tian et al., 2019b) | Switzerland | (45.9) | OCTA | 58 | 32:26 | IU (sarcoidosis, Behcet, Idiopathic) | previous medical record, clinical examination at baseline, FA imaging | analytical cross-sectional study | 8/8 |
| **(Tian et al., 2019a) | Switzerland | (45.5) | OCTA | 88 | 54:34 | IU (sarcoidosis, latent TB, Behcet's Disease, Idiopathic) | previous medical record, clinical examination at baseline, FA imaging | analytical cross-sectional study | 8/8 |
| (Emre et al., 2019) | Turkey | (39.44) | OCTA | 16 | 10:6 | Behcet's Disease | previous medical record, clinical examination at baseline, and FA imaging | analytical cross-sectional study | 6/8 |
|  | USA | No data | OCTA | 17 | No data | Birdshot Chorioretinopathy, pars planitis, intraocular lymphoma, syphilis, undifferentiated cause | previous medical record and FA imaging | case series | 7/10 |
| (Abroug et al., 2021) | Tunisia | (31.5) | OCTA | 284 | 117:167 | idiopathic retinal vasculitis, Eales disease, sarcoidosis, tuberculosis, Birdshot Chorioretinopathy, multiple sclerosis, SLE, acute retinal necrosis, Behcet's Disease, Toxoplasmosis, Rickettsial infection, idiopathic retinal vasculitis aneurysms and neuroretinitis syndrome, west Nile virus infection, cytomegalovirus retinitis, endogenous endophthalmitis, Susac syndrome, measles, poststreptococcal uveitis, Toxocariasis, syphilis and Crohn's disease. | previous medical record, clinical examination at baseline, and FA imaging | analytical cross-sectional study | 6/8 |

*, ** = same group of researchers, FA= fluorescein angiography

**Bias assessment**

We assessed the bias using JBI Critical Appraisal Checklist for analytical cross-sectional studies, prevalence studies, case-control or case series, depending on the type of study. All eligible studies that scored on more than half of the checklist are considered appropriate to include for synthesis, as shown in Table 5.1. Among the checklist, we noticed some common biases in these eligible articles. Five of thirteen analytical cross-sectional studies (Karampelas et al., 2015;Emre et al., 2019;Shirahama et al., 2019;Abroug et al., 2021;Zarei et al., 2021) did not mention possible confounding factors associated with observed imaging features in OCT related to the diagnosis of retinal vasculitis and did not state how to deal with associated confounding factors. For the case series, three studies did not report appropriate demographic data (Birnbaum et al., 2014;Abucham-Neto et al., 2018;Noori et al., 2021).

Of all primary studies related to OCT and retinal vasculitis, there was only one diagnostic test accuracy study. This study by Tian M et al. (Tian et al., 2019a) used accuracy type statistics, including sensitivity and specificity to compare OCT-A findings with fluorescein angiography, as the reference for diagnosing retinal vasculitis. One limitation of using fluorescein angiography as the reference is this technique mainly evaluates the superficial capillary plexus perfusion (Moussa et al., 2019). Although this study could complete all JBI Critical Appraisal Checklist, which made us considered included for synthesis, there was no other diagnostic test accuracy study to compare the results.

**OCT findings**

**OCT signs of active inflammation associated with retinal vasculitis**

Seven of the 8 studies reported OCT findings associated with the secondary effects of retinal vasculitis, including cystoid macular oedema, epiretinal membrane and disruption of

ellipsoid zone. One study reported on perivascular retinal thickness, but none of the 8 studies (Monnet et al., 2007;Karampelas et al., 2015;Maleki et al., 2016;Teussink et al., 2016;Goel et al., 2018;Knickelbein et al., 2018;Zarei et al., 2021;Silpa-Archa et al., 2022) reporting OCT features related to retinal vasculitis, reported primary vascular abnormalities.

Five studies reported the association between OCT findings and secondary effects in retinal vasculitis (Monnet et al., 2007;Maleki et al., 2016;Teussink et al., 2016;Goel et al., 2018). In the first study, Monnet et al. conducted an analytical cross-sectional study of 80 birdshot chorioretinopathy patients (160 eyes) (Monnet et al., 2007). They graded the retinal vascular leakage using fluorescein angiography, scoring from 0-4, with 4 being the most severe leakage. These leakage scores were compared with associated OCT findings, including epiretinal membranes and the third hyperreflective band (the hyperreflectivity band in the levels of photoreceptors)(Spaide and Curcio, 2011). This third band corresponds to the junction of the inner and outer segments of the photoreceptors. The result suggested that the increasing grade of fluorescein leakage was associated with the presence of epiretinal membranes (logistic regression models with the generalised estimating equation, adjusted p-value = 0.024) but not the intactness of third hyperreflective band (adjusted p-value= 0.386). It should be noted that this study was conducted in 2007, relatively older than other studies included in this systematic review. The study limitations were a smaller field of view of fluorescein angiography, only 60-degree and an older OCT machine (OCT3; Humphrey Instruments). They also compared the presence/absence of retinal vasculitis with the same OCT findings. The logistic regression models showed no association between the presence of retinal vasculitis and epiretinal membranes (adjusted p-value= 0.433) or the intactness of the third hyperreflective band (adjusted p-value= 0.418).

Maleki et al. conducted an analytical retrospective study of 80 patients with idiopathic retinal vasculitis (150 eyes) (Maleki et al., 2016). Poor visual outcome was defined as visual acuity lower than 20/40 or decrease in 2 or more lines. Poor visual outcome was associated with the OCT findings of cystoid macular oedema (Fischer's exact test, p=0.0001) and epiretinal membrane (p=0.008). Only cystoid macular oedema remained as an indicator after using multivariate binary logistic regression analysis to correct for confounding factors (OR 5.54, 95% CI 1.81-16.99, p=0.003); other prognostic factors were logMAR visual acuity at the first visit (OR 3.78, 95% CI 1.75-8.16, p=0.001) and macular ischemia (OR 5.12, 95% CI 1.12-23.04, p=0.036).

Teussink et al. reported a narrative case series of OCT findings in birdshot chorioretinopathy in 21 patients (42 eyes) in 2016 (Teussink et al., 2016), without statistical analysis. The authors noted disruption of the ellipsoid zone on OCT in 7 (33%) patients. Among these 7 patients, 4 had these disrupted ellipsoid zones reconstitution after resolution of the retinal vasculitis, whereas 3 with poorly responsive retinal vasculitis did not. The authors concluded that this ellipsoid zone disruption might relate to the activity of retinal vasculitis.

In a study published in 2018, Goel et al. conducted case series in 79 eyes of 66 patients with Eales disease and active vasculitis (Goel et al., 2018). The study did not report any association type of statistics. They indicated that OCT showed more macular complications in the eyes with active vasculitis than in the eyes with inactive vasculitis. In this study, macular complications included macular oedema, epiretinal membrane, macular thinning, hard exudates, haemorrhages, inner retinal or inner limiting membrane folds, pre-macular haemorrhages and macular hole.

Another study by Silpa-Archa et al. reported the OCT findings in 73 eyes of 48 patients with retinal vasculitis (Silpa-Archa et al., 2022). They compared OCT findings in patients with retinal vasculitis with the poor visual outcome (visual acuity worse than 20/200) and good visual outcome (visual acuity better or equal to 20/200). The results showed a higher proportion of OCT findings, including presence of epiretinal membrane and outer retinal disruption in the poor visual outcome group (Fischer's exact test, $p<0.05$), but there was no difference in the proportion of cystoid macular oedema, overlying vitritis and submacular fluid between two groups. The presence of outer retinal disruption remained as an indicator of poor visual outcome after using multivariate binary logistic regression analysis to correct for confounding factors (OR 21.12, 95% CI 1.39-320.28, p=0.028)

**Macular thickness alteration associated with the retinal vasculitis**

Two studies have highlighted that increased central macular thickness associated with retinal vasculitis (Monnet et al., 2007;Karampelas et al., 2015). The study by Monnet et al. of birdshot chorioretinopathy patients measured the macular thickness using OCT3 software (Zeiss-Humphrey) (Monnet et al., 2007). The program calculates the mean retinal thickness of 512 points within 1 mm of the fixation point. The study found that an increase in grading of fluorescein leakage severity was related to increased macular thickness (adjusted p-value <0.001). However, there was no difference when the mean macular thickness was compared between the presence and absence of retinal vasculitis groups (adjusted p-value = 0.247)

Another study by Karampelas et al. in 2015 reported an analytical cross-sectional study from 82 eyes of 82 uveitis patients (Karampelas et al., 2015). The central macular thickness was calculated using Topcon's FastMap software. The study graded the vasculitis by measuring macular and peripheral leakage index, defined as leakage area as a percentage of total area using wide-field fluorescein angiography images of the macula or the peripheral area. Their

result found that central macular thickness was positively correlated with macular leakage index (Spearman correlation coefficient (r) = 0.485, p-value < 0.001) and weakly with foveal avascular zone size (r = 0.291, p-value = 0.03), and not correlated with peripheral leakage index (r = -0.157, p-value = 0.248).

The perivascular retinal thickness in retinal vasculitis has been investigated by OCT. The case series by Knickelbein et al in 2018 characterised 11 patients (22 eyes) with retinal vasculitis from birdshot chorioretinopathy by using OCT scans centred on the proximal branches of the superior and inferior retinal vessels, fovea, and the optic nerve head (Knickelbein et al., 2018). They measured the perivascular retinal thickness by using system software (Zeiss Cirrus Viewer) on 6x6mm scans of the proximal temporal arcades. The mean perivascular retinal thickness at diagnosis (mean = 397.46 um) showed a decrease after one month of treatment with prednisolone (mean = 346.9 um; paired t-test, p-value<0.00001, n= 3 patients). For the other 8 patients, the authors concluded that 4 patients had perivascular retinal thickness increased during active disease and decreased during quiescence (no statistics applied), while another 4 patients did not have uveitis activity or perivascular retinal thickness change.

A study by Zarei et al. in 2021 correlated peripapillary OCT parameters and fluorescein angiography inflammatory score in 15 patients (28 eyes) with Behcet's disease and retinal vasculitis (Zarei et al., 2021). The fluorescein angiography inflammatory score was developed to indicate the inflammatory activity of each fluorescein angiography image ranging from 0 and 43. Central subfield macular thickness positively correlated with fluorescein angiography inflammatory score (Spearman correlation coefficient (r) = 0.413, p-value < 0.001). The fluorescein angiography inflammatory score also positively correlated with the peripapillary

retinal thickness measured at 2.2mm (r = 0.443, p-value < 0.001) and 3.45 mm diameter (r = 0.707, p-value < 0.001), and peripapillary retinal nerve fibre layer thickness (r = 0.850, p-value < 0.001).

**OCT-EDI finding**

**Choroidal thickness alteration as a finding associated with the retinal vasculitis**

Five studies have investigated subfoveal choroidal thickness alteration in retinal vasculitis (Boni et al., 2016;Shirahama et al., 2019;Bousquet et al., 2021;Kumar et al., 2021). Böni et al. conducted an analytical cross-sectional study of 86 patients (172 eyes) with birdshot chorioretinopathy in 2016(Boni et al., 2016). They compared the presence of retinal vasculitis with OCT-EDI findings, including change in choroidal thickness, suprachoroidal space, macular lesion (focal or diffuse lesion) and any choroidal lesion. There was no significant association between the presence of retinal vasculitis with choroidal thickness (OR 1.43, adjusted p-value = 0.37), suprachoroidal space (OR 0.91, adjusted p-value = 0.80), macular lesion (OR 0.80, adjusted p-value = 0.50) and any choroidal lesion (OR 1.04, adjusted p-value = 0.91).

The second study by Shirahama et al. was an analytical cross-sectional study that included 30 Behcet's uveitis patients (51 eyes) (Shirahama et al., 2019). This study graded vasculitis by a fluorescein angiography leakage score for the peripheral retina, macula, and optic disc on a scale from 0 to 3(Keino et al., 2011). The leakage score was then compared with the subfoveal choroidal thickness measured manually with OCT-EDI. They reported a significant positive correlation between the subfoveal choroidal thickness and leakage score in the total retina ($r^2$=0.210, p=0.0007, linear regression analysis).

Bousquet et al. conducted an analytical cross-sectional study of 80 birdshot chorioretinopathy patients (160 eyes) (Bousquet et al., 2021). The study found that subfoveal choroidal thickness was significantly greater in birdshot chorioretinopathy patients with vasculitis than without vasculitis (274.6 um vs 228.5 um, p-value=0.006, Student t-test). The presence of retinal vasculitis was associated with the choroidal vascularity index, which was defined by the ratio of the luminal area to the total choroidal area in OCT-EDI. The result showed that the choroidal vascularity index was positively associated with the presence of the retinal vasculitis in the univariate analysis (p-value < 0.001, generalised linear regression models with generalised estimating equation) but not the multivariate analysis (p-value = 0.24). Onal et al. reported the analytical cross-sectional study of 28 Behcet's uveitis patients (56 eyes). The study investigated the correlation of retinal/choroidal thickness with retinal vascular leakage using fluorescein angiography scores ranging from 0 to 40 developed by the ASUWOG (Onal et al., 2018). The result showed there was no statistically significant correlation between the fluorescein angiographic score and the subfoveal choroidal thickness (r=-0.221, p-value=0.105). However, the central foveal thickness was correlated with the fluorescein angiographic score (Spearman correlation coefficient (r) = 0.605, p-value < 0.001). The sub-analysis showed that retinal vascular staining/leakage score correlated with choroidal stroma to choroidal vessel lumen ratio in OCT (r=0.300, p-value=0.036).

Kumar et al., in a case-control study compared 23 acute idiopathic retinal vasculitis patients (36 eyes) with 25 control patients (50 eyes) using OCT-EDI (Kumar et al., 2021). There was a significant greater subfoveal choroidal thickness in the vasculitis group compared with the control group (338.86um vs 296.72um, p<0.001, Mann-Whitney U test).

**Other OCT-EDI findings associated with the retinal vasculitis**

A case-series of 14 birdshot chorioretinopathy patients (58 eyes) by Birnbaum et al., 2014 correlated the OCT-EDI findings with the retinal vasculitis using a fluorescein angiography leakage score ranged from 0 (none) to 2 (Birnbaum et al., 2014). The leakage score correlated with the presence of suprachoroidal fluid (Spearman correlation coefficient (r) = 0.45, p-value < 0.001). but not RPE disruption (r = -0.20, p-value = 0.15), retinal thickness (r = 0.01, p-value = 0.97) nor ellipsoid layer disruption (r = -0.21, p-value < 0.11).

**OCT-A finding**

**The primary sign of active inflammation in OCT-A**

The case-series by Abucham-Neto et al. examined the possibility of detecting the primary sign of active inflammation in retinal vasculitis, which they expected to see in relation to vascular sheathing in OCT-A. They explored 3x3 mm and 8x8 mm OCT-A of 10 patients (19 eyes) with retinal vasculitis (Abucham-Neto et al., 2018). They reported that they could not detect any primary sign of active inflammation around the affected vessels on OCT-A, even though 74% of eyes had shown active signs on fluorescein angiography images. However, secondary complications, including capillary dropout, foveal avascular zone, telangiectasia, shunts and area of neovascularisation, could be detected in 74% of eyes using OCT-A. This study did not do any association type of statistical analysis.

**Capillary vessel density alteration associated with the retinal vasculitis**

Four studies have reported retinal capillary vessel density alteration associated with retinal vasculitis (Emre et al., 2019;Tian et al., 2019a;Tian et al., 2019b). In the first one, Emre et al., 2019 conducted an analytical cross-sectional study of 16 patients (32 eyes) with Behcet's uveitis (Emre et al., 2019). They calculated the capillary vessel density up to 1.25 mm from the

foveolar centre. The results suggested that the eyes with a history of previous retinal vasculitis had significantly lower foveal capillary vessel density in superficial plexi (20.5% vasculitis vs 29.3% no vasculitis); and deep plexi (21.3% vasculitis vs 31.7% no vasculitis, p-value < 0.05, student t-test).

Tian et al., 2019 (Tian et al., 2019b) conducted an analytical cross-sectional study of 58 patients (93 eyes) with intermediate uveitis (IU). Here, they defined capillary non-perfusion on OCT-A as an area of total and profound capillary loss more than or equal to a quarter of the disc (Schaal et al., 2019). Capillary non-perfusion was compared between eyes with and without retinal vasculitis using the Chi-squared test. On the widefield montage scan, IU with vasculitis had a higher prevalence of non-perfusion of the superficial capillary plexus (19% vasculitis vs 3% no vasculitis, p-value=0.008); and deep capillary plexus (29% vasculitis vs 7% no vasculitis, p-value=0.008). However, OCT-A 3x3 scan did not show any difference in non-perfusion of the superficial capillary plexus (10% vasculitis vs 14% no vasculitis, p-value=0.6) and deep capillary plexus (29% vasculitis vs 18% no vasculitis, p-value=0.3). Foveal avascular zone parameters, including raw length, circularity and size, also differed between IU only and IU with vasculitis (p-value<0.05, ANOVA test). However, the multivariable regression analysis showed these effects were accounted for by epiretinal membrane and cystoid macular oedema rather than the disease entity.

A consecutive analytical cross-sectional study from the same group (Tian et al., 2019a) explored 88 IU patients (164 eyes). Capillary non-perfusion was defined as before, and capillary hypoperfusion was defined as an area of reduced capillary density less that one quarter of the disc (Schaal et al., 2019). The capillary non-perfusion and hypoperfusion on wide-field montage scans were compared with both the presence of retinal vasculitis and the presence of

capillary leakage on fluorescein angiography images. Their result showed that IU with vasculitis had non-perfusion and hypoperfusion in deep capillary plexus and superficial capillary plexus more frequently than IU without vasculitis (Phi and Cramer's V, p-value < 0.05); but not choriocapillaris nor choroid. There was no association between capillary leakage on fluorescein angiography and non-perfusion or reduced perfusion in superficial capillary plexus, deep capillary plexus, choriocapillaris or choroid. Furthermore, the study compared the diagnostic accuracy of capillary non-perfusion in OCT-A with the gold standard of capillary dropout and ischaemia finding in fluorescein angiography images. The sensitivity of detection of capillary dropout in superficial capillary plexus and deep capillary plexus were 15% and 24%, while the specificity was 97% and 94%, respectively.

The recent study by Abroug et al. retrospectively analysed 408 eyes of 284 retinal vasculitis patients (Abroug et al., 2021). Among these patients, OCT-A was performed in 110 eyes. They found that OCT-A of occlusive retinal vasculitis (50 eyes) showed more frequent areas of capillary nonperfusion or hypoperfusion comparing with non-occlusive retinal vasculitis (60 eyes) (Fischer's exact test, $p < 0.001$). So far, this study included the highest number of patients with retinal vasculitis. However, when interpreting the results in comparison with other studies, it should be noted that there were no control patients available for comparing the OCT findings with individuals who did not have vasculitis.

**Assessment of the perivascular retinal thickness**

The retrospective case series analysed 12x12mm sweptsource OCT-A scans of 17 patients with retinal vasculitis (Noori et al., 2021). These 12x12mm fovea-centred scans allowed the OCT-A machine to image a relatively large area without using a montage image. The authors combined total retinal thickness maps with retinal flow (customised slab between

49 and 149um beneath the internal limiting membrane) in an enface image. They found that the perivascular retinal thickening measured by this method was visually correlated with the leakage/staining on FA imaging (no statistical analysis). There was also a reduction in perivascular retinal thickening with successful treatment in a small subgroup of patients.

### 5.4 Discussion

Retinal vasculitis can present as part of many different uveitis entities, including infectious, noninfectious with systemic disease, purely ocular with known phenotype or idiopathic (Datoo O'Keefe and Rao, 2021;Agarwal et al., 2022). The clinical heterogeneity of retinal vasculitis and the fact that there are no currently standard criteria for diagnosis or classification of the disease can make the assessment of retinal vasculitis challenging (Agarwal et al., 2017;Diala et al., 2021). The SUN working group indicate that more studies are needed to define retinal vasculitis (Jabs et al., 2005), and there is also no consensus on grading its severity. Despite its invasiveness and time taken, fluorescein angiography is still the gold standard and clinical mainstay for diagnosing and assessing retinal vasculitis (Tugal-Tutkun et al., 2010a;Leder et al., 2013;Sheemar et al., 2019) usually in a widefield format (Reeves et al., 2013). This systematic review explored alternative imaging to understand OCT findings in retinal vasculitis. I have found that research into OCT, EDI-OCT and OCT-A in retinal vasculitis has predominantly focused on its secondary effects and complications. The OCT findings from imaging inflamed vessels and perivascular tissue has been mostly ignored. One study reported a decrease in perivascular retinal thickness after prednisolone treatment for retinal vasculitis, but in only 3 patients (Knickelbein et al., 2018). One case series of 11 patients investigated primary signs of retinal vasculitis in OCT-A (Abucham-Neto et al., 2018) but reported none detectable. Another case series utilising swept-source OCT-A reported perivascular retinal thickening visually correlated with vascular leakage/staining in FA

imaging but did not report their statistic calculation (Noori et al., 2021). To the best of our knowledge and through our searching strategy, there is no other study investigating the primary sign of inflammation in or around the retinal vessels in OCT, OCT-EDI or OCT-A. This may in part be because inflamed vessels are frequently located outside the standard field of view of OCT, and certainly a 3x3mm OCT-A.

The secondary effects of retinal vasculitis on the macula are much easier to observe with OCT. These OCT features include cystoid macule oedema (reported in 3 studies) (Monnet et al., 2007;Maleki et al., 2016;Goel et al., 2018), epiretinal membrane (reported in 4 studies) (Monnet et al., 2007;Maleki et al., 2016;Goel et al., 2018;Silpa-Archa et al., 2022), and the disruption in the ellipsoid zone (reported in 2 studies) (Teussink et al., 2016;Silpa-Archa et al., 2022). These secondary effects are non-specific so could not be used to diagnose retinal vasculitis. However, some of this research suggests unsurprisingly that secondary complications increase the risk of poorer visual prognosis (Mir et al., 2017;Sharief et al., 2017). This evidence supports using OCT to monitor these secondary complications in retinal vasculitis (Ali et al., 2014;Tugal-Tutkun et al., 2017).

The thickness of the retina or macula measured by OCT is a potential indicator of retinal inflammation, but again is non-specific and may be due to an inflammatory effect or intraretinal oedema. Four studies used OCT to measure retinal/macular thickness and compared it with the presence of retinal vasculitis or fluorescein angiography leakage score (Monnet et al., 2007;Karampelas et al., 2015;Knickelbein et al., 2018;Zarei et al., 2021). The results suggest that increased retinal/macular thickness correlates with retinal vasculitis, but it is not clear if this is purely driven by macular oedema. Two studies hypothesised that the increased thickness demonstrates retinal inflammation, and macular oedema could be the late consequence of

inflammation (Karampelas et al., 2015;Zarei et al., 2021). Retinal vasculitis showed some association to increased choroidal thickness measured by OCT-EDI in 4 studies, but not a fifth (Boni et al., 2016;Onal et al., 2018;Shirahama et al., 2019;Bousquet et al., 2021;Kumar et al., 2021). Two of these studies were in birdshot chorioretinopathy which is disease with a choroidal inflammatory component, so increased choroidal thickness is likely to reflect overall disease activity. An alteration in choroidal thickness was not present in Behcet's uveitis, a disease specifically causing inflammation of the retina and its vasculature (Onal et al., 2018). Unless retinal vasculitis is linked to choroidal inflammation (as in birdshot chorioretinopathy) it remains unclear how retinal vasculitis would be linked to an increase in choroidal thickness. Apart from choroidal inflammation, choroidal thickening could be caused by other diseases such as Pachychoroid Spectrum, including pachychoroid pigment epitheliopathy, central serous chorioretinopathy (CSC), pachychoroid neovasculopathy and polypoidal choroidal vasculopathy (Xie et al., 2021). Moreover, neoplastic lesions could also deform the choroidal profile. It is evident that further research is needed to investigate choroidal thickness parameters in retinal vasculitis in a range of uveitides.

In OCT-A, capillary vessel density seems to be a promising tool for assessing occlusive features of retinal vasculitis, although it is currently limited by the small field of view confined to the central macula. One study tried to overcome this with a montage OCT-A with more positive results. Four studies investigated capillary vessel density and non-perfusion using OCT-A and suggested decreased capillary vessel density or more non-perfusion in retinal vasculitis. One study reported the specificity of OCT-A to detect capillary dropout in superficial and deep capillary plexuses was 97% and 94% (Tian et al., 2019a), but the very low sensitivity will mean OCT-A will miss a high proportion with non-perfusion on fluorescein angiography. Capillary vessel density was also explored in a recent meta-analysis in Behcet's

patients regardless of retinal vasculitis (Ji et al., 2022) and showed decreased deep and superficial capillary vessel density in Behcet's disease.

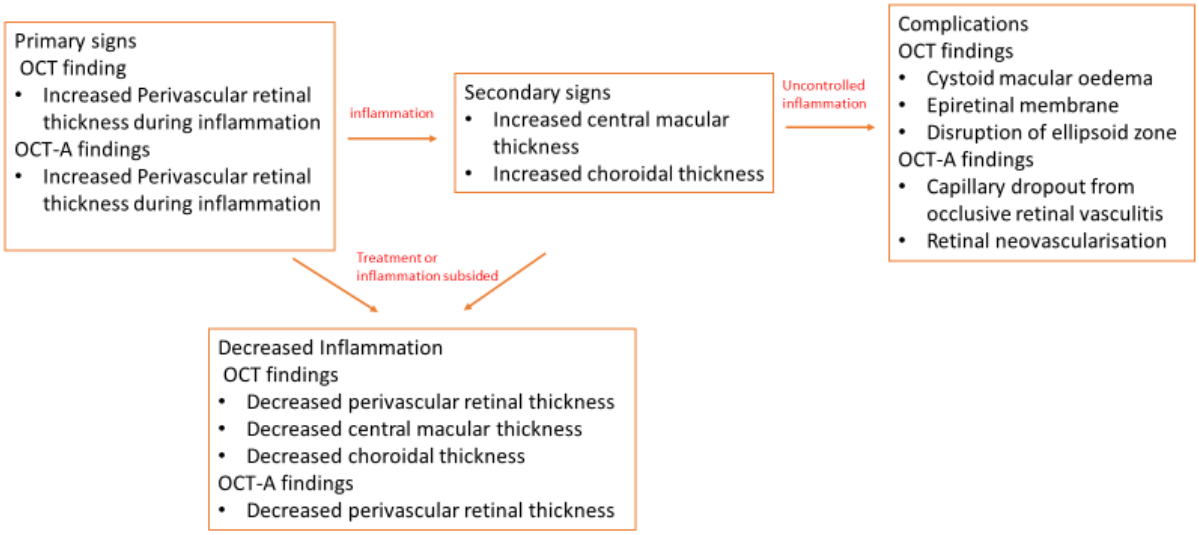


**Figure 5.3 Proposed mechanistic model of OCT/OCT-A findings related to pathogenic events of retinal vasculitis**

This diagram illustrates the proposed mechanistic model outlining the OCT and OCT-A findings associated with the pathogenic events of retinal vasculitis, including primary signs, secondary signs, complications, and changes during decreased inflammation. Although there is lack of strong evidence on OCT/OCT-A findings of retinal vasculitis, I propose here a mechanistic model of the pathogenic events of retinal vasculitis summarising from this systematic review. The primary sign of retinal vasculitis might exhibit an increase in perivascular retinal thickness during episodes of inflammation. This change is evident in both OCT and OCT-A. Beyond the primary sign, secondary signs are the extent of vascular inflammation on the retina and the choroid. The secondary signs could include an increase in central macular thickness and choroidal thickness. Retinal vasculitis could lead to various complications that have distinct OCT and OCT-A signatures. Among the OCT findings are cystoid macular oedema, epiretinal membrane formation, and the disruption of the ellipsoid

zone, all of which potentially contribute to visual impairment. On the OCT-A, we possibly observe capillary dropout and/or neovascularization, which are associated with disease progression and potential vision-threatening complications. As the inflammation subsides with appropriate treatment or disease remission, a reversal of certain findings is typically observed. OCT findings could show a decrease in perivascular retinal thickness, central macular thickness, and choroidal thickness. Monitoring these parameters could be crucial for assessing treatment response and disease activity. Similarly, on OCT-A, a decrease in perivascular retinal thickness is noted during the phase of decreased inflammation.

This study's limitations include limiting studies to those published in English which was a pragmatic approach to the resources available. Otherwise I am confident that these clear and broad search terms will have identified the relevant studies in this area. I only identified a small number of studies which were all retrospective or cross-sectional, investigating different features of the disease, at different stages (inactive or active or previous retinal vasculitis), and with different study designs. This made it impossible to conduct a meta-analysis or other statistical comparison between studies. Moreover, each study used different criteria to diagnose retinal vasculitis and different fluorescein angiography grading systems (Monnet et al., 2007;Birnbaum et al., 2014;Karampelas et al., 2015;Onal et al., 2018;Zarei et al., 2021).

There is clearly a large deficit in our knowledge of OCT, EDI-OCT and OCT-A in retinal vasculitis, especially when compared to other retinal diseases. There is evidently a need to investigate the OCT features of inflamed retinal vessels and perivascular retina, and the relationship between retinal vasculitis and structural changes in the macula and choroid, and how they might be used to monitor progressive disease. OCT-A has the potential to provide more information on capillary perfusion in retinal vasculitis but is limited by a narrow field of

view to the central macula at present. Swept-source OCT may overcome some of these issues, but further research investigating its findings in retinal vasculitis is awaited.

In conclusion, this systematic review found a paucity of research into OCT in retinal vasculitis and that it was mostly focused on the secondary effects of retinal vasculitis affecting the macula in specific uveitis entities. There is no evidence to suggest that in the near future current OCT technologies are likely to supersede fluorescein angiography in identifying active retinal vasculitis and associated non-perfusion, or grading its severity.

# Chapter 6 Develop clinical grading of retinal vasculitis in a wide-field fluorescence angiography

In this chapter, I present my study that was published in Retina.

Dhirachaikulpanich, D., Madhusudhan, S., Parry, D., Babiker, S., Zheng, Y., and Beare, N.A. V. (2023). Retinal vasculitis severity assessment: intra- and inter-observer reliability of a new scheme for grading wide-field fluorescein angiograms in retinal vasculitis. *Retina* 43, 1534-1543.

WFFA is commonly used to assess retinal vasculitis, which manifests as vascular leakage and occlusion. Currently, there is no standard grading scheme for retinal vasculitis severity. This study proposes a novel retinal vasculitis grading scheme and assesses its reliability and reproducibility. A grading scheme was developed to assess both leakage and occlusion in retinal vasculitis. WFFA images from 50 retinal vasculitis patients were graded by four graders, and one grader graded them twice. Intra-class correlation coefficient (ICC) was used to determine intra-interobserver reliability. Generalized linear models (GLM) were calculated to associate the scoring with visual acuity. Repeated grading by the same grader showed good intraobserver reliability for both leakage (ICC = 0.85, 95%CI 0.78-0.89) and occlusion (ICC = 0.82, 95%CI 0.75-0.88) scores. Interobserver reliability among 4 independent graders showed good agreement for both leakage (ICC = 0.66, 95%CI 0.49-0.77) and occlusion (ICC = 0.75, 95%CI 0.68-0.81) scores. Increasing leakage score was significantly associated with worse concurrent visual acuity (GLM, $\beta$=0.090, $p<0.01$) and at 1-year follow-up (GLM, $\beta$=0.063, $p<0.01$). This proposed grading scheme for retinal vasculitis has good to excellent intra and interobserver reliability across a range of graders. The leakage score related to present and future visual acuity.

## 6.1 Introduction

Retinal vasculitis is inflammation of the retinal vessels (Teussink et al., 2016), which constitute the inner blood-retina barrier. It has multiple causes, including infection, autoimmune diseases, inflammation, neoplastic disorders, and can be idiopathic(Rosenbaum et al., 2016;Agarwal et al., 2022). Retinal vasculitis potentially leads to visual loss due to macular edema and vascular occlusion.

Assessing retinal vasculitis can be challenging. Fundoscopic findings include perivascular haemorrhage, perivascular infiltrate, vessel sheathing, vessel calibre abnormalities, non-perfused retina and retinal neovascularization (Ebrahimiadib et al., 2021), but can be subtle or absent when retinal vasculitis is subclinical. Currently, fluorescein angiography, preferably wide-field, is the standard method to assess retinal vasculitis (Karampelas et al., 2015). Retinal vasculitis manifests as vascular leakage, occlusion of vessels, or vessel wall staining on the angiogram (Agarwal et al., 2017). Leakage or breakdown of the inner blood-retina barrier can affect arterioles, venules, or capillaries. It is generally accepted that vascular leakage, either segmental or widespread (Reeves et al., 2013), is an indicator of inflammation, and disease activity (Kang and Lee, 2014). Inflamed vessels, either capillary or larger vessels, can occlude, resulting in retinal non-perfusion and if extensive, lead to neovascularisation. Although an important indicator of severity, the presence of occlusion or non-perfusion is not a reliable indicator of active disease because it persists after inflammation has resolved.

Current clinical practice lacks agreement on a suitable severity classification or grading system for retinal vasculitis. Recent clinical trials have merely used the presence or absence of ‘active retinal vasculitis’ as an end-point, ignoring all information on severity (Anglade et al.,

2008;Nguyen et al., 2016;Suhler et al., 2018). The SUN working group announced in 2005 that "there was consensus that the definition of retinal vasculitis required more work" (Jabs et al., 2005). Later, the ASUWOG developed a 40-point scoring scheme to assess fluorescein angiography for posterior uveitis in standard images (Tugal-Tutkun et al., 2010a). The ASUWOG scheme has not been widely adopted despite showing high-interobserver reliability even in WFFA images (Moon et al., 2017). It has only been used in published studies of Behcet's uveitis (Kang and Lee, 2014) including monitoring response to adalimumab (Kim et al., 2022). The ASUWOG scoring scheme is too detailed for practical clinical use, or even for clinical trials.

Lack of a standardised grading system for retinal vasculitis could cause communication issues among clinicians and researchers and hinder the development of new treatments for retinal vasculitis. This study aimed to develop a grading scheme for retinal vasculitis which was meaningful and easy to use. The study focuses on vascular leakage and occlusion as the main criteria for WFFA imaging and their extent in the peripheral or central retinal zones. I tested the reliability of the novel grading scheme by analysing agreement between same and different graders and correlated severity scores with visual acuity.

## 6.2 Methods

### Study Design

This study was a single-centre, retrospective clinical study of patients diagnosed with retinal vasculitis and treated at St Paul's Eye Unit, Liverpool University Hospitals NHS Trust, Liverpool, UK, between 2009 and 2022. The study was conducted in accordance with the Declaration of Helsinki and was approved by the NHS Research Ethics Committee of the North of Scotland (reference number 19/NS/0186).

Two investigators identified patients attending St Paul's Eye Unit with retinal vasculitis based on electronic medical records. The diagnosis of uveitis was based on the SUN criteria (Jabs et al., 2005). Eligible patients were more than 18 years old with known retinal vasculitis in one or both eyes, and had previous WFFA. Patients with proliferative diabetic retinopathy, retinal vascular disease other than retinal vasculitis or other ocular diseases which would interfere with WFFA assessment were excluded. Informed consent was obtained from each patient.

Demographic data collected included age, gender, and race. I also collected the final etiological diagnosis of uveitis and the details of systemic immunosuppressant and local (ocular and periocular) treatment. Visual acuity was gathered as corrected visual acuity (CVA) (corrected with glasses or a pinhole) at the time of imaging and at 1-year follow-up. CVA was converted from Snellen to logarithm of the minimum angle of resolution (logMAR) for statistical analysis.

**Wide-field Fluorescein angiography**

Retinal angiography was performed using SPRECTALIS HRA (Heidelberg Engineering, Heidelberg, Germany)(105 degrees field of view) or HRA2 Scanning Laser Ophthalmoscope (SLO)(Heidelberg Engineering, Heidelberg, Germany) with the use of Staurenghi SLO 230 contact lens (Ocular Instruments Inc. Bellevue, WI, USA)(150 degrees field of view)(Reeves et al., 2013) or Optomap P200DTX (200 degrees field of view) or P200MA (200 degrees field of view)(Optos, Dunfermline, UK)(Patel et al., 2020). Angiograms were centred on the posterior pole of the fundus.

**New retinal vasculitis clinical grading for WFFA images**

The new grading scheme was based on graded scoring for degree of leakage and occlusion on WFFA per eye of a patient. First, the quality of images was assessed for focus and clarity and any obscuration from media opacity, and graded as ungradeable (0) where it was not possible to assess leakage from the retinal vessels or retinal perfusion with confidence, or when less than two retinal quadrants were seen (see below). For gradable images, image quality was noted as poor (1), fair (2), or good (3).

The fundus was divided into peripheral and central zones. Central zone was defined by a circle centred on the foveal centre with distance from the central fovea to the nasal optic disc edge as its radius. This zone was chosen to include all of the macula, the optic disc and the temporal vascular arcades, all of which are critical to maintaining central vision. Vascular leakage or occlusion in this zone is more likely to have consequences for vision and is therefore deemed more severe than changes in the peripheral zone. All of the visible retina external to the central zone was defined as the peripheral zone. Both zones were divided into 4 quadrants based on horizontal and vertical lines intersecting at the fovea (**Figure 6.1**).

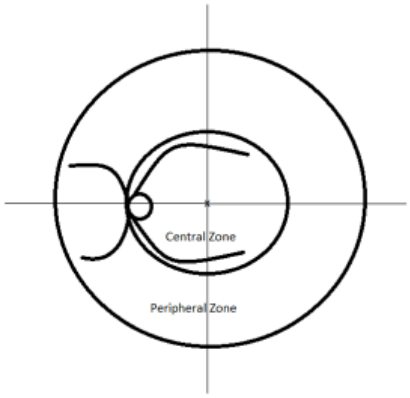


Zone description
Central Zone - Circle centred on the central fovea with radius of central fovea to nasal disc edge
Peripheral Zone - Zone peripheral to Central Zone (quadrants dividing peripheral and central zones meet at the fovea)

Leakage Score - fluorescein leakage from retinal vessels
L0 - no leakage
L1 - leakage in Peripheral Zone (1-2 quadrants)
L2 - leakage in Peripheral Zone (3-4 quadrants)
L3 - leakage includes Central Zone (1-2 quadrants) (with/ without peripheral leakage)
L4 - leakage includes Central Zone (3-4 quadrants) (with/ without peripheral leakage)

Occlusion Score - occluded retinal vessels (arterioles, venules or capillaries) with resulting non-perfusion or ischaemia. May be static, long-term change in absence leakage
O0 - no occlusion
O1 - Area of retinal ischaemia only in Peripheral Zone <=3 disc area
O2 - Area of retinal ischaemia only in Peripheral Zone >3 disc area
O3 - Area of retinal ischaemia includes Central Zone (<=3 disc area) (with/ without peripheral ischemia)
O4 - Area of retinal ischaemia in Central Zone (>3 disc area) (with/ without peripheral ischemia)

**Figure 6.1. Newly proposed retinal vasculitis grading scheme.**

Retinal vascular leakage or 'leakage' was defined as progressive hyperfluorescence coming from retinal vessels, either segments or full lengths of vessels (Tugal-Tutkun et al., 2010a;Johnson et al., 2013). Leakage is usually evident early in the fluorescein imaging and progresses to cover a larger area around vessels in later shots. Staining, defined as vessel wall hyperfluorescence evident from mid-run onwards without expansion (Johnson et al., 2013), was not included as it is deemed not indicative of active disease. It did not include leakage at the level of the retinal pigment epithelium (RPE) which forms the outer blood-retinal barrier, leakage from optic disc, new vessels, or hyperfluorescence due to fluid-filled cysts in macular edema alone.

The leakage score was based on the number of quadrants showing presence of leakage and their zone. Leakage in the peripheral zone, was graded as L1 when 1-2 quadrants were involved, or L2, when 3-4 quadrants were involved. Leakage in the central zone, was graded as L3 (1-2 quadrants) or L4 (3-4 quadrants) regardless of leakage in the peripheral zone. Thus, a leakage score of increasing severity from L0 to L4 was derived.

The occlusion score was based on the presence of occluded retinal vessels resulting in non-perfusion, or ischemia, the zone affected and the area of ischaemia. Occlusion in the peripheral zone was graded as O1 when non-perfusion covered an area of less than 3 disc areas, or O2 when more than 3 disc areas. Non-perfusion in the central zone was graded O3 when less than 3 disc areas, or O4 when more than 3 disc areas. The cut-off of 3 disc areas was derived from the AWOG grading scheme. All of the grading criteria are summarised in **Figure**

**6.1**. **Figures 6.2** and **6.3** show examples of grading the WFFA for retinal vasculitis using the proposed new scheme.

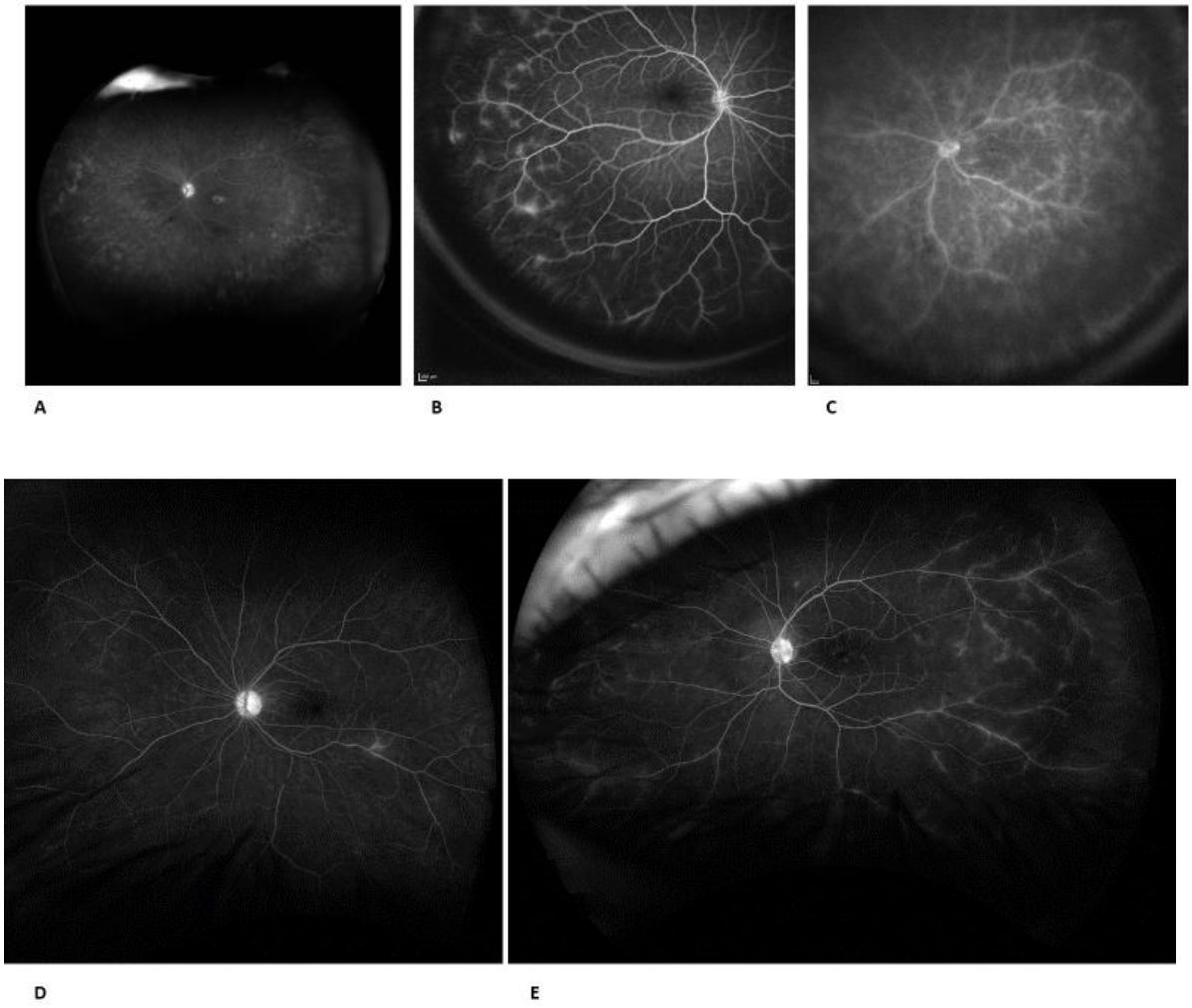


**Figure 6.2 Example images for leakage score.**

(A) Leakage from RPE L0 (not identified as retinal vasculitis leakage), (B) leakage from vessels in Peripheral Zone L2 (identified as retinal vasculitis leakage), (C) leakage from vessels in Central Zone L4 (identified as retinal vasculitis leakage), (D) leakage from vessels in Peripheral Zone L1 (identified as retinal vasculitis leakage) and (E) leakage from vessels in Central Zone L3 (identified as retinal vasculitis leakage).

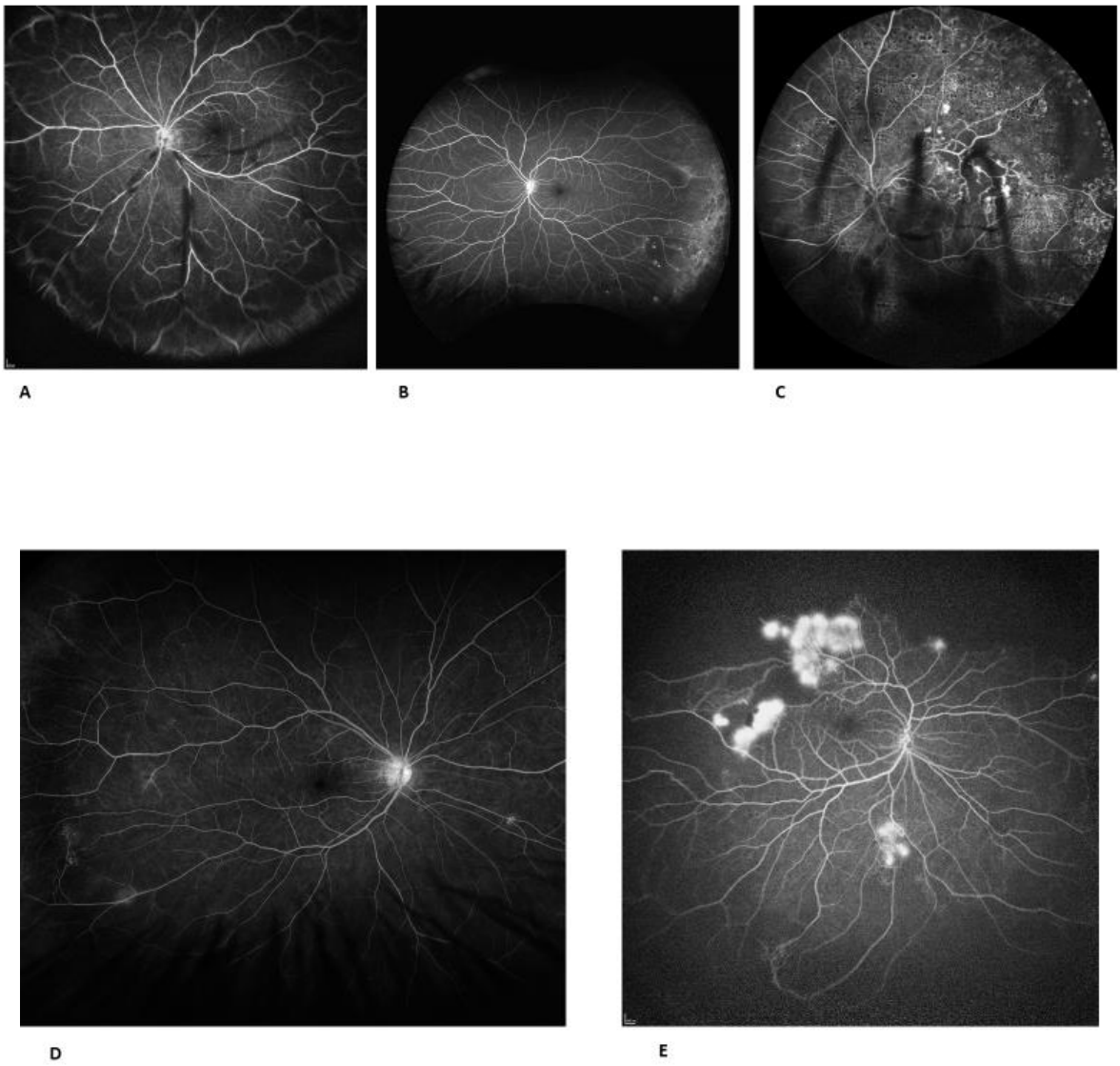


**Figure 6.3 Example images for occlusion score.**

(A) No occlusion O0, (B) occlusion in Peripheral Zone O2, (C) occlusion in Central Zone O4, (D) occlusion in Peripheral Zone O1 and (E) occlusion in Central Zone O3.

Additionally, I included further questions on the predominant vessel type involved, the presence of cystoid macular oedema (on WFFA only), and the presence of optic disc leakage (**Table 6.1**). This was to explore the utility of these assessments.

## Table 6.1 Patients' characteristics of 50 recruited patients

| | Number of Patients (N=50) (percentage) | | Number of Eyes (N=99) (percentage) | | |
|---|---|---|---|---|---|
| | | | Retinal vasculitis | | Fischer's exact |
| **Gender** | | **Type** | (+) (N=87) | (-) (N=12) | p-value <0.05 |
| Female | 29 (58%) | intermediate uveitis with/without retinal vasculitis | 22 (23.2%) | 1 (8.3%) | No |
| **Ethnicity** | | only posterior uveitis | 54 (57.6%) | 3 (25%) | Yes |
| White British | 38 (76%) | Panuveitis | 7 (8%) | 0 (0%) | No |
| Black or Black British African | 3 (6%) | **Clinical features** | | | |
| Other | 9 (18%) | cataract | 13 (14.9%) | 2 (16.7%) | No |
| **Age at diagnosis** | mean = 46.4 (IQR = 36.8-59) | Pseudophakia | 5 (5.7%) | 1 (8.3%) | No |
| **Bilateral** | 38 (76%) | vitreous haemorrhage | 4 (4.6%) | 0 (0%) | No |
| **Diagnosis** | | optic neuropathy | 3 (3.4%) | 0 (0%) | No |
| Idiopathic | 24 (48%) | epiretinal membrane | 7 (8%) | 0 (0%) | No |
| Behcet's uveitis | 4 (8%) | macular atrophy | 2 (2%) | 0 (0%) | No |
| Sarcoidosis | 3 (6%) | | | | |
| SLE | 3 (6%) | **logMAR CVA (at the time of imaging)** | Mean =0.295 SD = 0.54 | Mean =0.058 SD = 0.15 | t-test p =0.002 |
| Unspecified systemic vasculitis | 3 (6%) | -0.1 – 0 | 22 (25.3%) | 8 (66.7%) | |
| Multiple sclerosis | 3 (6%) | 0.1-0.2 | 30 (34.5%) | 3 (25%) | |
| Birdshot chorioretinopathy | 2 (4%) | 0.3-0.6 | 22 (25.3%) | 1 (8.3%) | |
| Tuberculosis | 2 (4%) | >0.8 | 13 (14.9%) | 0 (0%) | |
| Crohn's Disease | 1 (2%) | **Anterior chamber cell** | | | |
| Granulomatosis with polyangiitis (GPA) | 1 (2%) | 0 | 63 (72.4%) | 12 (75.8%) | |
| IRVAN | 1 (2%) | 0.5+ | 11 (12.6%) | 0 (0%) | |
| Psoriatic arthritis | 1 (2%) | 1+ | 5 (5.7%) | 0 (0%) | No |
| Rheumatoid arthritis | 1 (2%) | 2+ | 2 (2.3%) | 0 (0%) | |
| Vogt-Koyanagi-Harada disease | 1 (2%) | 3+ | 2 (2.3%) | 0 (0%) | |
| **Systemic treatment (at the time of imaging)** | | no data | 4 (4.6%) | 0 (0%) | |
| no systemic steroid | 23 (46%) | **Vitreous haze** | | | |
| prednisolone < 10 mg/day | 6 (12%) | 0 | 56 (64.4%) | 12 (100%) | |
| prednisolone >=10, <=20 mg/day | 8 (16%) | 0.5+ | 6 (6.9%) | 0 (0%) | |
| prednisolone >20, <=40 mg/day | 7 (14%) | 1+ | 14 (16.1%) | 0 (0%) | No |
| prednisolone >40 mg/day | 6 (12%) | 2+ | 4 (4.6%) | 0 (0%) | |
| MMF | 7 (14%) | 3+ | 3 (3.4%) | 0 (0%) | |
| Azathioprine | 2 (4%) | no data | 4 (4%) | 0 (0%) | |
| Cyclophosphamide | 2 (4%) | **Vitreous cells** | | | |
| Tacrolimus | 1 (2%) | Absent | 50 (57.5%) | 11 (91.7%) | No |
| Methotrexate | 1 (2%) | Present | 33 (34.3%) | 1 (8.3%) | |
| Adalimumab | 2 (4%) | no data | 4 (4%) | 0 (0%) | |
| Rituximab | 1 (2%) | **local treatment** | | | |
| | | topical steroid | 23 (26.4%) | 1 (8.3%) | No |
| | | intravitreal steroid (any previous) | 3 (3.4%) | 1 (8.3%) | No |
| | | Vitrectomy | 2 (2.2%) | 0 (0%) | No |
| | | Photocoagulation | 5 (5.7%) | 0 (0%) | No |

**Evaluation of the grading scheme**

One investigator (I) selected two images from each eye and masked the clinical data, and shuffled the participant order for intra-observer testing. This investigator was excluded from the grading exercise. The graders were two uveitis specialists (consultant 1 and 2), a trained senior ophthalmic image grader, and an ophthalmology higher specialist trainee(resident). All the graders were trained by the same example image sets before grading and undertook a pilot exercise on scoring for images independently. For intra-observer reliability, the ophthalmic image grader was asked to grade the same image set again after a gap of 1 month. For the purpose of analysing interobserver reliability, the first grading of the ophthalmic image grader was used. The grading outcomes of consultant 1 were used for subsequent analysis.

**Statistical analysis**

All analysis was performed using SPSS 22.0 (SPSS Inc., Chicago, IL). The data are shown as mean, percentage, and standard deviation. Student t-tests or Chi-square tests were applied to compare the variables. For intra and interobserver agreement, I calculated the intraclass correlation coefficient (ICC) for ordinal data (leakage score, occlusion score, quality of image) and Fleiss's kappa statistics for categorical data (presence of cystoid macular oedema, presence of optic disc leakage, and predominant vessel type involved). A single-measurement, absolute agreement with a 2-way mixed effects model was applied for ICC. The interpretation of both ICC and Fleiss's kappa were as follows: less than 0.40 as poor, 0.40-0.59 as fair, 0.60-0.74 as good, and 0.75-1.00 as excellent (Cicchetti, 1994).

Univariable and multivariable generalized linear regression analyses were used to calculate the association of the new grading scheme with CVA. The generalized estimating

equations (GEE) accounted for the elimination of inter-eyes correlation. Factors showing a p-value less than 0.1 in univariate analysis were consequently analysed in the multivariate analysis. A p-value less than 0.05 was considered statistically significant for all analyses.

### 6.3 Results

A total of 99 eyes from 50 patients with retinal vasculitis were recruited for this study. **Table 6.1** summarizes the patients' characteristics and diagnoses. Of the 50 patients, 29 (58%) were female, most were White British (38, 76%), and the mean age at diagnosis was 46.4 years (IQR = 36.8-59). Thirty-eight (76%) patients had bilateral retinal vasculitis. Of 99 eyes, there were 87 eyes with retinal vasculitis and 12 without. The most common presenting symptom of the eyes with retinal vasculitis was reduced/ blurred vision (49 with retinal vasculitis, 1 without retinal vasculitis, $p<0.05$). Anatomical type of uveitis from 87 retinal vasculitis eyes included 22 (23.2%) intermediate uveitis, 54 (57.6%) posterior uveitis, and 7 (8%) panuveitis. Other associated ophthalmologic complications in eyes with retinal vasculitis were cataracts (13, 14.9%), pseudophakia (5, 5.7%), vitreous haemorrhage (4, 4.6%), optic neuropathy (3, 3.4%), epiretinal membrane (7, 8%) and macular atrophy (2, 2%). At the time of WFFA imaging, the mean logMAR CVA of eyes with retinal vasculitis was 0.295, and 0.058 in eyes without retinal vasculitis (t-test, p-value < 0.05). Local treatment received in eyes with retinal vasculitis were topical steroid (23, 26.4%), intravitreal steroid (3, 3.4%), vitrectomy (2, 2.2%), and photocoagulation (5, 5.7%). From 50 patients, 27 (54%) received systemic treatment with oral prednisolone, 7 (14%) oral mycophenolate mofetil, 2 (4%) oral azathioprine, 2 (4%) intravenous cyclophosphamide, 1 (2%) oral tacrolimus, 1 (2%) oral methotrexate, 2 (4%) subcutaneous adalimumab, and 1 (2%) intravenous rituximab.

**Intra and interobserver reliability**

Intraobserver reliability showed excellent agreement for leakage (ICC 0.845, 95% CI 0.777-0.893), and good agreement for occlusion (ICC 0.824, 95% CI 0.747-0.878). For additional questions, the intraobserver reliability indicated fair agreement for CMO (kappa 0.579, 95% CI 0.573-0.586), fair agreement for optic disc leakage (kappa 0.509, 95% CI 0.503-0.575), excellent agreement for quality of imaging (ICC 0.822, 95% CI 0.742-0.879) and fair agreement for predominant vessel type involved (kappa 0.465, 95% CI 0.461-0.468).

The interobserver reliability was investigated for four graders scoring independently. The result revealed good agreement for the leakage score (ICC 0.655, 95% CI 0.491-0.769) and excellent agreement on occlusion score (ICC 0.750, 95% CI 0.679-0.813). It is noted that ICC between consultants 1 and 2 have the highest agreement for the leakage (ICC 0.795, excellent).

There were imbalances in the score distribution. For instance, using consultant 1 as ground truth, the commonest scores for leakage were L4 (37/96, 38.5%) and L0 (13/96, 13.5%). The raw agreement between consultants 1 and 2 was higher for L0 and L4 than L1-L3. As expected, there was more leakage than occlusion and O0 was the commonest occlusion score (64, 66.7%).

For additional questions assessing WFFA, the intraobserver reliability showed good agreement for CMO (kappa 0.638, 95%CI 0.635-0.640), poor agreement for optic disc leakage (kappa 0.293, 95%CI 0.291-0.296), fair agreement for quality of FA imaging (kappa 0.565, 95% CI 0.449-0.609) and poor agreement for predominant vessel type involved (kappa 0.266, 95%CI 0.265-0.267). The results of interobserver reliability are summarised in **Table 6.2**. As assessing CMO using WFFA is not standard practice, I additionally reviewed macular OCT scans acquired within 2 weeks (before or after) of WFFA in the study eyes for presence/

absence of CMO. Macular OCT scans were available in 82 study eyes. The result indicated fair agreement between assessing CMO by WFFA and OCT (kappa 0.444, 95%CI 0.317-0.571).

**Table 6.2 Intra and interobserver reliability of retinal vasculitis grading from 4 independent graders.**

| | Leakage Score (ICC) | Occlusion Score (ICC) | CMO (kappa) | Optic disc leakage (kappa) | Quality of FA imaging (ICC) | Predominant vessels (kappa) |
|---|---|---|---|---|---|---|
| **Intraobserver reliability** | 0.845 (95%CI 0.777-0.893) | 0.824 (95%CI 0.747-0.878) | 0.579 (95%CI 0.573-0.586) | 0.509 (95%CI 0.503-0.575) | 0.822 (95%CI 0.742-0.879) | 0.465 (95%CI 0.461-0.468) |
| **Interobserver reliability** | | | | | | |
| Consultant1 - Consultant2 | 0.795 | 0.741 | 0.836 | 0.276 | 0.498 | 0.424 |
| Consultant1 - Ophthalmic grader | 0.750 | 0.720 | 0.426 | 0.477 | 0.467 | 0.258 |
| Consultant1 - Resident | 0.525 | 0.856 | 0.779 | 0.497 | 0.570 | 0.226 |
| Consultant2 - Ophthalmic grader | 0.755 | 0.641 | 0.376 | 0.372 | 0.555 | 0.192 |
| Consultant2 - Resident | 0.519 | 0.771 | 0.765 | -0.191 | 0.617 | 0.298 |
| Ophthalmic grader - Resident | 0.574 | 0.770 | 0.554 | 0.092 | 0.702 | 0.133 |
| All (4 graders) | 0.655 (95%CI 0.491-0.769) | 0.750 (95%CI 0.679-0.813) | 0.638 (95%CI 0.635-0.640) | 0.293 (95%CI 0.291-0.296) | 0.565 (95%CI 0.449-0.669) | 0.266 (95%CI 0.265-0.267) |

**Association of retinal vasculitis scoring with visual acuity**

I compared the retinal vasculitis scoring with visual acuity using generalized linear regression analyses with GEE (**Table 6.3**, **Figure 6.4**). The univariable analysis showed worse visual acuity was associated with higher leakage score (β=0.105, p=0.001) as well as older age (β=0.005, p=0.04), male gender (β=0.162, p<0.05) and presence of optic disc leakage (β=0.202, p=0.027). The multivariable analysis showed only higher leakage score (β=0.090, p=0.008) and older age (β=0.006, p=0.016) as statistically significant associations with visual acuity.

**Table 6.3 Association between clinical variables includes retinal vasculitis grading with visual acuity using a Generalized Linear Model with a Generalized Estimating Equation.**

| Variables | date of imaging | | | | | | 1-year follow up | | | | | |
|---|---|---|---|---|---|---|---|---|---|---|---|---|
| | univariable | | | multivariable | | | univariable | | | multivariable | | |
| | Standardized coefficient β | | p-value | Standardized coefficient β | | p-value | Standardized coefficient β | | p-value | Standardized coefficient β | | p-value |
| | value | 95% CI | | value | 95% CI | | value | 95% CI | | value | 95% CI | |
| Age (years) | 0.005 | 0.00024-0.011 | 0.04 | 0.006 | 0.001-0.011 | 0.016 | 0.005 | 0.00049-0.0092 | 0.029 | 0.005 | 0.002-0.009 | 0.004 |
| Gender (females) | -0.162 | -0.323-0.000311 | 0.0495 | -0.111 | -0.278-0.056 | 0.192 | -0.066 | -0.246-0.114 | 0.474 | | | |
| Dose of prednisolone | 0.004 | -0.0003-0.009 | 0.067 | 0.003 | -0.002-0.008 | 0.290 | 0.02 | -0.002-0.005 | 0.360 | | | |
| Number of immunosuppressants | -0.006 | -0.085-0.073 | 0.879 | | | | -0.015 | -0.116-0.086 | 0.765 | | | |
| leakage score | 0.105 | 0.054-0.156 | 0.0001 | 0.090 | 0.023-0.158 | 0.008 | 0.089 | 0.037-0.141 | 0.001 | 0.063 | 0.018-0.107 | 0.006 |
| occlusion score | 0.073 | -0.002-0.148 | 0.056 | 0.048 | -0.024-0.121 | 0.190 | 0.059 | -0.005-0.123 | 0.071 | 0.050 | -0.007-0.106 | 0.083 |
| CMO | 0.169 | -0.008-0.346 | 0.061 | -0.041 | -0.269-0.186 | 0.721 | 0.1 | -0.079-0.278 | 0.273 | | | |
| Optic disc leakage | 0.202 | 0.022-0.381 | 0.027 | 0.144 | -0.049-0.336 | 0.143 | 0.241 | 0.022-0.46 | 0.031 | 0.233 | 0.048-0.418 | 0.014 |

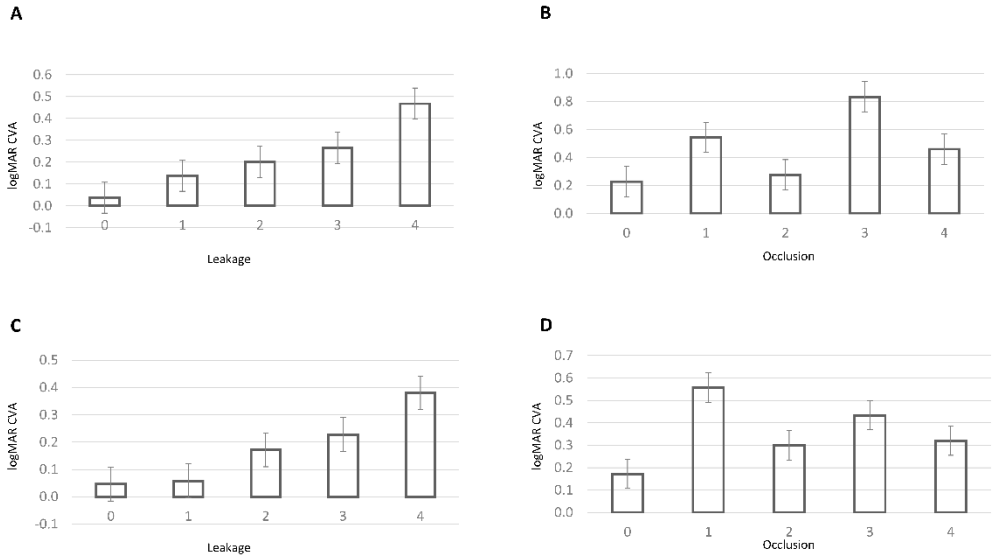


**Figure 6.4 Graph showing the relation between clinical grading and visual acuity**

(A) LogMAR CVA at date image obtained and leakage score, (B) logMAR CVA at date image obtained and occlusion score, (C) logMAR CVA at 1-year follow-up and leakage score and (D) logMAR CVA at 1-year follow-up and occlusion score. The error bars show the standard error.

At 1-year follow-up, the univariable analysis showed that higher leakage score(β=0.089, p=0.001), higher age(β=0.005, p=0.029), and presence of optic disc leakage(β=0.241, p=0.03) were associated with worse visual acuity. The multivariable analysis showed higher leakage score(β=0.063, p=0.006), older age(β=0.005, p=0.004), and optic disc leakage(β=0.233, p=0.014) as a statistically significant association with visual acuity.

## 6.4 Discussion

There is currently no accepted grading scheme for retinal vasculitis, resulting in unquantified clinical assessment, poor communication between clinicians and only a binary outcome for clinical trials in uveitis (present or absent) meaning much lost data. I present a

pragmatic grading scheme based on WFFA which is not time-consuming, and encompasses the important concepts of vascular leakage (activity) and occlusion (damage). I demonstrate that it has good to excellent intra and inter-observer reliability across different cadres of observers, and relates to function, in the form of visual acuity.

At present there are no SUN criteria for assessing severity of retinal vasculitis (Jabs et al., 2005). The ASUWOG scoring system (Tugal-Tutkun et al., 2010a) has been developed but has 40 points of assessment, and is not practical for use clinically or in clinical trials. It has has not been widely taken up and has only been tested in Behcet's Disease.

The recent decades have made significant progress in non-invasive imaging methods, specifically OCT and OCT-A, but these are not yet suitable alternatives to using WFFA for assessment of retinal vasculitis (Abucham-Neto et al., 2018;Kumar et al., 2021), which remains the standard method for diagnosis and severity assessment (Agarwal et al., 2017). In this current study, I emphasize two major angiographic features of retinal vasculitis, leakage and occlusion; and I propose grading their involvement within a peripheral zone and a central zone on a scale of severity. This investigation of intra and inter-observer agreement indicates that this grading scheme has good or excellent concordance, which means that it is reliable and reproducible between observers. The interobserver agreement in leakage score has a higher agreement between two uveitis consultants rather than an ophthalmic grader or trainee. This suggests that the accuracy of the assessment improves with clinical experience, and additional training may improve less experienced cadres. Clinical imaging panels might be the option for collaboratively assessing complex images.

Both univariable and multivariable analyses found that the leakage but not occlusion score was associated with visual acuity. The relationship between leakage and vision is meaningful in that it is measuring disease activity with an impact on visual function. Severity of vascular leakage thus may potentially serve as a clinical biomarker indicating the need for more intensive treatment (Kim et al., 2015;Onal et al., 2018). The current analysis did not show an association between occlusion grade and visual acuity. Occlusion will only directly affect visual acuity if it affects the fovea which will result in severe loss, so there is not an expected direct relationship with generalised severity. However, greater areas of occlusion, and involvement of the posterior pole rather than the periphery, have a greater chance of having a devastating impact on acuity. This is supported by previous research which indicated a relationship between foveal avascular zone size but not peripheral ischemia with poor visual outcome (Karampelas et al., 2015) in eyes with retinal vasculitis secondary to uveitis.

I found poor interobserver agreement for optic disc leakage. This feature may be related to overall uveitis activity, or specific optic nerve involvement as well as retinal vasculitis. I suggest that it not be included in the grading of retinal vasculitis severity. I also assessed the concordance of observers to identify the predominant type of vessel involved in inflammation which is said to aid diagnosis of the underlying disease. Unfortunately, this only had poor agreement and I suggest that this should not be included in a retinal vasculitis severity grading scale.

Besides clinician grading, automated computerised algorithms developed to grade retinal imaging are promising in many retinal diseases (Schmidt-Erfurth et al., 2018b). Automated algorithms could quantify areas affected by leakage and occlusion on continuous scales with weighting for central versus peripheral involvement. Attempts at automated grading

of retinal vascular leakage, including diabetic retinopathy patients (Ehlers et al., 2017) and malarial retinopathy patients (Zhao et al., 2015;Zhao et al., 2017), have given promising results. However, an automated computerized method incorporating both leakage and occlusion, specific to retinal vasculitis patients is still desirable.

This study was designed to retrospectively utilise images obtained in routine clinical practice from patients presenting with retinal vasculitis to a tertiary uveitis centre. Some patients with retinal vasculitis in this centre had no previous WFFA, so they were not included in this study. It was limited by using observers all from one centre, albeit from different cadres. There were more examples of leakage than occlusion, as is encountered in clinical practice. The images used were not equally distributed in terms of scores for leakage and occlusion; in particular there were more L4 images than L1, L2 or L3. This is in part a result of the simplicity of the scheme and also due to the limited sample size, but the relationship of the leakage grade to visual acuity supports this division of grades. Visual acuities were uniformly collected using Snellen charts and with the patients' own correction or pinhole, rather than refracted (best corrected) visual acuity.

Unlike the ASUWOG scoring system, which comprised a detailed assessment with 40 points, the current grading scheme was designed for practical use. However, by focusing primarily on evaluating only two critical features of retinal vasculitis, this grading scheme limits its ability to assess secondary complications that could be observed in WFFA, such as neovascularisation. The current grading scheme only includes leakage and occlusion. Although occlusion might not reflect the current disease activity (as it might be longstanding and not associated with current visual acuity based on our study), it remains an essential feature in retinal vasculitis. It may provide insights into the severity of the disease in the past or impact

treatment decisions. Another feature that the current grading scheme does not include is optic disc leakage. Although the optic disc leakage might be associated with poor visual acuity in follow-up assessments, this feature might not directly represent the primary feature of retinal vasculitis. It might be linked to overall uveitis activity or specific optic nerve involvement.

As one major limitation of this study was the imbalance in each score between leakage and occlusion, future studies should aim to address this imbalance by conducting image sets that are proportionally distributed, for example, ten images per class (totalling 50 images).

In conclusion, I have proposed a new severity grading scheme for retinal vasculitis focused on leakage and occlusion on retinal angiography, and initial assessment suggested promising levels of intra and inter-observer reliability. The leakage score relates to visual acuity, which supports its use as a biomarker for disease activity. Prospective studies could further validate this scoring scheme for retinal vasculitis and how it relates to treatment decisions and outcomes.

# Chapter 7 Develop computerised grading of retinal vasculitis on a wide-field fluorescence angiography

In this chapter, I present my study that has been submitted to Ocular Immunology and Inflammation.

Retinal vasculitis is characterised by retinal vascular leakage and occlusion on FA. There is no standard scheme available to segment retinal vasculitis features. This study aimed to develop a deep learning model to segment both vascular leakage and occlusion in retinal vasculitis. 463 FA images from 83 patients with retinal vasculitis were used to develop a deep learning model, in 60:20:20 ratio for training:validation:testing. Parameters, including deep learning architectures (DeeplabV3+, UNet++ and UNet), were altered to find the best binary segmentation model separately for retinal vascular leakage and occlusion, using a Dice score to determine the reliability of each model. The best model for vascular leakage had a Dice score of 0.6279 (95% confidence interval (CI) 0.5584-0.6974). For vascular occlusion, the best model achieved a Dice score of 0.6992 (95%CI 0.6109-0.7874). These retinal vasculitis segmentation models could perform reliable segmentation for retinal vascular leakage and occlusion in FAs of retinal vasculitis patients.

## 7.1 Introduction

Retinal vasculitis refers to inflammation of retinal blood vessels, which can lead to complications such as macular oedema and vascular occlusion, and progress to visual loss(Maleki et al., 2016). Retinal vasculitis, which may be subclinical or can present with vascular sheathing alone (Agarwal et al., 2017) or with additional findings such as retinal haemorrhages, cotton-wool spots, irregular vessel calibre, perivascular infiltrate and ghost vessels (Agarwal et al., 2017;Agarwal et al., 2022) . It may be difficult to confirm the diagnosis and assess the intensity of inflammation by routine fundoscopic examination alone or on standard colour fundus photography. Assessment of retinal vasculitis based on FA is widely accepted, and characterised by variable retinal vascular leakage and/or occlusion (Karampelas et al., 2015). The severity of leakage on FA could also correlate with disease activity and visual loss (Kim et al., 2015). However, there is no agreement on the definition or grading of retinal vasculitis as concluded by the SUN working group (Jabs et al., 2005), which therefore introduces an element of subjectivity in the human clinical assessment of retinal vasculitis.

Since 2012, artificial intelligence, specifically deep learning for image analysis, has proven its usability for image classification and segmentation (Schmidt-Erfurth et al., 2018b). Deep learning has facilitated diagnosing and classifying diseases in ophthalmology, especially retinal disease. Successful examples include the classification model to identify different stages of diabetic retinopathy using color fundus images (Tsiknakis et al., 2021), the classification of common retinal diseases such as diabetic retinopathy and AMD using OCT images (Kermany et al., 2018), and segmentation of sub and intraretinal fluid in neovascular AMD on OCT images (Schlegl et al., 2018). In more common eye diseases deep learning algorithms trained on large datasets showed some promising results but in the field of ocular inflammatory

diseases, it is challenging to obtain thousands of images, which has proved a limitation (Keino et al., 2022).

Only a few studies have applied deep learning in ocular inflammatory disease. Previously, researchers have applied to computerise the segmentation of retinal vascular leakage features in diabetic retinopathy (Ehlers et al., 2017), uveitis (Lee et al., 2022) and Behcet's disease (Keino et al., 2022) using WFFA images, but automated segmentation of both retinal vascular leakage and occlusion in retinal vasculitis has not been attempted. In real-world uveitis practice, FA images are obtained from various imaging machines, including Optos and Heidelberg (Patel et al., 2020) will include different fields of view; developing a segmentation algorithm based on a single machine might not reflect this reality. This current study aimed to develop computerised segmentation methods based on deep learning using combined datasets from Optos and Heidelberg images. This study focused on retinal vasculitis patients; and aimed to report the best binary segmentation model separately for retinal vascular leakage and occlusion.

## 7.2 Methods

### Study subjects

This study was undertaken at St Paul's Eye Unit, Liverpool University Hospitals NHS Trust, Liverpool, UK and Xiamen Eye Center of Xiamen University. The study followed the tenets of the Declaration of Helsinki and had prior ethical approval from the NHS Research Ethics Committee of the North of Scotland (reference number 19/NS/0186) and the institutional review board of Xiamen Eye Center of Xiamen University (reference number XMYKZX-KY-2022-008). FA images were obtained from St Paul's Eye Unit and Xiamen Eye Center of Xiamen University from patients who had a clinical diagnosis of retinal vasculitis based on the definition in the SUN criteria (Jabs et al., 2005). Study participants had undergone

FA between 2009 and 2022. FA images from the Heidelberg platform (Heidelberg Engineering, Heidelberg, Germany), including SPRECTALIS HRA (105 degrees field of view) or HRA2 Scanning Laser Ophthalmoscope (SLO) with the use of Staurenghi SLO 230 contact lens (Ocular Instruments Inc. Bellevue, WI, USA) (150 degrees field of view) (Reeves et al., 2013) and Optos platform (Optos, Dunfermline, UK) including Optomap P200DTX (200 degrees field of view), 200TX (200 degrees field of view) or P200MA (200 degrees field of view) were included (Patel et al., 2020). Patients with a past history of proliferative diabetic retinopathy, retinal vascular disease other than retinal vasculitis or other ocular diseases which might interfere with FA assessment were excluded. From St. Paul's Eye Unit, multiple images of both eyes were selected by two investigators (NAVB, consultant ophthalmologist and uveitis expert; and me). For the dataset from Xiamen Eye Center, images were selected by two local investigators (XC, ophthalmologist with special interest in retinal diseases and XL, consultant ophthalmologist with expertise in uveitis and medical retina). I included FA images from different time points, including 30 seconds- 60 seconds, 1-5 minutes and later than 5 minutes, deemed to be of sufficient quality to be gradable with at least 2 quadrants of the retina visible.

**Image characteristics**

The initial retinal vasculitis cohort included 86 patients - 50 patients from St Paul's Eye Unit and 36 patients from Xiamen Eye Center. The underlying diagnosis of retinal vasculitis for patients from St Paul's Eye Unit included idiopathic retinal vasculitis, Behcet's uveitis, sarcoidosis, SLE, unspecified systemic vasculitis, multiple sclerosis, birdshot chorioretinopathy, tuberculosis, Crohn's Disease, granulomatosis with polyangiitis, IRVAN, psoriatic arthritis, rheumatoid arthritis and Vogt-Koyanagi-Harada disease. The definitive diagnosis of retinal vasculitis for patients from Xiamen Eye Center included tuberculosis, sarcoidosis, intermediate uveitis, and Behcet's uveitis. After evaluation, four patients were

excluded due to the poor quality of FA images; 74 right eyes and 69 left eyes of 82 patients were included in the study. Some patients had more than one active retinal vasculitis episode, resulting in a total of 94 FA image sets. A total number of 463 FA images at various time points in the run were selected for manual segmentation. There were 316 images from the Optos platform and 147 from the Heidelberg platform. After manual segmentation, 340 images were determined to have retinal vascular leakage and 144 images to have occlusion. The FA images were randomly split into training, validating and testing datasets at an approximate 60:20:20 ratio, resulting in 273 images in the training dataset, 98 images in the validation dataset and 92 images in the test dataset. **Table 7.1** represents the number of the images after random splitting.

**Table 7.1. Dataset characteristics**

| | Train | Validate | Test |
|---|---|---|---|
| Number of patients | 47 | 16 | 19 |
| Number of episodes | 55 | 19 | 20 |
| Number of eyes | 83 | 29 | 31 |
| Number of images | 273 | 98 | 92 |
| Number of images with retinal vascular leakage | 212 | 66 | 62 |
| Number of images with occlusion | 91 | 21 | 32 |
| Number of Optos images | 180 | 67 | 69 |
| Number of Heidelberg images | 93 | 31 | 23 |

**Leakage and occlusion manual segmentation**

All images obtained were converted to jpeg files. The leakage and occlusion segmentation was manually annotated using the Labkit extension in ImageJ program and saved

in a tiff file format. Leakage and occlusion in the FA images were identified by NAVB and me. I used the Labkit segmentation tool (Arzt et al., 2022) to annotate the images to serve as ground truth. Retinal vascular leakage was defined as progressive increase in area and intensity of hyperfluorescence originating from retinal vessels within the first 60 seconds of the FA run, involving small segments or full length of any type of retinal vessel (arteries, veins, capillaries). It excluded vessel wall staining, leakage at the retinal pigment epithelium level (RPE) level, leakage from the optic disc, new vessels, or hyperfluorescence due to fluid-filled cysts in macular oedema alone. The retinal vascular leakage segmentation included the vasculature and the hyperfluorescent area around retinal vessels. Occlusion was defined as the presence of occluded retinal vessels resulting non-perfusion, or ischemia, and the zone affected by ischaemia, including areas of capillary drop-out, were segmented.

**Deep learning-based leakage and occlusion auto-segmentation**

Three well-known deep learning architectures (DeeplabV3+ (Chen et al., 2018a), UNet++ (Zhou et al., 2018) and UNet (Ronneberger et al., 2015)), were utilised for comparison in this work. For each architecture, two different encoder backbones (ResNet50 (He et al., 2016) and EfficientNet-B3 (Tan and Le, 2019)) were utilised respectively. In this study, a total of twelve deep learning models were trained for detection of leakage or occlusion. For each training exercise, the model was trained as binary segmentation with Dice loss function. Finally, the best model for retinal vascular leakage or occlusion segmentation was selected according to Dice score (Dice, 1945) on the test dataset. To compare the effect of image normalisation, image modification with a contrast limited adaptive histogram equalisation (CLAHE) (Zuiderveld, 1994) and without CLAHE (**Figure 7.1**) were trained separately. To boost the robustness, random augmentation was applied during the training process, including horizontal flipping, rotating less than 15 degrees, shifting and scaling.

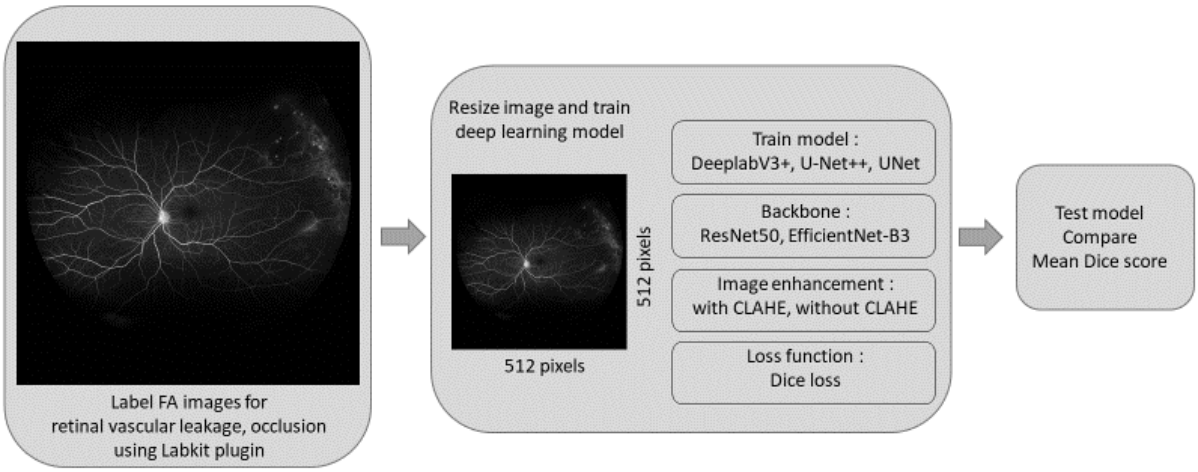


**Figure 7.1 Training and Testing diagrams**

All models were trained on Pytorch with the platform of Windows 10 Enterprise operating system using CPU Intel(R) Core(TM) i7-3770K CPU @ 3.50GHz 3.90 GHz and GPU NVIDIA Titan Xp. The image was firstly resized to 512*512 pixels, the models were trained for 200 epochs with learning rate of 0.0001 and Adam optimiser. Segmentation Models (SMP) (Iakubovskii, 2019) https://github.com/qubvel/segmentation_models.pytorch was utilised in this work. Dice score was utilised to justify the performance of the segmentation, and it is defined as Dice score = 2 TP / (2 TP + FP + FN), where using true positives (TP), true negatives (TN), false positives (FP) and false negatives (FN) were calculated according to the segmentation results and ground truth. The Dice score is the score measuring the similarity between two sets of data, in this case, the similarity between segmentation results and ground truth (Siddique et al., 2021). The score ranges from 0 to 1, where 0 suggests no overlap between two sets of data and 1 suggests a total overlap between two sets of data. However, no guideline or consensus indicates a fixed value for an acceptable Dice score.

## 7.3 Results

### Deep learning algorithm performances

After training with 200 epochs and varying parameters and image augmentation, the models were tested with the test dataset, which included 92 FA images from 19 patients. **Table 7.2** reports the Dice score of each model performed in the test dataset. The highest Dice score determined the best performance model for retinal vascular leakage and occlusion segmentation. The result suggested the best model for retinal vascular leakage was the UNet++ model architecture with efficientnet-b3 encoder backbone and no CLAHE image enhancement and achieved a Dice score of 0.6279 (95% confidence interval (CI) 0.5584-0.6974) for all images, and 0.6580 (95% CI 0.5833-0.7327), 0.5377 (95% 0.3673-0.7080) for only Optos images and only Heidelberg images respectively.

**Table 7.2 Dice score in different deep learning model to segment retinal vascular leakage and occlusion in retinal vasculitis**

| Model | DeeplabV3+ | | | | UNet++ | | | | UNet | | | |
|---|---|---|---|---|---|---|---|---|---|---|---|---|
| backbone | efficientnet-b3 | | resnet50 | | efficientnet-b3 | | resnet50 | | efficientnet-b3 | | resnet50 | |
| CLAHE image enhancement | No CLAHE | CLAHE | No CLAHE | CLAHE | No CLAHE | CLAHE | No CLAHE | CLAHE | No CLAHE | CLAHE | No CLAHE | CLAHE |
| Retinal vascular leakage | 0.5926 | 0.5775 | 0.5686 | 0.5751 | **0.6279** | 0.5932 | 0.6245 | 0.5302 | 0.5580 | 0.5610 | 0.6138 | 0.5782 |
| Occlusion | **0.6992** | 0.6167 | 0.6444 | 0.6713 | 0.6937 | 0.6944 | 0.6654 | 0.6478 | 0.6617 | 0.6380 | 0.6232 | 0.6696 |

For occlusion, the best model was the DeeplabV3+ model architecture with efficientnet-b3 encoder backbone and no CLAHE image enhancement; and it achieved a Dice score of 0.6992 (95% CI 0.6109-0.7874) for all images, and 0.6685 (95% CI 0.5637-0.7732), 0.7912 (95% CI 0.6229-0.9595) for only Optos images and only Heidelberg images respectively. **Figures 7.2** show examples of retinal vascular leakage, ground truth, and the algorithm-predicted segmentation, while **Figure 7.3** show occlusion segmentations in retinal vasculitis.

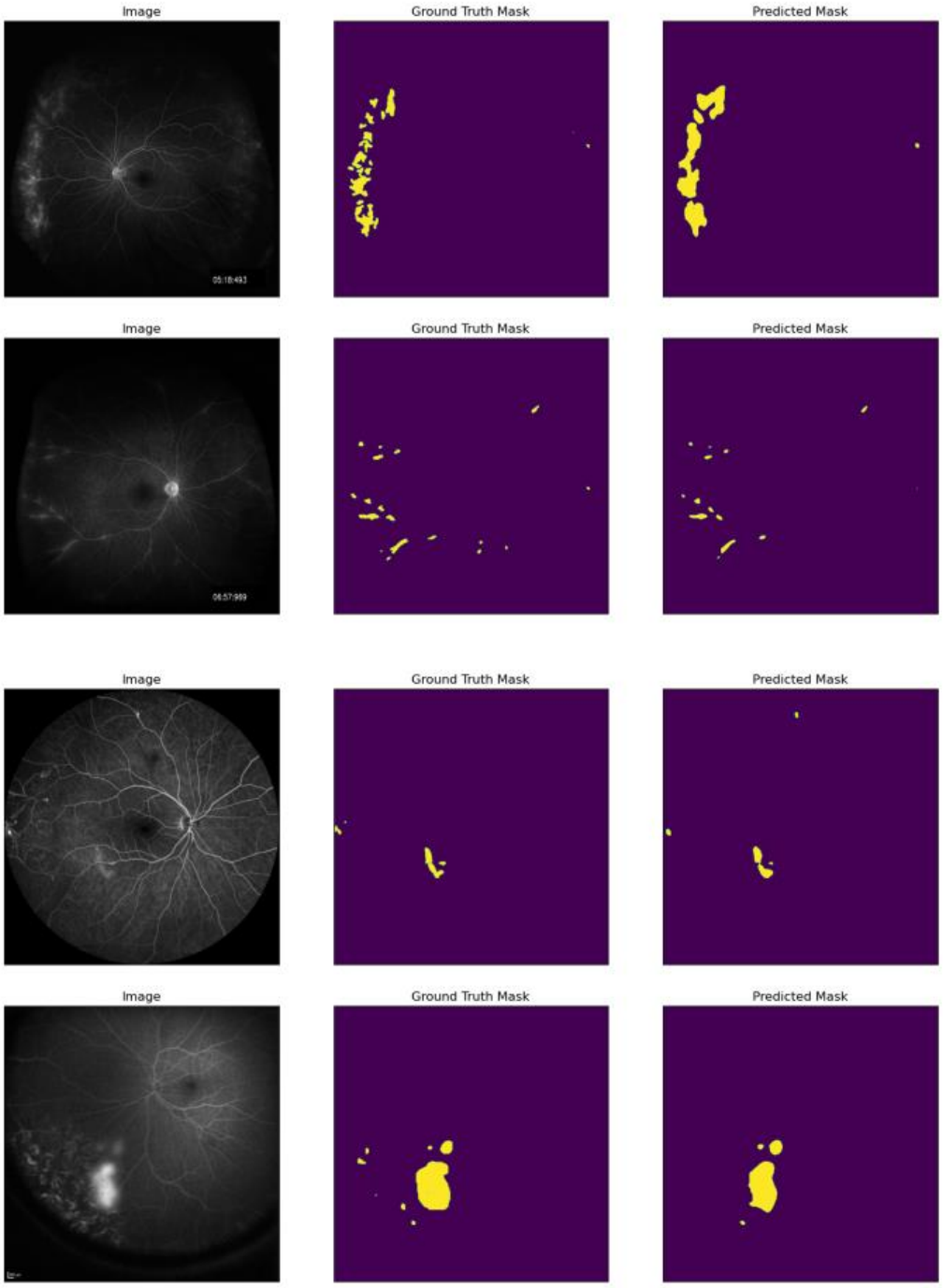


**Figure 7.2 Retinal vascular leakage image segmentation.**

OptosP200DTX (1st and 2nd row) and Heidelberg (3rd and 4th row)

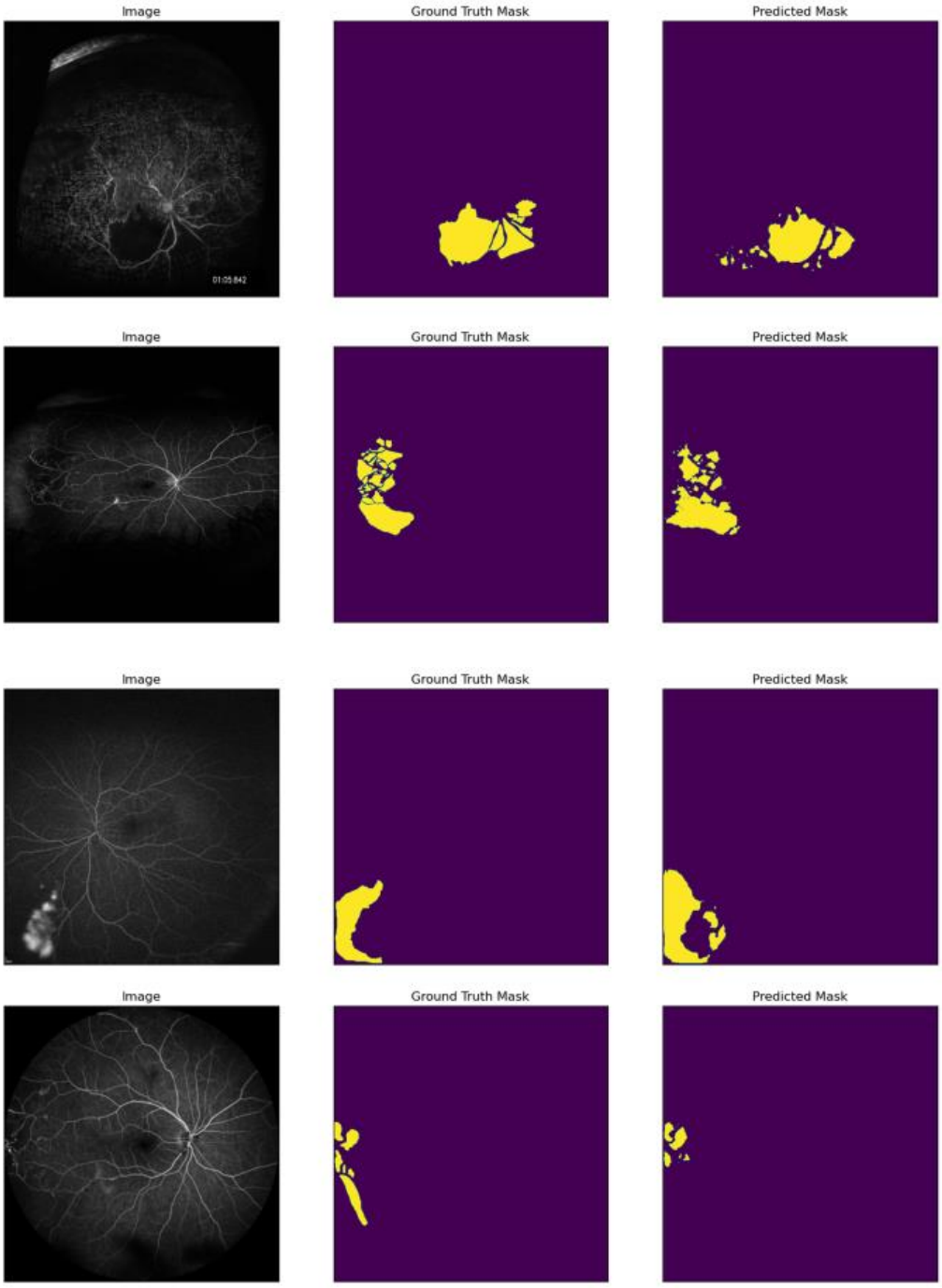


**Figure 7.3 Retinal vascular occlusion image segmentation.**

Optos200TX (1st row), P200DTX (2nd row) and Heidelberg (3rd and 4th row)

## 7.4 Discussion

Although retinal vasculitis is known to be diagnosed using FA as the choice of imaging and is expected to show retinal vascular leakage or occlusion on FA images (Agarwal et al., 2017), current clinical practice still lacks agreement in defining disease severity (Jabs et al., 2005). With the popularity of artificial intelligence and deep learning, it is possible to facilitate segmentation of retinal vasculitis. In this study, I have applied these deep learning models to develop computerised segmentation for retinal vascular leakage and occlusion in FA imaging.

To date there have been few attempts to segment retinal vascular leakage and occlusion on FA images using deep learning applications. Compared to previously published studies, I have used the highest number of FA images in uveitis patients. **Table 7.3** lists previous studies attempting segmentation of retinal vessel leakage and occlusion and performance in grading these parameters. For retinal vascular leakage, four studies used FA images from diabetic retinopathy (Ehlers et al., 2017), uveitis (Young et al., 2022), Behcet's uveitis (Keino et al., 2022), and malarial retinopathy (Zhao et al., 2015) . It is noteworthy that one study used only three participants to evaluate their retinal vascular leakage segmentation model (Keino et al., 2022),. Their performance comparison in uveitis shows a Dice score of 0.572 obtained from the deep learning method, compared with two clinicians' Dice score of 0.483 (Young et al., 2022). This result suggests a moderately acceptable performance in segmenting retinal vascular leakage, although less than the current study, with a best Dice score of 0.628.

**Table 7.3 Studies reported segmentation of retinal vascular leakage and occlusion in FA**

| Study | Country | Year | Lesion | Imaging machine | Disease | Total FA Images | Dice score | comments |
|---|---|---|---|---|---|---|---|---|
| (Zhao et al., 2015) | UK/Malawi | 2015 | Leakage | Topcon 50-EX optical unit | Malarial Retinopathy | 30 | NA | |
| (Ehlers et al., 2017) | USA | 2017 | Leakage | Optos200Tx | Diabetic Retinopathy | 56 | NA | |
| (Young et al., 2022) | USA | 2022 | Leakage | Optos200Tx | Uveitis | 250 | 0.572 | reported Dice score between two clinicians = 0.483 |
| (Keino et al., 2022) | Japan | 2022 | Leakage | Optos200Tx/ OptosP200DTx | Behcet's uveitis | 12 | 0.467 | |
| (Nunez do Rio et al., 2020) | UK | 2020 | Occlusion | Optos200Tx | Diabetic Retinopathy | 95 | 0.655 | |
| (Lee et al., 2022) | Korea | 2022 | Occlusion | OptosP200DTx | Diabetic Retinopathy | 951 | IOU = 0.681 | reported IOU score between two clinicians =0.793 |
| (Masayoshi et al., 2022) | Japan | 2022 | Occlusion | NA | Retinal vein occlusion | 403 | 0.736 | |

For occlusion, to the best of my knowledge, there has been no previous attempt on deep learning methods applied to FA images from eyes with uveitis/retinal vasculitis, although this has been done in diabetic retinopathy (Nunez do Rio et al., 2020;Lee et al., 2022) and retinal vein occlusion (Masayoshi et al., 2022). The best Dice score from the deep learning model reported in retinal vein occlusion was 0.736 (Masayoshi et al., 2022). In diabetic retinopathy, Lee et al. reported that the intersect over union score between two clinicians was 0.793, while the deep learning model's best performance was 0.681 (Lee et al., 2022). My model has obtained a Dice score of 0.699, showing acceptable segmentation for occlusion in FA imaging. In the retinal vein occlusion study (Masayoshi et al., 2022), occlusion was present in 323 out of 403 FA images (74.9%) In the diabetic retinopathy study (Ehlers et al., 2017) , 22.8% of the pixels in their FA images had vascular occlusion. The current retinal vasculitis dataset showed occlusion in 144 images from 463 FA images (31%); understandably rates of vascular occlusion will differ in different diseases, populations, and datasets.

The big challenge in artificial intelligence for image analysis is that the method is data-hungry and requires a large number of images (Choi et al., 2020a). In common retinal diseases such as diabetic retinopathy and age-related macular degeneration, available pooled image datasets have significantly large number of images, such as more than 100,000 macular OCT images (Kermany et al., 2018). However, in ocular inflammatory disease, the number of images obtained from a single dataset could be small (Keino et al., 2022). Therefore, an increasing number of images are needed in the deep learning model, and future analysis could include images from multi-centre biobanks or federated learning(Schmidt-Erfurth et al., 2018b). In addition, other examples of segmentation of FA imaging reported only using images from the Optos platform. The current result showed that it is possible to use FA images from Optos and

Heidelberg platforms which not only gave us a larger dataset but showed compatible performance results for segmentation models developed.

One limitation of this study is the retrospective nature of the image dataset used. FA images were at different time points in the run and not standardised. Although the algorithm might be comparable to other deep learning models in retinal vascular leakage and occlusion, the Dice score is lower when compared to segmentation algorithms developed for some other pathologies. For example, a score of 0.94 was reported for traumatic brain injury segmentation (Jadon et al., 2020), indicating a much tighter correlation between computerised segmentation and the clinicians' ground truth.  the current model is still not ready for real-life clinical practice. Another limitation is that it is known that eyes with severe intraocular inflammation may have more severe retinal vasculitis, but worse media opacity, such as vitritis which will affects the clarity of retinal images (Agarwal et al., 2017); for training the model and testing, we could only include images with good clarity. This meant that some severe retinal vasculitis might have been excluded on the basis that the images were ungradable.

In conclusion, this study demonstrates that it is possible to include images from different machines to develop deep learning methods for segmenting retinal vascular leakage and occlusion on FA in eyes with retinal vasculitis. Artificial intelligence applications in uveitis are promising as severity grading of wide-field images can involve a great deal of imaging data. Although a clinical grading scheme for retinal vasculitis is being developed, computerised grading can include all data on leakage and occlusion available in an FA image. A manual grading scheme in retinal vasculitis for clinicians will inevitably be simplified and limited by time constraints. However, larger image datasets are required to develop a more robust computerised segmentation model for clinical practice.

# Chapter 8 Conclusion

This thesis focuses on applying biomedical data analysis to the context of ageing and inflammatory retinal diseases. In this final chapter, I provide a comprehensive summary of the research, highlight the key findings and propose some potential ideas for future research.

## 8.1 Summary

The retina's complex structure constituting of the neural retina, RPE and retinal vasculatures, supports the human visual function. Retinal diseases are detrimental to our vision by altering these components. In this thesis, I utilise data-driven analysis to ageing and inflammatory retinal diseases. Two approaches from this work broaden the understanding and support the clinical diagnosis of retinal diseases.

The first approach in this work applies transcriptomic analysis to the RPE/choroid dataset to better understand the pathogenesis of ageing RPE/choroid and AMD. By integrating the microarray and RNAseq data, the differential gene expressions analysis of RPE/choroid transcriptomic led to two significant biological pathways in AMD: the neuroactive ligand-receptor interaction pathway and the extracellular matrix-receptor interaction signalling pathway. Next, the intercellular communication between RPE and choroidal endothelial cells has been explored by analysing the scRNA-seq and microarray datasets. The results highlighted VEGF-, BMP- and tenascin-mediated pathways associated with ageing and senescence in RPE/choroid tissues. Apart from the pathway analysis, the result in intercellular communication introduced that senescence status might differ by ageing RPE/choroid and among different subtypes of AMD. Together, the analysis of RPE/choroid transcriptomics in the first part of this thesis gives more biological insights into the ageing process and the pathogenesis of AMD.

For the second approach in this work, clinical imaging data of retinal vasculitis have been investigated. The systematic review of OCT and OCT-A in retinal vasculitis has been conducted to explore non-invasive imaging methods for retinal vasculitis. Although OCT and OCT-A might not demonstrate the primary sign of retinal vasculitis, they are useful in following up the complications such as macular oedema. At present OCT and OCT-A cannot replace FA imaging, emphasising FA as the gold standard imaging technique in retinal vasculitis patients. Despite the importance of FA, there is no accepted grading system specifically for retinal vasculitis. The work in this thesis has presented a newly developed WFFA grading system for retinal vasculitis, which grades on leakage and occlusion. The inter and intraobserver reliability has demonstrated this new grading scheme's repeatability. Additionally, the leakage score in this grading scheme correlates with visual acuity. Lastly, to apply data-driven application to retinal vasculitis, the WFFA images of retinal vasculitis have been used to develop a computerised grading system using deep learning. The resulting leakage and occlusion segmentation models from deep learning achieve acceptable performance, which could be a potential tool to help clinicians quantify WFFA images.

## 8.2 Main findings and contributions

This section explains how the main findings from this thesis answer the specific objectives mentioned in **Chapter 2.3**.

The first specific aim was to "To explore genes and functional pathways underpinning pathological processes occurring in ageing RPE/AMD by exploring existent AMD/controls RPE transcriptomic data."

The meta-analysis of microarray and RNAseq RPE/choroid transcriptomic data (**Chapter 3)** was conducted to address the problem, described in **Chapter 2.1**, that AMD RPE

transcriptomic studies are heterogeneous in techniques and methods. The result indicated 764 DE genes in macular AMD RPE/choroid and 445 DE genes in non-macular AMD RPE/choroid. The functional pathways analysis was determined using an over-representation analysis of KEGG pathways that suggested the neuroactive ligand-receptor interaction pathway and the extracellular matrix-receptor interaction signalling pathway as the possible biological processes associated with DE genes in macular AMD RPE/choroid.

The second specific aim was to "To investigate intercellular communication of the RPE/choroid in the context of ageing, senescence and AMD by using an integrated analysis of RPE transcriptomic datasets obtained through different approaches (microarrays and scRNA-seq)."

In **Chapter 4**, scRNA-seq and microarray of RPE/choroid have been re-analysed to understand the intercellular communication of the RPE/choroid. The cell-cell interaction analysis characterised VEGF-, BMP- and tenascin-mediated pathways as the intercellular communication pathways between RPE and choroidal endothelial cells. The linear regression analysis introduced that the genes in these three pathways might be differentially associated with ageing. The signalling strength of these three pathways was increased in the subpopulation of cells associated with senescence. In addition, senescence gene expression in RPE/choroid could positively correlate with ageing and differ between AMD types (geographic atrophy and neovascular).

The third specific aim was to "To conduct a systematic review to understand the features of retinal vasculitis in OCT imaging."

**Chapter 5** reported the systematic review of OCT and OCT-A in retinal vasculitis. The systemic search identified 20 relevant studies (8 OCT, 6 OCT-EDI and 6 OCT-A studies). The

data extraction from these publications illustrates no clear evidence of primary signs of retinal vasculitis on these imaging methods, although there is scope to develop vessel imaging analysis. However, they are certainly utilised for evaluating secondary complications of retinal vasculitis.

The fourth specific aim was to "To develop and test the reliability of a novel grading scheme for retinal vasculitis."

In **Chapter 6**, the new grading scheme of retinal vasculitis in WFFA has been proposed. This new grading scheme consisted of retinal vascular leakage and occlusion scores. The proposed grading scheme was then tested among 4 graders using WFFA images from 50 retinal vasculitis patients. The validation result from a single centre reported promising levels of intra and interobserver reliability, ranging from good to excellent.. Furthermore, increasing leakage score was related to worsened visual acuity.

"To develop a computerised analysis of retinal vasculitis grading using artificial intelligence."

As described in **Chapter 7**, deep learning models for image segmentation have been applied to develop computerised segmentation for WFFA images of retinal vasculitis. After training and testing using 463 images, the study reported reliable segmentation models for retinal vascular leakage and occlusion.

Taken together, these findings advance our understanding in ageing and inflammatory retinal diseases by using data-driven analysis. Additionally, how these works contribute to the current retinal research field is described below.

### 8.2.1 Data-driven application in retinal research – novel findings

This thesis mentions two aspects of data analysis in retinal diseases: biological and clinical data. By applying biological data analysis using transcriptome in **Chapter 3** and **4**, the results have contributed to the pathogenesis question of AMD. For clinical data, **Chapter 5-7** have explored the imaging of retinal vasculitis, one of the important features of inflammatory retinal diseases. Especially, **Chapter 7** has applied the deep learning method for image segmentation to WFFA images of retinal vasculitis.

### 8.2.2 Pathogenesis of AMD

Clinical data for AMD has previously supported epidemiological risk factors, i.e. ageing, and genetic associations, but the disease mechanism remains poorly understood (Handa et al., 2019). The transcriptomic analysis in **Chapter 3** and **4** added new information on specific pathways related to AMD RPE/choroid. **Chapter 3** applied the meta-analysis statistics for gene expression data, which had not previously been applied to AMD. With the combined data lead to identifying pathways related to AMD. Therefore, for the first time, the result suggests the potential significance of extracellular matrix alteration in AMD using combined transcriptomic data. Furthermore, **Chapter 4** is the first study that bioinformatically explored senescence gene expression in RPE/choroid using transcriptomic data. While senescence has been questioned its involvement in the pathogenesis of AMD, this chapter novelly proposed identifying senescences using transcriptomic data from post-mortem human RPE/choroid samples. Additionally, this novel result suggested the possibility that different types of AMD might have distinct levels of senescence gene expressions.

### 8.2.3 Clinical imaging of retinal vasculitis

The studies in this thesis focus on clinical imaging data for retinal vasculitis. **Chapter 5** identified the role of OCT and OCT-A throughout the literature, which had not previously been undertaken focusing on retinal vasculitis. While other retinal conditions move away from FA, this review supported its continued use in posterior uveitis whilst identifying future research needs to develop non-invasive imaging to assess retinal vasculitis. **Chapter 6** added the new retinal vasculitis grading scheme for WFFA images. As no validated, straight-forward, clinical grading scheme exists for retinal vasculitis this is a novel development for uveitis care and research. Regarding data-driven application, computerised application in imaging inflammatory retinal diseases, such as identifying retinal vascular leakage (Young et al., 2022) and quantifying vitreous inflammation in uveitis (Liu et al., 2022) have had variable success. **Chapter 7** then introduced a novel computerised segmentation method for retinal vasculitis. The result of this novel computerised method is the first study comparing different deep learning architectures focused on retinal vascular leakage and occlusion in retinal vasculitis patients.

## 8.3 Future work

### 8.3.1 Future work on ageing retinal disease

#### Validation of biological pathways associated with AMD

The transcriptomic experiments in RPE/choroid are still limited to small sample sizes. More transcriptomic data are needed from various populations and subtypes of AMD to confirm the results are generalisable. Data analysis alone cannot replace molecular experiments, however it can guide experimental hypotheses and methodology to confirm exact biology. Molecular biology in retinal disease is always limited by difficulty obtaining tissue, poor animal models and tissue culture models, so needs any additional information to guide it.

In keeping with other pathways in AMD, whether senescence cells occur in the retina still needs more evidence to confirm, including biological mechanism studies integrating with clinical studies.

The results from **Chapter 3** suggested possible functional pathways, including neuroactive ligand-receptor interaction and extracellular matrix-receptor interaction signalling. Some suggested possible studies that could be undertaken from these findings include:

- Inhibition or overexpression of genes in these two pathways and identify the molecular consequences using cellular models such as primary human RPE culture or human RPE generated from stem cell culture.
- Conduct a similar transcriptomic study comparing AMD RPE/choroid with postmortem normal RPE/choroid in other countries/regions and having more detailed clinical and pathological data.
- Combine the current transcriptomic results with other omics, including genomic, proteomic and metabolomics.

For **Chapter 4**, the results suggested that senescence might be involved in AMD, but this suggestion developed from analysing a small number of scRNA-seq samples. The validation should be conducted by increasing the sample to validate this hypothesis, applying the proposed senescence score from the current thesis, and testing the difference between AMD RPE/choroid and normal RPE/choroid. Although there is no consensus on how many samples are needed to design the transcriptomic study. One study recommended at least six samples per condition (Schurch et al., 2016), although the experimental designs would be limited by the scarcity of postmortem RPE/choroid samples and the cost of sequencing technology.

Moreover, this score might be potentially used to evaluate senotherapy treatments in RPE cellular culture.

**Discovery of the pathogenesis of AMD using other omics**

Apart from omics data, there is progress in clinical imaging; future research could combine the omics and advanced imaging data in AMD to create more understanding of pathogenesis. The result in this thesis used only transcriptomic data to understand AMD. Other novel experiments in omics data, including spatial omics and multi-omics data analysis (Vandereyken et al., 2023), could be applied to retinal tissues.

**Omics and AMD treatment**

Although the treatment option has not been explored in the current analysis, omics testing, such as using genomics on AMD patients, might lead to precision medicine. For example, if a future clinical trial could show that some treatments option are preferable in specific genotypes, the genomics could be used in future clinical practice. This is being explored in some current studies of treatment for geographic atrophy.

### 8.3.2 Future work on inflammatory retinal disease

**Validation of clinical grading**

The current validation of new clinical WFFA grading on retinal vasculitis was done using graders from a single centre. The future validation needs more images from the different centres and validated with more graders in multicentres. More specifically, the follow-up study could be conducted using the grading scheme provided in **Chapter 6** to validate interoperator reliability among uveitis experts in different centres. Additionally, the correlation between the leakage score and visual acuity should incorporate data from various centres. Also the grading

scheme needs to be validated against clinical response to treatment, which could be done in the context of a clinical trial or prospective clinical study. This new clinical grading may already be used clinically, but after further validation could be used in clinical trials in the inclusion criteria and outcome measures.

**Role of OCT and OCT-A in retinal vasculitis**

Although the current systematic review concluded that there were insufficient data for OCT and OCT-A to be diagnosic tools for retinal vasculitis, conducting OCT and OCT-A image analysis specifically on inflammed retinal vessels has not been done. As **Chapter 5** suggested possible features of OCT/OCT-A related to retinal vasculitis, future studies might focus on these features including perivascular retinal thickness (OCT, OCT-A), central macular thickness (OCT), choroidal thickness (OCT-EDI), cystoid macular oedema (OCT), epiretinal membrane formation (OCT), disruption of the ellipsoid zone (OCT), and capillary dropout (OCT-A). Wider field OCT such as swept-source OCT may identify features which could diagnose or severity-assess retinal vasculitis and this has not yet been investigated, Other options include applied deep learning classification on OCT and OCT-A images, which may potentially extract some features from the images.

**Training segmentation models of retinal vasculitis**

Because the computerised segmentation model for retinal vasculitis was developed in **Chapter 7** using images from the internal dataset, future studies could involve external validation by utilising images from various medical centres. Similar to clinical grading, more images are needed to improve and train the deep learning model, including images from multiple centres. The future computerised method needs to include a wide range of uveitis conditions and ambiguous images. Following training and validation with more images to

achieve a confident performance, this artificial intelligence system could be used as a decision support system (Vasey et al., 2022) while clinicians interpret WFFA images. A clinical ordinal severity scale inevitably loses most available information on WFFA, whereas AI can include all information in a continuous scale which accounts for extent and position of abnormalities. However, the reproducibility of computerised methods needs several prospective clinical evaluations before implementing in clinical practice.

**Omics data and inflammatory retinal diseases**

Even though not mentioned in this thesis, omics data analysis is potential rich research avenue for uveitis and inflammatory retinal diseases, including retinal vasculitis. Some researchers recently reported using metagenomic techniques to find the pathogens involved in intraocular infection (Ma et al., 2019). If sample scarcity could be overcome, omics techniques could be applied to uveitis research incorporating clinical image analysis to powerfully illuminate pathogenic pathways which are likely to be more complex and multifactorial than AMD.

## References


Abràmoff, M., and Kay, C.N. (2013). "Image Processing," in *Retina,* eds. S.J. Ryan, S.R. Sadda, D.R. Hinton, A.P. Schachat, S.R. Sadda, C.P. Wilkinson, P. Wiedemann & A.P. Schachat. (London: W.B. Saunders), 151-176.

Abroug, N., Khairallah, M., Ksiaa, I., Ben Amor, H., Zina, S., Attia, S., Jelliti, B., Khochtali, S., and Khairallah, M. (2021). A Comparative Study between Occlusive and Non-occlusive Retinal Vasculitis: Data from a Referral Center in Tunisia, North Africa. *Ocul Immunol Inflamm***,** 1-8.

Abucham-Neto, J.Z., Torricelli, A.a.M., Lui, A.C.F., Guimaraes, S.N., Nascimento, H., and Regatieri, C.V. (2018). Comparison between optical coherence tomography angiography and fluorescein angiography findings in retinal vasculitis. *Int J Retina Vitreous* 4**,** 15.

Acar, I.E., Lores-Motta, L., Colijn, J.M., Meester-Smoor, M.A., Verzijden, T., Cougnard-Gregoire, A., Ajana, S., Merle, B.M.J., De Breuk, A., Heesterbeek, T.J., Van Den Akker, E., Daha, M.R., Claes, B., Pauleikhoff, D., Hense, H.W., Van Duijn, C.M., Fauser, S., Hoyng, C.B., Delcourt, C., Klaver, C.C.W., Galesloot, T.E., Den Hollander, A.I., and Consortium, E.-R. (2020). Integrating Metabolomics, Genomics, and Disease Pathways in Age-Related Macular Degeneration: The EYE-RISK Consortium. *Ophthalmology* 127**,** 1693-1709.

Accorinti, M., Gilardi, M., De Geronimo, D., Iannetti, L., Giannini, D., and Parravano, M. (2020). Optical Coherence Tomography Angiography Findings in Active and Inactive Ocular Behcet Disease. *Ocul Immunol Inflamm* 28**,** 589-600.

Ach, T., Huisingh, C., Mcgwin, G., Jr., Messinger, J.D., Zhang, T., Bentley, M.J., Gutierrez, D.B., Ablonczy, Z., Smith, R.T., Sloan, K.R., and Curcio, C.A. (2014). Quantitative autofluorescence and cell density maps of the human retinal pigment epithelium. *Invest Ophthalmol Vis Sci* 55**,** 4832-4841.

Agarwal, A., Afridi, R., Agrawal, R., Do, D.V., Gupta, V., and Nguyen, Q.D. (2017). Multimodal Imaging in Retinal Vasculitis. *Ocul Immunol Inflamm* 25**,** 424-433.

Agarwal, A., Rubsam, A., Zur Bonsen, L., Pichi, F., Neri, P., and Pleyer, U. (2022). A Comprehensive Update on Retinal Vasculitis: Etiologies, Manifestations and Treatments. *J Clin Med* 11**,** 2525.

Age-Related Eye Disease Study Research, G. (2001a). The Age-Related Eye Disease Study system for classifying age-related macular degeneration from stereoscopic color fundus photographs: the Age-Related Eye Disease Study Report Number 6. *Am J Ophthalmol* 132**,** 668-681.

Age-Related Eye Disease Study Research, G. (2001b). A randomized, placebo-controlled, clinical trial of high-dose supplementation with vitamins C and E, beta carotene, and zinc for age-related macular degeneration and vision loss: AREDS report no. 8. *Arch Ophthalmol* 119**,** 1417-1436.

Agrawal, R., Gunasekeran, D.V., Gonzalez-Lopez, J.J., Cardoso, J., Gupta, B., Addison, P.K., Westcott, M., and Pavesio, C.E. (2017). PERIPHERAL RETINAL VASCULITIS: Analysis of 110 Consecutive Cases and a Contemporary Reappraisal of Tubercular Etiology. *Retina* 37**,** 112-117.

Al-Khuzaei, S., Broadgate, S., Foster, C.R., Shah, M., Yu, J., Downes, S.M., and Halford, S. (2021). An Overview of the Genetics of ABCA4 Retinopathies, an Evolving Story. *Genes (Basel)* 12**,** 1241.

Al-Zamil, W.M., and Yassin, S.A. (2017). Recent developments in age-related macular degeneration: a review. *Clin Interv Aging* 12**,** 1313-1330.

Albacete-Albacete, L., Sanchez-Alvarez, M., and Del Pozo, M.A. (2021). Extracellular Vesicles: An Emerging Mechanism Governing the Secretion and Biological Roles of Tenascin-C. *Front Immunol* 12**,** 671485.

Albloushi, A.F., Dheyab, A.M., Al-Swaina, N.F., Al-Obailan, M., Daif, A.K., and Abu El-Asrar, A.M. (2021). Clinical findings and outcomes of uveitis associated with multiple sclerosis. *Eur J Ophthalmol* 31**,** 482-490.

Alge, C.S., Suppmann, S., Priglinger, S.G., Neubauer, A.S., May, C.A., Hauck, S., Welge-Lussen, U., Ueffing, M., and Kampik, A. (2003). Comparative proteome analysis of native differentiated and cultured dedifferentiated human RPE cells. *Invest Ophthalmol Vis Sci* 44**,** 3629-3641.

Ali, A., Ku, J.H., Suhler, E.B., Choi, D., and Rosenbaum, J.T. (2014). The course of retinal vasculitis. *Br J Ophthalmol* 98**,** 785-789.

Alimadadi, A., Munroe, P.B., Joe, B., and Cheng, X. (2020). Meta-Analysis of Dilated Cardiomyopathy Using Cardiac RNA-Seq Transcriptomic Datasets. *Genes (Basel)* 11**,** 60.

Anderson, K.W., Chen, J., Wang, M., Mast, N., Pikuleva, I.A., and Turko, I.V. (2015). Quantification of histone deacetylase isoforms in human frontal cortex, human retina, and mouse brain. *PLoS One* 10**,** e0126592.

Anglade, E., Aspeslet, L.J., and Weiss, S.L. (2008). A new agent for the treatment of noninfectious uveitis: rationale and design of three LUMINATE (Lux Uveitis Multicenter Investigation of a New Approach to Treatment) trials of steroid-sparing voclosporin. *Clin Ophthalmol* 2**,** 693-702.

Apinyawasisuk, S., Rothova, A., Kunavisarut, P., and Pathanapitoon, K. (2013). Clinical features and etiology of retinal vasculitis in Northern Thailand. *Indian J Ophthalmol* 61**,** 739-742.

Ardeljan, D., and Chan, C.C. (2013). Aging is not a disease: distinguishing age-related macular degeneration from aging. *Prog Retin Eye Res* 37**,** 68-89.

Armingol, E., Officer, A., Harismendy, O., and Lewis, N.E. (2021). Deciphering cell-cell interactions and communication from gene expression. *Nat Rev Genet* 22**,** 71-88.

Arzt, M., Deschamps, J., Schmied, C., Pietzsch, T., Schmidt, D., Tomancak, P., Haase, R., and Jug, F. (2022). LABKIT: Labeling and Segmentation Toolkit for Big Image Data. *Frontiers in Computer Science* 4.

Ashikawa, Y., Nishimura, Y., Okabe, S., Sato, Y., Yuge, M., Tada, T., Miyao, H., Murakami, S., Kawaguchi, K., Sasagawa, S., Shimada, Y., and Tanaka, T. (2017). Potential protective function of the sterol regulatory element binding factor 1-fatty acid desaturase 1/2 axis in early-stage age-related macular degeneration. *Heliyon* 3**,** e00266.

Aumann, S., Donner, S., Fischer, J., and Muller, F. (2019). "Optical Coherence Tomography (OCT): Principle and Technical Realization," in *High Resolution Imaging in Microscopy and Ophthalmology: New Frontiers in Biomedical Optics,* ed. J.F. Bille. (Cham (CH): Springer International Publishing), 59-85.

Badar, M., Haris, M., and Fatima, A. (2020). Application of deep learning for retinal image analysis: A review. *Computer Science Review* 35**,** 100203.

Badr, M.T., and Hacker, G. (2019). Gene expression profiling meta-analysis reveals novel gene signatures and pathways shared between tuberculosis and rheumatoid arthritis. *PLoS One* 14**,** e0213470.

Balbaba, M., Ulas, F., Postaci, S.A., Celiker, U., and Gurgoze, M.K. (2020). Clinical and Demographic Features of Pediatric-Onset Behcet's Disease and Evaluation of Optical Coherence Tomography Findings. *Ocul Immunol Inflamm* 28**,** 606-612.

Barbie, D.A., Tamayo, P., Boehm, J.S., Kim, S.Y., Moody, S.E., Dunn, I.F., Schinzel, A.C., Sandy, P., Meylan, E., Scholl, C., Frohling, S., Chan, E.M., Sos, M.L., Michel, K., Mermel, C., Silver, S.J., Weir, B.A., Reiling, J.H., Sheng, Q., Gupta, P.B., Wadlow, R.C., Le, H., Hoersch, S., Wittner, B.S., Ramaswamy, S., Livingston, D.M., Sabatini, D.M., Meyerson, M., Thomas, R.K., Lander, E.S., Mesirov, J.P., Root, D.E., Gilliland, D.G., Jacks, T., and Hahn, W.C. (2009). Systematic RNA interference reveals that oncogenic KRAS-driven cancers require TBK1. *Nature* 462**,** 108-112.

Barrie, E.S., Hartmann, K., Lee, S.H., Frater, J.T., Seweryn, M., Wang, D., and Sadee, W. (2017). The CHRNA5/CHRNA3/CHRNB4 Nicotinic Receptor Regulome: Genomic Architecture, Regulatory Variants, and Clinical Associations. *Hum Mutat* 38**,** 112-119.

Basisty, N., Kale, A., Jeon, O.H., Kuehnemann, C., Payne, T., Rao, C., Holtz, A., Shah, S., Sharma, V., Ferrucci, L., Campisi, J., and Schilling, B. (2020). A proteomic atlas of senescence-associated secretomes for aging biomarker development. *PLoS Biol* 18**,** e3000599.

Baumal, C.R., Bodaghi, B., Singer, M., Tanzer, D.J., Seres, A., Joshi, M.R., Feltgen, N., and Gale, R. (2021). Expert Opinion on Management of Intraocular Inflammation, Retinal Vasculitis, and Vascular Occlusion after Brolucizumab Treatment. *Ophthalmol Retina* 5**,** 519-527.

Baumal, C.R., Spaide, R.F., Vajzovic, L., Freund, K.B., Walter, S.D., John, V., Rich, R., Chaudhry, N., Lakhanpal, R.R., Oellers, P.R., Leveque, T.K., Rutledge, B.K., Chittum, M., Bacci, T., Enriquez, A.B., Sund, N.J., Subong, E.N.P., and Albini, T.A. (2020). Retinal Vasculitis and Intraocular Inflammation after Intravitreal Injection of Brolucizumab. *Ophthalmology* 127**,** 1345-1359.

Beranova-Giorgianni, S., and Giorgianni, F. (2018). Proteomics of Human Retinal Pigment Epithelium (RPE) Cells. *Proteomes* 6**,** 22.

Bermond, K., Wobbe, C., Tarau, I.S., Heintzmann, R., Hillenkamp, J., Curcio, C.A., Sloan, K.R., and Ach, T. (2020). Autofluorescent Granules of the Human Retinal Pigment Epithelium: Phenotypes, Intracellular Distribution, and Age-Related Topography. *Invest Ophthalmol Vis Sci* 61**,** 35.

Biernacka, J.M., Geske, J., Jenkins, G.D., Colby, C., Rider, D.N., Karpyak, V.M., Choi, D.S., and Fridley, B.L. (2013). Genome-wide gene-set analysis for identification of pathways associated with alcohol dependence. *Int J Neuropsychopharmacol* 16**,** 271-278.

Birnbaum, A.D., Fawzi, A.A., Rademaker, A., and Goldstein, D.A. (2014). Correlation between clinical signs and optical coherence tomography with enhanced depth imaging findings in patients with birdshot chorioretinopathy. *JAMA Ophthalmol* 132**,** 929-935.

Blaauwgeers, H.G., Holtkamp, G.M., Rutten, H., Witmer, A.N., Koolwijk, P., Partanen, T.A., Alitalo, K., Kroon, M.E., Kijlstra, A., Van Hinsbergh, V.W., and Schlingemann, R.O. (1999). Polarized vascular endothelial growth factor secretion by human retinal pigment epithelium and localization of vascular endothelial growth factor receptors on the inner choriocapillaris. Evidence for a trophic paracrine relation. *Am J Pathol* 155**,** 421-428.

Blasiak, J. (2020). Senescence in the pathogenesis of age-related macular degeneration. *Cell Mol Life Sci* 77**,** 789-805.

Blasiak, J., Piechota, M., Pawlowska, E., Szatkowska, M., Sikora, E., and Kaarniranta, K. (2017). Cellular Senescence in Age-Related Macular Degeneration: Can Autophagy and DNA Damage Response Play a Role? *Oxid Med Cell Longev* 2017**,** 5293258.

Blokland, K.E.C., Pouwels, S.D., Schuliga, M., Knight, D.A., and Burgess, J.K. (2020). Regulation of cellular senescence by extracellular matrix during chronic fibrotic diseases. *Clin Sci (Lond)* 134**,** 2681-2706.

Boni, C., Thorne, J.E., Spaide, R.F., Ostheimer, T.A., Sarraf, D., Levinson, R.D., Goldstein, D.A., Rifkin, L.M., Vitale, A.T., Jaffe, G.J., and Holland, G.N. (2016). Choroidal Findings in Eyes With Birdshot Chorioretinitis Using Enhanced-Depth Optical Coherence Tomography. *Invest Ophthalmol Vis Sci* 57**,** OCT591-599.

Booij, J.C., Ten Brink, J.B., Swagemakers, S.M., Verkerk, A.J., Essing, A.H., Van Der Spek, P.J., and Bergen, A.A. (2010). A new strategy to identify and annotate human RPE-specific gene expression. *PLoS One* 5**,** e9341.

Booij, J.C., Van Soest, S., Swagemakers, S.M., Essing, A.H., Verkerk, A.J., Van Der Spek, P.J., Gorgels, T.G., and Bergen, A.A. (2009). Functional annotation of the human retinal pigment epithelium transcriptome. *BMC Genomics* 10**,** 164.

Borcherding, N., Vishwakarma, A., Voigt, A.P., Bellizzi, A., Kaplan, J., Nepple, K., Salem, A.K., Jenkins, R.W., Zakharia, Y., and Zhang, W. (2021). Mapping the immune environment in clear cell renal carcinoma by single-cell genomics. *Commun Biol* 4**,** 122.

Boulton, M., and Dayhaw-Barker, P. (2001). The role of the retinal pigment epithelium: topographical variation and ageing changes. *Eye (Lond)* 15**,** 384-389.

Boulton, M., Moriarty, P., Jarvis-Evans, J., and Marcyniuk, B. (1994). Regional variation and age-related changes of lysosomal enzymes in the human retinal pigment epithelium. *Br J Ophthalmol* 78**,** 125-129.

Boulton, M., Roanowska, M., and Wess, T. (2004). Ageing of the retinal pigment epithelium: implications for transplantation. *Graefes Arch Clin Exp Ophthalmol* 242**,** 76-84.

Boulton, M.E. (2013). "Ageing of the Retina and Retinal Pigment Epithelium," in *Age-related Macular Degeneration*. Springer Berlin Heidelberg), 45-63.

Bousquet, E., Khandelwal, N., Seminel, M., Mehanna, C., Salah, S., Eymard, P., Bodin Hassani, S., Monnet, D., Brezin, A., and Agrawal, R. (2021). Choroidal Structural Changes in Patients with Birdshot Chorioretinopathy. *Ocul Immunol Inflamm* 29**,** 346-351.

Brown, L.A., Williams, J., Taylor, L., Thomson, R.J., Nolan, P.M., Foster, R.G., and Peirson, S.N. (2017). Meta-analysis of transcriptomic datasets identifies genes enriched in the mammalian circadian pacemaker. *Nucleic Acids Res* 45**,** 9860-9873.

Burlina, P.M., Joshi, N., Pekala, M., Pacheco, K.D., Freund, D.E., and Bressler, N.M. (2017). Automated Grading of Age-Related Macular Degeneration From Color Fundus Images Using Deep Convolutional Neural Networks. *JAMA Ophthalmol* 135**,** 1170-1176.

Butler, J.M., Supharattanasitthi, W., Yang, Y.C., and Paraoan, L. (2021). RNA-seq analysis of ageing human retinal pigment epithelium: Unexpected up-regulation of visual cycle gene transcription. *J Cell Mol Med* 25**,** 5572-5585.

Cabrera, A.P., Bhaskaran, A., Xu, J., Yang, X., Scott, H.A., Mohideen, U., and Ghosh, K. (2016). Senescence Increases Choroidal Endothelial Stiffness and Susceptibility to Complement Injury: Implications for Choriocapillaris Loss in AMD. *Invest Ophthalmol Vis Sci* 57**,** 5910-5918.

Caceres, P.S., and Rodriguez-Boulan, E. (2020). Retinal pigment epithelium polarity in health and blinding diseases. *Curr Opin Cell Biol* 62**,** 37-45.

Cao, D., Leong, B., Messinger, J.D., Kar, D., Ach, T., Yannuzzi, L.A., Freund, K.B., and Curcio, C.A. (2021). Hyperreflective Foci, Optical Coherence Tomography Progression Indicators in Age-Related Macular Degeneration, Include Transdifferentiated Retinal Pigment Epithelium. *Invest Ophthalmol Vis Sci* 62**,** 34.

Cao, L., Wang, H., Wang, F., Xu, D., Liu, F., and Liu, C. (2013). Abeta-induced senescent retinal pigment epithelial cells create a proinflammatory microenvironment in AMD. *Invest Ophthalmol Vis Sci* 54**,** 3738-3750.

Chatsirisupachai, K., Palmer, D., Ferreira, S., and De Magalhaes, J.P. (2019). A human tissue-specific transcriptomic analysis reveals a complex relationship between aging, cancer, and cellular senescence. *Aging Cell* 18**,** e13041.

Chaum, E., Winborn, C.S., and Bhattacharya, S. (2015). Genomic regulation of senescence and innate immunity signaling in the retinal pigment epithelium. *Mamm Genome* 26**,** 210-221.

Chen, J., Liu, C.-H., and Sapieha, P. (2016). "Retinal Vascular Development," in *Anti-Angiogenic Therapy in Ophthalmology*. Springer International Publishing), 1-19.

Chen, J., and Sampath, A.P. (2017). "Structure and Function of Rod and Cone Photoreceptors," in *Ryan's Retina E-Book,* eds. A.P. Schachat, C.P. Wilkinson, D.R. Hinton, S.R. Sadda & P. Wiedemann. 6 ed: Elsevier), 387-407.

Chen, L.-C., Zhu, Y., Papandreou, G., Schroff, F., and Adam, H. (2018a). "Encoder-Decoder with Atrous Separable Convolution for Semantic Image Segmentation," in *Computer Vision – ECCV 2018*. Springer International Publishing), 833-851.

Chen, L.C., Papandreou, G., Kokkinos, I., Murphy, K., and Yuille, A.L. (2018b). DeepLab: Semantic Image Segmentation with Deep Convolutional Nets, Atrous Convolution, and Fully Connected CRFs. *IEEE Trans Pattern Anal Mach Intell* 40**,** 834-848.

Choi, R.Y., Coyner, A.S., Kalpathy-Cramer, J., Chiang, M.F., and Campbell, J.P. (2020a). Introduction to Machine Learning, Neural Networks, and Deep Learning. *Transl Vis Sci Technol* 9**,** 14.

Choi, Y.E., Song, M.J., Hara, M., Imanaka-Yoshida, K., Lee, D.H., Chung, J.H., and Lee, S.T. (2020b). Effects of Tenascin C on the Integrity of Extracellular Matrix and Skin Aging. *Int J Mol Sci* 21**,** 8693.

Choudhry, N., Duker, J.S., Freund, K.B., Kiss, S., Querques, G., Rosen, R., Sarraf, D., Souied, E.H., Stanga, P.E., Staurenghi, G., and Sadda, S.R. (2019). Classification and Guidelines for

Widefield Imaging: Recommendations from the International Widefield Imaging Study Group. *Ophthalmol Retina* 3**,** 843-849.

Cicchetti, D.V. (1994). Guidelines, criteria, and rules of thumb for evaluating normed and standardized assessment instruments in Psychology. *Psychological Assessment* 6**,** 284-290.

Cipriani, V., Leung, H.T., Plagnol, V., Bunce, C., Khan, J.C., Shahid, H., Moore, A.T., Harding, S.P., Bishop, P.N., Hayward, C., Campbell, S., Armbrecht, A.M., Dhillon, B., Deary, I.J., Campbell, H., Dunlop, M., Dominiczak, A.F., Mann, S.S., Jenkins, S.A., Webster, A.R., Bird, A.C., Lathrop, M., Zelenika, D., Souied, E.H., Sahel, J.A., Leveillard, T., French, A.M.D.I., Cree, A.J., Gibson, J., Ennis, S., Lotery, A.J., Wright, A.F., Clayton, D.G., and Yates, J.R. (2012). Genome-wide association study of age-related macular degeneration identifies associated variants in the TNXB-FKBPL-NOTCH4 region of chromosome 6p21.3. *Hum Mol Genet* 21**,** 4138-4150.

Colijn, J.M., Buitendijk, G.H.S., Prokofyeva, E., Alves, D., Cachulo, M.L., Khawaja, A.P., Cougnard-Gregoire, A., Merle, B.M.J., Korb, C., Erke, M.G., Bron, A., Anastasopoulos, E., Meester-Smoor, M.A., Segato, T., Piermarocchi, S., De Jong, P., Vingerling, J.R., Topouzis, F., Creuzot-Garcher, C., Bertelsen, G., Pfeiffer, N., Fletcher, A.E., Foster, P.J., Silva, R., Korobelnik, J.F., Delcourt, C., Klaver, C.C.W., Consortium, E.-R., and European Eye Epidemiology, C. (2017). Prevalence of Age-Related Macular Degeneration in Europe: The Past and the Future. *Ophthalmology* 124**,** 1753-1763.

Conley, S.M., Cai, X., Makkia, R., Wu, Y., Sparrow, J.R., and Naash, M.I. (2012). Increased cone sensitivity to ABCA4 deficiency provides insight into macular vision loss in Stargardt's dystrophy. *Biochim Biophys Acta* 1822**,** 1169-1179.

Conti-Fine, B.M., Navaneetham, D., Lei, S., and Maus, A.D. (2000). Neuronal nicotinic receptors in non-neuronal cells: new mediators of tobacco toxicity? *Eur J Pharmacol* 393**,** 279-294.

Corridoni, D., Antanaviciute, A., Gupta, T., Fawkner-Corbett, D., Aulicino, A., Jagielowicz, M., Parikh, K., Repapi, E., Taylor, S., Ishikawa, D., Hatano, R., Yamada, T., Xin, W., Slawinski, H., Bowden, R., Napolitani, G., Brain, O., Morimoto, C., Koohy, H., and Simmons, A. (2020). Single-cell atlas of colonic CD8(+) T cells in ulcerative colitis. *Nat Med* 26**,** 1480-1490.

Costanzo, L.S. (2017). "Neurophysiology," in *Physiology E-Book,* ed. L.S. Costanzo. 6 ed: Elsevier), 69-116.

Crossman, A.R., and Neary, D. (2020). "Visual system," in *Neuroanatomy : an illustrated colour text,* eds. A.R. Crossman, D. Neary & B. Crossman. 6 ed: Elsevier), 150-153.

Curcio, C.A. (2018a). Antecedents of Soft Drusen, the Specific Deposits of Age-Related Macular Degeneration, in the Biology of Human Macula. *Invest Ophthalmol Vis Sci* 59**,** AMD182-AMD194.

Curcio, C.A. (2018b). Soft Drusen in Age-Related Macular Degeneration: Biology and Targeting Via the Oil Spill Strategies. *Invest Ophthalmol Vis Sci* 59**,** AMD160-AMD181.

Curcio, C.A., and Johnson, M. (2017). "Structure, Function, and Pathology of Bruch's Membrane," in *Ryan's Retina E-Book,* eds. A.P. Schachat, C.P. Wilkinson, D.R. Hinton, S.R. Sadda & P. Wiedemann. 6 ed: Elsevier), 522-543.

Curcio, C.A., Johnson, M., Huang, J.D., and Rudolf, M. (2009). Aging, age-related macular degeneration, and the response-to-retention of apolipoprotein B-containing lipoproteins. *Prog Retin Eye Res* 28**,** 393-422.

Datoo O'keefe, G.A., and Rao, N. (2021). Retinal vasculitis: A framework and proposal for a classification system. *Surv Ophthalmol* 66**,** 54-67.

De Fauw, J., Ledsam, J.R., Romera-Paredes, B., Nikolov, S., Tomasev, N., Blackwell, S., Askham, H., Glorot, X., O'donoghue, B., Visentin, D., Van Den Driessche, G., Lakshminarayanan, B., Meyer, C., Mackinder, F., Bouton, S., Ayoub, K., Chopra, R., King, D., Karthikesalingam, A., Hughes, C.O., Raine, R., Hughes, J., Sim, D.A., Egan, C., Tufail, A., Montgomery, H., Hassabis, D., Rees, G., Back, T., Khaw, P.T., Suleyman, M., Cornebise, J., Keane, P.A., and Ronneberger, O. (2018). Clinically applicable deep learning for diagnosis and referral in retinal disease. *Nat Med* 24**,** 1342-1350.

De Magalhaes, J.P., Curado, J., and Church, G.M. (2009). Meta-analysis of age-related gene expression profiles identifies common signatures of aging. *Bioinformatics* 25**,** 875-881.

Deangelis, M.M., Owen, L.A., Morrison, M.A., Morgan, D.J., Li, M., Shakoor, A., Vitale, A., Iyengar, S., Stambolian, D., Kim, I.K., and Farrer, L.A. (2017). Genetics of age-related macular degeneration (AMD). *Hum Mol Genet* 26**,** R45-R50.

Del Priore, L.V., Kuo, Y.H., and Tezel, T.H. (2002). Age-related changes in human RPE cell density and apoptosis proportion in situ. *Invest Ophthalmol Vis Sci* 43**,** 3312-3318.

Dhirachaikulpanich, D., Li, X., Porter, L.F., and Paraoan, L. (2020a). Integrated Microarray and RNAseq Transcriptomic Analysis of Retinal Pigment Epithelium/Choroid in Age-Related Macular Degeneration. *Front Cell Dev Biol* 8**,** 808.

Dhirachaikulpanich, D., Paraoan, R.a.I., Carlsson, E., and Paraoan, L. (2020b). The quest of vision: retina's daily challenges. *The Biochemist* 42**,** 4-10.

Diala, F.G.I., Mccarthy, K., Chen, J.L., and Tsui, E. (2021). Multimodal imaging in pediatric uveitis. *Ther Adv Ophthalmol* 13**,** 25158414211059244.

Dice, L.R. (1945). Measures of the Amount of Ecologic Association Between Species. *Ecology* 26**,** 297-302.

Dimitrov, D., Türei, D., Boys, C., Nagai, J.S., Ramirez Flores, R.O., Kim, H., Szalai, B., Costa, I.G., Dugourd, A., Valdeolivas, A., and Saez-Rodriguez, J. (2021). "Comparison of Resources and Methods to infer Cell-Cell Communication from Single-cell RNA Data". Cold Spring Harbor Laboratory).

Dimitrov, D., Turei, D., Garrido-Rodriguez, M., Burmedi, P.L., Nagai, J.S., Boys, C., Ramirez Flores, R.O., Kim, H., Szalai, B., Costa, I.G., Valdeolivas, A., Dugourd, A., and Saez-Rodriguez, J. (2022). Comparison of methods and resources for cell-cell communication inference from single-cell RNA-Seq data. *Nat Commun* 13**,** 3224.

Do, B.K., and Giovinazzo, J. (2016). Retinal Vasculitis. *Advances in Ophthalmology and Optometry* 1**,** 69-84.

Dong, L., Yang, Q., Zhang, R.H., and Wei, W.B. (2021). Artificial intelligence for the detection of age-related macular degeneration in color fundus photographs: A systematic review and meta-analysis. *EClinicalMedicine* 35**,** 100875.

Ebrahimiadib, N., Maleki, A., Fadakar, K., Manhapra, A., Ghassemi, F., and Foster, C.S. (2021). Vascular abnormalities in uveitis. *Surv Ophthalmol* 66**,** 653-667.

Ehlers, J.P., Wang, K., Vasanji, A., Hu, M., and Srivastava, S.K. (2017). Automated quantitative characterisation of retinal vascular leakage and microaneurysms in ultra-widefield fluorescein angiography. *Br J Ophthalmol* 101**,** 696-699.

El-Nimri, N.W., Moore, S.M., Zangwill, L.M., Proudfoot, J.A., Weinreb, R.N., Skowronska-Krawczyk, D., and Baxter, S.L. (2020). Evaluating the neuroprotective impact of senolytic drugs on human vision. *Sci Rep* 10**,** 21752.

Ellis, L.M., and Hicklin, D.J. (2008). VEGF-targeted therapy: mechanisms of anti-tumour activity. *Nat Rev Cancer* 8**,** 579-591.

Emre, S., Guven-Yilmaz, S., Ulusoy, M.O., and Ates, H. (2019). Optical coherence tomography angiography findings in Behcet patients. *Int Ophthalmol* 39**,** 2391-2399.

Esengonul, M., Marta, A., Beirao, J., Pires, I.M., and Cunha, A. (2022). A Systematic Review of Artificial Intelligence Applications Used for Inherited Retinal Disease Management. *Medicina (Kaunas)* 58**,** 504.

Ferrara, N., Gerber, H.P., and Lecouter, J. (2003). The biology of VEGF and its receptors. *Nat Med* 9**,** 669-676.

Ferris, F.L., 3rd, Wilkinson, C.P., Bird, A., Chakravarthy, U., Chew, E., Csaky, K., Sadda, S.R., and Beckman Initiative for Macular Research Classification, C. (2013). Clinical classification of age-related macular degeneration. *Ophthalmology* 120**,** 844-851.

Finnemann, S.C., Bonilha, V.L., Marmorstein, A.D., and Rodriguez-Boulan, E. (1997). Phagocytosis of rod outer segments by retinal pigment epithelial cells requires alpha(v)beta5 integrin for binding but not for internalization. *Proc Natl Acad Sci U S A* 94**,** 12932-12937.

Fisher, R.A. (1992). "Statistical Methods for Research Workers," in *Breakthroughs in Statistics,* eds. S. Kotz & N.L. Johnson. (New York, NY: Springer New York), 66-70.

Fleckenstein, M., Keenan, T.D.L., Guymer, R.H., Chakravarthy, U., Schmitz-Valckenberg, S., Klaver, C.C., Wong, W.T., and Chew, E.Y. (2021). Age-related macular degeneration. *Nat Rev Dis Primers* 7**,** 31.

Forrester, J.V., Dick, A.D., Mcmenamin, P.G., Roberts, F., and Pearlman, E. (2016). "Anatomy of the eye and orbit," in *The Eye,* eds. J.V. Forrester, A.D. Dick, P.G. Mcmenamin, F. Roberts & E. Pearlman. 4 ed: W.B. Saunders), 1-102.e102.

Forrester, J.V., Kuffova, L., and Dick, A.D. (2018). Autoimmunity, Autoinflammation, and Infection in Uveitis. *Am J Ophthalmol* 189**,** 77-85.

Franklin, S., and Vondriska, T.M. (2011). Genomes, proteomes, and the central dogma. *Circ Cardiovasc Genet* 4**,** 576.

Friedrichson, T., Kalbach, H.L., Buck, P., and Van Kuijk, F.J. (1995). Vitamin E in macular and peripheral tissues of the human eye. *Curr Eye Res* 14**,** 693-701.

Fritsche, L.G., Chen, W., Schu, M., Yaspan, B.L., Yu, Y., Thorleifsson, G., Zack, D.J., Arakawa, S., Cipriani, V., Ripke, S., Igo, R.P., Jr., Buitendijk, G.H., Sim, X., Weeks, D.E., Guymer, R.H., Merriam, J.E., Francis, P.J., Hannum, G., Agarwal, A., Armbrecht, A.M., Audo, I., Aung, T., Barile, G.R., Benchaboune, M., Bird, A.C., Bishop, P.N., Branham, K.E., Brooks, M., Brucker, A.J., Cade, W.H., Cain, M.S., Campochiaro, P.A., Chan, C.C., Cheng, C.Y., Chew, E.Y., Chin, K.A., Chowers, I., Clayton, D.G., Cojocaru, R., Conley, Y.P., Cornes, B.K., Daly, M.J., Dhillon, B., Edwards, A.O., Evangelou, E., Fagerness, J., Ferreyra, H.A., Friedman, J.S., Geirsdottir, A., George, R.J., Gieger, C., Gupta, N., Hagstrom, S.A., Harding, S.P., Haritoglou, C., Heckenlively, J.R., Holz, F.G., Hughes, G., Ioannidis, J.P., Ishibashi, T., Joseph, P., Jun, G., Kamatani, Y., Katsanis, N., C, N.K., Khan, J.C., Kim, I.K., Kiyohara, Y., Klein, B.E., Klein, R., Kovach, J.L., Kozak, I., Lee, C.J., Lee, K.E., Lichtner, P., Lotery, A.J., Meitinger, T., Mitchell, P., Mohand-Said, S., Moore, A.T., Morgan, D.J., Morrison, M.A., Myers, C.E., Naj, A.C., Nakamura, Y., Okada, Y., Orlin, A., Ortube, M.C., Othman, M.I., Pappas, C., Park, K.H., Pauer, G.J., Peachey, N.S., Poch, O., Priya, R.R., Reynolds, R., Richardson, A.J., Ripp, R., Rudolph, G., Ryu, E., et al. (2013). Seven new loci associated with age-related macular degeneration. *Nat Genet* 45**,** 433-439, 439e431-432.

Fritsche, L.G., Igl, W., Bailey, J.N., Grassmann, F., Sengupta, S., Bragg-Gresham, J.L., Burdon, K.P., Hebbring, S.J., Wen, C., Gorski, M., Kim, I.K., Cho, D., Zack, D., Souied, E., Scholl, H.P., Bala, E., Lee, K.E., Hunter, D.J., Sardell, R.J., Mitchell, P., Merriam, J.E., Cipriani, V., Hoffman, J.D., Schick, T., Lechanteur, Y.T., Guymer, R.H., Johnson, M.P., Jiang, Y., Stanton, C.M., Buitendijk, G.H., Zhan, X., Kwong, A.M., Boleda, A., Brooks, M., Gieser, L., Ratnapriya, R., Branham, K.E., Foerster, J.R., Heckenlively, J.R., Othman, M.I., Vote, B.J., Liang, H.H., Souzeau, E., Mcallister, I.L., Isaacs, T., Hall, J., Lake, S., Mackey, D.A., Constable, I.J., Craig, J.E., Kitchner, T.E., Yang, Z., Su, Z., Luo, H., Chen, D., Ouyang, H., Flagg, K., Lin, D., Mao, G., Ferreyra, H., Stark, K., Von Strachwitz, C.N., Wolf, A., Brandl, C., Rudolph, G., Olden, M., Morrison, M.A., Morgan, D.J., Schu, M., Ahn, J., Silvestri, G., Tsironi, E.E., Park, K.H., Farrer, L.A., Orlin, A., Brucker, A., Li, M., Curcio, C.A., Mohand-Said, S., Sahel, J.A., Audo, I., Benchaboune, M., Cree, A.J., Rennie, C.A., Goverdhan, S.V., Grunin, M., Hagbi-Levi, S., Campochiaro, P., Katsanis, N., Holz, F.G., Blond, F., Blanche, H., Deleuze, J.F., Igo, R.P., Jr., Truitt, B., Peachey, N.S., Meuer, S.M., Myers, C.E., Moore, E.L., Klein, R., et al. (2016). A large genome-wide association study of age-related macular degeneration highlights contributions of rare and common variants. *Nat Genet* 48**,** 134-143.

Fujinami, K., Zernant, J., Chana, R.K., Wright, G.A., Tsunoda, K., Ozawa, Y., Tsubota, K., Webster, A.R., Moore, A.T., Allikmets, R., and Michaelides, M. (2013). ABCA4 gene screening by next-generation sequencing in a British cohort. *Invest Ophthalmol Vis Sci* 54**,** 6662-6674.

Gallagher, M.J., Yilmaz, T., Cervantes-Castaneda, R.A., and Foster, C.S. (2007). The characteristic features of optical coherence tomography in posterior uveitis. *Br J Ophthalmol* 91**,** 1680-1685.

Gao, H., and Hollyfield, J.G. (1992). Aging of the human retina. Differential loss of neurons and retinal pigment epithelial cells. *Invest Ophthalmol Vis Sci* 33**,** 1-17.

Gardner, G.G., Keating, D., Williamson, T.H., and Elliott, A.T. (1996). Automatic detection of diabetic retinopathy using an artificial neural network: a screening tool. *Br J Ophthalmol* 80**,** 940-944.

Glenn, J.V., and Stitt, A.W. (2009). The role of advanced glycation end products in retinal ageing and disease. *Biochim Biophys Acta* 1790**,** 1109-1116.

Goder, A., Emmerich, C., Nikolova, T., Kiweler, N., Schreiber, M., Kuhl, T., Imhof, D., Christmann, M., Heinzel, T., Schneider, G., and Kramer, O.H. (2018). HDAC1 and HDAC2 integrate checkpoint kinase phosphorylation and cell fate through the phosphatase-2A subunit PR130. *Nat Commun* 9**,** 764.

Goel, N., Kumar, V., Arora, S., Jain, P., and Ghosh, B. (2018). Spectral domain optical coherence tomography evaluation of macular changes in Eales disease. *Indian J Ophthalmol* 66**,** 433-438.

Gogat, K., Le Gat, L., Van Den Berghe, L., Marchant, D., Kobetz, A., Gadin, S., Gasser, B., Quere, I., Abitbol, M., and Menasche, M. (2004). VEGF and KDR gene expression during human embryonic and fetal eye development. *Invest Ophthalmol Vis Sci* 45**,** 7-14.

Gonzalez-Gualda, E., Baker, A.G., Fruk, L., and Munoz-Espin, D. (2021). A guide to assessing cellular senescence in vitro and in vivo. *FEBS J* 288**,** 56-80.

Gopinath, B., Liew, G., Kifley, A., and Mitchell, P. (2016). Thyroid Dysfunction and Ten-Year Incidence of Age-Related Macular Degeneration. *Invest Ophthalmol Vis Sci* 57**,** 5273-5277.

Gorska, E., Popko, K., Stelmaszczyk-Emmel, A., Ciepiela, O., Kucharska, A., and Wasik, M. (2010). Leptin receptors. *Eur J Med Res* 15 Suppl 2**,** 50-54.

Gosálvez, J., and Horcajadas, J.A. (2018). "Introduction: Human Genome Projects: The Omics Starting Point," in *Reproductomics,* eds. J.A. Horcajadas & J. Gosálvez. Academic Press), xvii-xxix.

Gregg, R.G., Singer, J., Kamermans, M., Mccall, M.A., and Massey, S.C. (2017). "Function and Anatomy of the Mammalian Retina," in *Ryan's Retina E-Book,* eds. A.P. Schachat, C.P. Wilkinson, D.R. Hinton, S.R. Sadda & P. Wiedemann. 6 ed: Elsevier), 408-450.

Group, A.R., Chew, E.Y., Clemons, T., Sangiovanni, J.P., Danis, R., Domalpally, A., Mcbee, W., Sperduto, R., and Ferris, F.L. (2012). The Age-Related Eye Disease Study 2 (AREDS2): study design and baseline characteristics (AREDS2 report number 1). *Ophthalmology* 119**,** 2282-2289.

Gu, X., Neric, N.J., Crabb, J.S., Crabb, J.W., Bhattacharya, S.K., Rayborn, M.E., Hollyfield, J.G., and Bonilha, V.L. (2012). Age-related changes in the retinal pigment epithelium (RPE). *PLoS One* 7**,** e38673.

Hammond, C.J., Webster, A.R., Snieder, H., Bird, A.C., Gilbert, C.E., and Spector, T.D. (2002). Genetic influence on early age-related maculopathy: a twin study. *Ophthalmology* 109**,** 730-736.

Hamza, T.H., Chen, H., Hill-Burns, E.M., Rhodes, S.L., Montimurro, J., Kay, D.M., Tenesa, A., Kusel, V.I., Sheehan, P., Eaaswarkhanth, M., Yearout, D., Samii, A., Roberts, J.W., Agarwal, P., Bordelon, Y., Park, Y., Wang, L., Gao, J., Vance, J.M., Kendler, K.S., Bacanu, S.A., Scott, W.K., Ritz, B., Nutt, J., Factor, S.A., Zabetian, C.P., and Payami, H. (2011). Genome-wide gene-environment study identifies glutamate receptor gene GRIN2A as a Parkinson's disease modifier gene via interaction with coffee. *PLoS Genet* 7**,** e1002237.

Handa, J.T. (2017). "Cell Biology of the Retinal Pigment Epithelium," in *Ryan's Retina E-Book,* eds. A.P. Schachat, C.P. Wilkinson, D.R. Hinton, S.R. Sadda & P. Wiedemann. 6 ed: Elsevier), 451-465.

Handa, J.T., Bowes Rickman, C., Dick, A.D., Gorin, M.B., Miller, J.W., Toth, C.A., Ueffing, M., Zarbin, M., and Farrer, L.A. (2019). A systems biology approach towards understanding and treating non-neovascular age-related macular degeneration. *Nat Commun* 10**,** 3347.

Haner, N.U., Dysli, C., and Munk, M.R. (2023). Imaging in retinal vascular disease: A review. *Clin Exp Ophthalmol* 51**,** 217-228.

Hanzelmann, S., Castelo, R., and Guinney, J. (2013). GSVA: gene set variation analysis for microarray and RNA-seq data. *BMC Bioinformatics* 14**,** 7.

Hao, Y., Hao, S., Andersen-Nissen, E., Mauck, W.M., 3rd, Zheng, S., Butler, A., Lee, M.J., Wilk, A.J., Darby, C., Zager, M., Hoffman, P., Stoeckius, M., Papalexi, E., Mimitou, E.P., Jain, J., Srivastava, A., Stuart, T., Fleming, L.M., Yeung, B., Rogers, A.J., Mcelrath, J.M., Blish, C.A., Gottardo, R., Smibert, P., and Satija, R. (2021). Integrated analysis of multimodal single-cell data. *Cell* 184**,** 3573-3587 e3529.

Hardy, J. (2010). Genetic analysis of pathways to Parkinson disease. *Neuron* 68**,** 201-206.

Harley, M.E., Allan, L.A., Sanderson, H.S., and Clarke, P.R. (2010). Phosphorylation of Mcl-1 by CDK1-cyclin B1 initiates its Cdc20-dependent destruction during mitotic arrest. *EMBO J* 29**,** 2407-2420.

Harman, A.M., Fleming, P.A., Hoskins, R.V., and Moore, S.R. (1997). Development and aging of cell topography in the human retinal pigment epithelium. *Invest Ophthalmol Vis Sci* 38**,** 2016-2026.

Hassig, C.A., Tong, J.K., Fleischer, T.C., Owa, T., Grable, P.G., Ayer, D.E., and Schreiber, S.L. (1998). A role for histone deacetylase activity in HDAC1-mediated transcriptional repression. *Proc Natl Acad Sci U S A* 95**,** 3519-3524.

He, K., Zhang, X., Ren, S., and Sun, J. (Year). "Deep Residual Learning for Image Recognition", in: *2016 IEEE Conference on Computer Vision and Pattern Recognition (CVPR)*), 770-778.

He, L., Zhang, Q., Zhang, Y., Fan, Y., Yuan, F., and Li, S. (2021). Single-cell analysis reveals cell communication triggered by macrophages associated with the reduction and exhaustion of CD8(+) T cells in COVID-19. *Cell Commun Signal* 19**,** 73.

Hocking, J.C., and Mcfarlane, S. (2007). Expression of Bmp ligands and receptors in the developing Xenopus retina. *Int J Dev Biol* 51**,** 161-165.

Hou, X.W., Wang, Y., Ke, C.F., Li, M.Y., and Pan, C.W. (2022). Metabolomics and Biomarkers in Retinal and Choroidal Vascular Diseases. *Metabolites* 12**,** 814.

Hu, C., Chu, C., Liu, L., Wang, C., Jin, S., Yang, R., Rung, S., Li, J., Qu, Y., and Man, Y. (2021). Dissecting the microenvironment around biosynthetic scaffolds in murine skin wound healing. *Sci Adv* 7**,** eabf0787.

Huang, D., Swanson, E.A., Lin, C.P., Schuman, J.S., Stinson, W.G., Chang, W., Hee, M.R., Flotte, T., Gregory, K., Puliafito, C.A., and Et Al. (1991). Optical coherence tomography. *Science* 254**,** 1178-1181.

Hughes, E.H., and Dick, A.D. (2003). The pathology and pathogenesis of retinal vasculitis. *Neuropathol Appl Neurobiol* 29**,** 325-340.

Hussain, A.A., Lee, Y., and Marshall, J. (2020). Understanding the complexity of the matrix metalloproteinase system and its relevance to age-related diseases: Age-related macular degeneration and Alzheimer's disease. *Prog Retin Eye Res* 74**,** 100775.

Hyttinen, J.M.T., Viiri, J., Kaarniranta, K., and Blasiak, J. (2018). Mitochondrial quality control in AMD: does mitophagy play a pivotal role? *Cell. Mol. Life Sci.* 75**,** 2991-3008.

Iakubovskii, P. (2019). Segmentation Models Pytorch. *GitHub repository*.

Ibrahim, A.S., Hussein, K., Wang, F., Wan, M., Saad, N., Essa, M., Kim, I., Shakoor, A., Owen, L.A., Deangelis, M.M., and Al-Shabrawey, M. (2020). Bone Morphogenetic Protein (BMP)4 But Not BMP2 Disrupts the Barrier Integrity of Retinal Pigment Epithelia and Induces Their Migration: A Potential Role in Neovascular Age-Related Macular Degeneration. *J Clin Med* 9**,** 2293.

Ikuta, T., Ariga, H., and Matsumoto, K. (2000). Extracellular matrix tenascin-X in combination with vascular endothelial growth factor B enhances endothelial cell proliferation. *Genes Cells* 5**,** 913-927.

International Human Genome Sequencing, C. (2004). Finishing the euchromatic sequence of the human genome. *Nature* 431**,** 931-945.

Invernizzi, A., Cozzi, M., and Staurenghi, G. (2019). Optical coherence tomography and optical coherence tomography angiography in uveitis: A review. *Clin Exp Ophthalmol* 47**,** 357-371.

Itahana, K., Campisi, J., and Dimri, G.P. (2007). "Methods to Detect Biomarkers of Cellular Senescence." Humana Press), 21-31.

Jabs, D.A., Nussenblatt, R.B., Rosenbaum, J.T., and Standardization of Uveitis Nomenclature Working, G. (2005). Standardization of uveitis nomenclature for reporting clinical data. Results of the First International Workshop. *Am J Ophthalmol* 140**,** 509-516.

Jadon, S., Leary, O., Pan, I., Harder, T., Wright, D., Merck, L., and Merck, D. (2020). *A comparative study of 2D image segmentation algorithms for traumatic brain lesions using CT data from the ProTECTIII multicenter clinical trial.* SPIE.

Jager, R.D., Mieler, W.F., and Miller, J.W. (2008). Age-related macular degeneration. *N Engl J Med* 358**,** 2606-2617.

Jay, N.L., and Gillies, M. (2012). Proteomic analysis of ophthalmic disease. *Clin Exp Ophthalmol* 40**,** 755-763.

Ji, K.B., Hu, Z., Zhang, Q.L., Mei, H.F., and Xing, Y.Q. (2022). Retinal microvasculature features in patients with Behcet's disease: a systematic review and meta-analysis. *Sci Rep* 12**,** 752.

Ji, X., Bosse, Y., Landi, M.T., Gui, J., Xiao, X., Qian, D., Joubert, P., Lamontagne, M., Li, Y., Gorlov, I., De Biasi, M., Han, Y., Gorlova, O., Hung, R.J., Wu, X., Mckay, J., Zong, X., Carreras-Torres, R., Christiani, D.C., Caporaso, N., Johansson, M., Liu, G., Bojesen, S.E., Le Marchand, L., Albanes, D., Bickeboller, H., Aldrich, M.C., Bush, W.S., Tardon, A., Rennert, G., Chen, C., Teare, M.D., Field, J.K., Kiemeney, L.A., Lazarus, P., Haugen, A., Lam, S., Schabath, M.B., Andrew, A.S., Shen, H., Hong, Y.C., Yuan, J.M., Bertazzi, P.A., Pesatori, A.C., Ye, Y., Diao, N., Su, L., Zhang, R., Brhane, Y., Leighl, N., Johansen, J.S., Mellemgaard, A., Saliba, W., Haiman, C., Wilkens, L., Fernandez-Somoano, A., Fernandez-Tardon, G., Van Der Heijden, E., Kim, J.H., Dai, J., Hu, Z., Davies, M.P.A., Marcus, M.W., Brunnstrom, H., Manjer, J., Melander, O., Muller, D.C., Overvad, K., Trichopoulou, A., Tumino, R., Doherty, J., Goodman, G.E., Cox, A., Taylor, F., Woll, P., Bruske, I., Manz, J., Muley, T., Risch, A., Rosenberger, A., Grankvist, K., Johansson, M., Shepherd, F., Tsao, M.S., Arnold, S.M., Haura, E.B., Bolca, C., Holcatova, I., Janout, V., Kontic, M., Lissowska, J., Mukeria, A., Ognjanovic, S., Orlowski, T.M., Scelo, G., Swiatkowska, B., Zaridze, D., Bakke, P., Skaug, V., Zienolddiny, S., et al. (2018). Identification of susceptibility pathways for the role of chromosome 15q25.1 in modifying lung cancer risk. *Nat Commun* 9**,** 3221.

Jin, S., Guerrero-Juarez, C.F., Zhang, L., Chang, I., Ramos, R., Kuan, C.H., Myung, P., Plikus, M.V., and Nie, Q. (2021). Inference and analysis of cell-cell communication using CellChat. *Nat Commun* 12**,** 1088.

Johnson, R.N., Fu, A.D., Mcdonald, H.R., Jumper, J.M., Ai, E., Cunningham, E.T., and Lujan, B.J. (2013). "Fluorescein Angiography," in *Retina,* eds. S.J. Ryan, S.R. Sadda, D.R. Hinton, A.P. Schachat, S.R. Sadda, C.P. Wilkinson, P. Wiedemann & A.P. Schachat. (London: W.B. Saunders), 2-50.e51.

Johnson, W.E., Li, C., and Rabinovic, A. (2007). Adjusting batch effects in microarray expression data using empirical Bayes methods. *Biostatistics* 8**,** 118-127.

Jung, J.J., Chen, C.Y., Mrejen, S., Gallego-Pinazo, R., Xu, L., Marsiglia, M., Boddu, S., and Freund, K.B. (2014). The incidence of neovascular subtypes in newly diagnosed neovascular age-related macular degeneration. *Am J Ophthalmol* 158**,** 769-779 e762.

Kanehisa, M., Sato, Y., Kawashima, M., Furumichi, M., and Tanabe, M. (2016). KEGG as a reference resource for gene and protein annotation. *Nucleic Acids Res* 44**,** D457-462.

Kang, G.Y., Bang, J.Y., Choi, A.J., Yoon, J., Lee, W.C., Choi, S., Yoon, S., Kim, H.C., Baek, J.H., Park, H.S., Lim, H.J., and Chung, H. (2014). Exosomal proteins in the aqueous humor as novel biomarkers in patients with neovascular age-related macular degeneration. *J Proteome Res* 13**,** 581-595.

Kang, H.M., Koh, H.J., and Lee, S.C. (2018). Spectral domain optical coherence tomography as an adjunctive tool for screening Behcet uveitis. *PLoS One* 13**,** e0208254.

Kang, H.M., and Lee, S.C. (2014). Long-term progression of retinal vasculitis in Behcet patients using a fluorescein angiography scoring system. *Graefes Arch Clin Exp Ophthalmol* 252**,** 1001-1008.

Karampelas, M., Sim, D.A., Chu, C., Carreno, E., Keane, P.A., Zarranz-Ventura, J., Westcott, M., Lee, R.W., and Pavesio, C.E. (2015). Quantitative analysis of peripheral vasculitis, ischemia, and vascular leakage in uveitis using ultra-widefield fluorescein angiography. *Am J Ophthalmol* 159**,** 1161-1168 e1161.

Kay, P., Yang, Y.C., Hiscott, P., Gray, D., Maminishkis, A., and Paraoan, L. (2014). Age-related changes of cystatin C expression and polarized secretion by retinal pigment epithelium: potential age-related macular degeneration links. *Invest Ophthalmol Vis Sci* 55**,** 926-934.

Kay, P., Yang, Y.C., and Paraoan, L. (2013). Directional protein secretion by the retinal pigment epithelium: roles in retinal health and the development of age-related macular degeneration. *J Cell Mol Med* 17**,** 833-843.

Keino, H., Okada, A.A., Watanabe, T., and Taki, W. (2011). Decreased ocular inflammatory attacks and background retinal and disc vascular leakage in patients with Behcet's disease on infliximab therapy. *Br J Ophthalmol* 95**,** 1245-1250.

Keino, H., Okada, A.A., Watanabe, T., and Taki, W. (2014). Long-term efficacy of infliximab on background vascular leakage in patients with Behcet's disease. *Eye (Lond)* 28**,** 1100-1106.

Keino, H., Wakitani, T., Sunayama, W., and Hatanaka, Y. (2022). Quantitative Analysis of Retinal Vascular Leakage in Retinal Vasculitis Using Machine Learning. *Applied Sciences* 12**,** 12751.

Kermany, D.S., Goldbaum, M., Cai, W., Valentim, C.C.S., Liang, H., Baxter, S.L., Mckeown, A., Yang, G., Wu, X., Yan, F., Dong, J., Prasadha, M.K., Pei, J., Ting, M.Y.L., Zhu, J., Li, C., Hewett, S., Dong, J., Ziyar, I., Shi, A., Zhang, R., Zheng, L., Hou, R., Shi, W., Fu, X., Duan, Y., Huu, V.a.N., Wen, C., Zhang, E.D., Zhang, C.L., Li, O., Wang, X., Singer, M.A., Sun, X., Xu, J., Tafreshi, A., Lewis, M.A., Xia, H., and Zhang, K. (2018). Identifying Medical Diagnoses and Treatable Diseases by Image-Based Deep Learning. *Cell* 172**,** 1122-1131 e1129.

Kersten, E., Paun, C.C., Schellevis, R.L., Hoyng, C.B., Delcourt, C., Lengyel, I., Peto, T., Ueffing, M., Klaver, C.C.W., Dammeier, S., Den Hollander, A.I., and De Jong, E.K. (2018). Systemic and ocular fluid compounds as potential biomarkers in age-related macular degeneration. *Surv Ophthalmol* 63**,** 9-39.

Kevany, B.M., and Palczewski, K. (2010). Phagocytosis of retinal rod and cone photoreceptors. *Physiology (Bethesda)* 25**,** 8-15.

Khan, M., Cornelis, S.S., Pozo-Valero, M.D., Whelan, L., Runhart, E.H., Mishra, K., Bults, F., Alswaiti, Y., Altalbishi, A., De Baere, E., Banfi, S., Banin, E., Bauwens, M., Ben-Yosef, T., Boon, C.J.F., Van Den Born, L.I., Defoort, S., Devos, A., Dockery, A., Dudakova, L., Fakin, A., Farrar, G.J., Sallum, J.M.F., Fujinami, K., Gilissen, C., Glavac, D., Gorin, M.B., Greenberg, J., Hayashi, T., Hettinga, Y.M., Hoischen, A., Hoyng, C.B., Hufendiek, K., Jagle, H., Kamakari, S., Karali, M., Kellner, U., Klaver, C.C.W., Kousal, B., Lamey, T.M., Macdonald, I.M., Matynia, A., Mclaren, T.L., Mena, M.D., Meunier, I., Miller, R., Newman, H., Ntozini, B., Oldak, M., Pieterse, M., Podhajcer, O.L., Puech, B., Ramesar, R., Ruther, K., Salameh, M., Salles, M.V., Sharon, D., Simonelli, F., Spital, G., Steehouwer, M., Szaflik, J.P., Thompson, J.A., Thuillier, C., Tracewska, A.M., Van Zweeden, M., Vincent, A.L., Zanlonghi, X., Liskova, P., Stohr, H., Roach, J.N., Ayuso, C., Roberts, L., Weber, B.H.F., Dhaenens, C.M., and Cremers, F.P.M. (2020). Resolving the dark matter of ABCA4 for 1054 Stargardt disease probands through integrated genomics and transcriptomics. *Genet Med* 22**,** 1235-1246.

Kiel, J.W. (2010). "Integrated Systems Physiology: from Molecule to Function to Disease," in *The Ocular Circulation*. (San Rafael (CA): Morgan & Claypool Life Sciences

Copyright © 2010 by Morgan & Claypool Life Sciences.).

Kim, B.H., Park, U.C., Park, S.W., and Yu, H.G. (2022). Ultra-Widefield Fluorescein Angiography to Monitor Therapeutic Response to Adalimumab in Behcet's Uveitis. *Ocul Immunol Inflamm* 30**,** 1347-1353.

Kim, E.J., Grant, G.R., Bowman, A.S., Haider, N., Gudiseva, H.V., and Chavali, V.R.M. (2018). Complete Transcriptome Profiling of Normal and Age-Related Macular Degeneration Eye Tissues Reveals Dysregulation of Anti-Sense Transcription. *Sci Rep* 8**,** 3040.

Kim, L.A., and D'amore, P.A. (2012). A brief history of anti-VEGF for the treatment of ocular angiogenesis. *Am J Pathol* 181**,** 376-379.

Kim, M., Kwon, H.J., Choi, E.Y., Kim, S.S., Koh, H.J., and Lee, S.C. (2015). Correlation between Fluorescein Angiographic Findings and Visual Acuity in Behcet Retinal Vasculitis. *Yonsei Med J* 56**,** 1087-1096.

Kirkwood, T.B. (1977). Evolution of ageing. *Nature* 270**,** 301-304.

Kiser, P.D., Golczak, M., Maeda, A., and Palczewski, K. (2012). Key enzymes of the retinoid (visual) cycle in vertebrate retina. *Biochim Biophys Acta* 1821**,** 137-151.

Klein, R. (2007). Overview of progress in the epidemiology of age-related macular degeneration. *Ophthalmic Epidemiol* 14**,** 184-187.

Klein, R., Klein, B.E., Knudtson, M.D., Meuer, S.M., Swift, M., and Gangnon, R.E. (2007). Fifteen-year cumulative incidence of age-related macular degeneration: the Beaver Dam Eye Study. *Ophthalmology* 114**,** 253-262.

Klein, R., Meuer, S.M., Myers, C.E., Buitendijk, G.H., Rochtchina, E., Choudhury, F., De Jong, P.T., Mckean-Cowdin, R., Iyengar, S.K., Gao, X., Lee, K.E., Vingerling, J.R., Mitchell, P., Klaver, C.C., Wang, J.J., and Klein, B.E. (2014). Harmonizing the classification of age-related macular degeneration in the three-continent AMD consortium. *Ophthalmic Epidemiol* 21**,** 14-23.

Knickelbein, J.E., Tucker, W., Kodati, S., Akanda, M., and Sen, H.N. (2018). Non-invasive method of monitoring retinal vasculitis in patients with birdshot chorioretinopathy using optical coherence tomography. *Br J Ophthalmol* 102**,** 815-820.

Kobayashi, Y., Yoshida, S., Zhou, Y., Nakama, T., Ishikawa, K., Arima, M., Nakao, S., Sassa, Y., Takeda, A., Hisatomi, T., Ikeda, Y., Matsuda, A., Sonoda, K.H., and Ishibashi, T. (2016a). Tenascin-C promotes angiogenesis in fibrovascular membranes in eyes with proliferative diabetic retinopathy. *Mol Vis* 22**,** 436-445.

Kobayashi, Y., Yoshida, S., Zhou, Y., Nakama, T., Ishikawa, K., Kubo, Y., Arima, M., Nakao, S., Hisatomi, T., Ikeda, Y., Matsuda, A., Sonoda, K.H., and Ishibashi, T. (2016b). Tenascin-C secreted by transdifferentiated retinal pigment epithelial cells promotes choroidal neovascularization via integrin alphaV. *Lab Invest* 96**,** 1178-1188.

Kong, Y., Liang, X., Liu, L., Zhang, D., Wan, C., Gan, Z., and Yuan, L. (2015). High Throughput Sequencing Identifies MicroRNAs Mediating alpha-Synuclein Toxicity by Targeting Neuroactive-Ligand Receptor Interaction Pathway in Early Stage of Drosophila Parkinson's Disease Model. *PLoS One* 10**,** e0137432.

Koo, I., Wei, X., and Zhang, X. (2014). "Chapter Sixteen - Analysis of Metabolomic Profiling Data Acquired on GC–MS," in *Methods in Enzymology,* eds. L. Galluzzi & G. Kroemer. Academic Press), 315-324.

Kozlowski, M.R. (2012). RPE cell senescence: a key contributor to age-related macular degeneration. *Med Hypotheses* 78**,** 505-510.

Kozlowski, M.R. (2015). Senescent retinal pigment epithelial cells are more sensitive to vascular endothelial growth factor: implications for "wet" age-related macular degeneration. *J Ocul Pharmacol Ther* 31**,** 87-92.

Kritsilis, M., S, V.R., Koutsoudaki, P.N., Evangelou, K., Gorgoulis, V.G., and Papadopoulos, D. (2018). Ageing, Cellular Senescence and Neurodegenerative Disease. *Int J Mol Sci* 19**,** 2937.

Krizhevsky, A., Sutskever, I., and Hinton, G.E. (2017). ImageNet classification with deep convolutional neural networks. *Communications of the ACM* 60**,** 84-90.

Krohne, T.U., Kaemmerer, E., Holz, F.G., and Kopitz, J. (2010). Lipid peroxidation products reduce lysosomal protease activities in human retinal pigment epithelial cells via two different mechanisms of action. *Exp Eye Res* 90**,** 261-266.

Kumar, A., Ambiya, V., Mishra, S.K., and Jhanwar, M. (2021). Choroidal thickness alterations in idiopathic acute retinal vasculitis. *Ther Adv Ophthalmol* 13**,** 25158414211022875.

Lagger, C., Ursu, E., Equey, A., Avelar, R.A., Pisco, A.O., Tacutu, R., and De Magalhães, J.P. (2021). "scAgeCom: a murine atlas of age-related changes in intercellular communication inferred with the package scDiffCom". Cold Spring Harbor Laboratory).

Lains, I., Duarte, D., Barros, A.S., Martins, A.S., Gil, J., Miller, J.B., Marques, M., Mesquita, T., Kim, I.K., Cachulo, M.D.L., Vavvas, D., Carreira, I.M., Murta, J.N., Silva, R., Miller, J.W., Husain, D., and Gil, A.M. (2017). Human plasma metabolomics in age-related macular degeneration (AMD) using nuclear magnetic resonance spectroscopy. *PLoS One* 12**,** e0177749.

Lakkaraju, A., Umapathy, A., Tan, L.X., Daniele, L., Philp, N.J., Boesze-Battaglia, K., and Williams, D.S. (2020). The cell biology of the retinal pigment epithelium. *Prog Retin Eye Res***,** 100846.

Lamb, L.E., and Simon, J.D. (2007). A2E: A Component of Ocular Lipofuscin¶. *Photochemistry and Photobiology* 79**,** 127-136.

Landau, K., and Kurz-Levin, M. (2011). Retinal disorders. *Handb Clin Neurol* 102**,** 97-116.

Landowski, M., Kelly, U., Klingeborn, M., Groelle, M., Ding, J.D., Grigsby, D., and Bowes Rickman, C. (2019). Human complement factor H Y402H polymorphism causes an age-related macular degeneration phenotype and lipoprotein dysregulation in mice. *Proc Natl Acad Sci U S A* 116**,** 3703-3711.

Laovirojjanakul, W., Acharya, N., and Gonzales, J.A. (2019). Ultra-Widefield Fluorescein Angiography in Intermediate Uveitis. *Ocul Immunol Inflamm* 27**,** 356-361.

Laviers, H., and Zambarakji, H. (2014). Enhanced depth imaging-OCT of the choroid: a review of the current literature. *Graefes Arch Clin Exp Ophthalmol* 252**,** 1871-1883.

Lecun, Y., Bengio, Y., and Hinton, G. (2015). Deep learning. *Nature* 521**,** 436-444.

Leder, H.A., Campbell, J.P., Sepah, Y.J., Gan, T., Dunn, J.P., Hatef, E., Cho, B., Ibrahim, M., Bittencourt, M., Channa, R., Do, D.V., and Nguyen, Q.D. (2013). Ultra-wide-field retinal imaging in the management of non-infectious retinal vasculitis. *J Ophthalmic Inflamm Infect* 3**,** 30.

Lee, C.S., Tyring, A.J., Deruyter, N.P., Wu, Y., Rokem, A., and Lee, A.Y. (2017a). Deep-learning based, automated segmentation of macular edema in optical coherence tomography. *Biomed Opt Express* 8**,** 3440-3448.

Lee, J.G., Jun, S., Cho, Y.W., Lee, H., Kim, G.B., Seo, J.B., and Kim, N. (2017b). Deep Learning in Medical Imaging: General Overview. *Korean J Radiol* 18**,** 570-584.

Lee, K.S., Lin, S., Copland, D.A., Dick, A.D., and Liu, J. (2021). Cellular senescence in the aging retina and developments of senotherapies for age-related macular degeneration. *J Neuroinflammation* 18**,** 32.

Lee, P.K., Ra, H., and Baek, J. (2022). Automated segmentation of ultra-widefield fluorescein angiography of diabetic retinopathy using deep learning. *Br J Ophthalmol*.

Levi, N., Papismadov, N., Solomonov, I., Sagi, I., and Krizhanovsky, V. (2020). The ECM path of senescence in aging: components and modifiers. *FEBS J* 287**,** 2636-2646.

Levy-Clarke, G.A., and Nussenblatt, R. (2005). Retinal vasculitis. *Int Ophthalmol Clin* 45**,** 99-113.

Li, Z., Hu, F., Li, Q., Wang, S., Chen, C., Zhang, Y., Mao, Y., Shi, X., Zhou, H., Cao, X., and Peng, X. (2022). Ocular Adverse Events after Inactivated COVID-19 Vaccination. *Vaccines (Basel)* 10**,** 918.

Liao, Y., Wang, J., Jaehnig, E.J., Shi, Z., and Zhang, B. (2019). WebGestalt 2019: gene set analysis toolkit with revamped UIs and APIs. *Nucleic Acids Res* 47**,** W199-W205.

Lin, M.K., Yang, J., Hsu, C.W., Gore, A., Bassuk, A.G., Brown, L.M., Colligan, R., Sengillo, J.D., Mahajan, V.B., and Tsang, S.H. (2018). HTRA1, an age-related macular degeneration protease, processes extracellular matrix proteins EFEMP1 and TSP1. *Aging Cell* 17**,** e12710.

Liu, X., Kale, A.U., Ometto, G., Montesano, G., Sitch, A.J., Capewell, N., Radovanovic, C., Bucknall, N., Beare, N.a.V., Moore, D.J., Keane, P.A., Crabb, D.P., and Denniston, A.K. (2022). OCT Assisted Quantification of Vitreous Inflammation in Uveitis. *Transl Vis Sci Technol* 11**,** 3.

Lutty, G.A., Mcleod, D.S., Bhutto, I.A., Edwards, M.M., and Seddon, J.M. (2020). Choriocapillaris dropout in early age-related macular degeneration. *Exp Eye Res* 192**,** 107939.

Ma, H., Yang, F., and Ding, X.Q. (2020a). Inhibition of thyroid hormone signaling protects retinal pigment epithelium and photoreceptors from cell death in a mouse model of age-related macular degeneration. *Cell Death Dis* 11**,** 24.

Ma, L., Jakobiec, F.A., and Dryja, T.P. (2019). A Review of Next-Generation Sequencing (NGS): Applications to the Diagnosis of Ocular Infectious Diseases. *Semin Ophthalmol* 34**,** 223-231.

Ma, L.L., Wang, Y.Y., Yang, Z.H., Huang, D., Weng, H., and Zeng, X.T. (2020b). Methodological quality (risk of bias) assessment tools for primary and secondary medical studies: what are they and which is better? *Mil Med Res* 7**,** 7.

Ma, T., Liang, F., Oesterreich, S., and Tseng, G.C. (2017). A Joint Bayesian Model for Integrating Microarray and RNA Sequencing Transcriptomic Data. *J Comput Biol* 24**,** 647-662.

Ma, W., Cojocaru, R., Gotoh, N., Gieser, L., Villasmil, R., Cogliati, T., Swaroop, A., and Wong, W.T. (2013). Gene expression changes in aging retinal microglia: relationship to microglial support functions and regulation of activation. *Neurobiol Aging* 34**,** 2310-2321.

Ma, W., Lee, S.E., Guo, J., Qu, W., Hudson, B.I., Schmidt, A.M., and Barile, G.R. (2007). RAGE ligand upregulation of VEGF secretion in ARPE-19 cells. *Invest Ophthalmol Vis Sci* 48**,** 1355-1361.

Malek, G., Campisi, J., Kitazawa, K., Webster, C., Lakkaraju, A., and Skowronska-Krawczyk, D. (2022). Does senescence play a role in age-related macular degeneration? *Exp Eye Res* 225**,** 109254.

Maleki, A., Cao, J.H., Silpa-Archa, S., and Foster, C.S. (2016). Visual Outcome and Poor Prognostic Factors in Isolated Idiopathic Retinal Vasculitis. *Retina* 36**,** 1979-1985.

Mao, J.R., Taylor, G., Dean, W.B., Wagner, D.R., Afzal, V., Lotz, J.C., Rubin, E.M., and Bristow, J. (2002). Tenascin-X deficiency mimics Ehlers-Danlos syndrome in mice through alteration of collagen deposition. *Nat Genet* 30**,** 421-425.

Marazita, M.C., Dugour, A., Marquioni-Ramella, M.D., Figueroa, J.M., and Suburo, A.M. (2016). Oxidative stress-induced premature senescence dysregulates VEGF and CFH expression in retinal pigment epithelial cells: Implications for Age-related Macular Degeneration. *Redox Biol* 7**,** 78-87.

Marmor, M.F. (2019). "Retinal Pigment Epithelium," in *Ophthalmology,* ed. M. Yanoff. 5 ed: Elsevier), 423-425.e421.

Marneros, A.G. (2016). Increased VEGF-A promotes multiple distinct aging diseases of the eye through shared pathomechanisms. *EMBO Mol Med* 8**,** 208-231.

Martinez-Cue, C., and Rueda, N. (2020). Cellular Senescence in Neurodegenerative Diseases. *Front Cell Neurosci* 14**,** 16.

Masayoshi, K., Katada, Y., Ozawa, N., Ibuki, M., Negishi, K., and Kurihara, T. (2022). Automatic segmentation of non-perfusion area from fluorescein angiography using deep learning with uncertainty estimation. *Informatics in Medicine Unlocked* 32**,** 101060.

Mathis, T., Holz, F.G., Sivaprasad, S., Yoon, Y.H., Eter, N., Chen, L.J., Koh, A., Cunha De Souza, E., and Staurenghi, G. (2023). Characterisation of macular neovascularisation subtypes in age-related macular degeneration to optimise treatment outcomes. *Eye (Lond)* 37**,** 1758-1765.

Matsumoto, K.I., and Aoki, H. (2020). The Roles of Tenascins in Cardiovascular, Inflammatory, and Heritable Connective Tissue Diseases. *Front Immunol* 11**,** 609752.

Mcclellan, K.A., and Coster, D.J. (1987). Uveitis: a strategy for diagnosis. *Aust N Z J Ophthalmol* 15**,** 227-241.

Melzer, D., Pilling, L.C., and Ferrucci, L. (2020). The genetics of human ageing. *Nat Rev Genet* 21**,** 88-101.

Miller, W.L. (2020). Tenascin-X-Discovery and Early Research. *Front Immunol* 11**,** 612497.

Mir, T.A., Reddy, A.K., Burkholder, B.M., Walsh, J., Shifera, A.S., Khan, I.R., and Thorne, J.E. (2017). Clinical Features and Incidence Rates of Ocular Complications in Patients With Retinal Vasculitis. *Am J Ophthalmol* 179**,** 171-178.

Miraldi Utz, V., Coussa, R.G., Antaki, F., and Traboulsi, E.I. (2018). Gene therapy for RPE65-related retinal disease. *Ophthalmic Genet* 39**,** 671-677.

Mitchell, P., Liew, G., Gopinath, B., and Wong, T.Y. (2018). Age-related macular degeneration. *Lancet* 392**,** 1147-1159.

Mitter, S.K., Rao, H.V., Qi, X., Cai, J., Sugrue, A., Dunn, W.A., Grant, M.B., and Boulton, M.E. (2012). "Autophagy in the Retina: A Potential Role in Age-Related Macular Degeneration." Springer US), 83-90.

Mohamed, S., Chan, C.K., Tsang, C.W., Szeto, S.K., Fong, A.H., Chan, J.C., and Wong, C.Y. (2023). Case Report: Retinal Vasculitis in Two Adolescents After COVID-19 Vaccination. *Ocul Immunol Inflamm* 31**,** 1245-1249.

Molday, R.S., and Moritz, O.L. (2015). Photoreceptors at a glance. *J Cell Sci* 128**,** 4039-4045.

Mones, J., Srivastava, S.K., Jaffe, G.J., Tadayoni, R., Albini, T.A., Kaiser, P.K., Holz, F.G., Korobelnik, J.F., Kim, I.K., Pruente, C., Murray, T.G., and Heier, J.S. (2021). Risk of Inflammation, Retinal Vasculitis, and Retinal Occlusion-Related Events with Brolucizumab: Post Hoc Review of HAWK and HARRIER. *Ophthalmology* 128**,** 1050-1059.

Monnet, D., Levinson, R.D., Holland, G.N., Haddad, L., Yu, F., and Brezin, A.P. (2007). Longitudinal cohort study of patients with birdshot chorioretinopathy. III. Macular imaging at baseline. *Am J Ophthalmol* 144**,** 818-828.

Moon, S.W., Kim, B.H., Park, U.C., and Yu, H.G. (2017). Inter-observer Variability in Scoring Ultra-wide-field Fluorescein Angiography in Patients with Behcet Retinal Vasculitis. *Ocul Immunol Inflamm* 25**,** 20-28.

Moreno, P., Huang, N., Manning, J.R., Mohammed, S., Solovyev, A., Polanski, K., Chazarra, R., Talavera-Lopez, C., Doyle, M., Marnier, G., Grüning, B., Rasche, H., Bacon, W., Perez-Riverol, Y., Haeussler, M., Meyer, K.B., Teichmann, S., and Papatheodorou, I. (2020). "User-friendly, scalable tools and workflows for single-cell analysis". Cold Spring Harbor Laboratory).

Morgan, D.J., and Deangelis, M.M. (2014). Differential Gene Expression in Age-Related Macular Degeneration. *Cold Spring Harb Perspect Med* 5**,** a017210.

Moussa, M., Leila, M., Bessa, A.S., Lolah, M., Abou Shousha, M., El Hennawi, H.M., and Hafez, T.A. (2019). Grading of macular perfusion in retinal vein occlusion using en-face swept-source optical coherence tomography angiography: a retrospective observational case series. *BMC Ophthalmol* 19**,** 127.

Mullins, R.F., Schoo, D.P., Sohn, E.H., Flamme-Wiese, M.J., Workamelahu, G., Johnston, R.M., Wang, K., Tucker, B.A., and Stone, E.M. (2014). The membrane attack complex in aging human choriocapillaris: relationship to macular degeneration and choroidal thinning. *Am J Pathol* 184**,** 3142-3153.

Munn, Z., Moola, S., Lisy, K., Riitano, D., and Tufanaru, C. (2015). Methodological guidance for systematic reviews of observational epidemiological studies reporting prevalence and cumulative incidence data. *Int J Evid Based Healthc* 13**,** 147-153.

Nazifova-Tasinova, N., Radeva, M., Galunska, B., and Grupcheva, C. (2020). Metabolomic analysis in ophthalmology. *Biomed Pap Med Fac Univ Palacky Olomouc Czech Repub* 164**,** 236-246.

Newman, A.M., Gallo, N.B., Hancox, L.S., Miller, N.J., Radeke, C.M., Maloney, M.A., Cooper, J.B., Hageman, G.S., Anderson, D.H., Johnson, L.V., and Radeke, M.J. (2012). Systems-level analysis of age-related macular degeneration reveals global biomarkers and phenotype-specific functional networks. *Genome Med* 4**,** 16.

Nguyen, Q.D., Merrill, P.T., Jaffe, G.J., Dick, A.D., Kurup, S.K., Sheppard, J., Schlaen, A., Pavesio, C., Cimino, L., Van Calster, J., Camez, A.A., Kwatra, N.V., Song, A.P., Kron, M., Tari, S., and Brezin, A.P. (2016). Adalimumab for prevention of uveitic flare in patients with inactive non-infectious uveitis controlled by corticosteroids (VISUAL II): a multicentre, double-masked, randomised, placebo-controlled phase 3 trial. *Lancet* 388**,** 1183-1192.

Nicolo, M., Piccolino, F.C., Zardi, L., Giovannini, A., and Mariotti, C. (2000). Detection of tenascin-C in surgically excised choroidal neovascular membranes. *Graefes Arch Clin Exp Ophthalmol* 238**,** 107-111.

Noh, S.J., Jeong, W.J., Rho, J.H., Shin, D.M., Ahn, H.B., Park, W.C., Rho, S.H., Soung, Y.H., Kim, T.H., Park, B.S., and Yoo, Y.H. (2008). Sensitization of RPE cells by alphaB-crystallin siRNA to SAHA-induced stage 1 apoptosis through abolishing the association of alphaB-crystallin with HDAC1 in SC35 speckles. *Invest Ophthalmol Vis Sci* 49**,** 4753-4759.

Noori, J., Shi, Y., Yang, J., Gregori, G., Albini, T.A., Rosenfeld, P.J., and Davis, J.L. (2021). A Novel Method to Detect and Monitor Retinal Vasculitis Using Swept-Source OCT Angiography. *Ophthalmol Retina* 5**,** 1226-1234.

Nordgaard, C.L., Berg, K.M., Kapphahn, R.J., Reilly, C., Feng, X., Olsen, T.W., and Ferrington, D.A. (2006). Proteomics of the retinal pigment epithelium reveals altered protein expression at progressive stages of age-related macular degeneration. *Invest Ophthalmol Vis Sci* 47**,** 815-822.

Nunez Do Rio, J.M., Sen, P., Rasheed, R., Bagchi, A., Nicholson, L., Dubis, A.M., Bergeles, C., and Sivaprasad, S. (2020). Deep Learning-Based Segmentation and Quantification of Retinal Capillary Non-Perfusion on Ultra-Wide-Field Retinal Fluorescein Angiography. *J Clin Med* 9**,** 2537.

Onal, S., Tugal-Tutkun, I., Neri, P., and C, P.H. (2014). Optical coherence tomography imaging in uveitis. *Int Ophthalmol* 34**,** 401-435.

Onal, S., Uludag, G., Oray, M., Mengi, E., Herbort, C.P., Akman, M., Metin, M.M., Koc Akbay, A., and Tugal-Tutkun, I. (2018). Quantitative Analysis of Structural Alterations in the Choroid of Patients with Active Behcet Uveitis. *Retina* 38**,** 828-840.

Orozco, L.D., Chen, H.H., Cox, C., Katschke, K.J., Jr., Arceo, R., Espiritu, C., Caplazi, P., Nghiem, S.S., Chen, Y.J., Modrusan, Z., Dressen, A., Goldstein, L.D., Clarke, C., Bhangale, T., Yaspan, B., Jeanne, M., Townsend, M.J., Van Lookeren Campagne, M., and Hackney, J.A. (2020). Integration of eQTL and a Single-Cell Atlas in the Human Eye Identifies Causal Genes for Age-Related Macular Degeneration. *Cell Rep* 30**,** 1246-1259 e1246.

Ouyang, Y., Heussen, F.M., Hariri, A., Keane, P.A., and Sadda, S.R. (2013). Optical coherence tomography-based observation of the natural history of drusenoid lesion in eyes with dry age-related macular degeneration. *Ophthalmology* 120**,** 2656-2665.

Page, M.J., Mckenzie, J.E., Bossuyt, P.M., Boutron, I., Hoffmann, T.C., Mulrow, C.D., Shamseer, L., Tetzlaff, J.M., Akl, E.A., Brennan, S.E., Chou, R., Glanville, J., Grimshaw, J.M., Hrobjartsson, A., Lalu, M.M., Li, T., Loder, E.W., Mayo-Wilson, E., Mcdonald, S., Mcguinness, L.A., Stewart, L.A., Thomas, J., Tricco, A.C., Welch, V.A., Whiting, P., and Moher, D. (2021). The PRISMA 2020 statement: an updated guideline for reporting systematic reviews. *BMJ* 372**,** n71.

Panda-Jonas, S., Jonas, J.B., and Jakobczyk-Zmija, M. (1996). Retinal pigment epithelial cell count, distribution, and correlations in normal human eyes. *Am J Ophthalmol* 121**,** 181-189.

Papatheodorou, I., Moreno, P., Manning, J., Fuentes, A.M., George, N., Fexova, S., Fonseca, N.A., Fullgrabe, A., Green, M., Huang, N., Huerta, L., Iqbal, H., Jianu, M., Mohammed, S., Zhao, L., Jarnuczak, A.F., Jupp, S., Marioni, J., Meyer, K., Petryszak, R., Prada Medina, C.A., Talavera-Lopez, C., Teichmann, S., Vizcaino, J.A., and Brazma, A. (2020). Expression Atlas update: from tissues to single cells. *Nucleic Acids Res* 48**,** D77-D83.

Paraoan, L., Grierson, I., and Maden, B.E. (2000). Analysis of expressed sequence tags of retinal pigment epithelium: cystatin C is an abundant transcript. *Int J Biochem Cell Biol* 32**,** 417-426.

Paraoan, L., Sharif, U., Carlsson, E., Supharattanasitthi, W., Mahmud, N.M., Kamalden, T.A., Hiscott, P., Jackson, M., and Grierson, I. (2020). Secretory proteostasis of the retinal pigmented epithelium: Impairment links to age-related macular degeneration. *Prog Retin Eye Res* 79**,** 100859.

Patel, S.N., Shi, A., Wibbelsman, T.D., and Klufas, M.A. (2020). Ultra-widefield retinal imaging: an update on recent advances. *Ther Adv Ophthalmol* 12**,** 2515841419899495.

Pawlak, A.M., Glenn, J.V., Beattie, J.R., Mcgarvey, J.J., and Stitt, A.W. (2008). Advanced glycation as a basis for understanding retinal aging and noninvasive risk prediction. *Ann N Y Acad Sci* 1126**,** 59-65.

Pichi, F., Invernizzi, A., Tucker, W.R., and Munk, M.R. (2020). Optical coherence tomography diagnostic signs in posterior uveitis. *Prog Retin Eye Res* 75**,** 100797.

Porritt, K., Gomersall, J., and Lockwood, C. (2014). JBI's Systematic Reviews: Study selection and critical appraisal. *Am J Nurs* 114**,** 47-52.

Porter, L.F., Saptarshi, N., Fang, Y., Rathi, S., Den Hollander, A.I., De Jong, E.K., Clark, S.J., Bishop, P.N., Olsen, T.W., Liloglou, T., Chavali, V.R.M., and Paraoan, L. (2019). Whole-genome methylation profiling of the retinal pigment epithelium of individuals with age-related macular degeneration reveals differential methylation of the SKI, GTF2H4, and TNXB genes. *Clin Epigenetics* 11**,** 6.

Pouw, A.E., Greiner, M.A., Coussa, R.G., Jiao, C., Han, I.C., Skeie, J.M., Fingert, J.H., Mullins, R.F., and Sohn, E.H. (2021). Cell-Matrix Interactions in the Eye: From Cornea to Choroid. *Cells* 10**,** 687.

Prete, M., Guerriero, S., Dammacco, R., Fatone, M.C., Vacca, A., Dammacco, F., and Racanelli, V. (2014). Autoimmune uveitis: a retrospective analysis of 104 patients from a tertiary reference center. *J Ophthalmic Inflamm Infect* 4**,** 17.

Provis, J.M., Penfold, P.L., Cornish, E.E., Sandercoe, T.M., and Madigan, M.C. (2005). Anatomy and development of the macula: specialisation and the vulnerability to macular degeneration. *Clin Exp Optom* 88**,** 269-281.

Ramrattan, R.S., Van Der Schaft, T.L., Mooy, C.M., De Bruijn, W.C., Mulder, P.G., and De Jong, P.T. (1994). Morphometric analysis of Bruch's membrane, the choriocapillaris, and the choroid in aging. *Invest Ophthalmol Vis Sci* 35**,** 2857-2864.

Raychaudhuri, S., Iartchouk, O., Chin, K., Tan, P.L., Tai, A.K., Ripke, S., Gowrisankar, S., Vemuri, S., Montgomery, K., Yu, Y., Reynolds, R., Zack, D.J., Campochiaro, B., Campochiaro, P., Katsanis, N., Daly, M.J., and Seddon, J.M. (2011). A rare penetrant mutation in CFH confers high risk of age-related macular degeneration. *Nat Genet* 43**,** 1232-1236.

Reeves, G.M., Kumar, N., Beare, N.A., and Pearce, I.A. (2013). Use of Staurenghi lens angiography in the management of posterior uveitis. *Acta Ophthalmol* 91**,** 48-51.

Reinhard, J., Roll, L., and Faissner, A. (2017). Tenascins in Retinal and Optic Nerve Neurodegeneration. *Front Integr Neurosci* 11**,** 30.

Ritchie, M.E., Phipson, B., Wu, D., Hu, Y., Law, C.W., Shi, W., and Smyth, G.K. (2015). limma powers differential expression analyses for RNA-sequencing and microarray studies. *Nucleic Acids Res* 43**,** e47.

Romdhoniyyah, D.F., Harding, S.P., Cheyne, C.P., and Beare, N.a.V. (2021). Metformin, A Potential Role in Age-Related Macular Degeneration: A Systematic Review and Meta-Analysis. *Ophthalmol Ther* 10**,** 245-260.

Ronneberger, O., Fischer, P., and Brox, T. (2015). "U-Net: Convolutional Networks for Biomedical Image Segmentation," in *Medical Image Computing and Computer-Assisted Intervention – MICCAI 2015*. Springer International Publishing), 234-241.

Rosenbaum, J.T., Ku, J., Ali, A., Choi, D., and Suhler, E.B. (2012). Patients with Retinal Vasculitis Rarely Suffer from Systemic Vasculitis. *Seminars in Arthritis and Rheumatism* 41**,** 859-865.

Rosenbaum, J.T., Sibley, C.H., and Lin, P. (2016). Retinal vasculitis. *Curr Opin Rheumatol* 28**,** 228-235.

Rozing, M.P., Durhuus, J.A., Krogh Nielsen, M., Subhi, Y., Kirkwood, T.B., Westendorp, R.G., and Sorensen, T.L. (2020). Age-related macular degeneration: A two-level model hypothesis. *Prog Retin Eye Res* 76**,** 100825.

Saptarshi, N., Green, D., Cree, A., Lotery, A., Paraoan, L., and Porter, L.F. (2021). Epigenetic Age Acceleration Is Not Associated with Age-Related Macular Degeneration. *Int J Mol Sci* 22**,** 13457.

Schaal, K.B., Munk, M.R., Wyssmueller, I., Berger, L.E., Zinkernagel, M.S., and Wolf, S. (2019). Vascular Abnormalities in Diabetic Retinopathy Assessed with Swept-Source Optical Coherence Tomography Angiography Widefield Imaging. *Retina* 39**,** 79-87.

Schlegl, T., Waldstein, S.M., Bogunovic, H., Endstrasser, F., Sadeghipour, A., Philip, A.M., Podkowinski, D., Gerendas, B.S., Langs, G., and Schmidt-Erfurth, U. (2018). Fully Automated Detection and Quantification of Macular Fluid in OCT Using Deep Learning. *Ophthalmology* 125**,** 549-558.

Schmidt-Erfurth, U., Bogunovic, H., Sadeghipour, A., Schlegl, T., Langs, G., Gerendas, B.S., Osborne, A., and Waldstein, S.M. (2018a). Machine Learning to Analyze the Prognostic Value of Current Imaging Biomarkers in Neovascular Age-Related Macular Degeneration. *Ophthalmol Retina* 2**,** 24-30.

Schmidt-Erfurth, U., Chong, V., Loewenstein, A., Larsen, M., Souied, E., Schlingemann, R., Eldem, B., Mones, J., Richard, G., Bandello, F., and European Society of Retina, S. (2014). Guidelines for the management of neovascular age-related macular degeneration by the European Society of Retina Specialists (EURETINA). *Br J Ophthalmol* 98**,** 1144-1167.

Schmidt-Erfurth, U., Sadeghipour, A., Gerendas, B.S., Waldstein, S.M., and Bogunovic, H. (2018b). Artificial intelligence in retina. *Prog Retin Eye Res* 67**,** 1-29.

Schubert, H.D. (2019). "Structure of the Neural Retina," in *Ophthalmology,* ed. M. Yanoff. 5 ed: Elsevier), 419-422.e411.

Schurch, N.J., Schofield, P., Gierlinski, M., Cole, C., Sherstnev, A., Singh, V., Wrobel, N., Gharbi, K., Simpson, G.G., Owen-Hughes, T., Blaxter, M., and Barton, G.J. (2016). How many biological replicates are needed in an RNA-seq experiment and which differential expression tool should you use? *RNA* 22**,** 839-851.

Senger, D.R., Galli, S.J., Dvorak, A.M., Perruzzi, C.A., Harvey, V.S., and Dvorak, H.F. (1983). Tumor cells secrete a vascular permeability factor that promotes accumulation of ascites fluid. *Science* 219**,** 983-985.

Seo, S., and Suh, W. (2017). Antiangiogenic effect of dasatinib in murine models of oxygen-induced retinopathy and laser-induced choroidal neovascularization. *Mol Vis* 23**,** 823-831.

Seshasai, S., Liao, J., Toh, Q.C., Cheng, C.Y., Cheung, G.C., Sethi, S., Wong, T.Y., and Sabanayagam, C. (2015). Serum leptin and age-related macular degeneration. *Invest Ophthalmol Vis Sci* 56**,** 1880-1886.

Sharief, L., Lightman, S., Blum-Hareuveni, T., Bar, A., and Tomkins-Netzer, O. (2017). Clinical Outcome of Retinal Vasculitis and Predictors for Prognosis of Ischemic Retinal Vasculitis. *Am J Ophthalmol* 177**,** 206-212.

Sharif, U., Mahmud, N.M., Kay, P., Yang, Y.C., Harding, S.P., Grierson, I., Kamalden, T.A., Jackson, M.J., and Paraoan, L. (2019). Advanced glycation end products-related modulation of cathepsin L and NF-kappaB signalling effectors in retinal pigment epithelium lead to augmented response to TNFalpha. *J Cell Mol Med* 23**,** 405-416.

Sheemar, A., Temkar, S., Takkar, B., Sood, R., Sinha, S., Chawla, R., Vohra, R., and Venkatesh, P. (2019). Ultra-Wide Field Imaging Characteristics of Primary Retinal Vasculitis: Risk Factors for Retinal Neovascularization. *Ocul Immunol Inflamm* 27**,** 383-388.

Sheffield, V.C., and Stone, E.M. (2011). Genomics and the eye. *N Engl J Med* 364**,** 1932-1942.

Shirahama, S., Kaburaki, T., Nakahara, H., Tanaka, R., Komae, K., Fujino, Y., Kawashima, H., and Aihara, M. (2019). Association between subfoveal choroidal thickness and leakage site on fluorescein angiography in Behcet's uveitis. *Sci Rep* 9**,** 8612.

Shulman, S., Kramer, M., Amer, R., Sorkin, N., Schaap-Fogler, M., Rosenblatt, A., and Habot-Wilner, Z. (2015). Characteristics and Long-Term Outcome of Patients with Noninfectious Retinal Vasculitis. *Retina* 35**,** 2633-2640.

Siddique, N., Paheding, S., Elkin, C.P., and Devabhaktuni, V. (2021). U-Net and Its Variants for Medical Image Segmentation: A Review of Theory and Applications. *IEEE Access* 9**,** 82031-82057.

Sieber, C., Kopf, J., Hiepen, C., and Knaus, P. (2009). Recent advances in BMP receptor signaling. *Cytokine Growth Factor Rev* 20**,** 343-355.

Silpa-Archa, S., Sapthanakorn, W., and Foster, C.S. (2022). ISOLATED RETINAL VASCULITIS: Prognostic Factors and Expanding the Role of Immunosuppressive Treatment in Retinal Vasculitis Associated With Positive QuantiFERON-TB Gold Test. *Retina* 42**,** 1897-1908.

Slakter, J.S., and Stur, M. (2005). Quality of life in patients with age-related macular degeneration: impact of the condition and benefits of treatment. *Surv Ophthalmol* 50**,** 263-273.

Solursh, M., Langille, R.M., Wood, J., and Sampath, T.K. (1996). Osteogenic protein-1 is required for mammalian eye development. *Biochem Biophys Res Commun* 218**,** 438-443.

Spaide, R.F. (2020). CHOROIDAL BLOOD FLOW: Review and Potential Explanation for the Choroidal Venous Anatomy Including the Vortex Vein System. *Retina* 40**,** 1851-1864.

Spaide, R.F., and Curcio, C.A. (2011). Anatomical correlates to the bands seen in the outer retina by optical coherence tomography: literature review and model. *Retina* 31**,** 1609-1619.

Spaide, R.F., Fujimoto, J.G., Waheed, N.K., Sadda, S.R., and Staurenghi, G. (2018). Optical coherence tomography angiography. *Prog Retin Eye Res* 64**,** 1-55.

Spaide, R.F., Jaffe, G.J., Sarraf, D., Freund, K.B., Sadda, S.R., Staurenghi, G., Waheed, N.K., Chakravarthy, U., Rosenfeld, P.J., Holz, F.G., Souied, E.H., Cohen, S.Y., Querques, G., Ohno-Matsui, K., Boyer, D., Gaudric, A., Blodi, B., Baumal, C.R., Li, X., Coscas, G.J., Brucker, A., Singerman, L., Luthert, P., Schmitz-Valckenberg, S., Schmidt-Erfurth, U., Grossniklaus, H.E., Wilson, D.J., Guymer, R., Yannuzzi, L.A., Chew, E.Y., Csaky, K., Mones, J.M., Pauleikhoff, D., Tadayoni, R., and Fujimoto, J. (2020). Consensus Nomenclature for Reporting Neovascular Age-Related Macular Degeneration Data: Consensus on Neovascular Age-Related Macular Degeneration Nomenclature Study Group. *Ophthalmology* 127**,** 616-636.

Sparrow, J.R., Gregory-Roberts, E., Yamamoto, K., Blonska, A., Ghosh, S.K., Ueda, K., and Zhou, J. (2012). The bisretinoids of retinal pigment epithelium. *Prog Retin Eye Res* 31**,** 121-135.

Sparrow, J.R., Hicks, D., and Hamel, C.P. (2010). The retinal pigment epithelium in health and disease. *Curr Mol Med* 10**,** 802-823.

Sreekumar, P.G., Hinton, D.R., and Kannan, R. (2020). The Emerging Role of Senescence in Ocular Disease. *Oxid Med Cell Longev* 2020**,** 2583601.

Staurenghi, G., Bottoni, F., and Giani, A. (2013). "Clinical Applications of Diagnostic Indocyanine Green Angiography," in *Retina,* eds. S.J. Ryan, S.R. Sadda, D.R. Hinton, A.P. Schachat, S.R. Sadda, C.P. Wilkinson, P. Wiedemann & A.P. Schachat. (London: W.B. Saunders), 51-81.

Strauss, O. (2005). The retinal pigment epithelium in visual function. *Physiol Rev* 85**,** 845-881.

Su, L., Chen, S., Zheng, C., Wei, H., and Song, X. (2019). Meta-Analysis of Gene Expression and Identification of Biological Regulatory Mechanisms in Alzheimer's Disease. *Front Neurosci* 13**,** 633.

Suhler, E.B., Adan, A., Brezin, A.P., Fortin, E., Goto, H., Jaffe, G.J., Kaburaki, T., Kramer, M., Lim, L.L., Muccioli, C., Nguyen, Q.D., Van Calster, J., Cimino, L., Kron, M., Song, A.P., Liu, J., Pathai, S., Camez, A., Schlaen, A., Van Velthoven, M.E.J., Vitale, A.T., Zierhut, M., Tari, S., and Dick, A.D. (2018). Safety and Efficacy of Adalimumab in Patients with Noninfectious Uveitis in an Ongoing Open-Label Study: VISUAL III. *Ophthalmology* 125**,** 1075-1087.

Suhler, E.B., Smith, J.R., Wertheim, M.S., Lauer, A.K., Kurz, D.E., Pickard, T.D., and Rosenbaum, J.T. (2005). A prospective trial of infliximab therapy for refractory uveitis: preliminary safety and efficacy outcomes. *Arch Ophthalmol* 123**,** 903-912.

Sura, A.A., Chen, L., Messinger, J.D., Swain, T.A., Mcgwin, G., Jr., Freund, K.B., and Curcio, C.A. (2020). Measuring the Contributions of Basal Laminar Deposit and Bruch's Membrane in Age-Related Macular Degeneration. *Invest Ophthalmol Vis Sci* 61**,** 19.

Swaroop, A., and Zack, D.J. (2002). Transcriptome analysis of the retina. *Genome Biol* 3**,** REVIEWS1022.

Szklarczyk, D., Gable, A.L., Lyon, D., Junge, A., Wyder, S., Huerta-Cepas, J., Simonovic, M., Doncheva, N.T., Morris, J.H., Bork, P., Jensen, L.J., and Mering, C.V. (2019). STRING v11: protein-protein association networks with increased coverage, supporting functional discovery in genome-wide experimental datasets. *Nucleic Acids Res* 47**,** D607-D613.

Tajiri, K., Yonebayashi, S., Li, S., and Ieda, M. (2021). Immunomodulatory Role of Tenascin-C in Myocarditis and Inflammatory Cardiomyopathy. *Front Immunol* 12**,** 624703.

Tam, V., Patel, N., Turcotte, M., Bosse, Y., Pare, G., and Meyre, D. (2019). Benefits and limitations of genome-wide association studies. *Nat Rev Genet* 20**,** 467-484.

Tan, M., and Le, Q.V. (2019). EfficientNet: Rethinking Model Scaling for Convolutional Neural Networks. *ArXiv* abs/1905.11946.

Tang, J., Yan, H., and Zhuang, S. (2013). Histone deacetylases as targets for treatment of multiple diseases. *Clin Sci (Lond)* 124**,** 651-662.

Tanna, P., Strauss, R.W., Fujinami, K., and Michaelides, M. (2017). Stargardt disease: clinical features, molecular genetics, animal models and therapeutic options. *Br J Ophthalmol* 101**,** 25-30.

Telegina, D.V., Korbolina, E.E., Ershov, N.I., Kolosova, N.G., and Kozhevnikova, O.S. (2015). Identification of functional networks associated with cell death in the retina of OXYS rats during the development of retinopathy. *Cell Cycle* 14**,** 3544-3556.

Terao, R., Ahmed, T., Suzumura, A., and Terasaki, H. (2022). Oxidative Stress-Induced Cellular Senescence in Aging Retina and Age-Related Macular Degeneration. *Antioxidants (Basel)* 11**,** 2189.

Terrano, D.T., Upreti, M., and Chambers, T.C. (2010). Cyclin-dependent kinase 1-mediated Bcl-xL/Bcl-2 phosphorylation acts as a functional link coupling mitotic arrest and apoptosis. *Mol Cell Biol* 30**,** 640-656.

Teussink, M.M., Huis in Het Veld, P.I., De Vries, L.A., Hoyng, C.B., Klevering, B.J., and Theelen, T. (2016). Multimodal imaging of the disease progression of birdshot chorioretinopathy. *Acta Ophthalmol* 94**,** 815-823.

Tian, L., Kazmierkiewicz, K.L., Bowman, A.S., Li, M., Curcio, C.A., and Stambolian, D.E. (2015). Transcriptome of the human retina, retinal pigmented epithelium and choroid. *Genomics* 105**,** 253-264.

Tian, M., Tappeiner, C., Zinkernagel, M.S., Huf, W., Wolf, S., and Munk, M.R. (2019a). Evaluation of vascular changes in intermediate uveitis and retinal vasculitis using swept-source wide-field optical coherence tomography angiography. *Br J Ophthalmol* 103**,** 1289-1295.

Tian, M., Tappeiner, C., Zinkernagel, M.S., Wolf, S., and Munk, M.R. (2019b). Swept-source optical coherence tomography angiography reveals vascular changes in intermediate uveitis. *Acta Ophthalmol* 97**,** e785-e791.

Ting, D.S.W., Cheung, C.Y., Lim, G., Tan, G.S.W., Quang, N.D., Gan, A., Hamzah, H., Garcia-Franco, R., San Yeo, I.Y., Lee, S.Y., Wong, E.Y.M., Sabanayagam, C., Baskaran, M., Ibrahim, F., Tan, N.C., Finkelstein, E.A., Lamoureux, E.L., Wong, I.Y., Bressler, N.M., Sivaprasad, S., Varma, R., Jonas, J.B., He, M.G., Cheng, C.Y., Cheung, G.C.M., Aung, T., Hsu, W., Lee, M.L., and Wong, T.Y. (2017). Development and Validation of a Deep Learning System for Diabetic Retinopathy and Related Eye Diseases Using Retinal Images From Multiethnic Populations With Diabetes. *JAMA* 318**,** 2211-2223.

Ting, D.S.W., Peng, L., Varadarajan, A.V., Keane, P.A., Burlina, P.M., Chiang, M.F., Schmetterer, L., Pasquale, L.R., Bressler, N.M., Webster, D.R., Abramoff, M., and Wong, T.Y. (2019). Deep learning in ophthalmology: The technical and clinical considerations. *Prog Retin Eye Res* 72**,** 100759.

Tong, Y., Lu, W., Yu, Y., and Shen, Y. (2020). Application of machine learning in ophthalmic imaging modalities. *Eye Vis (Lond)* 7**,** 22.

Tseng, G.C., Ghosh, D., and Feingold, E. (2012). Comprehensive literature review and statistical considerations for microarray meta-analysis. *Nucleic Acids Res* 40**,** 3785-3799.

Tsiknakis, N., Theodoropoulos, D., Manikis, G., Ktistakis, E., Boutsora, O., Berto, A., Scarpa, F., Scarpa, A., Fotiadis, D.I., and Marias, K. (2021). Deep learning for diabetic retinopathy detection and classification based on fundus images: A review. *Comput Biol Med* 135**,** 104599.

Tsirouki, T., Dastiridou, A., Symeonidis, C., Tounakaki, O., Brazitikou, I., Kalogeropoulos, C., and Androudi, S. (2018). A Focus on the Epidemiology of Uveitis. *Ocul Immunol Inflamm* 26**,** 2-16.

Tugal-Tutkun, I., Herbort, C.P., Khairallah, M., and Angiography Scoring for Uveitis Working, G. (2010a). Scoring of dual fluorescein and ICG inflammatory angiographic signs for the grading of posterior segment inflammation (dual fluorescein and ICG angiographic scoring system for uveitis). *Int Ophthalmol* 30**,** 539-552.

Tugal-Tutkun, I., Herbort, C.P., Khairallah, M., and Mantovani, A. (2010b). Interobserver agreement in scoring of dual fluorescein and ICG inflammatory angiographic signs for the grading of posterior segment inflammation. *Ocul Immunol Inflamm* 18**,** 385-389.

Tugal-Tutkun, I., Ozdal, P.C., Oray, M., and Onal, S. (2017). Review for Diagnostics of the Year: Multimodal Imaging in Behcet Uveitis. *Ocul Immunol Inflamm* 25**,** 7-19.

Turk, M.A., Hayworth, J.L., Nevskaya, T., and Pope, J.E. (2021). Ocular manifestations of Behcet's disease in children and adults: a systematic review and meta-analysis. *Clin Exp Rheumatol* 39 Suppl 132**,** 94-101.

Ueda, D., Shimazaki, A., and Miki, Y. (2019). Technical and clinical overview of deep learning in radiology. *Jpn J Radiol* 37**,** 15-33.

Ueda, S., Nunn, B.M., Chauhan, R., Mcdonald, K., Kaplan, H.J., O'toole, M.G., and Tamiya, S. (2021). Sustained dasatinib treatment prevents early fibrotic changes following ocular trauma. *Graefes Arch Clin Exp Ophthalmol* 259**,** 1103-1111.

Umazume, A., Kezuka, T., Usui, Y., Suzuki, J., and Goto, H. (2018). Evaluation of efficacy of infliximab for retinal vasculitis and extraocular symptoms in Behcet disease. *Jpn J Ophthalmol* 62**,** 390-397.

Vandereyken, K., Sifrim, A., Thienpont, B., and Voet, T. (2023). Methods and applications for single-cell and spatial multi-omics. *Nat Rev Genet* 24**,** 494-515.

Vasey, B., Nagendran, M., Campbell, B., Clifton, D.A., Collins, G.S., Denaxas, S., Denniston, A.K., Faes, L., Geerts, B., Ibrahim, M., Liu, X., Mateen, B.A., Mathur, P., Mccradden, M.D., Morgan, L., Ordish, J., Rogers, C., Saria, S., Ting, D.S.W., Watkinson, P., Weber, W., Wheatstone, P., Mcculloch, P., and Group, D.-a.E. (2022). Reporting guideline for the early stage clinical evaluation of decision support systems driven by artificial intelligence: DECIDE-AI. *BMJ* 377**,** e070904.

Voigt, A.P., Mulfaul, K., Mullin, N.K., Flamme-Wiese, M.J., Giacalone, J.C., Stone, E.M., Tucker, B.A., Scheetz, T.E., and Mullins, R.F. (2019). Single-cell transcriptomics of the human retinal pigment epithelium and choroid in health and macular degeneration. *Proc Natl Acad Sci U S A* 116**,** 24100-24107.

Voigt, A.P., Mullin, N.K., Mulfaul, K., Lozano, L.P., Wiley, L.A., Flamme-Wiese, M.J., Boese, E.A., Han, I.C., Scheetz, T.E., Stone, E.M., Tucker, B.A., and Mullins, R.F. (2022). Choroidal endothelial and macrophage gene expression in atrophic and neovascular macular degeneration. *Hum Mol Genet* 31**,** 2406-2423.

Voigt, A.P., Mullin, N.K., Stone, E.M., Tucker, B.A., Scheetz, T.E., and Mullins, R.F. (2021). Single-cell RNA sequencing in vision research: Insights into human retinal health and disease. *Prog Retin Eye Res* 83**,** 100934.

Voigt, A.P., Whitmore, S.S., Mulfaul, K., Chirco, K.R., Giacalone, J.C., Flamme-Wiese, M.J., Stockman, A., Stone, E.M., Tucker, B.A., Scheetz, T.E., and Mullins, R.F. (2020). Bulk and single-cell gene

expression analyses reveal aging human choriocapillaris has pro-inflammatory phenotype. *Microvasc Res* 131**,** 104031.

Von Zglinicki, T., Wan, T., and Miwa, S. (2021). Senescence in Post-Mitotic Cells: A Driver of Aging? *Antioxid Redox Signal* 34**,** 308-323.

Walton, R.C., and Ashmore, E.D. (2003). Retinal vasculitis. *Curr Opin Ophthalmol* 14**,** 413-419.

Wang, J., Duncan, D., Shi, Z., and Zhang, B. (2013). WEB-based GEne SeT AnaLysis Toolkit (WebGestalt): update 2013. *Nucleic Acids Res* 41**,** W77-83.

Wang, J., Feng, Y., Han, P., Wang, F., Luo, X., Liang, J., Sun, X., Ye, J., Lu, Y., and Sun, X. (2018a). Photosensitization of A2E triggers telomere dysfunction and accelerates retinal pigment epithelium senescence. *Cell Death Dis* 9**,** 178.

Wang, J., Vasaikar, S., Shi, Z., Greer, M., and Zhang, B. (2017). WebGestalt 2017: a more comprehensive, powerful, flexible and interactive gene set enrichment analysis toolkit. *Nucleic Acids Res* 45**,** W130-W137.

Wang, J.J., Rochtchina, E., Lee, A.J., Chia, E.M., Smith, W., Cumming, R.G., and Mitchell, P. (2007). Ten-year incidence and progression of age-related maculopathy: the blue Mountains Eye Study. *Ophthalmology* 114**,** 92-98.

Wang, S., Wang, X., Cheng, Y., Ouyang, W., Sang, X., Liu, J., Su, Y., Liu, Y., Li, C., Yang, L., Jin, L., and Wang, Z. (2019). Autophagy Dysfunction, Cellular Senescence, and Abnormal Immune-Inflammatory Responses in AMD: From Mechanisms to Therapeutic Potential. *Oxid Med Cell Longev* 2019**,** 3632169.

Wang, Z., Arat, S., Magid-Slav, M., and Brown, J.R. (2018b). Meta-analysis of human gene expression in response to Mycobacterium tuberculosis infection reveals potential therapeutic targets. *BMC Syst Biol* 12**,** 3.

Wauman, J., Zabeau, L., and Tavernier, J. (2017). The Leptin Receptor Complex: Heavier Than Expected? *Front Endocrinol (Lausanne)* 8**,** 30.

Wen, Y., Alshikho, M.J., and Herbert, M.R. (2016). Pathway Network Analyses for Autism Reveal Multisystem Involvement, Major Overlaps with Other Diseases and Convergence upon MAPK and Calcium Signaling. *PLoS One* 11**,** e0153329.

Wenick, A.S., Bressler, N.M., and Bressler, S.B. (2017). "Age-Related Macular Degeneration: Non-Neovascular Early AMD, Intermediate AMD, and Geographic Atrophy," in *Ryan's Retina E-Book,* eds. A.P. Schachat, C.P. Wilkinson, D.R. Hinton, S.R. Sadda & P. Wiedemann. 6 ed: Elsevier), 1293-1344.

Whitmore, S.S., Braun, T.A., Skeie, J.M., Haas, C.M., Sohn, E.H., Stone, E.M., Scheetz, T.E., and Mullins, R.F. (2013). Altered gene expression in dry age-related macular degeneration suggests early loss of choroidal endothelial cells. *Mol Vis* 19**,** 2274-2297.

Whitmore, S.S., Sohn, E.H., Chirco, K.R., Drack, A.V., Stone, E.M., Tucker, B.A., and Mullins, R.F. (2015). Complement activation and choriocapillaris loss in early AMD: implications for pathophysiology and therapy. *Prog Retin Eye Res* 45**,** 1-29.

Whitmore, S.S., Wagner, A.H., Deluca, A.P., Drack, A.V., Stone, E.M., Tucker, B.A., Zeng, S., Braun, T.A., Mullins, R.F., and Scheetz, T.E. (2014). Transcriptomic analysis across nasal, temporal, and macular regions of human neural retina and RPE/choroid by RNA-Seq. *Exp Eye Res* 129**,** 93-106.

Witkin, A.J., Chang, D.F., Jumper, J.M., Charles, S., Eliott, D., Hoffman, R.S., Mamalis, N., Miller, K.M., and Wykoff, C.C. (2017). Vancomycin-Associated Hemorrhagic Occlusive Retinal Vasculitis: Clinical Characteristics of 36 Eyes. *Ophthalmology* 124**,** 583-595.

Wong, C.W., Yanagi, Y., Lee, W.K., Ogura, Y., Yeo, I., Wong, T.Y., and Cheung, C.M.G. (2016). Age-related macular degeneration and polypoidal choroidal vasculopathy in Asians. *Prog Retin Eye Res* 53**,** 107-139.

Wong, W.L., Su, X., Li, X., Cheung, C.M., Klein, R., Cheng, C.Y., and Wong, T.Y. (2014). Global prevalence of age-related macular degeneration and disease burden projection for 2020 and 2040: a systematic review and meta-analysis. *Lancet Glob Health* 2**,** e106-116.

Xia, J., Benner, M.J., and Hancock, R.E. (2014). NetworkAnalyst--integrative approaches for protein-protein interaction network analysis and visual exploration. *Nucleic Acids Res* 42**,** W167-174.

Xia, J., Gill, E.E., and Hancock, R.E. (2015). NetworkAnalyst for statistical, visual and network-based meta-analysis of gene expression data. *Nat Protoc* 10**,** 823-844.

Xie, R., Qiu, B., Chhablani, J., and Zhang, X. (2021). Evaluation of Choroidal Thickness Using Optical Coherent Tomography: A Review. *Front Med (Lausanne)* 8**,** 783519.

Xu, Y., Yan, K., Kim, J., Wang, X., Li, C., Su, L., Yu, S., Xu, X., and Feng, D.D. (2017). Dual-stage deep learning framework for pigment epithelium detachment segmentation in polypoidal choroidal vasculopathy. *Biomed Opt Express* 8**,** 4061-4076.

Yamada, R., Okada, D., Wang, J., Basak, T., and Koyama, S. (2021). Interpretation of omics data analyses. *J Hum Genet* 66**,** 93-102.

Yang, A.C., Kern, F., Losada, P.M., Agam, M.R., Maat, C.A., Schmartz, G.P., Fehlmann, T., Stein, J.A., Schaum, N., Lee, D.P., Calcuttawala, K., Vest, R.T., Berdnik, D., Lu, N., Hahn, O., Gate, D., Mcnerney, M.W., Channappa, D., Cobos, I., Ludwig, N., Schulz-Schaeffer, W.J., Keller, A., and Wyss-Coray, T. (2021). Dysregulation of brain and choroid plexus cell types in severe COVID-19. *Nature* 595**,** 565-571.

Yang, F., Ma, H., and Ding, X.Q. (2018). Thyroid Hormone Signaling in Retinal Development, Survival, and Disease. *Vitam Horm* 106**,** 333-349.

Yang, P., Troncone, L., Augur, Z.M., Kim, S.S.J., Mcneil, M.E., and Yu, P.B. (2020). The role of bone morphogenetic protein signaling in vascular calcification. *Bone* 141**,** 115542.

Yao, H., Ge, T., Zhang, Y., Li, M., Yang, S., Li, H., and Wang, F. (2019). BMP7 antagonizes proliferative vitreoretinopathy through retinal pigment epithelial fibrosis in vivo and in vitro. *FASEB J* 33**,** 3212-3224.

Yatsenko, A.N., Shroyer, N.F., Lewis, R.A., and Lupski, J.R. (2001). Late-onset Stargardt disease is associated with missense mutations that map outside known functional regions of ABCR (ABCA4). *Hum Genet* 108**,** 346-355.

Yi, Z., Chen, L., Zheng, H., and Chen, C. (2023). Retinal Vasculitis Following COVID-19 Vaccination: Causation or Coincidence? *Ocul Immunol Inflamm* 31**,** 1283-1285.

Yin, X.X., Sun, L., Fu, Y., Lu, R., and Zhang, Y. (2022). U-Net-Based Medical Image Segmentation. *J Healthc Eng* 2022**,** 4189781.

Yoo, S.S., Lee, S.M., Do, S.K., Lee, W.K., Kim, D.S., and Park, J.Y. (2014). Unmethylation of the CHRNB4 gene is an unfavorable prognostic factor in non-small cell lung cancer. *Lung Cancer* 86**,** 85-90.

Young, L.H., Kim, J., Yakin, M., Lin, H., Dao, D.T., Kodati, S., Sharma, S., Lee, A.Y., Lee, C.S., and Sen, H.N. (2022). Automated Detection of Vascular Leakage in Fluorescein Angiography - A Proof of Concept. *Transl Vis Sci Technol* 11**,** 19.

Zapata, M.A., Royo-Fibla, D., Font, O., Vela, J.I., Marcantonio, I., Moya-Sanchez, E.U., Sanchez-Perez, A., Garcia-Gasulla, D., Cortes, U., Ayguade, E., and Labarta, J. (2020). Artificial Intelligence to Identify Retinal Fundus Images, Quality Validation, Laterality Evaluation, Macular Degeneration, and Suspected Glaucoma. *Clin Ophthalmol* 14**,** 419-429.

Zarei, M., Pesarakli, H., Yaseri, M., Etesali, H., and Ebrahimiadib, N. (2021). Peripapillary optical coherence tomography as an alternative to fluorescein angiography for monitoring Behcet's retinal vasculitis. *Sci Rep* 11**,** 20037.

Zhang, B., Kirov, S., and Snoddy, J. (2005). WebGestalt: an integrated system for exploring gene sets in various biological contexts. *Nucleic Acids Res* 33**,** W741-748.

Zhao, Y., Maccormick, I.J., Parry, D.G., Leach, S., Beare, N.A., Harding, S.P., and Zheng, Y. (2015). Automated detection of leakage in fluorescein angiography images with application to malarial retinopathy. *Sci Rep* 5**,** 10425.

Zhao, Y., Zheng, Y., Liu, Y., Yang, J., Zhao, Y., Chen, D., and Wang, Y. (2017). Intensity and Compactness Enabled Saliency Estimation for Leakage Detection in Diabetic and Malarial Retinopathy. *IEEE Trans Med Imaging* 36**,** 51-63.

Zhou, D., Borsa, M., and Simon, A.K. (2021). Hallmarks and detection techniques of cellular senescence and cellular ageing in immune cells. *Aging Cell* 20**,** e13316.

Zhou, G., Soufan, O., Ewald, J., Hancock, R.E.W., Basu, N., and Xia, J. (2019). NetworkAnalyst 3.0: a visual analytics platform for comprehensive gene expression profiling and meta-analysis. *Nucleic Acids Res* 47**,** W234-W241.

Zhou, G., Stevenson, M.M., Geary, T.G., and Xia, J. (2016). Comprehensive Transcriptome Meta-analysis to Characterize Host Immune Responses in Helminth Infections. *PLoS Negl Trop Dis* 10**,** e0004624.

Zhou, Z., Rahman Siddiquee, M.M., Tajbakhsh, N., and Liang, J. (2018). "UNet++: A Nested U-Net Architecture for Medical Image Segmentation." Springer International Publishing), 3-11.

Zhu, Q., Liu, M., He, Y., and Yang, B. (2019). Quercetin protect cigarette smoke extracts induced inflammation and apoptosis in RPE cells. *Artif Cells Nanomed Biotechnol* 47**,** 2010-2015.

Zuiderveld, K.J. (1994). "Contrast Limited Adaptive Histogram Equalization", in: *Graphics gems.*).